A PERFORMANCE BASED ASSESMENT OF BIOLOGICAL SELF-HEALING CEMENT-BASED MORTAR

A Thesis

by

Ilgın Sandalcı

Submitted to the
Graduate School of Sciences and Engineering
In Partial Fulfillment of the Requirements for
the Degree of

Master of Science

in the
Department of Civil Engineering

Özyeğin University
August 2022

Copyright © 2022 by Ilgın Sandalcı

A PERFORMANCE BASED ASSESMENT OF BIOLOGICAL SELF-HEALING CEMENT-BASED MORTAR

Approved by:

Asst. Prof. Dr. Zeynep Başaran Bundur, Advisor,
Department of Civil Engineering
Özyeğin University

Asst. Prof. Dr. Derya Deniz,
Department of Civil Engineering
Özyeğin University

Prof. Dr. Nilüfer Özyurt Zihnioğlu
Department of Civil Engineering
Boğaziçi University

Date Approved: 11 August 2022

To my parents.

Feride and Deniz Sandalcı

ABSTRACT

Concrete is the second most used material after water, and the demand for cement-based systems is rapidly increasing due to the urbanization. Because of the cement content, the concrete induces approximately 8% of total carbon emissions. It becomes a necessity to make the concrete industry more sustainable and decrease the carbon dioxide (CO_2) emissions. Unfortunately, it is unfeasible to produce a concrete by not using cement.

We have to reshape how we consume cement-based materials to achieve carbon neutrality in the sector. To date, it is evident that eliminating cement from structural concrete is not feasible, thus it will be more efficient to improve the service life of the structures. A major problem in concrete structures is early age microcracking. Early age microcracks occurring in concrete increase the permeability, consequently decreasing the durability. Recent studies showed that it might be possible to remediate microcracks in the cement-based materials by microbial-induced calcium carbonate precipitation (MICP). However, the main challenge of the application is to provide a suitable carrier to keep the bacterial cells viable in highly alkaline cement paste matrix. This study aims to develop a biological additive to trigger self-healing in cement-based systems by immobilizing *Sporosarcina pasteurii (S. pasteurii)* cells on natural minerals zeolite, metakaolin and perlite. Self-healing ability of bio-based additive was evaluated through healing of flexural cracks in early-age mortar (14 days and 28 days after mixing) samples. Screening of the healing process was done with stereomicroscopy analysis, ultrasonic pulse velocity test (UPV) and water absorption tests. An accelerated corrosion test was applied to self-healed reinforced mortars to evaluate impact of crack sealing on rebar

corrosion. Moreover, the impact of biological additive on the drying shrinkage and the performance of cement-based mortar was also evaluated.

According to conducted analyses, zeolite itself was found to be efficient in autogenous self-healing through its reactivity and internal curing mechanism. Metakaolin and perlite were not found to be suitable to immobilizing bacteria cells. It was concluded that the pore structure and the water absorption capacities of minerals are the main criteria to select a suitable carrier for bacteria cells. While the biological additive had not a significant impact on the initial setting time of cement-based mortar, the addition of bacteria cells decreased the early age compressive strength. Lastly, the mineral and bacteria addition increased the free drying shrinkage of the cement-based mortar.

ÖZETÇE

Beton, kentleşmeden dolayı dünyada sudan sonra en çok kullanılan ikinci malzemedir ve şehirleşmeden dolayı çimento bazlı sistemlere talep gittikçe artmaktadır. Çimento içeriğinden dolayı, beton yaklaşık olarak 8% karbon salınımına neden olur. Beton endüstrisinin daha sürdürülebilir olması ve CO_2 salınımının düşürülmesi gerekmektedir. Fakat çimento kullanmadan, beton üretmek olanaksızdır.

İnşaat sektöründe karbon nötre ulaşmak için, çimento bazlı malzeme tüketimini yeniden şekillendirmek gerekmektedir. Bugüne dek, açıkça anlaşılmıştır ki yapısal betondan çimentoyu çıkarmak uygulanabilir değildir. Bu nedenle, yapıların hizmet ömürlerini uzatmak daha etkili bir yöntemdir. Beton yapılardaki ana sorun erken dönem mikro çatlaklardır. Erken yaşta betonda oluşan mikro çatlaklar, betonun geçirgenliğini arttırır, bunun sonucunda betonun dayanıklılığı azalır. Son çalışmalar, mikro çatlakların bakteri kaynaklı kalsiyum karbonat çökeltisi ile onarılabileceğini göstermiştir. Ancak bu uygulamadaki en büyük zorluk, bakteri hücrelerinin canlılığını çimento hamurunun alkali ortamından koruyacak bir katman oluşturmaktır. Bu çalışma, *Sporosarcina pasteurii (S. pasteurii)* hücrelerini doğal mineraller olan zeolite, metakaolin ve perlite sabitleyerek çimento bazlı sistemde kendiliğinden iyileşmeyi sağlayacak biyolojik bir katkı geliştirmeyi amaçlamaktadır. Biyolojik katkının kendiliğinden iyileşmeye olan etkisi, erken dönemde (karşımdan 14 ve 28 gün sonra) çimento harç numunelerinde oluşturulan çatlakların onarılması ile değerlendirilmiştir. Onarım süreci, stereo mikroskop analizleri, ultra ses geçiş hızı ve su emme kapasitesi testleri ile gözlemlenmiştir. Kendiliğinden iyileşme ile sağlanan onarımın korozyona olan etkisini incelemek için hızlandırılmış

korozyon testi gerçekleştirilmiştir. Ayrıca geliştirilen biyolojik katkının kuruma rötresine ve çimento esaslı harcın performansına olan etkisi de değerlendirilmiştir.

Yapılan analizlere göre, zeolit, reaktivitesi ve iç kürlenme mekanizmasından dolayı, otojen kendiliğinden iyileşmede etkili bulunmuştur. Metakaolin ve perlit, bakteri hücresini sabitlemek için uygun bulunmamıştır. Mineralin gözenekli yapısının ve su emme kapasitesinin, bakteri hücreleri için uygun koruyucu katman seçiminde ana kriterler olduğu sonucuna varılmıştır. Biyolojik katkının çimento esaslı harcın priz süresine önemli bir etkisinin olmadığı fakat erken dönemde basınç dayanımını düşürdüğü gözlemlenmiştir. Son olarak, mineral ve bakteri ilavesi çimento harcının serbest kuruma rötresini arttırmıştır.

ACKNOWLEDGMENTS

I would like to express my deepest gratitude to my advisor, Asst. Prof. Dr. Zeynep Başaran Bundur for her patient guidance, encouragement, and support. I have been extremely lucky to have an advisor who believed in me, allowed me to work freely, and offered me valuable opportunities.

I would also like to thank my thesis committee members, Prof. Dr. Nilüfer Özyurt Zihnioğlu and Asst. Prof. Dr. Derya Deniz for their attention and advice.

This research was conducted with financial assistance from the Scientific and Technical Research Council (TUBITAK) of Turkey Project: MAG-118M327. I would like to acknowledge TUBITAK for financial support.

I would like to thank Asst. Prof. Dr. Serhan Ulukaya for his advice and support.

I would like to extend my sincere thanks to Engin Aydın and Ozan Eray Aydın for their contribution and support to my experimental studies.

Special thanks to my dear friends Efe Kurtoğlu, Necdet Cem Ayla, Yağız Can Atasoy, Gamze Gaye Alsan, Ege Gediksiz and Barış Baysal for their friendships, motivation, and support. I would like to acknowledge my friends and colleagues Ayça Gisu Güldoğan and Mustafa Mert Tezer for their guidance and contribution to my study.

I would like to thank all the members of OZU SAM research group.

Finally, I would like to thank my mother and father for supporting me in my every decision and tolerating me in every situation.

TABLE OF CONTENTS

ABSTRACT ..... **iv**

ÖZETÇE ..... **vi**

ACKNOWLEDGMENTS ..... **viii**

TABLE OF CONTENTS ..... **ix**

LIST OF TABLES ..... **xi**

LIST OF FIGURES ..... **xiii**

CHAPTER I **1**

INTRODUCTION **1**

Goal and Objectives 4

CHAPTER II **6**

LITERATURE REVIEW **6**

CHAPTER III **11**

MATERIALS AND METHODOLOGY **11**

3.1 Microorganism selection and growth 11

3.2 Material selection 12

3.3 Immobilization procedure 14

3.4 Preparing of mortar samples 16

3.5 Crack formation and curing conditions 18

3.6 Evaluation of self-healing ability 19

3.6.1 Stereomicroscope and image analysis 19

3.6.2 Ultrasonic pulse velocity (UPV) 20

3.6.3 Water absorption capacity 21

3.6.4 Characterization of the precipitates 21

3.7 Performance evaluation of bio-based mortar samples 22

3.7.1 Vicat needle test 22
3.7.2 Compressive strength test 22
3.8 Influence of biological additive on free drying shrinkage 23
3.9 Effects of crack sealing on corrosion resistance 24
CHAPTER IV 26
RESULTS AND DISCUSSION 26
4.1 Evaluation of self-healing ability 26
4.1.1 Use of micro-size Zeolite (200 μm) as a protection barrier: 26
4.1.2 Use of Zeolite (1.6 mm) aggregate as a protection barrier: 37
4.1.3 Use of perlite as a protection barrier: 43
4.1.4 Use of metakaolin as a protection barrier: 49
4.1.5 A comparative evaluation of mineral immobilization barriers: 55
4.2 Performance evaluation of bio-based mortar samples 57
4.2.1 Evaluation of initial setting time 57
4.2.2 Evaluation of compressive strength 59
4.3 Influence of biological additive on free drying shrinkage 62
4.4 Effects of crack sealing on corrosion resistance 68
CHAPTER V 71
CONCLUSION AND FUTURE STUDIES 71
5.1 Key findings of the study 71
5.2 Future works 73
APPENDIX A – IMAGE ANAYLSES 75
APPENDIX B – FTIR ANALYSES 129
APPENDIX C – ONGOING WORKS 134
BIBLIOGRAPHY 136
VITA 142

LIST OF TABLES

1 The characteristic of minerals and cement used in the mixture..... 12

2 Biological additive design. ZEO: zeolite, PER: perlite, MET: metakaolin; B: mineral was saturated with bacterial cells and PBS, BN: half of mineral was saturated with bacterial cells and PBS and the other half of mineral was saturated with UCSL-CA 15

3 Mix design of prepared mortars and their flow rate. ZEO: zeolite, PER: perlite, MET: metakaolin; C: only includes minerals, B: mineral was saturated with bacterial cells and PBS, BN: half of mineral was saturated with bacterial cells and PBS and the other half of mineral was saturated with UCSL-CA..... 17

4 Crack closure rates %. ZEO: zeolite, PER: perlite, MET: metakaolin. C: only includes minerals, B: mineral was saturated with bacterial cells and PBS, BN: half of mineral was saturated with bacterial cells and PBS and the other half of mineral was saturated with UCSL-CA, UCSL-CA: nutrient medium curing, W: water curing, NC: at ambient conditions. 27

5 FTIR analysis results. ZEO: zeolite, C: only includes minerals, B: mineral was saturated with bacterial cells and PBS, BN: half of mineral was saturated with bacterial cells and PBS and the other half of mineral was saturated with UCSL-CA. 35

6 Crack closure rates %. BT: bentonite, DE: diatomaceous earth, SEP: sepiolite, ZEO: zeolite, PER: perlite, MET: metakaolin, PUM: pumice. C: only includes minerals, B: mineral was saturated with bacterial cells and PBS, BN: half of mineral was saturated with bacterial cells and PBS and the other half of mineral was saturated with UCSL-CA, UCSL-CA: nutrient medium curing, W: water curing, NC: at ambient conditions. 55

7 The variation at the compressive strength with respect to cement-based mortar without any mineral and bacteria. ZEO: zeolite, PER: perlite, DE: diatomaceous earth, BT: bentonite, PUM: pumice, MET: metakaolin, SEP: sepiolite, C: only includes minerals, B: mineral was saturated with bacterial cells and PBS, BN: half of mineral was saturated with bacterial cells and PBS and the other half of mineral was saturated with UCSL-CA..... 62

8 Assessment of corrosion by current measurement after crack healing. DE: diatomaceous earth, BT: bentonite, PUM: pumice, SEP: sepiolite, C: only includes minerals, BN: half of mineral was saturated with bacterial cells and PBS and the other half of mineral was saturated with UCSL-CA. 68
A.1 The crack width analysis of 14-day old samples cured with UCSL-CA nutrient medium. BT: bentonite, DE: diatomaceous earth, SEP: sepiolite, ZEO: zeolite, PER: perlite, MET: metakaolin, PUM: pumice. C: only includes minerals, B: mineral was saturated with bacterial cells and PBS, BN: half of mineral was saturated with bacterial cells and PBS and the other half of mineral was saturated with UCSL-CA. 125
A.2 The crack width analysis of 28-day old samples cured with UCSL-CA nutrient medium. BT: bentonite, DE: diatomaceous earth, SEP: sepiolite, ZEO: zeolite, PER: perlite, MET: metakaolin, PUM: pumice. C: only includes minerals, B: mineral was saturated with bacterial cells and PBS, BN: half of mineral was saturated with bacterial cells and PBS and the other half of mineral was saturated with UCSL-CA. 126
A.3 The crack width analysis of 14-day old samples cured with water. BT: bentonite, DE: diatomaceous earth, SEP: sepiolite, ZEO: zeolite, PER: perlite, MET: metakaolin, PUM: pumice. C: only includes minerals, B: mineral was saturated with bacterial cells and PBS, BN: half of mineral was saturated with bacterial cells and PBS and the other half of mineral was saturated with UCSL-CA. 127
A.4 The crack width analysis of 28-day old samples cured with water. BT: bentonite, DE: diatomaceous earth, SEP: sepiolite, ZEO: zeolite, PER: perlite, MET: metakaolin, PUM: pumice. C: only includes minerals, B: mineral was saturated with bacterial cells and PBS, BN: half of mineral was saturated with bacterial cells and PBS and the other half of mineral was saturated with UCSL-CA. 128

LIST OF FIGURES

1 Particle size distribution of OPC CEM I 42.5 R, zeolite (200µm) and metakaolin. 13

2 Sieve analysis of perlite and zeolite (1.6mm). 13

3 ESEM images of minerals (a) Zeolite (200 µm) (b) Metakaolin (c) Perlite. Scale 5µm. 14

4 ESEM images after the immobilization (a) Zeolite (200 µm) (b) Metakaolin (c) Perlite. Scale 5µm (left), 2µm (right). 16

5 Schematic presentation of casted mortar series. 19

6 Crack width evaluation (a) Image taken from the stereomicroscope (b) Image applied threshold filter. 20

7 Accelerated corrosion test set up. 25

8 The crack images of 28-day old ZEOC-200 samples (a, b, c) right after cracking, (d, e, f) after 7 days of water curing, (g, h, i) after 14 days of water curing, (j, k, l) after 21 days of water curing, (m, n, o) after 28 days of water curing. 27

9 The crack images of 28-day old ZEOB-200. (a, b, c) right after cracking, (d, e, f) after 7 days of UCSL-CA curing, (g, h, i) after 14 days of UCSL-CA curing, (j, k, l) after 21 days of UCSL-CA curing, (m, n, o) after 28 days of UCSL-CA curing. 30

10 The crack images of 28-day old ZEOBN-200 samples. (a, b, c) right after cracking, (d, e, f) after 7 days of UCSL-CA curing, (g, h, i) after 14 days of UCSL-CA curing, (j, k, l) after 21 days of UCSL-CA curing, (m, n, o) after 28 days of UCSL-CA curing. 31

11 Ultrasonic pulse velocity changes of samples containing zeolite 200µm, after 28 days curing. (a) cracked on day 14th (b) cracked on day 28th. ZEO: zeolite, C: only includes minerals, B: mineral was saturated with bacterial cells and PBS, BN: half of mineral was saturated with bacterial cells and PBS and the other half of mineral was saturated with UCSL-CA, C: UCSL-CA nutrient medium curing, W: water curing, NC: at ambient conditions, NCR: no crack. 33

12 120-hour water absorption capacities of samples containing zeolite 200µm, after 28 days curing. (a) cracked on day 14th (b) cracked on day 28th. ZEO: zeolite,

C: only includes minerals, B: mineral was saturated with bacterial cells and PBS, BN: half of mineral was saturated with bacterial cells and PBS and the other half of mineral was saturated with UCSL-CA, C: UCSL-CA nutrient medium curing, W: water curing, NC: at ambient conditions, NCR: no crack. 34
13 ESEM images of the crack surface obtained from specimens (a) 14-day ZEOB-200 cured with UCSL-CA (b) 28-day ZEOC-200 cured with water. Scale: 5µm. 36
14 The crack images of 14-day old ZEOC-1.6 samples. (a, b, c) right after cracking, (d, e, f) after 7 days of UCSL-CA curing, (g, h, i) after 14 days of UCSL-CA curing, (j, k, l) after 21 days of UCSL-CA curing, (m, n, o) after 28 days of UCSL-CA curing..... 38
15 The crack images of 14-day old ZEOB-1.6 samples. (a, b, c) right after cracking, (d, e, f) after 7 days of UCSL-CA curing, (g, h, i) after 14 days of UCSL-CA curing, (j, k, l) after 21 days of UCSL-CA curing, (m, n, o) after 28 days of UCSL-CA curing..... 39
16 The crack images of 14-day old ZEOBN-1.6 samples. (a, b, c) right after cracking, (d, e, f) after 7 days of water curing, (g, h, i) after 14 days of water curing, (j, k, l) after 21 days of water curing, (m, n, o) after 28 days of water curing 40
17 Ultrasonic pulse velocity changes of samples containing zeolite 1.6mm, after 28 days curing. (a) cracked on day 14th (b) cracked on day 28th. ZEO: zeolite, C: only includes minerals, B: mineral was saturated with bacterial cells and PBS, BN: half of mineral was saturated with bacterial cells and PBS and the other half of mineral was saturated with UCSL-CA, C: UCSL-CA nutrient medium curing, W: water curing, NC: at ambient conditions, NCR: no crack. 41
18 120-hour water absorption capacities of samples containing zeolite 1.6mm, after 28 days curing. (a) cracked on day 14th (b) cracked on day 28th. ZEO: zeolite, C: only includes minerals, B: mineral was saturated with bacterial cells and PBS, BN: half of mineral was saturated with bacterial cells and PBS and the other half of mineral was saturated with UCSL-CA, C: UCSL-CA nutrient medium curing, W: water curing, NC: at ambient conditions, NCR: no crack. 42

19 The crack images of 14-day old PERC samples (a, b, c) right after cracking, (d, e, f) after 7 days of UCSL-CA curing, (g, h, i) after 28 days of UCSL-CA curing. 44
20 The crack images of 14-day old PERB samples (a, b, c) right after cracking, (d, e, f) after 7 days of UCSL-CA curing, (g, h, I) after 14 days of UCSL-CA curing, (j, k, l) after 28 days of UCSL-CA curing. 45
21 The crack images of 14-day old PERBN (a, b, c) right after cracking, (d, e, f) after 7 days of UCSL-CA curing, (g, h, I) after 21 days of UCSL-CA curing, (j, k, l) after 28 days of UCSL-CA curing. 46
22 Ultrasonic pulse velocity changes of samples containing perlite, after 28 days curing. (a) cracked on day 14th (b) cracked on day 28th. PER: perlite, C: only includes minerals, B: mineral was saturated with bacterial cells and PBS, BN: half of mineral was saturated with bacterial cells and PBS and the other half of mineral was saturated with UCSL-CA, C: UCSL-CA nutrient medium curing, W: water curing, NC: at ambient conditions, NCR: no crack 47
23 120-hour water absorption capacities of samples containing perlite, after 28 days curing. (a) cracked on day 14th (b) cracked on day 28th. PER: perlite, C: only includes minerals, B: mineral was saturated with bacterial cells and PBS, BN: half of mineral was saturated with bacterial cells and PBS and the other half of mineral was saturated with UCSL-CA, C: UCSL-CA nutrient medium curing, W: water curing, NC: at ambient conditions, NCR: no crack. 48
24 The crack images of 14-day old METC samples. (a, b, c) right after cracking, (d, e, f) after 7 days of water curing, (g, h, i) after 21 days of water curing, (j, k, l) after 28 days of water curing. 49
25 The crack images of 28-day old METB samples. (a, b, c) right after cracking, (d, e, f) after 7 days of UCSL-CA curing, (g, h, i) after 14 days of UCSL-CA curing, (j, k, l) after 21 days of UCSL-CA curing (m, n, o) after 28 days of UCSL-CA curing. 51
26 The crack images of 14-day old METBN samples. (a, b, c) right after cracking, (d, e, f) after 7 days of UCSL-CA curing, (g, h, i) after 14 days of UCSL-CA curing, (j, k, l) after 28 days of UCSL-CA curing. 52

27 Ultrasonic pulse velocity changes of samples containing metakaolin, after 28 days curing. (a) cracked on day 14th (b) cracked on day 28th. MET: metakaolin, C: only includes minerals, B: mineral was saturated with bacterial cells and PBS, BN: half of mineral was saturated with bacterial cells and PBS and the other half of mineral was saturated with UCSL-CA, C: UCSL-CA nutrient medium curing, W: water curing, NC: at ambient conditions, NCR: no crack 53
28 120-hour water absorption capacities of samples containing metakaolin, after 28 days curing. (a) cracked on day 14th (b) cracked on day 28th. MET: metakaolin, C: only includes minerals, B: mineral was saturated with bacterial cells and PBS, BN: half of mineral was saturated with bacterial cells and PBS and the other half of mineral was saturated with UCSL-CA, C: UCSL-CA nutrient medium curing, W: water curing, NC: at ambient conditions, NCR: no crack 55
29 Vicat Needle test results. ZEO: zeolite, PER: perlite, DE: diatomaceous earth, BT: bentonite, PUM: pumice, MET: metakaolin, SEP: sepiolite, C: only includes minerals, B: mineral was saturated with bacterial cells and PBS, BN: half of mineral was saturated with bacterial cells and PBS and the other half of mineral was saturated with UCSL-CA..... 57
30 Compressive Strength test result. [68] (a) C series samples (b) B series samples (c) BN series samples. ZEO: zeolite, PER: perlite, DE: diatomaceous earth, BT: bentonite, PUM: pumice, MET: metakaolin, SEP: sepiolite, C: only includes minerals, B: mineral was saturated with bacterial cells and PBS, BN: half of mineral was saturated with bacterial cells and PBS and the other half of mineral was saturated with UCSL-CA..... 60
31 Free shrinkage by time. (a) C series (b) BN series. DE: diatomaceous earth, BT: bentonite, PUM: pumice, SEP: sepiolite, C: only includes minerals, BN: half of mineral was saturated with bacterial cells and PBS and the other half of mineral was saturated with UCSL-CA..... 65
32 The change of length after 112 days. DE: diatomaceous earth, BT: bentonite, PUM: pumice, SEP: sepiolite, C: only includes minerals, BN: half of mineral was saturated with bacterial cells and PBS and the other half of mineral was saturated with UCSL-CA. 65

33 Weight loss by time. (a) C series (b) BN series. DE: diatomaceous earth, BT: bentonite, PUM: pumice, SEP: sepiolite, C: only includes minerals, BN: half of mineral was saturated with bacterial cells and PBS and the other half of mineral was saturated with UCSL-CA. 67
34 The change of weight after 112 days. DE: diatomaceous earth, BT: bentonite, PUM: pumice, SEP: sepiolite, C: only includes minerals, BN: half of mineral was saturated with bacterial cells and PBS and the other half of mineral was saturated with UCSL-CA. 67
35 The tensile strength results after accelerated corrosion test. DE: diatomaceous earth, BT: bentonite, PUM: pumice, SEP: sepiolite, C: only includes minerals, BN: half of mineral was saturated with bacterial cells and PBS and the other half of mineral was saturated with UCSL-CA. 69
36 Conditions of rebars after the accelerated corrosion test 70
A.1 The crack images of 14- day old ZEOC-200 samples. (a, b, c) right after cracking, (d, e, f) after 7 days of UCSL-CA curing, (g, h, i) after 14 days of UCSL-CA curing, (j, k, l) after 21 days of UCSL-CA curing, (m, n, o) after 28 days of UCSL-CA curing. 75
A.2 The crack images of 14-day old ZEOC-200. (a, b, c) right after cracking, (d, e, f) after 7 days of water curing, (g, h) after 21 days of water curing, (i, j) after 28 days of water curing. (Due to crack sealing, the measurement point couldn't be found therefore some of images were missing.) 76
A.3 The crack images of 14-day old ZEOC-200 samples. (a, b, c) right after cracking, (d, e, f) after 7 days, (g, h, i) after 14 days, (j, k, l) after 21 days, (m, n) after 28 days. 77
A.4 The crack images of 28-day old ZEOC-200. (a, b, c) right after cracking, (d, e, f) after 7 days of UCSL-CA curing, (g, h, i) after 14 days of UCSL-CA curing, (j, k, l) after 21 days of UCSL-CA curing, (m, n, o) after 28 days of UCSL-CA curing. 78
A.5 The crack images of 28-day old ZEOC-200 samples kept at ambient conditions. (a, b, c) right after cracking, (d, e, f) after 7, (g, h, i) after 14 days, (j, k, l) after 21 days, (m, n, o) after 28 days. 79

A.6The crack images of 14-day old ZEOB-200. (a, b, c) right after cracking, (d, e, f) after 7 days of UCSL-CA curing, (g, h, i) after 14 days of UCSL-CA curing, (j, k, l) after 21 days of UCSL-CA curing, (m, n, o) after 28 days of UCSL-CA curing. 80
A.7The crack images of 14-day old ZEOB-200 samples. (a, b, c) right after cracking, (d, e, f) after 7 days of water curing, (g, h, i) after 14 days of water curing, (j, k, l) after 21 days of water curing, (m, n, o) after 28 days of water curing. 81
A.8The crack images of 14-day old ZEOB-200 samples kept at ambient conditions. (a, b, c) right after cracking, (d, e, f) after 7 days, (g, h, i) after 14 days, (j, k, l) after 21 days, (m, n, o) after 28 days. 82
A.9The crack images of 28-day old ZEOB-200. (a, b, c) right after cracking, (d, e, f) after 7 days of water curing, (g, h, i) after 14 days of water curing, (j, k, l) after 21 days of water curing, (m, n, o) after 28 days of water curing. 83
A.10The crack images of 28-day old ZEOB-200 samples kept at ambient conditions. (a, b, c) right after cracking, (d, e, f) after 7 days, (g, h, i) after 14 days, (j, k, l) after 21 days, (m, n, o) after 28 days. 84
A.11The crack images of 14-day old ZEOBN-200 samples. (a, b, c) right after cracking, (d, e, f) after 7 days of UCSL-CA curing, (g, h, i) after 14 days of UCSL-CA curing, (j, k, l) after 21 days of UCSL-CA curing, (m, n, o) after 28 days of UCSL-CA curing. 85
A.12The crack images of 14-day old ZEOBN-200. (a, b, c) right after cracking, (d, e, f) after 7 days of water curing, (g, h, i) after 14 days of water curing, (j, k, l) after 21 days of water curing, (m, n, o) after 28 days of water curing. 86
A.13The crack images of 14-day old ZEOBN-200 samples kept at ambient conditions. (a, b, c) right after cracking, (d, e, f) after 7 days, (g, h, i) after 14 days, (j, k, l) after 21 days, (m, n, o) after 28 days. 87
A.14The crack images of 28-day old ZEOBN-200 samples. (a, b, c) right after cracking, (d, e, f) after 7 days of water curing, (g, h, i) after 14 days of water curing, (j, k, l) after 21 days of water curing, (m, n, o) after 28 days of water curing. 88

A.15The crack images of 28-day old ZEOBN-200 samples kept at ambient conditions. (a, b, c) right after cracking, (d, e, f) after 7 days, (g, h, i) after 14 days, (j, k, l) after 28 days. 89
A.16The crack images of 14-day old ZEOC-1.6 samples. (a, b, c) right after cracking, (d, e, f) after 7 days of water curing, (g, h, i) after 14 days of water curing, (j, k, l) after 21 days of water curing, (m, n, o) after 28 days of water curing. 90
A.17The crack images of 14-day old ZEOC-1.6 samples kept at ambient conditions. (a, b, c) right after cracking, (d, e, f) after 7 days, (g, h, i) after 14 days, (j, k, l) after 21 days, (m, n, o) after 28 days. 91
A.18The crack images of 28-day old ZEOC-1.6 samples. (a, b, c) right after cracking, (d, e, f) after 7 days of UCSL-CA curing, (g, h, i) after 14 days of UCSL-CA curing, (j, k, l) after 21 days of UCSL-CA curing, (m, n, o) after 28 days of UCSL-CA curing..... 92
A.19The crack images of 28-day old ZEOC-1.6 samples. (a, b, c) right after cracking, (d, e, f) after 7 days of water curing, (g, h, i) after 14 days of water curing, (j, k, l) after 21 days of water curing, (m, n, o) after 28 days of water curing. 93
A.20The crack images of 28-day old ZEOC-1.6 samples kept at ambient conditions. (a, b, c) right after cracking, (d, e, f) after 7 days, (g, h, i) after 14 days, (j, k, l) after 21 days, (m, n, o) after 28 days. 94
A.21The crack images of 14-day old ZEOB-1.6 samples. (a, b, c) right after cracking, (d, e, f) after 7 days of water curing, (g, h, i) after 14 days of water curing, (j, k, l) after 21 days of water curing, (m, n, o) after 28 days of water curing. 95
A.22The crack images of 14-day old ZEOB-1.6 kept at ambient conditions. (a, b, c) right after cracking, (d, e, f) after 7 days, (g, h, i) after 14 days, (j, k, l) after 21 days, (m, n, o) after 28 days..... 96
A.23The crack images of 28-day old ZEOB-1.6 samples. (a, b, c) right after cracking, (d, e, f) after 7 days of UCSL-CA curing, (g, h, i) after 14 days of UCSL-CA curing, (j, k, l) after 21 days of UCSL-CA curing, (m, n, o) after 28 days of UCSL-CA curing..... 97
A.24The crack images of 28-day old ZEOB-1.6 samples. (a, b, c) right after cracking, (d, e, f) after 7 days of water curing, (g, h, i) after 14 days of water curing, (j, k, l) after 21 days of water curing, (m, n, o) after 28 days of water curing. 98

A.25The crack images of 28-day old ZEOB-1.6 samples kept at ambient conditions. (a, b, c) right after cracking, (d, e, f) after 7 days, (g, h, i) after 14 days, (j, k, l) after 21 days, (m, n, o) after 28 days. 99
A.26The crack images of 14-day old ZEOBN-1.6 samples. (a, b, c) right after cracking, (d, e, f) after 7 days of UCSL-CA curing, (g, h, i) after 14 days of UCSL-CA curing, (j, k, l) after 21 days of UCSL-CA curing, (m, n, o) after 28 days of UCSL-CA curing. 100
A.27The crack images of 14-day old ZEOBN-1.6 samples kept at ambient conditions. (a, b, c) right after cracking, (d, e, f) after 7 days, (g, h, i) after 14 days, (j, k, l) after 21 days, (m, n, o) after 28 days. 101
A.28The crack images of 28-day old ZEOBN-1.6 samples. (a, b, c) right after cracking, (d, e, f) after 7 days of UCSL-CA curing, (g, h, i) after 14 days of UCSL-CA curing, (j, k, l) after 21 days of UCSL-CA curing, (m, n, o) after 28 days of UCSL-CA curing. 102
A.29The crack images of 28-day old ZEOBN-1.6 samples. (a, b, c) right after cracking, (d, e, f) after 7 days of water curing, (g, h, i) after 14 days of water curing, (j, k, l) after 21 days of water curing, (m, n, o) after 28 days of water curing. 103
A.30The crack images of 28-day old ZEOBN-1.6 samples kept at ambient conditions. (a, b, c) right after cracking, (d, e, f) after 7 days, (g, h, i) after 14 days, (j, k, l) after 28 days 104
A.31The crack images of 14-day old PERC samples. (a, b, c) right after cracking, (d, e, f) after 7 days of water curing, (g, h, i) after 28 days of water curing. 105
A.32The crack images of 14-day old PERC samples kept at ambient conditions. (a, b, c) right after cracking, (d, e, f) after 7 days, (g, h, i) after 14 days, (j, k, l) after 28 days. 105
A.33The crack images of 28-day old PERC samples. (a, b, c) right after cracking, (d, e, f) after 7 days of UCSL-CA curing, (g, h, i) after 14 days of UCSL-CA curing. (j, k, l) after 28 days of UCSL-CA curing. 106
A.34The crack images of 28-day old PERC samples. (a, b, c) right after cracking, (d, e, f) after 7 days of water curing, (g, h, i) after 21 days of water curing. (j, k, l) after 28 days of water curing. 107

A.35The crack images of 28-day old PERC samples kept at ambient conditions. (a, b, c) right after cracking, (d, e, f) after 28 days. 107
A.36The crack images of 14-day old PERB samples. (a, b, c) right after cracking, (d, e, f) after 7 days of water curing, (g, h, i) after 14 days of water curing. (j, k, l) after 28 days of water curing. 108
A.37The crack images of 14-day old PERB samples kept at ambient conditions. (a, b, c) right after cracking, (d, e, f) after 28 days. 108
A.38T he crack images of 28-day old PERB samples. (a, b, c) right after cracking, (d, e, f) after 7 days of UCSL-CA curing, (g, h, i) after 14 days of UCSL-CA curing. (j, k, l) after 28 days of UCSL-CA curing. 109
A.39The crack images of 28-day old PERB samples. (a, b, c) right after cracking, (d, e, f) after 7 days of water curing, (g, h, i) after 14 days of water curing. (j, k, l) after 28 days of water curing. 110
A.40The crack images of 28-day old PERB samples kept at ambient conditions. (a, b, c) right after cracking, (d, e, f) after 28 days. 110
A.41The crack images of 14-day old PERBN samples. (a, b, c) right after cracking, (d, e, f) after 7 days of water curing, (g, h, i) after 21 days of water curing. (j, k, l) after 28 days of water curing. 111
A.42The crack images of 14-day old PERBN samples kept at ambient conditions. (a, b, c) right after cracking, (d, e, f) after 7 days, (g, h, i) after 14 days, (j, k, l) after 28 days. 112
A.43The crack images of 28-day old PERBN samples. (a, b, c) right after cracking, (d, e, f) after 7 days of UCSL-CA curing, (g, h, i) after 21 days of UCSL-CA curing, (j, k, l) after 28 days of UCSL-CA curing. 112
A.44The crack images of 28-day old PERBN samples. (a, b, c) right after cracking, (d, e, f) after 7 days of water curing, (g, h, i) after 14 days of water curing, (j, k, l) after 21 days of water curing, (m, n) after 28 days of water curing. 113
A.45The crack images of 28-day old PERBN samples kept at ambient conditions. (a, b, c) right after cracking, (d, e, f) after 28 days. 114
A.46The crack images of 14-day old METC samples. (a, b, c) right after cracking, (d, e, f) after 14 days of UCSL-CA curing, (g, h, i) after 21 days of UCSL-CA curing, (j, k, l) after 28 days of UCSL-CA curing. 115

A.47The crack images of 14-day old METC samples kept at ambient conditions. (a, b, c) right after cracking, (d, e, f) after 28 days. 115
A.48The crack images of 28-day old METC samples. (a, b, c) right after cracking, (d, e, f) after 21 days of UCSL-CA curing, (g, h, i) after 28 days of UCSL-CA curing. 116
A.49The crack images of 28-day old METC samples. (a, b, c) right after cracking, (d, e, f) after 14 days of water curing, (g, h, i) after 28 days of water curing.. 116
A.50The crack images of 28-day old METC samples kept at ambient conditions. (a, b, c) right after cracking, (d, e, f) after 28 days. 117
A.51The crack images of 14-day old METB samples. (a, b, c) right after cracking, (d, e, f) after 21 days of UCSL-CA curing, (g, h, i) after 28 days of UCSL-CA curing. 117
A.52The crack images of 14-day old METB samples. (a, b, c) right after cracking, (d, e, f) after 14 days of water curing, (g, h, i) after 28 days of water curing.. 118
A.53The crack images of 14-day old METB samples kept at ambient conditions. (a, b, c) right after cracking, (d, e, f) after 28 days. 118
A.54The crack images of 28-day old METB samples. (a, b, c) right after cracking, (d, e, f) after 7 days of water curing, (g, h, i) after 14 days water curing, (j, k, l) after 21 days of water curing (m, n, o) after 28 days of water curing. 119
A.55The crack images of 28-day old METB samples kept at ambient conditions. (a, b, c) right after cracking, (d, e, f) after 28 days. 120
A.56The crack images of 14-day old METBN samples. (a, b, c) right after cracking, (d, e, f) after 7 days of water curing, (g, h, i) after 14 days of water curing, (j, k, l) 28 days of water curing. 121
A.57The crack images of 14-day old METBN samples kept at ambient conditions. (a, b, c) right after cracking, (d, e, f) after 7 days, (g, h, i) after 28 days..... 121
A.58The crack images of 28-day old METBN samples. (a, b, c) right after cracking, (d, e, f) after 7 days of UCSL-CA curing, (g, h, i) after 14 days of UCSL-CA curing, (j, k, l) after 21 days of UCSL-CA curing (m, n, o) after 28 days of UCSL-CA curing..... 122

A.59 The crack images of 28-day old METBN samples. (a, b, c) right after cracking, (d, e, f) after 7 days of water curing, (g, h, i) after 14 days of water curing, (j, k, l) after 21 days of water curing (m, n, o) after 28 days of water curing. 123
A.60 The crack images of 28-day old METBN samples kept at ambient conditions. (a, b, c) right after cracking, (d, e, f) after 7 days, (g, h, i) after 28 days..... 124
B.1 FTIR spectra of 28-day old samples cured with UCSL-CA nutrient medium. (a) DEB (b) DEBN (c) BTB (d) BTBN (e) SEPB (f) SEPBN (g) PUMB (h) PUMBN 131
B.2 FTIR spectra of ZEO-200 samples. (a) Zeolite-200μm (b) ZEOC-200-14D-NC (c) ZEOC-200-28D-W (d) ZEOC-200-28D-C (e) ZEB-200-14D-W (f) ZEOB-200-14D-C (g) ZEOB-200-28D-W (h) ZEOB-200-28D-C (i) ZEOBN-200-14D-W..... 133
C.1 The designed restrained shrinkage system to obtain micro cracks. 134
C.2 First trial of restrained shrinkage (a) control sample (b) BTBN sample (c) the initial crack was observed in BTBN sample after 15 days without any curing. 134
C.3 The reinforced cement-based mortars for corrosion test. 135

CHAPTER I

INTRODUCTION

Concrete is still the most popular construction material due to its high performance, and cost efficiency [1]. While the cement and concrete industry plays an important role in the European economy, their production process is a major contributor to global warming and responsible for 8% of the global CO_2 emissions [1], [2]. With the recent Paris Agreement, the cement and concrete industry must develop more sustainable strategies to decrease CO_2 emissions to reach the goals of governments to keep global warming below 2˚C [3], [4]. A solution to decrease the negative environmental impact of the concrete and cement industry propounded by the International Energy Authority is capture and store/utilize CO_2 (CCS/CCU). However, the implementation of CCS/CCU technologies requires a massive investment at this stage because of high volume cement production [1]. To date, it is evident that eliminating cement from structural concrete is not feasible, thus it might be more efficient to extend the service life of structures which will decrease the demand to cement production and lessen the economic burden on the cement industry to implement breakthrough technologies.

Extending the service life of concrete structures could be achieved by limiting the crack formation and decreasing the permeability of the material. Due to its brittle nature, low tensile strength, and shrinkage, cracking is inevitable in concrete and these cracks reduce the durability, and the life span of concrete structures decreases [5]. Microcracks can lead to durability problems as carbonation, corrosion, sulphate attack etc. due to increasing permeability of the concrete. Traditional repair methods could not be effective

procedure to remediate microcracks under the consideration of scale of construction and accessibility to damaged zone [6]. Moreover, traditional repair methods are not environmentally friendly due to epoxy-, acrylic-, or cement-based content. Therefore, self-healing mechanism in concrete could be sustainable and economical approach to remediate microcracks.

Self-healing concrete could be defined as the capability of concrete to seal micro cracks naturally without any external influence [5]. The autogenous self-healing is a crack remediation mechanism due to the latent hydration in cement paste matrix. Autogenous self-healing can be explained as the hydration of un-hydrated particles with the ingress of water from cracks in mature concrete and consequently, sealing of cracks by the formation of calcium silicate hydrate gels (CSH) and calcium carbonate (CaCO3). There is an extensive amount of research conducted to increase the self-healing ability of concrete. Integrating supplementary cementitious materials (fly ash, silica fume, blast-furnace slag), calcined clays, natural minerals, superabsorbent polymers, crystalline, and microfibers into the cement matrix enhances the efficiency of the autogenous self-healing ability of the concrete [7]–[11]. Nevertheless, the crack width sealed by autogenous self-healing mechanism is limited (<300 μm) and depends on the presence of water and the composition of the cement matrix [7]. Therefore, various autonomous self-healing systems have been improved to increase the self-healing capacity of the cementitious materials.

Autonomous healing methodology is based on non-traditional engineering applications embedded the cementitious systems instead of un-hydrated cement particles [5]. Autonomous self-healing systems are based on encapsulation of healing agent (urea-formaldehyde or epoxy-based microcapsules, lightweight aggregates impregnated with

sodium silicate, immobilization of microorganisms, oil core/silica gel shell microcapsules including methylmeth-acrylate) or vascular systems (tubular capsules, polymethylmethacrylate, glass, ceramic or starch based tubes filled with healing agent, super elastic shape memory alloy wires including adhesives) [7], [12]–[20]. It was proven that cracks widths up to 1 mm can be healed and the impermeability of cement-based materials increases by autonomous self-healing mechanism [5], [21].

Throughout the literature, there were series of studies suggesting that so-called autonomous self-healing of microcracks could be obtained by incorporation of microorganisms to the mix and led to a decrease in water permeability. Relatedly, these microorganisms could survive when they were incorporated within mortar (or concrete) mix via various methods. These approaches generally include encapsulation of the bacteria in organic or synthetic protections barriers before incorporating in concrete. However, these methods generally require additional processing and labor, which mainly increases the cost of the application. Moreover, some of these encapsulation methods led to a decrease in both workability and strength. Another approach can be integrating the microorganisms without any extra intervention [22], [23]. With this approach, flexural cracks in 7-day old samples were sealed by biogenic CaCO3 and water absorption capacity of the samples was reduced upon healing [23]. However, it would be hard to incorporate the cells with their growth medium in practice. Thus, it is crucial to develop a simpler, economically feasible and sustainable protection system to improve the robustness of the bacterial cells against the restrictive environment. While most of the studies in the literature focused on reducing the permeability, it is still not known if the crack healing through biomineralization actually improves the durability of the material. In such a case, it is important to determine the influence of self-healing sealant on

corrosion. Throughout the literature, there is a limited number of studies focused on impact of nutrient medium and bacterial cells on corrosion. However, it is much more crucial to protect the rebar after the cracks were sealed. And yet, there is not any information about the effects of bacterial cells and self-healing on drying shrinkage.

Goal and Objectives

The main goal of this study is to develop a biological additive to remediate microcracks in the cementitious systems by biomineralization. To achieve this goal, the bacteria cells were immobilized on zeolite, metakaolin and perlite. These minerals were selected due to usage of natural resources criteria of sustainable development [24]. Self-healing ability of designed biological additive was evaluated through stereomicroscope, ultrasonic pulse velocity (UPV), water absorption test and scanning electron microscopy (SEM). At last, the viability of bacterial cells was correlated with the efficiency of crack healing for different immobilization barriers. Accelerated corrosion and drying shrinkage tests were applied to bio-based cement-based mortars including different type of natural minerals or light weight aggregates pursuant to the crack healing abilities. At last, the effects of the biological additive on the performance of designed mortar were evaluated.

The specific objectives of the study are as follows:

1. Characterization of suitable natural minerals (zeolite, metakaolin and perlite),
2. Development the biological additive by immobilizing the cells on natural minerals,
3. Evaluating the effects of biological additives on performance (initial setting and compressive strength),

4. Establishing a qualitative analysis for crack healing through visual inspection, water absorption and UPV,

5. Identifying the chemistry of precipitates within the crack surface,

6. Assessing the influence of crack healing on corrosion resistance,

7. Evaluating the effects of biological additive on drying shrinkage.

CHAPTER II

LITERATURE REVIEW

Microbial induced calcite precipitation (MICP) is a promising autonomous self-healing process that microorganisms trigger the formation of calcium carbonate ($CaCO_3$) and remediate microcracks into the cementitious materials [25]. The key factors affecting calcium carbonate ($CaCO_3$) precipitation could be stated as (1) the calcium concentration, (2) the concentration of dissolved inorganic carbon (DIC), (3) the pH in environment and (4) the presence of nucleation site provided by the surface of bacteria cell [17].

The ureolytic bacteria cultures are the most common self-healing agents used to trigger MICP in cement-based materials due to their enzymatic activity (urease). The ureolytic bacteria culture can produce carbonate and ammonium ions (NH4+) by using urea as an energy source [26]. The produced ammonia (NH4+) increases the pH in environment and results in CaCO3 precipitation towards calcium source (Ca+) [27], [28]. The reactions of urea hydrolysis are given in Equations (1-4) [29]:

$$CO(NH_2)_2 + H_2O \rightarrow H_2COOH + NH_3 \quad (1)$$

$$NH_2COOH + H_2O \rightarrow NH_3 + H_2CO_3 \quad (2)$$

$$2NH_3 + 2H_2O \leftrightarrow 2{NH_4}^+ + 2OH^- \quad (3)$$

$$2OH^- + H_2CO_3 \leftrightarrow {CO_3}^{2-} + 2H_2O \quad (4)$$

The hydrolysis of urea can be summarized as following reaction [29]:

$$CO(NH_2)_2 + 2H_2O \leftrightarrow 2NH_4{}^+ + CO_3{}^{2-}$$

After the negative charge of the bacteria surface, bacteria attract cations containing Ca^{2+} from surroundings and holds on its cell surface. Thereafter, the Ca^{2+} ions react with the CO_3 ions and calcium carbonate ($CaCO_3$) precipitation is formed as follows [17]:

$$CaCO_3 \leftrightarrow Ca^{2+} + CO_3{}^{2-}$$

The main facts considered to incorporate microorganisms into the cementitious system are that bacteria cells stay viable (1) at the high alkaline conditions of the cement paste (pH=12-13) (2) the concrete mixing process, and (3) the lack of nutrients [30]. Bacillus genus *(Bacillus pasteurii* (*Sporosarcina pasteurii), bacillus alkalinitrilicus, bacillus pseudofirmus, bacillus cohnii, bacillus sphaericus etc.)* are the most frequently used bacteria cultures as a self-healing agent due to alkaline resistant [27], [31]–[35].

The study conducted by Jonkers et. al. showed that the bacteria cells *(b. pseudofirmus, and b. cohnii)* stayed viable for 4 months when they were inoculated in the cement matrix directly [32]. On the other hand, the addition of a high quantity of bacteria spores induced decrease in 3-, 7-, 28- day old compressive strengths less than 10%.

Bundur et. al. incorporated *s. pasteurii* cells into the cement mortar to evaluate the impact of bacteria on the strength and porosity of mortar [30]. Bacteria cells were found to be viable up to 330 days. The study showed that the bacteria addition decreased the porosity of mortar and enhance the compressive strength in comparation with control samples.

Other study showed that *s. pasteurii* cells remained viable up to 11 months when they were inoculated to the cement-based mixture [23]. The bacteria cells and nutrient medium were incorporated into the cement-based mortar by replacing the water of mixture. According to visual inspection and water absorption test results, this methodology was found to be effective in healing 0.30-0.35 mm cracks in 7-day old samples and reduction in water absorption of samples. However, decrease in the amount of $CaCO_3$ was detected through the crack depth due to the limited viability and lack of O_2.

The main issues of inoculation bacteria cells into the cement-based materials are the viability of microorganism and consequently decreasing calcite precipitation in the long term [32]. Thus, cell immobilization or encapsulation methodologies have been developed by using a protective barrier (polyurethane (PU), lightweight aggregates, nanomaterials, natural minerals, hydrogels) in the repairment of microcracks to extend the viability of bacteria cells [33], [35]–[40].

In a study, *b. sphaericus* immobilized on melamine-based microcapsules were inoculated in the cement-based mortar [14]. In addition, microcapsules including calcium and urea source were also added into the mixture. Self-healing ability was investigated through crack healing ratio and water absorption of mortar specimen. According to microscopic analysis, the samples including bacteria-based microcapsules showed higher crack closure than control samples. The maximum remediated crack width was detected as 970 μm. Moreover, partial crack closure was observed in samples without bacteria due to the autogenous healing. The water absorption capacities of samples with bacteria were lower than control series samples. On the other hand, the addition of microcapsules reduced the compressive strength of cement mortar.

In other study, expanded perlite was used as a protective carrier for *b. cohnii* [38]. Bacteria cells were immobilized on expanded perlite particles under vacuum pressure and then a solution including calcium lactate and yeast extract were sprayed on the particles. Lastly, metakaolin and sodium silicate-based coating was applied on the particles. At the end of 28 days of water curing, the complete healing was observed in 0.79 mm crack. Jiang et. al. prepared concrete samples including a sugar-coated expanded perlite as a protective barrier for *b. cohnii* [41]. The visual analysis and the water permeability test were done to evaluate the self-healing ability of concrete samples cured with water for 28 days. According to results, it was observed that 1.24 mm crack was healed completely and in addition the water permeability of samples decreased.

Tezer developed a biological self-healing cement-based mortar by immobilizing *sporosarcina pasteurii* cells on natural minerals or lightweight aggregate (LWA) as diatomaceous earth, bentonite, sepiolite, and pumice [42]. The biological additive was prepared by saturating half of mineral with bacteria cells and other half with nutrient. The self-healing ability was evaluated by stereomicroscope analysis, ultrasonic pulse velocity and water absorption capacity. According to conducted analyses to evaluate self-healing system, it was seen that the bacteria cells were immobilized on diatomaceous earth, bentonite, sepiolite, and pumice. The full crack (0.3-0.4 mm) closure regardless of mineral type was observed in samples cured with nutrient medium before 28 days. However, the influence of biological additive on the performance and drying shrinkage of cement-based mortar was not investigated. Moreover, effects of crack sealing on corrosion resistance are unknown.

In this study, zeolite, metakaolin and perlite were used as a protective barrier to develop a biological additive. Moreover, the impact of biological additive on the performance and drying shrinkage of the cementitious system was evaluated.

CHAPTER III

MATERIALS AND METHODOLOGY

3.1 Microorganism selection and growth

Sporosarcina pasteurii (S. pasteurii) from Leibniz institute – German collection of microorganisms and cell cultures (DSMZ 33) was selected as a self-healing agent in cement-based materials. This strain was selected based on the findings obtained from previous studies which showed that incorporating *S. pasteurii* cells could remediate 0.3-0.35 mm microcracks when they were incorporated to the mortar without any encapsulation [23]. The cells were aerobically incubated (IKA KS 4000) in sterilized nutrient medium at pH=9 (UCSLS) which included 0.13 M tris base, 20 g/L urea, 10 g/L corn steep liqueur (CSL) and 10 g/L sodium acetate per liter of distilled (DI) water. The nutrient medium was sterilized at 121 ˚ C for 45 minutes (NUVE NC 40M, Istanbul, Turkey). The cells were grown in sterilized nutrient medium with shaking conditions (175 rpm) at 30˚ C until the stationary phase obtained (10^9 CFU/mL) [42]. After the incubation, the cells were collected from the culture by centrifuging at 8,000 g for 10 minutes. The cells were washed twice by PBS (Phosphate Buffer Solution, pH=9). The collected *S. pasteurii* cells were stored at 4˚C until the immobilization procedure.

3.2 Material selection

Mortar samples were prepared with Ordinary Portland Cement (OPC) CEM I 42.5 R and *S. pasteurii* cells were immobilized on zeolite (200µm and 1.6mm), metakaolin (< 1 of 00 µm) and perlite (2 mm). Bio-based additive was obtained by submerging the minerals to aqueous solution, either PBS or UCSL-CA medium for 24-h. The absorption capacity was defined in terms of *24-hours absorption capacity* for each protection mineral. This was determined by submerging the oven-dried minerals and aggregates in water for 24 hours and calculating the total absorbed water within the specified time frame. The 24-h absorption capacities of the minerals and aggregates are summarized in Table 1.

Table 1: The characteristic of minerals and cement used in the mixture

Sample	Particle Size Range	Water Absorption Capacity
Cement	5-70 µm	-
Zeolite-200 µm	<200 µm	25%
Zeolite-1.6mm	0.7-1.6 mm	25%
Perlite	0-2 mm	9%
Metakaolin	<45 µm	11%

Particle size distributions of fine minerals were determined by a Mastersizer 200 particle analyzer with a Hydro MU 2000 (Malvern, Worcestershire, United Kingdom) wet dispersion unit. The cement particles were dispersed in ethanol to prevent further hydration of the cement particles. Figure 1 demonstrates the particle size distribution of OPC CEM I 42.5 R and the minerals (<200 µm) used for immobilization. The particle size distribution of zeolite (1.6mm) and perlite (2mm) was determined by sieve analysis regarding to ASTM C136 Standard Test Method for Sieve Analysis of Fine and Coarse

Aggregates [43]. The sieve analyses of perlite (2mm) and zeolite (1.6mm) are shown in Figure 2.

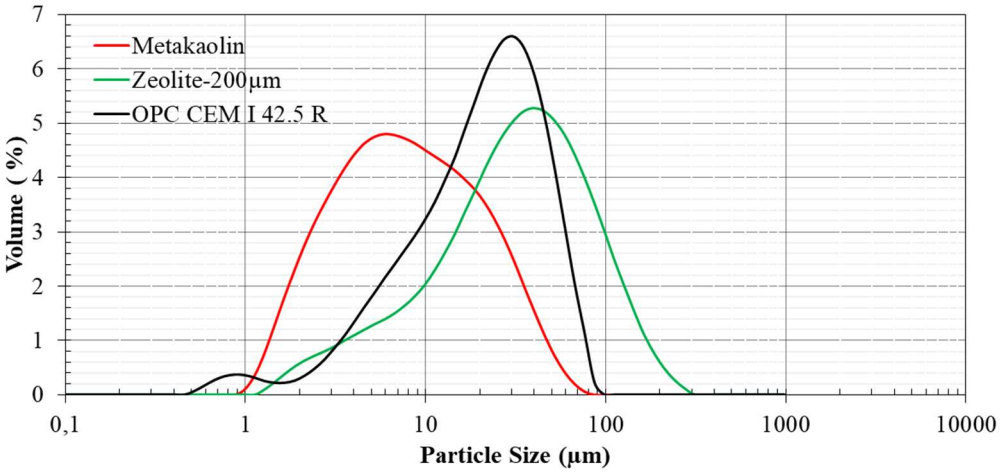

Figure 1: Particle size distribution of OPC CEM I 42.5 R, zeolite (200µm) and metakaolin.

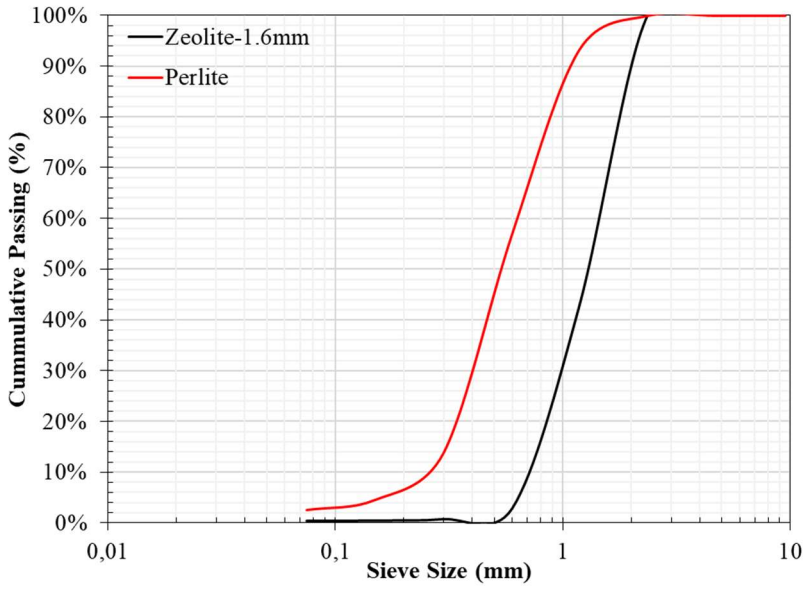

Figure 2: Sieve analysis of perlite and zeolite (1.6mm).

Moreover, ESEM (FEI-Philips XL30 Environmental Scanning Electron Microscope with Field Emission Gun) analysis was conducted to examine microstructure of minerals. Figure 3 shows ESEM images of minerals.

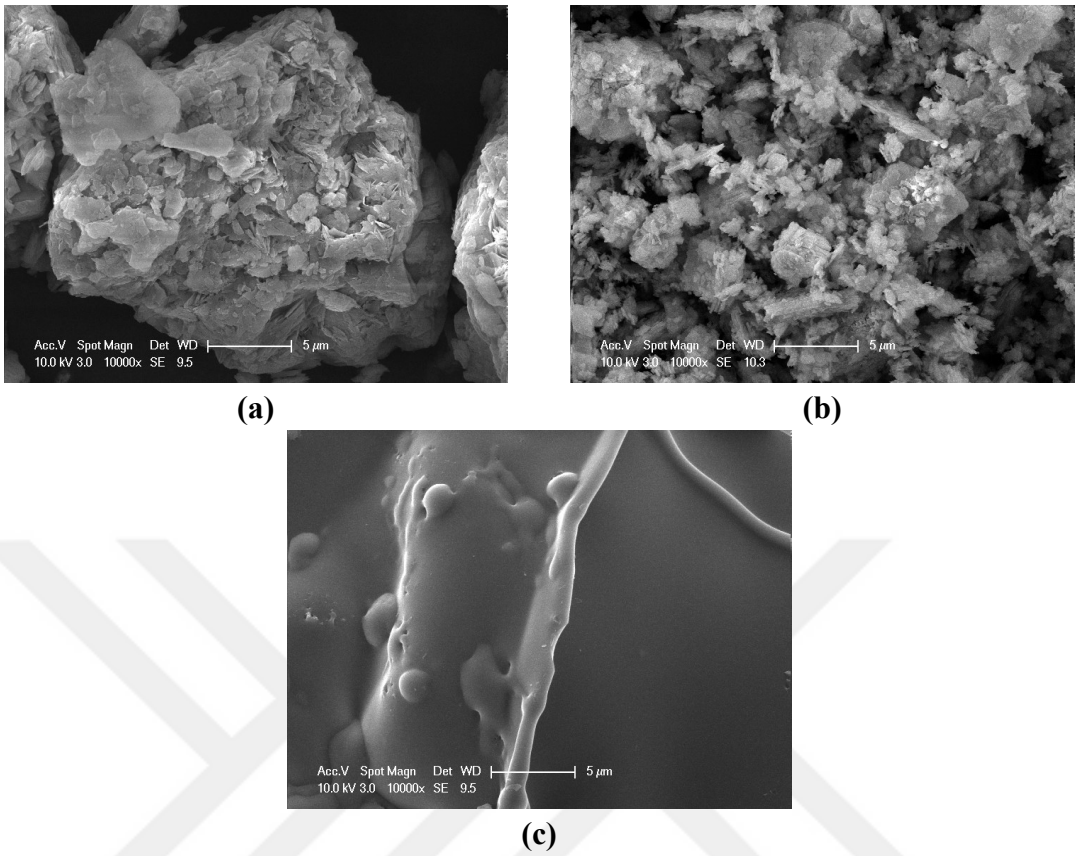

Figure 3: ESEM images of minerals (a) Zeolite (200 μm) (b) Metakaolin (c) Perlite. Scale 5μm.

3.3 Immobilization procedure

To develop a biological additive, the vegetative bacteria cells were immobilized on the minerals by two different procedures; B series that mineral was saturated with bacteria cells and PBS, and BN series that half of mineral was saturated with bacteria cells and PBS, and the other half of mineral was saturated nutrient medium including calcium acetate and labelled UCSL-CA. UCSL-CA nutrient medium (pH=9) contains 0.13 M tris base, 20 g/L urea, 10 g/L CSL and 10 g/L calcium acetate per liter of distilled water.

For B series immobilization procedure, 2 g of viable S. pasteurii cells were suspended in 87.5 mL PBS and added to 22.5 g (5% of cement weight) of fine powder mineral without any nutrient medium. Due to the larger particle size, 6 g of bacterial cells

suspended in 262.5 mL PBS were added to 67.5 g (5% of standard sand) of perlite and zeolite (1.6mm) instead of 22.5 g. BN series of immobilization was achieved by saturating half of mineral (11.25 g) with 1 g of vegetative bacteria cells suspended in 45 mL PBS and saturating the other half (11.25 g) with UCSL-CA nutrient medium. For perlite and zeolite (1.6mm), 3 g of bacteria cells suspended in 135 mL PBS were immobilized 33.75 g of mineral. Immobilization of minerals was achieved with shaking conditions (175 rpm) at 30˚ C for 24 hours. Then slurry was removed from incubation and kept at 40˚ C in an oven for an additional 12 hours. A saturated surface dry (SSD) biological additive was obtained by filtering the excess solutions through MN615 A Grade I filter paper and drying the mineral-cell compound in an oven at 40˚ C. The final composition of biological additives is demonstrated in Table 2.

Table 2: Biological additive design. ZEO: zeolite, PER: perlite, MET: metakaolin; B: mineral was saturated with bacterial cells and PBS, BN: half of mineral was saturated with bacterial cells and PBS and the other half of mineral was saturated with UCSL-CA

Sample Name	Mineral (g)	Bacteria (g)	PBS (mL)	UCSL-CA (mL)
ZEO-B-200 µm	22.5	2	87.5	-
ZEO-B-1.6mm	67.5	6	262.5	-
PER-B	67.5	6	262.5	-
MET-B	22.5	2	87.5	-
ZEO-BN-200 µm	22.5	1	45	42.5
ZEO-BN-1.6mm	67.5	3	135	127.5
PER-BN	67.5	3	135	127.5
MET-BN	22.5	1	45	42.5

To evaluate the immobilization, ESEM analyses were conducted for the biological additives. Figure 4 shows ESEM images after immobilization.

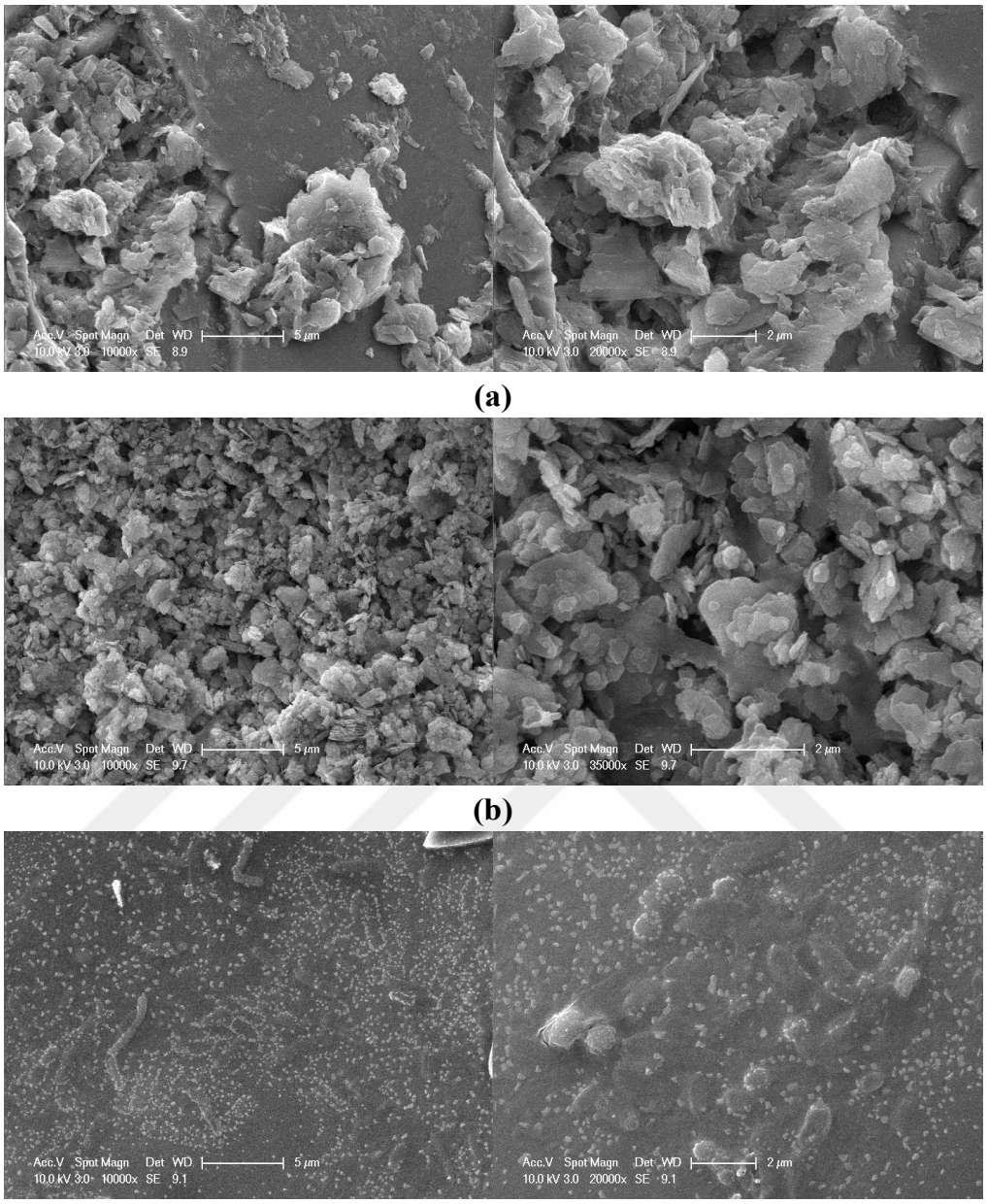

Figure 4: ESEM images after the immobilization (a) Zeolite (200 μm) (b) Metakaolin (c) Perlite. Scale 5μm (left), 2μm (right).

3.4 Preparing of mortar samples

Cement-based mortars were prepared by using OPC CEM I 42.5 R cement and standard sand complied with the norm EN-196-1, according to ASTM C305-14 Standard Practice for Mechanical Mixing of Hydraulic Cement Pastes and Mortars of Plastic Consistency

[44]. Water to cement ratio (w/c) and sand to cement ratio were kept at 0.45 and 3, respectively. Table 4 summarizes the mix proportions of prepared samples. The amounts of mineral and sand were replaced depending on used minerals' type and size.

To maintain the same flowability of the mortars, polycarboxylate ether (PCE)-based superplasticizer (BASF) was used. The amount of PCE superplasticizer was determined according to flow table diameter of mortars based on ASTM C230/C230M-14 Standard Specification for Flow Table for Use in Tests of Hydraulic Cement [45] and desired as 13±2 cm. The flowability of mortars were calculated by given formula.

$$\text{Flow rate } \% = \left(\frac{\text{A}}{\text{d}_{\text{base}}}\right) \text{x } 100 \qquad (5)$$

where A is the average of four readings minus the diameter of the cone base. The flow diameter of each mix is summarized in Table 3.

Table 3: Mix design of prepared mortars and their flow rate. ZEO: zeolite, PER: perlite, MET: metakaolin; C: only includes minerals, B: mineral was saturated with bacterial cells and PBS, BN: half of mineral was saturated with bacterial cells and PBS and the other half of mineral was saturated with UCSL-CA.

Sample	Cement (g)	Sand (g)	Mineral (g)	Superplasticizer (g)	Flow Rate (%)
ZEOC-200 µm	450	1350	22.5	4	19.2±0.5
ZEOC-1.6mm	450	1282.5	67.5	3	22.6±0.7
PER-C	450	1282.5	67.5	3	28.8±0.4
MET-C	450	1350	22.5	3	28.4±0.3
ZEO-B-200 µm	450	1350	22.5	4	21.0±0.4
ZEO-B-1.6mm	450	1282.5	67.5	2	33.1±0.5
PER-B	450	1282.5	67.5	2	24.7±0.4
MET-B	450	1350	22.5	3	37.7±0.7
ZEO-BN-200 µm	450	1350	22.5	4	17.3±0.4
ZEO-BN-1.6mm	450	1282.5	67.5	2.5	33.7±0.4

PER-BN	450	1282.5	67.5	2.5	21.9±0.3
MET-BN	450	1350	22.5	3	41.1±0.9

3.5 Crack formation and curing conditions

Mortar mixes were casted in 40x40x160 mm beams molds. To strengthen to the flexural strength of beams during the formation of cracks, 12 mm synthetic fibers (6 g/m^3 of mortar) were used. After casting, beams were kept in 100% humidity until the day of cracking. A total of 24 beams were casted for each series of mix (Table 3). Nine of beams were cracked on day 14th and the other nine of beams were cracked on day 28th. Six remained beams were not cracked and kept at the ambient conditions. Cracks having a width of 0.30-0.60 mm were formed under a 3-point flexural loading using a servo hydraulic displacement-controlled device. Loading rate was recorded as 0.005 mm/sec.

Beams cracked on specified days were cured in there different conditions. Six beams were cured in tap water, another six beams were cured in UCSL-CA nutrient medium. Along curing, samples after submerging in curing solution (water/UCSL-CA) for 48 hours were kept at ambient temperature for 48 hours. This procedure was applied for 28 days. The curing solution was refreshed every week. The curing procedure was limited to 4 weeks due to the observation of high crack closure rates at samples in previous studies carried out same procedure [42]. At last, the rest of cracked beams were kept at ambient conditions in order to evaluate the impact of curing to the self-healing ability. Figure 5 summarizes the experimental protocol of this study.

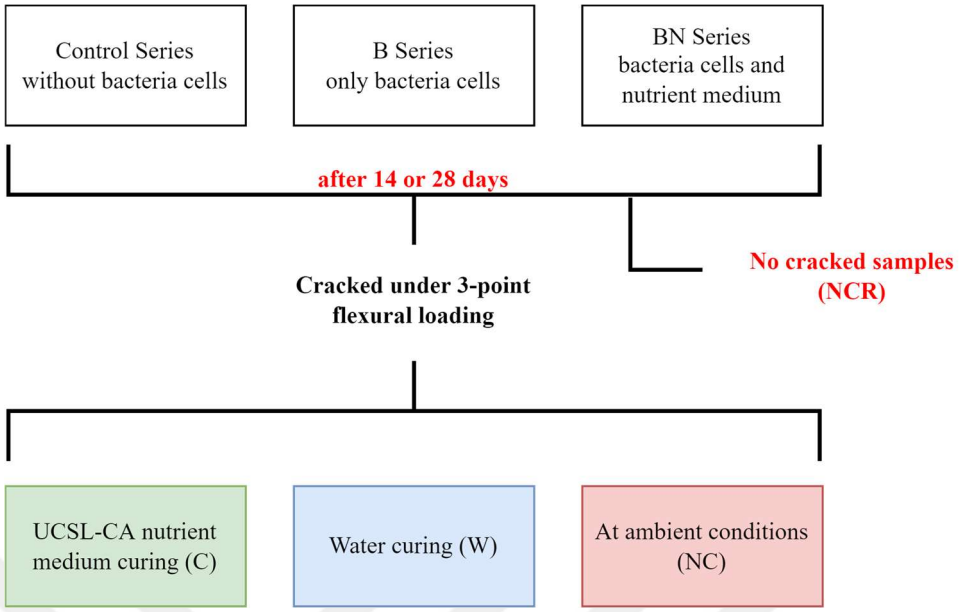

Figure 5: Schematic presentation of casted mortar series.

3.6 Evaluation of self-healing ability

3.6.1 Stereomicroscope and image analysis

Visual closure at cracks were periodically observed with a stereomicroscope. The images were taken from cracked samples at 6.7x and 50x scales by using Stereomicroscope (NIKON Inc. SMZ745T) were examined with Clemex Vision Lite software.

For determining the percent of visual crack closure, a Java-based image processing program "Image J" was used. First the scale of 50x images taken from stereomicroscope was transformed to pixel/µm. (50x scale corresponds to 1000µm.) After adjusting the scale of images, "Threshold" filter was applied to images to make crack surfaces more apparent. (See Figure 6). The crack width was measured at 10 different points along the crack on each sample after cracked formed and after 7, 14, 21, and 28 days of curing. Attention was paid to take the measurements at same points for different days. The crack closure was determined by following formula.

$$\text{visual crack sealing } \% = \frac{\sum_{n=1}^{10} w_i - \sum_{n=1}^{10} w_{7.,14.,21.,28.}}{\sum_{n=1}^{10} w_i} \quad (6)$$

where w_i is initial crack measurement and $w_{7.,14.,21.,28.}$ is the measurements taken after 7, 14, 21 and 28 days of curing.

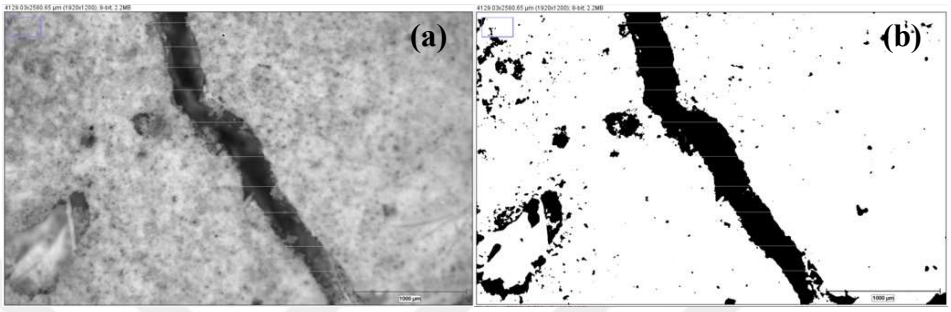

Figure 6: Crack width evaluation (a) Image taken from the stereomicroscope (b) Image applied threshold filter.

3.6.2 Ultrasonic pulse velocity (UPV)

To evaluate crack closure, ultrasonic pulse velocity test was applied each sample in accordance with ASTM C597-16 Standard Test Method for Pulse Velocity Through Concrete [46]. This test is applied to specify the existence of voids and cracks into concrete [47]. A UPV meter test setup was used to measure transit time. The transit time was measured from the long axis (160 mm) of the air-dried beam. A petroleum jelly was applied to the transducers to obtain a smooth contact zone between the beam surface and transducer. Transducers were pressed to the beam surfaces which are opposite to each other, until a stable transit time was showed. Measurements were taken before and after crack formed and 7, 14, 21, 28 days. The ultrasonic pulse velocity was calculated according to given formula:

$$\text{ultrasonic pulse velocity (m/s)} = \frac{\text{the length of sample (m)}}{\text{transit time (s)}} \quad (7)$$

3.6.3 Water absorption capacity

The impact of the biological additive to self-healing ability was investigated by conducting water absorption capacity test regarding to RILEM 25 PEM II-6 [48]. Samples were dried at 40˚C in an oven until the mass change maintained ±0.1% range. Uncracked surfaces of dried samples were covered with waterproof silicone-based cover. 40x40 mm area of cracked surface was not covered. After dried mass of samples were measured, samples were immersed into water bath to a height of 2 mm. To keep the water level constant, water was added when needed. Periodically (15 and 30 minute, 1, 3, 5, 8, 24, 48, 72, 96 and 120 hour), samples were removed from the water bath and after wiped with towel, the wet mass of samples were measured. Water absorption coefficients (k) of samples were calculated with given formula.

$$k\,(t^{0.5}) = Q/A \qquad (8)$$

where;

k: water absorption coefficient (kg/ (m^2.$s^{0.5}$))

t: time (second)

Q: the amount of water absorbed (kg)

A: submerged area (m^2)

3.6.4 Characterization of the precipitates

After the water absorption test, samples were divided into two parts from crack zone to characterize the morphology of precipitation occurred at crack surface. 1 cm^2 taken sample covered with gold was examined by FEI-Philips XL30 ESEM. ESEM voltage was kept at 10 kV and the operating distance was kept at 10 mm.

The chemical component of precipitation was evaluated by Fourier Transform Infrared (FTIR) analysis. Approximately 5 mg sample collected from crack surface was characterized chemically with a resolution of 4 cm^{-1} in the range of 4.000 – 600 cm^{-1} by using FTIR (Bruker Equinox 55IR Spectrometer). These analyses were conducted at samples observed enough crack closure.

3.7 Performance evaluation of bio-based mortar samples

3.7.1 Vicat needle test

The initial setting time of cement pastes containing biological additive and negative control pastes were determined with a modified ASTM C191-19 Standard Test Methods for Time of Setting of Hydraulic Cement by Vicat Needle [49], instead of determining the w/c ratio that will yield a "normal consistency" paste as suggested in the standard, the w/c ratios were kept constant at 0.45 to be consistent with the ratios used throughout the other analysis conducted in the study. The penetration depth of the Vicat needle was measured to decide the initial setting of cement pastes. Tests were performed based on triplicates of samples.

3.7.2 Compressive strength test

For compressive strength test, cement-based mortar samples containing biological additive and negative control mortars were prepared according to ASTM C305-14 Standard Practice for Mechanical Mixing of Hydraulic Cement Pastes and Mortars of Plastic Consistency [44]. Water to cement ratio and sand to cement ratio were kept at 0.45 and 3, respectively. The mortar samples were casted in 5x5x5 cm cubes and kept in a humid environment at 21˚C for 24 h. Then the molds were removed, and the samples

were further cured in 100% humidity at 23˚C. The compressive strength was conducted according to ASTM C109/C109M-21 Standard Test Method for Compressive Strength of Hydraulic Cement Mortars (Using 2-in. or [50 mm] Cube Specimens) at 3, 7, 28 and 90 days after casting [50].

3.8 Influence of biological additive on free drying shrinkage

Drying shrinkage is one of the main factors caused microcracks in the hardened concrete. The drying shrinkage is the result of realizing of water in the capillary pores of the hydrated cement paste and consequently, the absorbed water loss of C-S-H gel [51]. The mortar mixes showing a higher crack healing efficiency were selected for shrinkage evaluation. Herein, C and BN series of BT, DE, SEP, PUM and ZEO (only C series) samples were prepared. These mixes were selected because both B and BN series of these mixes showed a visual crack healing efficiency higher than 80% and a reduced water absorption capacity upon healing.

The influence of biological additive on drying shrinkage was evaluated based on ASTM C596-18 Standard Test Method for Drying Shrinkage of Mortar Containing Hydraulic Cement [52]. The samples containing 750 g cement to 1500 g standard sand were prepared and the flow diameter was kept at 110±5 mm. The w/c was kept 0.45. To examine the impact of minerals and biological additive separately, mortars were prepared with and without bacteria cells. Prepared mixtures were placed into 25x25x250 mm beam molds and without demolding samples were kept in 100% relative humidity (RH) at 23˚C for 24 hours. Upon demolding, the samples were submerged into lime-saturated water for 48 hours. At the end of 48 hours, the beams were removed from lime-saturated water and wiped with a towel. The initial weight and length measurements were recorded right after

the samples were dried. The length measurements of beams were carried out with comparator based on ASTM C157/C157M-17 Standard Test Method for Length Change of Hardened Hydraulic-Cement [53]. Following the first measurement, the samples were moved to the controlled climate chamber at 23˚C and 50% RH for 16 weeks. The length and weight of the samples were measured at 4, 7, 11, 18, 25 days, 8 and 16 weeks. The length changes of triplicates of samples were calculated based on Equation 5. [53]

$$\Delta L_x = \frac{CRD - initial\ CRD}{G} \times 100 \quad (9)$$

where:

ΔL_X: length change of sample at any day, %

CRD: difference between the comparator reading of the sample and the reference bar at any day

G: the gage length (205 mm)

3.9 Effects of crack sealing on corrosion resistance

An accelerated reinforced corrosion test was performed to samples which showed visually higher crack sealing [54]. Similar to drying shrinkage tests, C and BN series of BT, DE, SEP, PUM and ZEO (only C series) samples were selected for corrosion test. Mortar samples were casted in 40x40x160 mm molds. 8 mm steel rebars (200 mm length) were embedded into prepared mortars.

To induce self-healing, an artificial crack with a 0.4 mm width and 16 mm depth was formed at the mid-section of the samples during casting. Upon casting, the beams were kept in 95% humidity at 20±2˚C for 3 days and following they were kept at ambient conditions for 11 days. After that, BN series samples were cured in UCSL-CA nutrient

solution until 80% crack closure observed. A set of negative control samples were kept at ambient conditions.

After healing process, beams connected in series each other from rebars were submerged in 3.5% sodium chloride (NaCl) solution [54]. Then, the beams were immersed in NaCl solution. A steel mesh was wrapped around the beams as the steel mesh was completely immersed in solution.

For accelerated corrosion test, the set up was connected to 40V power supply. While rebars were connected to the anode of power supply, the steel mesh was connected to the cathode. Moreover, a resistor was connected to the set up to reduce the current of the system, and the current was kept to 0.1A (See Figure 7). A 40V was applied to the system for 7 days. After 7 days, the samples were removed from the solution and the degree of corrosion was measured with CorMap Corrosion Measurement System (James Instruments Inc.) Then, the uniaxial tension test was conducted to rebars in samples with a loading of 10 mm/sec. The analyses were done with triplicates of samples.

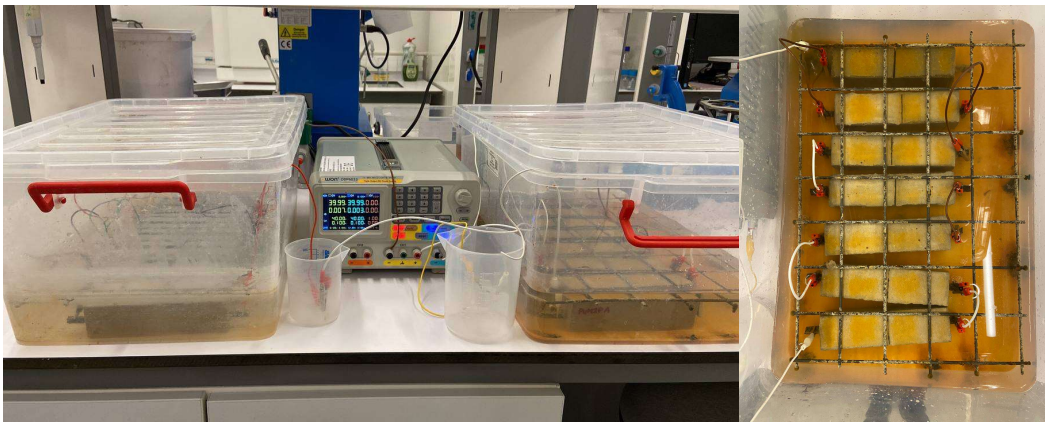

Figure 7: Accelerated corrosion test set up.

CHAPTER IV

RESULTS AND DISCUSSION

4.1 Evaluation of self-healing ability

In this study, three different series specimens C, B and BN containing zeolite, metakaolin and perlite were casted, and 0.3-0.6 mm micro cracks were formed on the samples in 14 and 28 days under a 3-point flexural loading. Cracked samples were cured under three different conditions: ponding cycles of UCSL-CA nutrient medium (1), water (2), and ambient conditions (3). The initial evaluation was done via stereomicroscope analysis and ultrasonic pulse velocity (UPV) test on triplicates of samples in each series for 4 weeks. The specimens belonging to the same series showed similar crack-healing trend. Since the visual crack healing was almost the same for each set, herein one representative image of series was shown. Stereomicroscopy images are given in Appendix A.

4.1.1 Use of micro-size Zeolite (200 µm) as a protection barrier:

Figure 8 shows representative images for 28-day old ZEOC-200 samples containing only saturated minerals without any bacterial cells. The difference in % crack closure for both ZEO samples (and all samples) was summarized in Table 4. The visual crack healing was determined quantitively as described in Section 3.6.1.

(a) **(b)** **(c)**

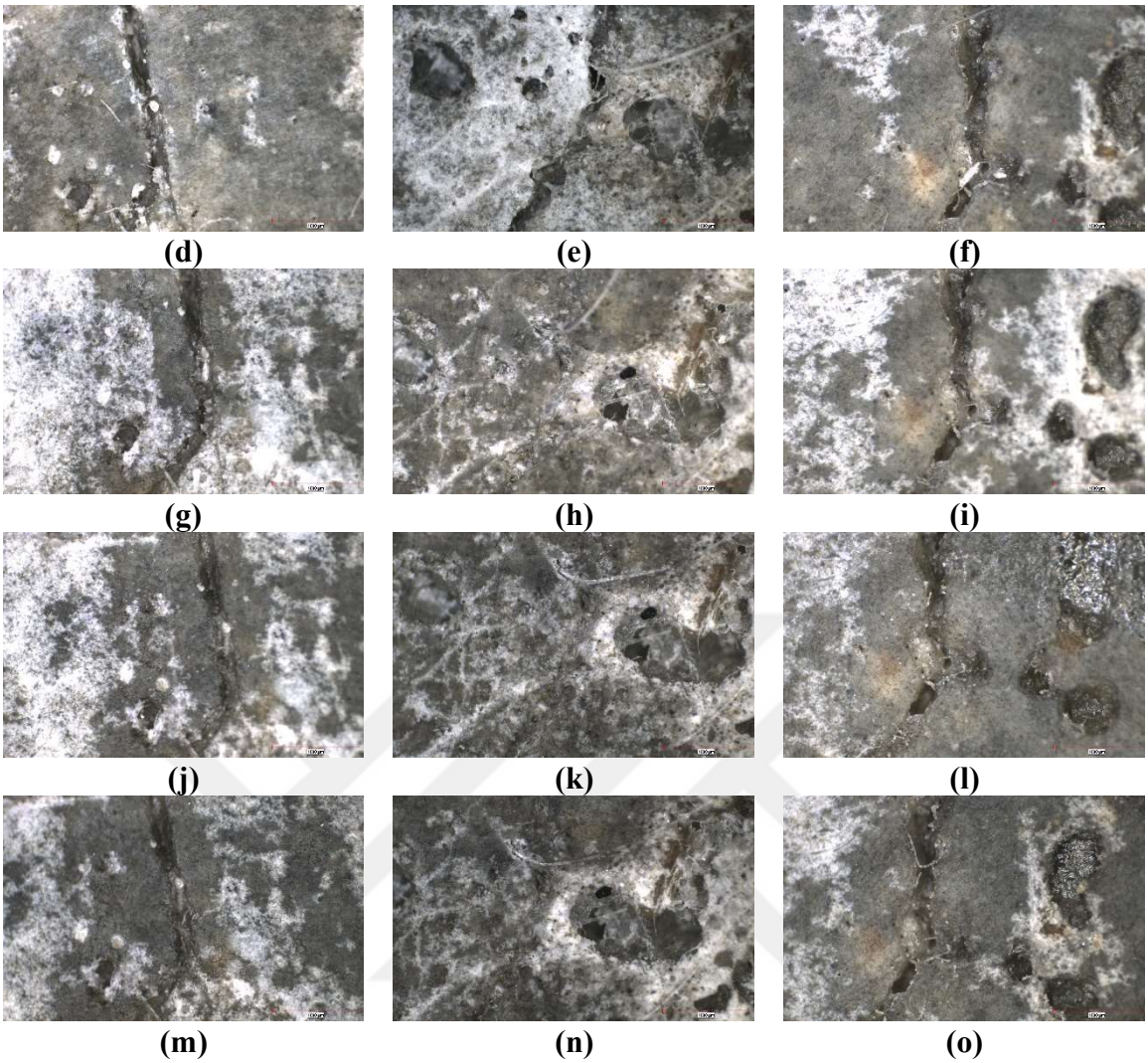

Figure 8: The crack images of 28-day old ZEOC-200 samples (a, b, c) right after cracking, (d, e, f) after 7 days of water curing, (g, h, i) after 14 days of water curing, (j, k, l) after 21 days of water curing, (m, n, o) after 28 days of water curing.

Table 4: Crack closure rates %. ZEO: zeolite, PER: perlite, MET: metakaolin. C: only includes minerals, B: mineral was saturated with bacterial cells and PBS, BN: half of mineral was saturated with bacterial cells and PBS and the other half of mineral was saturated with UCSL-CA, UCSL-CA: nutrient medium curing, W: water curing, NC: at ambient conditions.

Crack Closure %						
Sample Name	**14. Day**			**28. Day**		
	UCSL-CA	**W**	**NC**	**UCSL-CA**	**W**	**NC**
ZEOC-200	33,61	63,3	44,36	52,86	71,87	15,27
ZEOC-1.6	52,07	37,12	11,11	55,9	24,11	17,28
METC	20,05	12,91	10,35	15,83	9,57	16,81

PERC	42,39	17,73	3,2	32,6	8,69	4,73
ZEOB-200	84,19	23,6	15,05	69,55	61,48	13,77
ZEOB-1.6	37,1	30,43	2,27	34,55	23,3	12,64
METB	38,79	0,64	10,40	30,02	11,03	10,47
PERB	34,73	21,09	7,86	21,84	12,42	9,84
ZEOBN-200	53,88	23,13	9,49	28,37	13,86	23,64
ZEOBN-1.6	40,16	43,02	29,14	29,65	24,65	23,19
METBN	25,7	8,0	15,11	33,42	17,03	8,36
PERBN	56,23	6,51	6,17	17,32	22,72	3,2

Incorporation of zeolite mineral in control sample resulted in over 70% crack closure in samples cured with water. This could be attributed to the fact that zeolites could be classified as a very reactive natural pozzolan [55]. The clinoptilolite zeolite used in this study contained 65-75% SiO_2 and 10-12% Al_2O_3 with a d_{50} of 60 μm. The surface area, cation content, and ease of cation exchange in the zeolites were effective for short term reactivity [56]. The clinoptilolite zeolites containing high K^+ content and ease of K^+ exchange could react very fast after 3 days compared to those possessing Ca^+ exchange and Na^+ exchange. Correlatively, the clinoptilolite zeolite used in this study contains 2.5-3.8% K_2O and CaO. Although the exact reaction kinetics is not known, the autogenous self-healing in ZEOC-200 samples could be related to pozzolanic activity. Moreover, due to its porous structure and high-water absorption capacity, zeolite could be used as internal curing agent in the cementitious systems [57]. Saturated zeolite particles can desorb its absorbed moisture content and could trigger the secondary hydration under the dry conditions [58]. Once again, partial crack sealings were observed in ZEOC-200 samples kept in ambient conditions especially, 44% crack closure was measured in 14-day old ZEOC-200 upon cracking.

On the other hand, the crack sealing in ZEOC-200 samples were found to be less efficient when the samples were cured in UCSL-CA medium at pH 9. In the literature, it was known that the reaction of zeolites depends on the ions in the environment and pH

of the environment [55], [56]. Therefore, the higher pH of nutrient medium might be limited the cation exchange in zeolite and reduced the reactivity.

Figure 9 demonstrates representative images of ZEOB-200 series for 28-day old samples where the bacterial cells were immobilized on the zeolite without any nutrient medium. When ZEOB-200 series samples were examined, approximately 85% and 70% crack closure was observed in 14- and 28- day old samples. According to ZEOC-200 series samples, it was seen that UCSL-CA curing decreased the reactivity of zeolite, consequently reduced cracked closure. Therefore, it was considered that crack sealing occurred in ZEOB-200 series samples cured with UCSL-CA was solely based on the bacterial activity. In addition to this, crack sealing observed in ZEOB-200 series samples cured with water was similar to ZEOC-200 series sample in same conditions. Herein, the crystal formation in ZEOB-200 cured in water might be due to the reactivity of zeolite rather than a possible biomineralization reaction. In fact, it was also known that the bacterial cells require nutrients to survive and trigger biomineralization [59]. In water cured ZEOB-200 the bacterial cells could not access to nutrients at any point. Therefore, the viability of cells could be hindered in an environment without any nutrients.

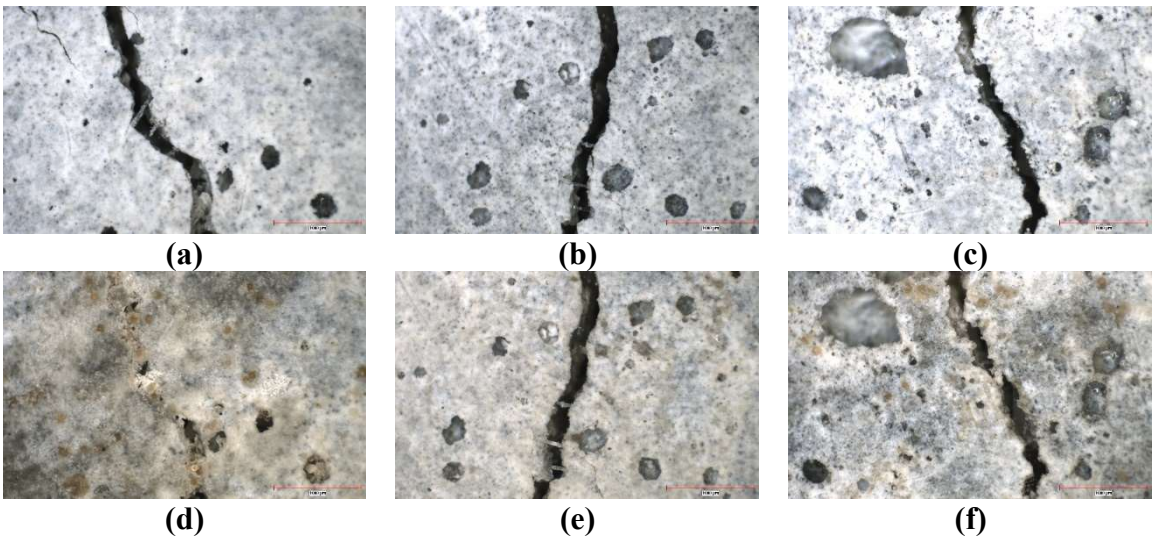

(a) **(b)** **(c)**

(d) **(e)** **(f)**

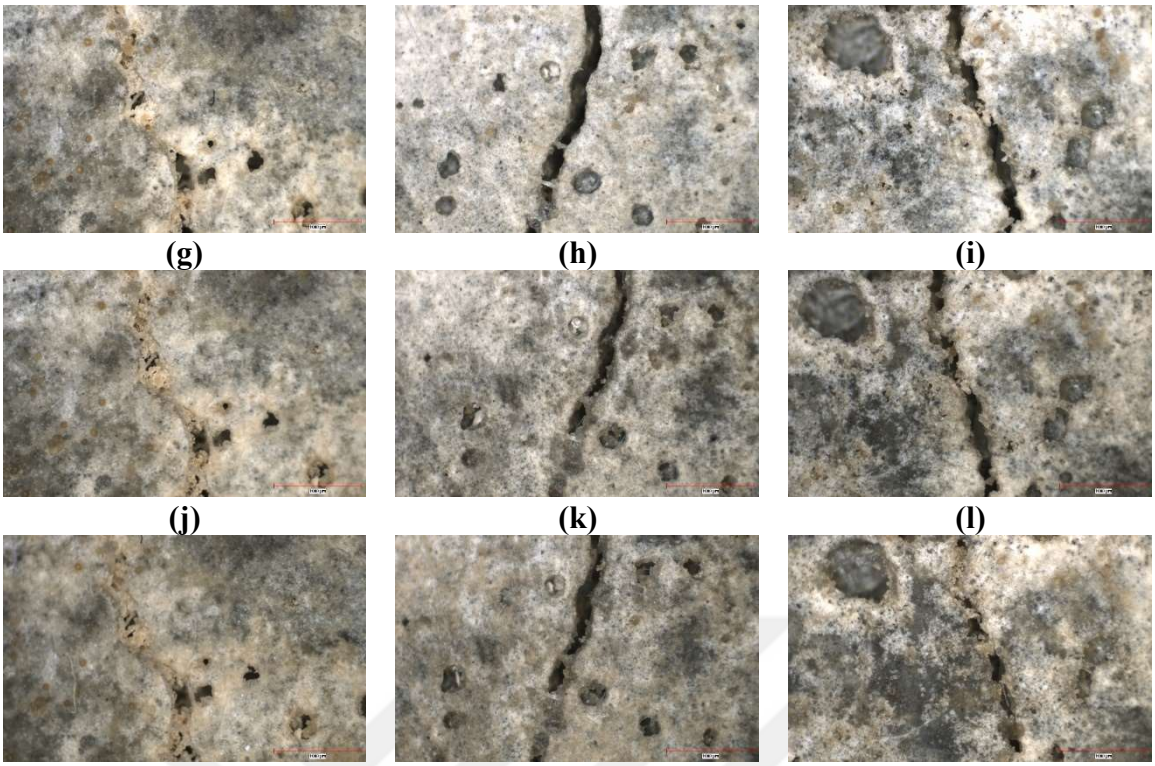

Figure 9: The crack images of 28-day old ZEOB-200. (a, b, c) right after cracking, (d, e, f) after 7 days of UCSL-CA curing, (g, h, i) after 14 days of UCSL-CA curing, (j, k, l) after 21 days of UCSL-CA curing, (m, n, o) after 28 days of UCSL-CA curing.

Finally, ZEOBN-200 series specimens were analyzed as shown in Figure 10. In that series samples, half of mineral was saturated with bacterial cells and PBS and the other half of mineral was saturated with UCSL-CA. Lower crack closure rates were measured in ZEOBN-200 series samples regardless of curing condition in comparison to ZEOC-200 and ZEOB-200. Considering the fact that UCSL-CA addition reduced the % crack closure in samples containing zeolite, it could be concluded that the relative high pH of the nutrient medium reduces the reactivity of the mineral.

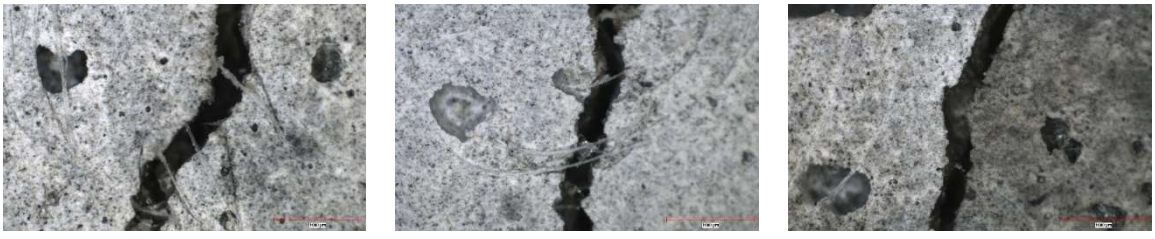

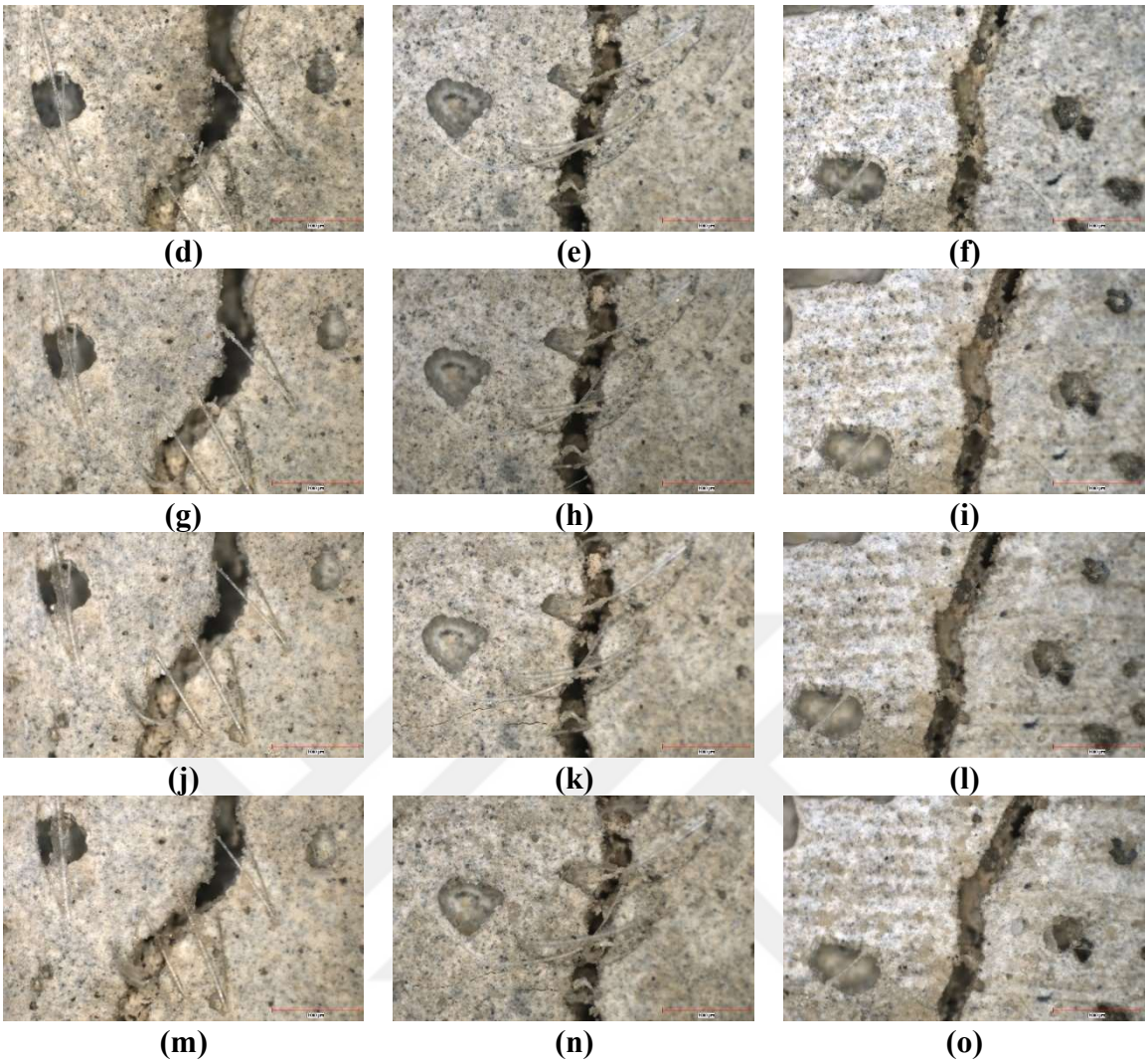

Figure 10: The crack images of 28-day old ZEOBN-200 samples. (a, b, c) right after cracking, (d, e, f) after 7 days of UCSL-CA curing, (g, h, i) after 14 days of UCSL-CA curing, (j, k, l) after 21 days of UCSL-CA curing, (m, n, o) after 28 days of UCSL-CA curing.

To monitor the crack healing through the crack depth, a UPV test was conducted as a semi-quantitative method. Figure 11 represents the change in UPV before cracking, right after cracking, and following a 28-day curing period for both 14-day and 28-day cracked ZEO-200 samples. Comparing the UPV values measured before cracking, similar values were obtained from ZEOC-200, ZEOB-200 and ZEOBN-200 series samples both 14-day and 28-day. It shows that the mortars casted were in same quality and the bacteria addition has no impact on the initial performance of cement-based mortar. After cracking, approximately 5±2% decrease was recorded in UPV which indicates a deformation in the

sample. While the sudden decrease in UPV upon cracking indicating a reduction in quality and the relative increase in UPV during curing is a sign of improved quality.

In accordance with the visual analysis, there was an increase in UPV ZEOC-200 sample through the 28-day water curing period. Both 14-day and 28-day samples showed a higher UPV values when they were cured in water compared to their counterpart samples cured in nutrient medium. The increase in velocity during the curing period could be an indicator of an improvement in quality of the material [60].

The change in UPV for ZEOB-200 specimens cured in both water and UCSL-CA were equivalent to the uncracked ZEOB-200 sample. This is in line with the visual evaluation where there was more than 80% crack healing in UCSL-CA cured ZEOB-200 sample.

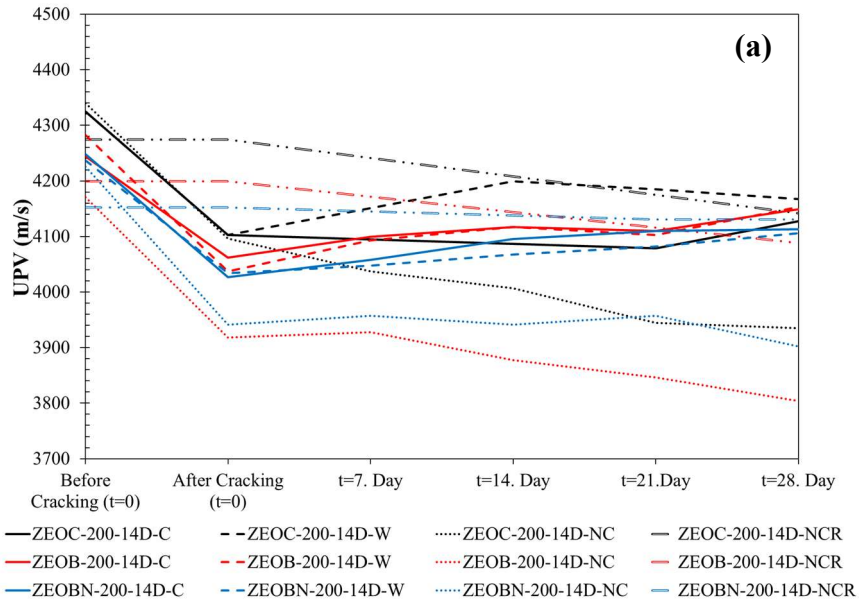

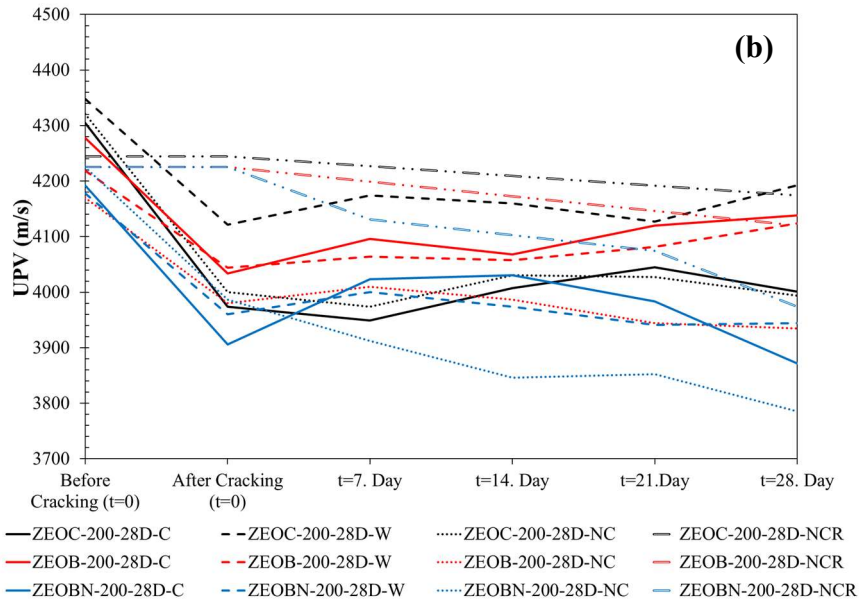

Figure 11: Ultrasonic pulse velocity changes of samples containing zeolite 200µm, after 28 days curing. (a) cracked on day 14th (b) cracked on day 28th. ZEO: zeolite, C: only includes minerals, B: mineral was saturated with bacterial cells and PBS, BN: half of mineral was saturated with bacterial cells and PBS and the other half of mineral was saturated with UCSL-CA, C: UCSL-CA nutrient medium curing, W: water curing, NC: at ambient conditions, NCR: no crack.

It was known that the most significant effect of self-healing on the performance of material is the water absorption or the permeability. The previous studies shows that the crack remediation provided by biological self-healing was not effective in the enhancement of the flexural strength, it only reduced the permeability of the material [61]. Therefore, to determine the impact of self-healing on the performance of sample, the water absorption capacity test was conducted according to RILEM 25 PEM II-6 [48]. Figure 12 represents the 120h water absorption coefficients of samples. There was approximately 40% increase in the water absorption capacity of samples upon its crack formation both at 14-day and 28-day old samples (compare NCR and NC samples). The water absorption capacities of all series of samples (ZEOC-200, ZEOB-200, and ZEOBN-200) cured with nutrient medium and water were slightly decreased in comparison with corresponding samples kept at ambient conditions. While the distinct crack closure was visually observed in 28 -day ZEOC-200 sample cured with water and

14-day ZEOB-200 sample cured with nutrient, this affect was not reflected as a decrease in water absorption coefficient. This could be attributed to the stability of sealing precipitation. Such that the morphology of the sealant might affect the efficiency of the crack healing [23]. If the $CaCO_3$ precipitate is vaterite instead of calcite, even though it visually seals the crack, water can still access through the crack.

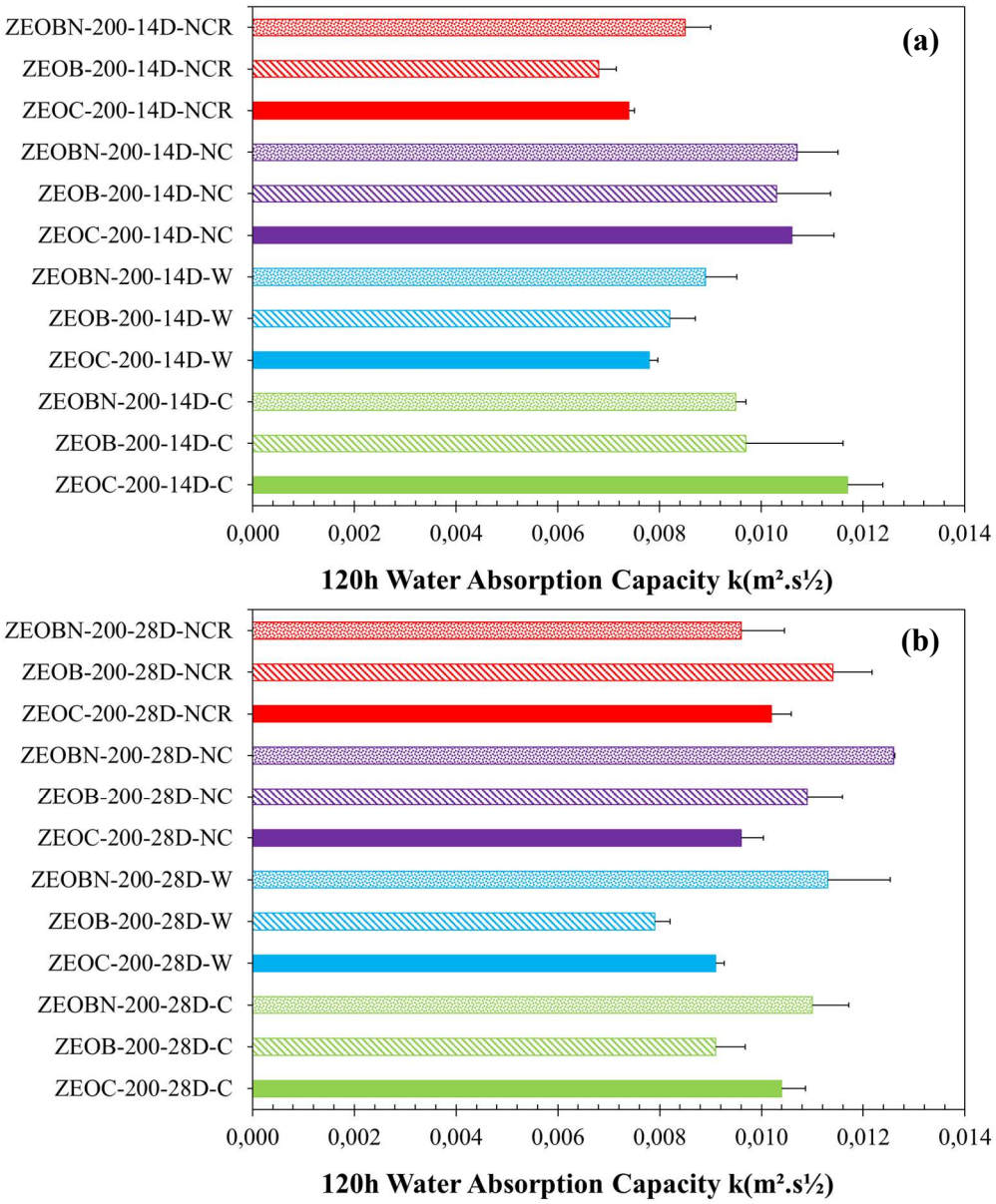

Figure 12: 120-hour water absorption capacities of samples containing zeolite 200µm, after 28 days curing. (a) cracked on day 14th (b) cracked on day 28th. ZEO: zeolite, C: only includes minerals, B: mineral was saturated with bacterial cells and PBS, BN: half of mineral was saturated with bacterial cells and PBS and the other half of mineral was saturated with UCSL-CA, C: UCSL-CA nutrient medium curing, W: water curing, NC: at ambient conditions, NCR: no crack.

Upon completion of a water absorption test, the specimens were cracked into two pieces and further FTIR and ESEM analyses were conducted on precipitates collected from specimens. Table 5 summarizes the FTIR characterization for all zeolite-containing samples. The FTIR spectra for all samples are summarized in Appendix B. The information collected from the samples obtained from crack surfaces also confirmed that the sealing precipitate is mostly CaCO3 and CSH. Besides calcite, different polymorphs, such as aragonite and vaterite were also found in samples. This indicates that, zeolite-containing samples exhibited a mutual reaction mechanism of latent hydration and carbonation. In addition, the influence of crack sealing efficiency of ZEO-200 series samples was less pronounced in decreasing the water absorption. This might be explained by the vaterite precipitation which is a less stable for of CaCO3 than calcite in water [23].

Table 5: FTIR analysis results. ZEO: zeolite, C: only includes minerals, B: mineral was saturated with bacterial cells and PBS, BN: half of mineral was saturated with bacterial cells and PBS and the other half of mineral was saturated with UCSL-CA.

Sample Name	UCSL-CA Curing		Water Curing	
	14. Day	**28. Day**	**14. Day**	**28. Day**
ZEOC-200	No crystal	Vaterite	CSH, Vaterite	Vaterite
ZEOB-200	Calcite, CSH, AFm	Calcite, Vaterite, Aragonite, CSH	Calcite, CSH, AFm	AFm
ZEOBN-200	Calcite, CSH	No crystal	Calcite, Vaterite, Aragonite, CSH	Calcite, CSH

Furthermore, Figure 13 shows ESEM images of the collected precipitates of zeolite samples with high crack closure rate. In accordance with FTIR results, ettringite and partially calcite was detected.

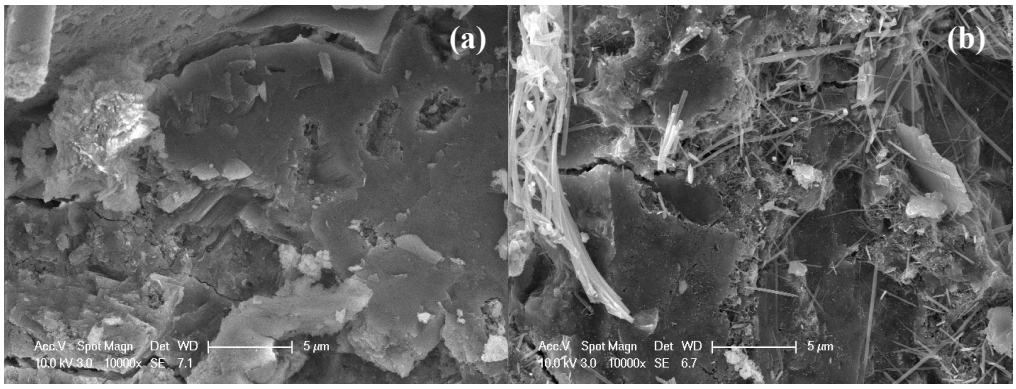

Figure 13: ESEM images of the crack surface obtained from specimens (a) 14-day ZEOB-200 cured with UCSL-CA (b) 28-day ZEOC-200 cured with water. Scale: 5µm.

These results indicate that suitable conditions have to be maintained when zeolite was used as an immobilization bedding for the bacterial cells. The cells can be incorporated without, and nutrients and the cells were able to seal cracks only at 14-day old samples. Compared to our previous findings, efficiency of zeolite as a bacterial bedding was not as high as what was observed in bentonite, sepiolite, diatomaceous earth, and pumice. This could be attributed to the pore size limitation of zeolites where the pores are mostly at a nanoscale range [62]. In such a case, the bacterial cells were absorbed on the surface of zeolite particles rather than actually being absorbed in these nano-sized pores. Moreover, the pores in zeolites generally filled by dust, cations as magnesium and calcium which prevents to the embedding of bacteria cells [63]. Since the bacterial cells were not actually embedded in the mineral, they might be more prone to the negative impacts of an alkaline environment. It might be possible that most of the cells could be dead, thus could only trigger limited precipitation. Even though zeolites were not a suitable bedding material for the bacterial cells, there is still a high potential of application to actually trigger self-healing with zeolites through an internal curing mechanism and the pozzolanic activity.

4.1.2 Use of Zeolite (1.6 mm) aggregate as a protection barrier:

A similar crack closure trend to ZEO-200 series was observed at ZEO-1.6 series. The highest crack closure rates, 52%, 40%, 43% and 55% were measured in 14-day old ZEOC-1.6, ZEOBN-1.6 cured with nutrient, ZEOBN-1.6 cured with water and 28-day old ZEOC-1.6 cured with nutrient, respectively. It was detected that the impact of nutrient on ZEO-1.6 was lower than ZEO-200. Figure 14, Figure 15, and Figure 16 show the crack images of 14-day C, B and BN series samples cured with different conditions.

The crack sealing rates of ZEOC-1.6 samples cured with water were almost half of the crack sealing % of ZEOC-200 samples cured with water. This could be explained by the different working mechanisms occur in these zeolites having two different particle sizes. While ZEO-200 reacts with water and induces a latent hydration, ZEO-1.6 can desorb a higher amount of absorbed water leading to a higher degree of internal curing but does not possess pozzolanic activity. By comparing these 2 series, it is clear that pozzolanic activity leads to a higher degree of healing compared to an internal curing mechanism. Herein, it is also possible that the higher amount of zeolite-1.6mm used in the mortar mix could led to the densification of the cement matrix and prevent to the access of external water [58]. It can be explained as the high amount of water supplied by internal curing agent increases the hydration rate of cement matrix and densifies it. Therefore, the densification of matrix prevents to transport of water discharged from the internal curing agent to seal the crack in the absence of water.

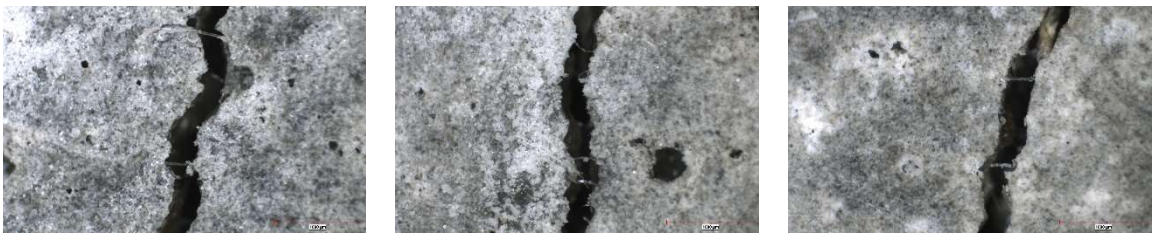

(a) **(b)** **(c)**

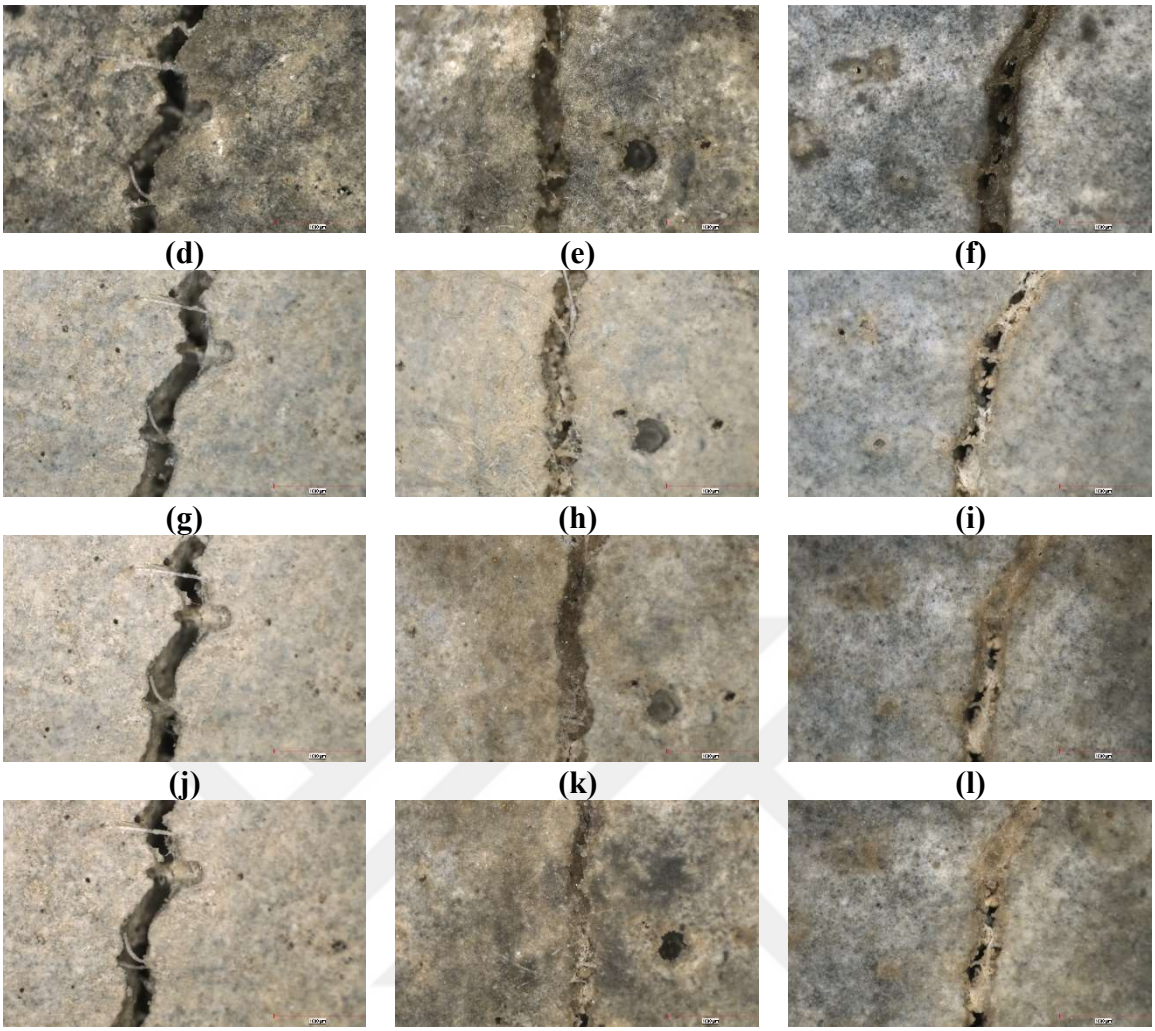

Figure 14: The crack images of 14-day old ZEOC-1.6 samples. (a, b, c) right after cracking, (d, e, f) after 7 days of UCSL-CA curing, (g, h, i) after 14 days of UCSL-CA curing, (j, k, l) after 21 days of UCSL-CA curing, (m, n, o) after 28 days of UCSL-CA curing.

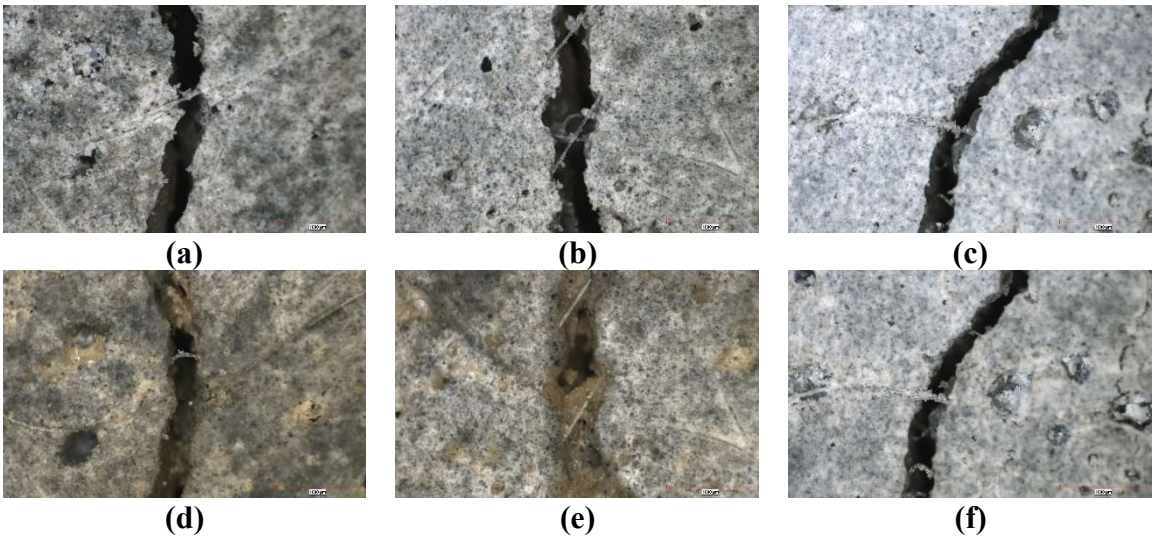

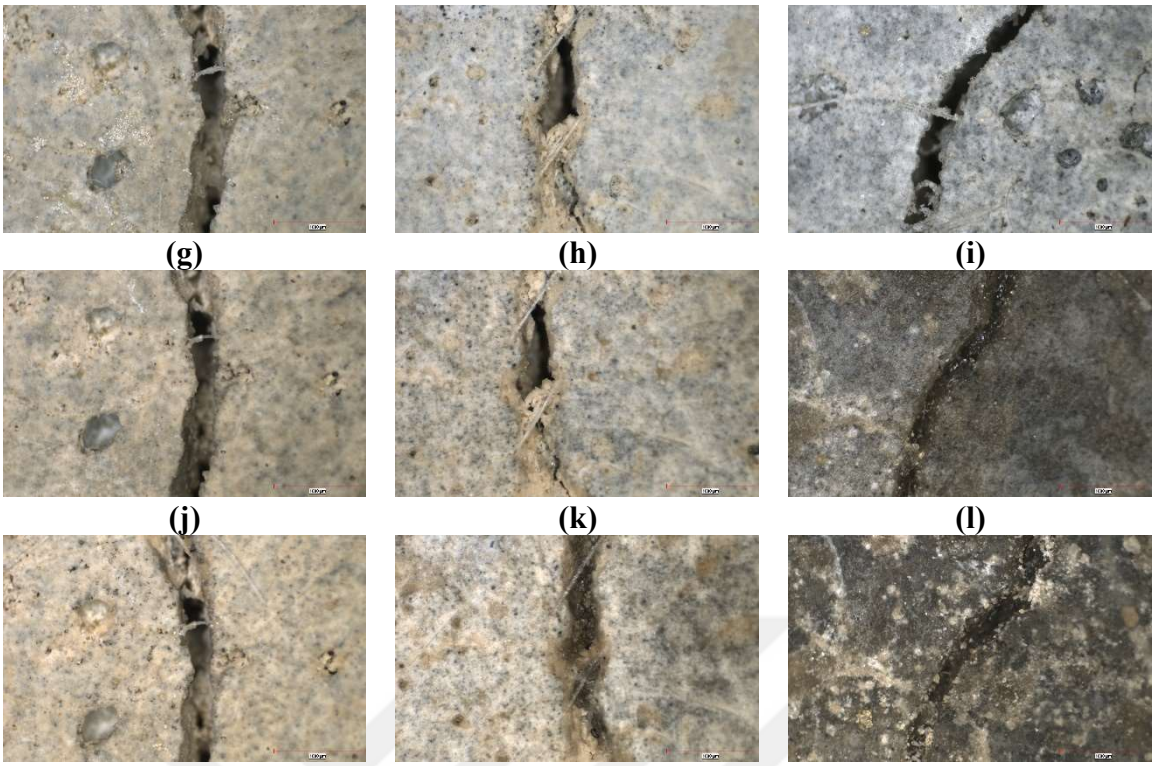

Figure 15: The crack images of 14-day old ZEOB-1.6 samples. (a, b, c) right after cracking, (d, e, f) after 7 days of UCSL-CA curing, (g, h, i) after 14 days of UCSL-CA curing, (j, k, l) after 21 days of UCSL-CA curing, (m, n, o) after 28 days of UCSL-CA curing.

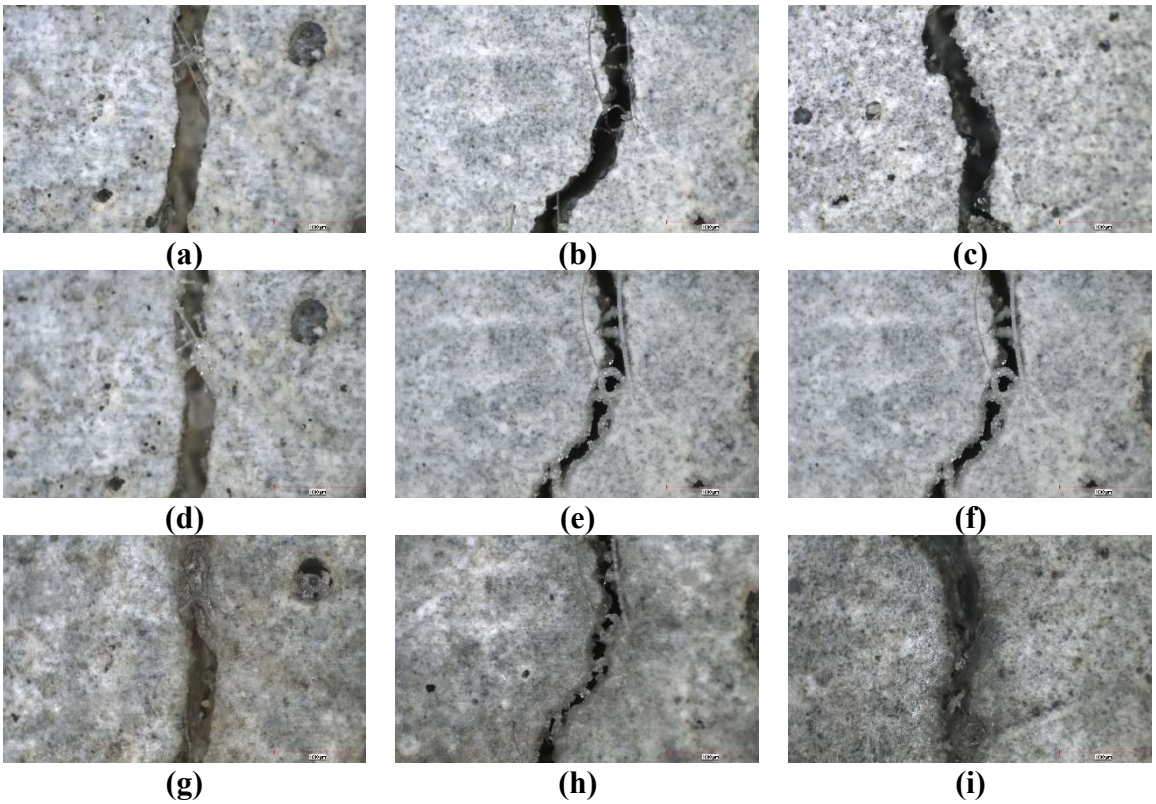

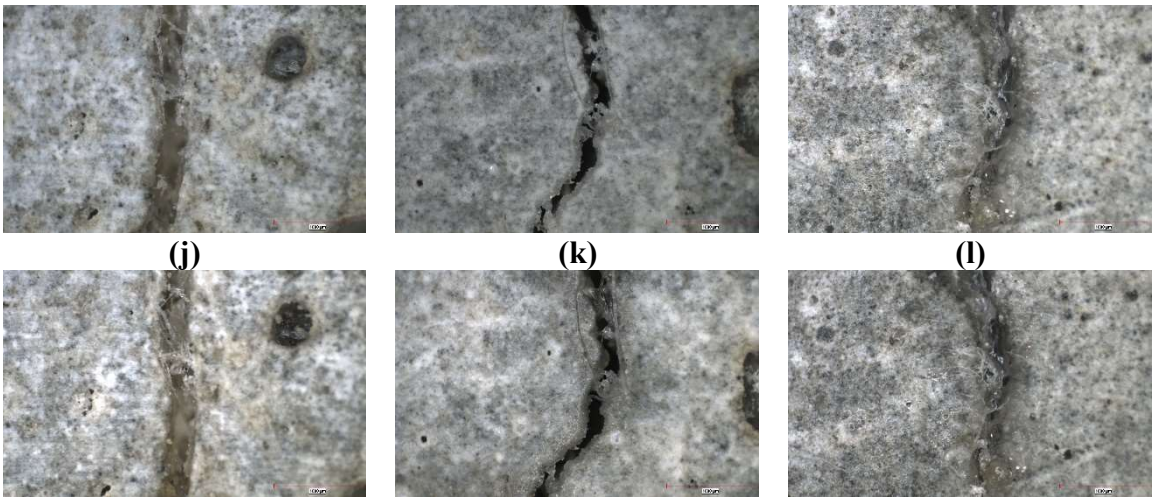

Figure 16: The crack images of 14-day old ZEOBN-1.6 samples. (a, b, c) right after cracking, (d, e, f) after 7 days of water curing, (g, h, i) after 14 days of water curing, (j, k, l) after 21 days of water curing, (m, n, o) after 28 days of water curing

Figure 17 shows UPV changes of ZEO-1.6 samples cracked after 14- and 28-day of mixing. The decrease in UPV was observed in both no cure and no cracked (NC and NCR) samples in all series. It might be due to the fact that the specimens were saturated in the first measurement, but they were unsaturated in the following measurements because of no curing process applied. The UPV enhancement in ZEOC-1.6-14D-C, ZEOBN-1.6-14D-C, ZEOBN-1.6-14D-W, and ZEOBN-1.6-28D-C were in compliance with the crack closure percentages. This again shows that the crack healing occurs through the depth of the crack as well as the crack mouth. Moreover, even low crack-healing was observed visually, the highest rate of UPV enhancement in ZEOC-1.6-28D-W and ZEOBN-1.6-28D-W was measured. This situation might be explained by the crack sealing phenomenon occurs through the depth of the crack which could be attributed to the reactivity and the internal curing property of zeolite as aforementioned.

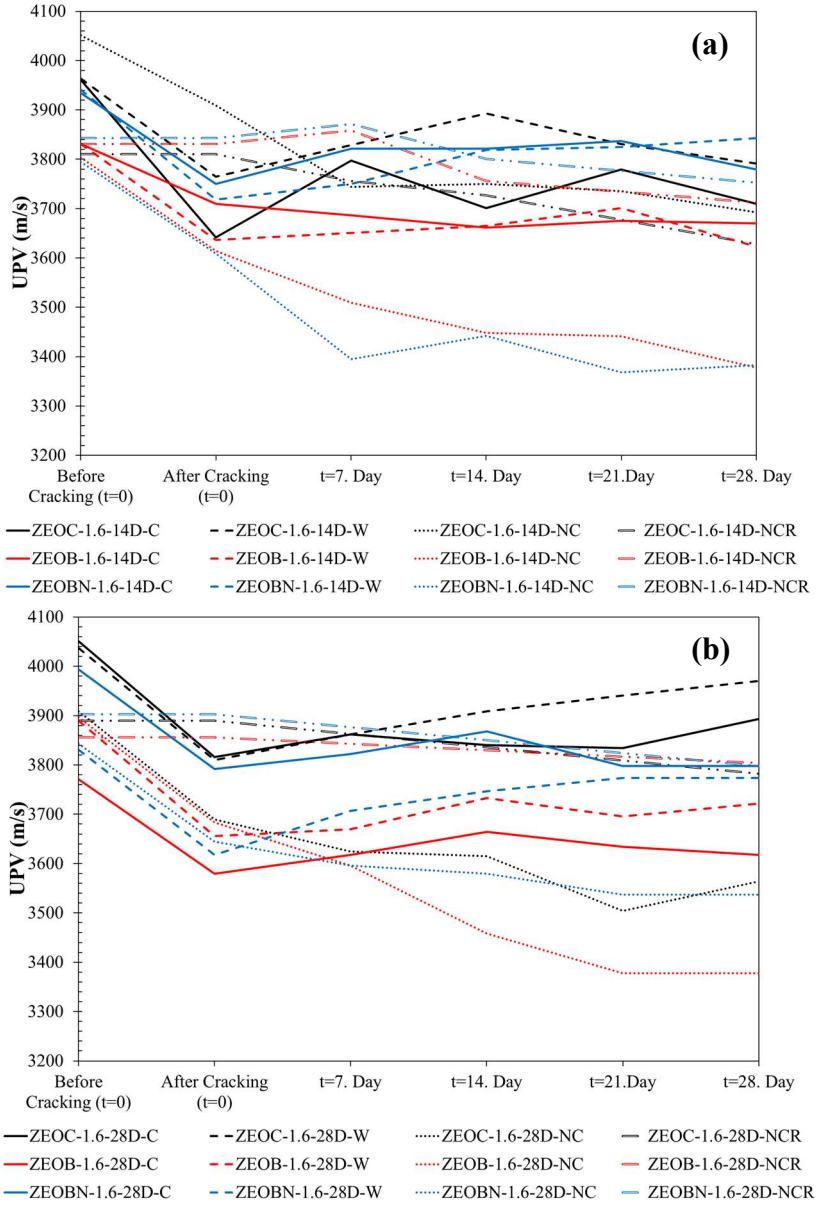

Figure 17: Ultrasonic pulse velocity changes of samples containing zeolite 1.6mm, after 28 days curing. (a) cracked on day 14th (b) cracked on day 28th. ZEO: zeolite, C: only includes minerals, B: mineral was saturated with bacterial cells and PBS, BN: half of mineral was saturated with bacterial cells and PBS and the other half of mineral was saturated with UCSL-CA, C: UCSL-CA nutrient medium curing, W: water curing, NC: at ambient conditions, NCR: no crack.

The crack healing performance of ZEO-1.6 was also quantified by the change in water absorption coefficient. Herein, slightly high-water absorption coefficients were observed in no cracked ZEO-1.6 samples. This could again be related to the degree of saturation of samples. A possible explanation for this result might be the unsaturated condition of specimens as it affected the UPV results. Generally, the decreases in water

absorption capacities were obtained in all series regardless curing type in comparation to corresponding no cure samples. Since there was not enough precipitate in ZEO-1.6 samples, it was not possible to conduct FTIR and SEM to the cracks surface.

All three evaluations for ZEO-1.6 series showed that immobilization of bacterial cells on ZEO-1.6 is not an efficient source for self-healing mechanisms. ZEO-200 is a more preferable protection barrier for the proposed biological additive.

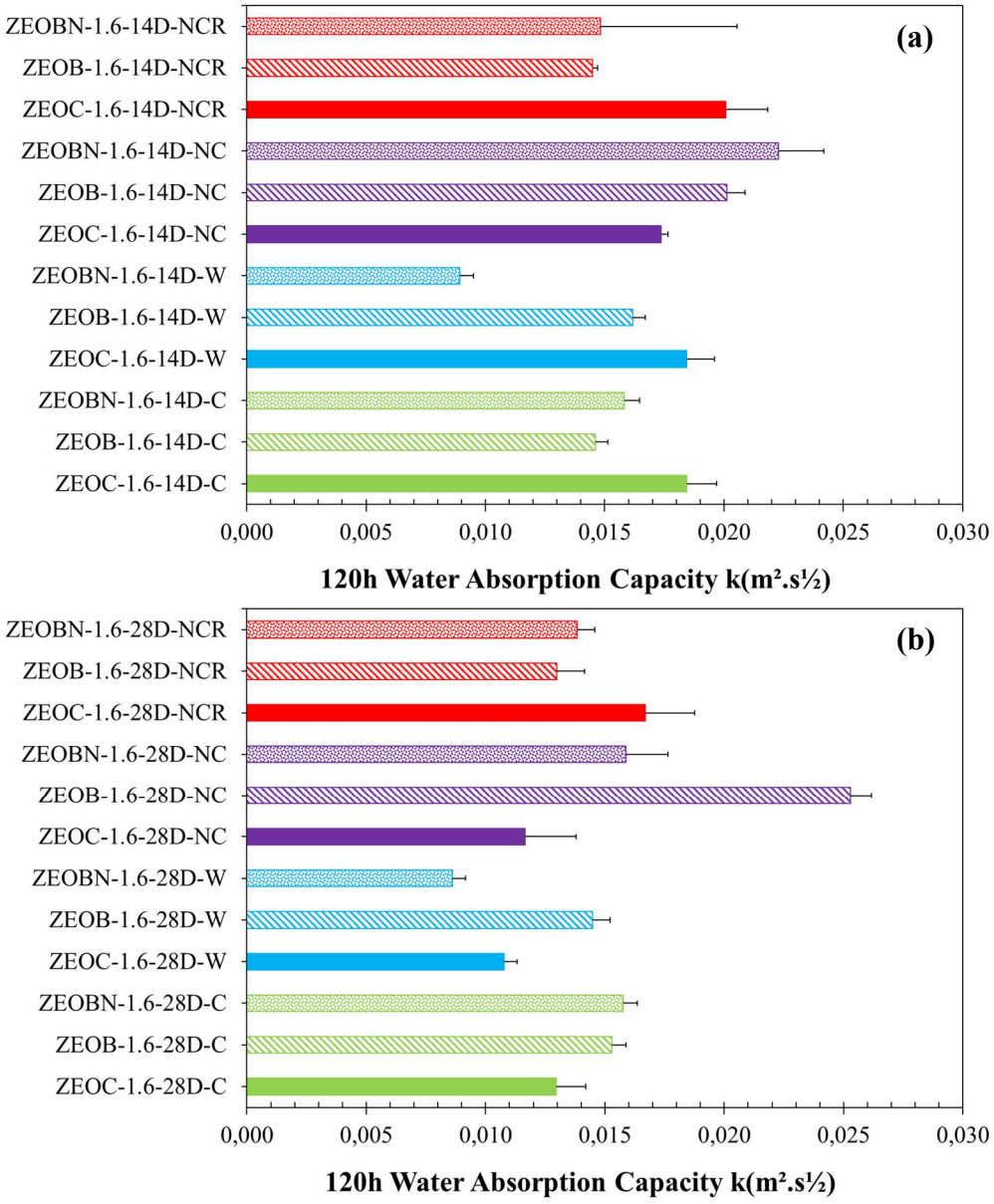

Figure 18: 120-hour water absorption capacities of samples containing zeolite 1.6mm, after 28 days curing. (a) cracked on day 14th (b) cracked on day 28th. ZEO: zeolite, C: only includes minerals, B: mineral was saturated with bacterial cells and

PBS, BN: half of mineral was saturated with bacterial cells and PBS and the other half of mineral was saturated with UCSL-CA, C: UCSL-CA nutrient medium curing, W: water curing, NC: at ambient conditions, NCR: no crack.

4.1.3 Use of perlite as a protection barrier:

Figures 19, 20 and 21 summarize the stereoscopy images obtained from samples prepared by immobilizing *S. pasteurii* on perlite (PERC, PERB and PERBN series). PERC samples exhibited a similar behavior with zeolites such that the control PERC sample exhibited a partial crack sealing. A difference that occurred in both ZEOC-1.6 and PERC samples compared to ZEOC-200 is both ZEOC-1.6 and PERC induced a higher % crack closure when they were cured in UCSL-CA medium rather than water curing (*see* Table 5 in section 4.1.1). But it was the opposite ZEOC-200 sample. Herein, it could be due to the different particle size of these 3 minerals. While ZEO-200 induces reactivity due to its fine particle size, ZEO-1.6 and PER acts as an internal curing reservoir. Based on their higher efficiency in UCSL-CA medium, it could be concluded that additional ions in the nutrient medium ($[Ca^{+2}]$, $[NO_3^-]$, etc.) might induce a reaction for precipitation.

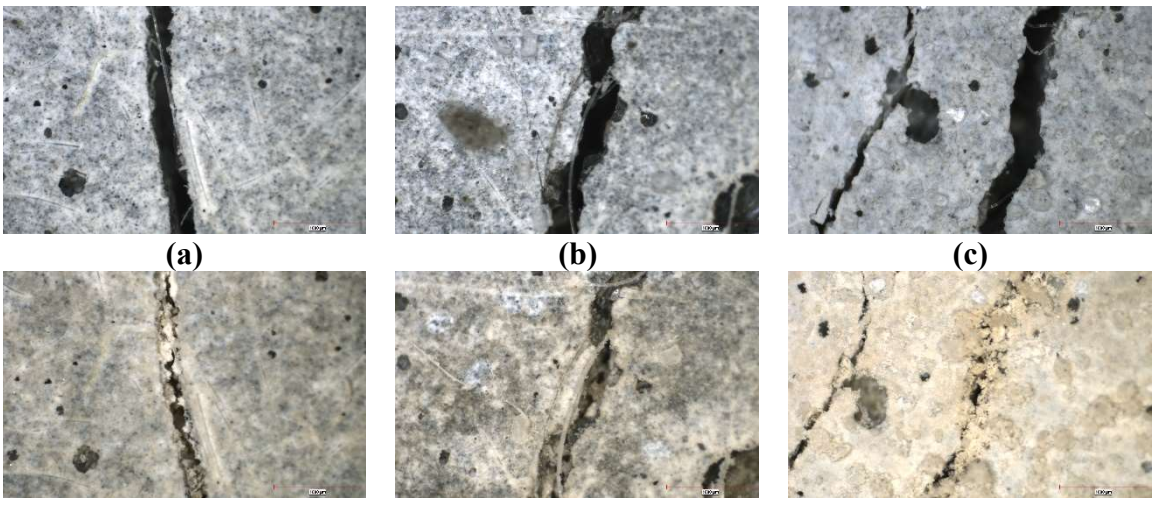

(a) **(b)** **(c)**

(d) **(e)** **(f)**

(g) (h) (i)

Figure 19: The crack images of 14-day old PERC samples (a, b, c) right after cracking, (d, e, f) after 7 days of UCSL-CA curing, (g, h, i) after 28 days of UCSL-CA curing.

Incorporation of bacterial cells in PERB sample did not affect the self-healing potential. In fact, the addition of cells PERB sample cured in UCSL-CA reduced the % crack sealing compared to PERC sample cured in UCSL-CA. This could be cells attached on the surface of perlite might consume [NO_3^-] which limits the crack healing %. It was evident that the cells did not trigger biomineralization. This suggests these ions might trigger a partial reactivity in perlite.

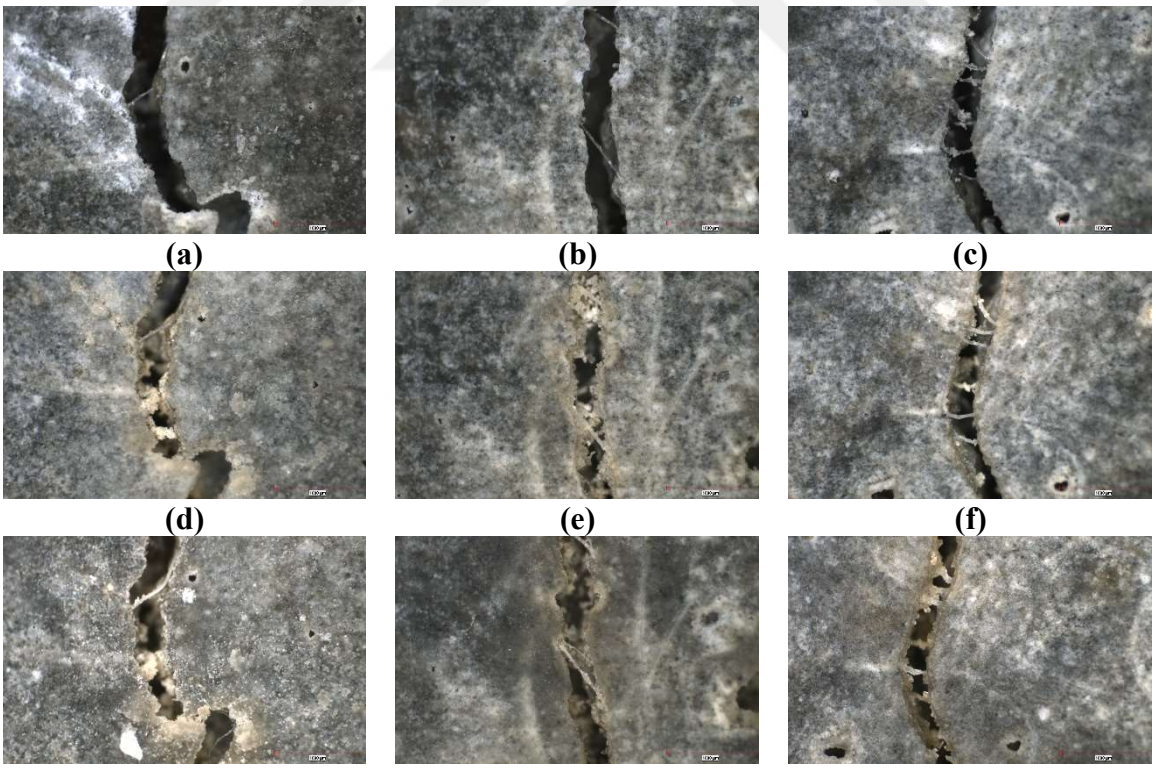

(a) (b) (c)

(d) (e) (f)

(g) (h) (i)

(j) (k) (l)

Figure 20: The crack images of 14-day old PERB samples (a, b, c) right after cracking, (d, e, f) after 7 days of UCSL-CA curing, (g, h, I) after 14 days of UCSL-CA curing, (j, k, l) after 28 days of UCSL-CA curing.

At last, addition of cells along with their nutrients in PERBN sample did not yield a significant change compared to PERB series, except 14-day old PERBN sample. Evaluating the results in perlite overall, the increase in 14-day old PERBN sample could also be due to the interaction the nutrient medium with the perlite rather than a possible biomineralization reaction.

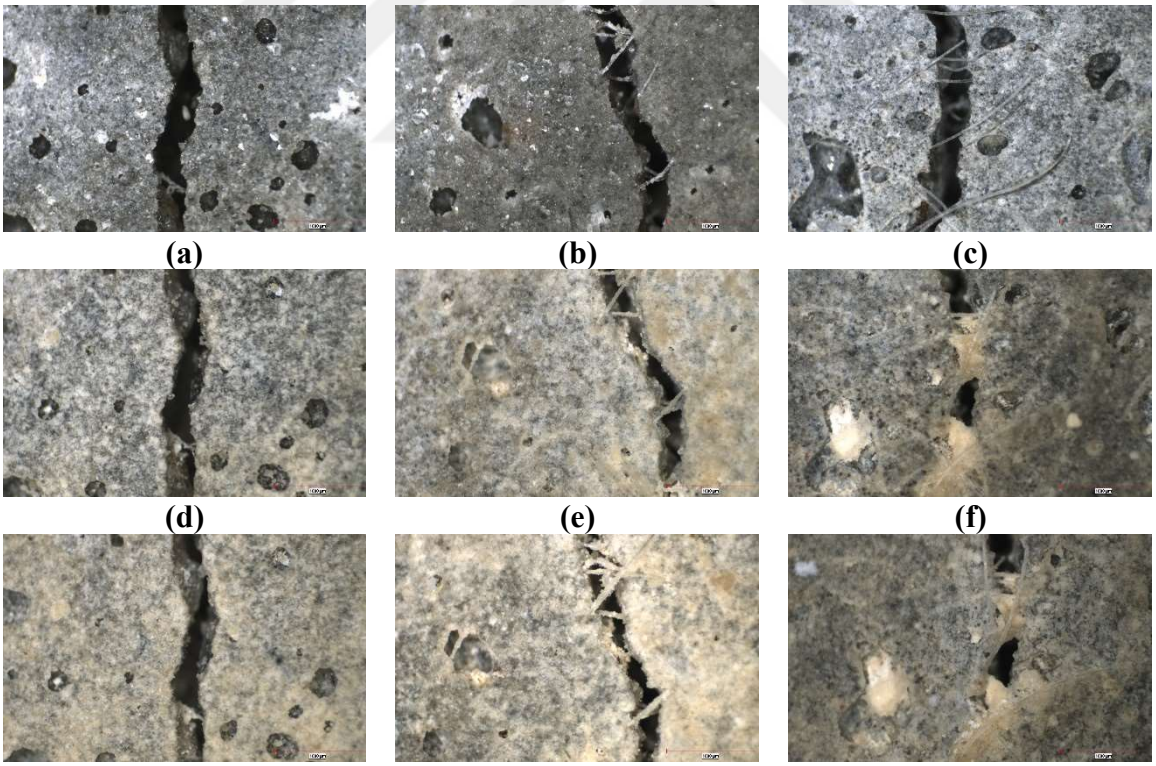

(a) (b) (c)

(d) (e) (f)

(g) (h) (i)

(j) **(k)** **(l)**

Figure 21: The crack images of 14-day old PERBN (a, b, c) right after cracking, (d, e, f) after 7 days of UCSL-CA curing, (g, h, I) after 21 days of UCSL-CA curing, (j, k, l) after 28 days of UCSL-CA curing.

The results obtained from UPV measurement of samples containing perlite cracked after 14- and 28-day are presented in Figure 22. The higher UPV change was observed in samples cured in UCSL-CA medium. Comparing the 14-day old PERC, PERB and PERBN sample cured in UCSL-CA medium, the highest UPV change was observed in PERBN sample. This is in line with the visual evaluation and also shows that the crack healing occurs through the depth of the crack. However, while the % crack closure was lower in water cured 14-day old PERBN sample compared to counterpart PERB and PERC sample, the UPV change in water cured 14-day old PERBN sample was the highest among these 3 samples. This again could be a validation of the interaction between the UCSL-CA medium and perlite. Since the nutrient medium was incorporated in the mix in BN series, the limited interaction between the ions and perlite might trigger a healing which might be localized around the UCSL-CA saturated perlite aggerate inside the mix. Further studies have to be done to understand the reaction mechanism of perlite at high pH and different ionic concentrations.

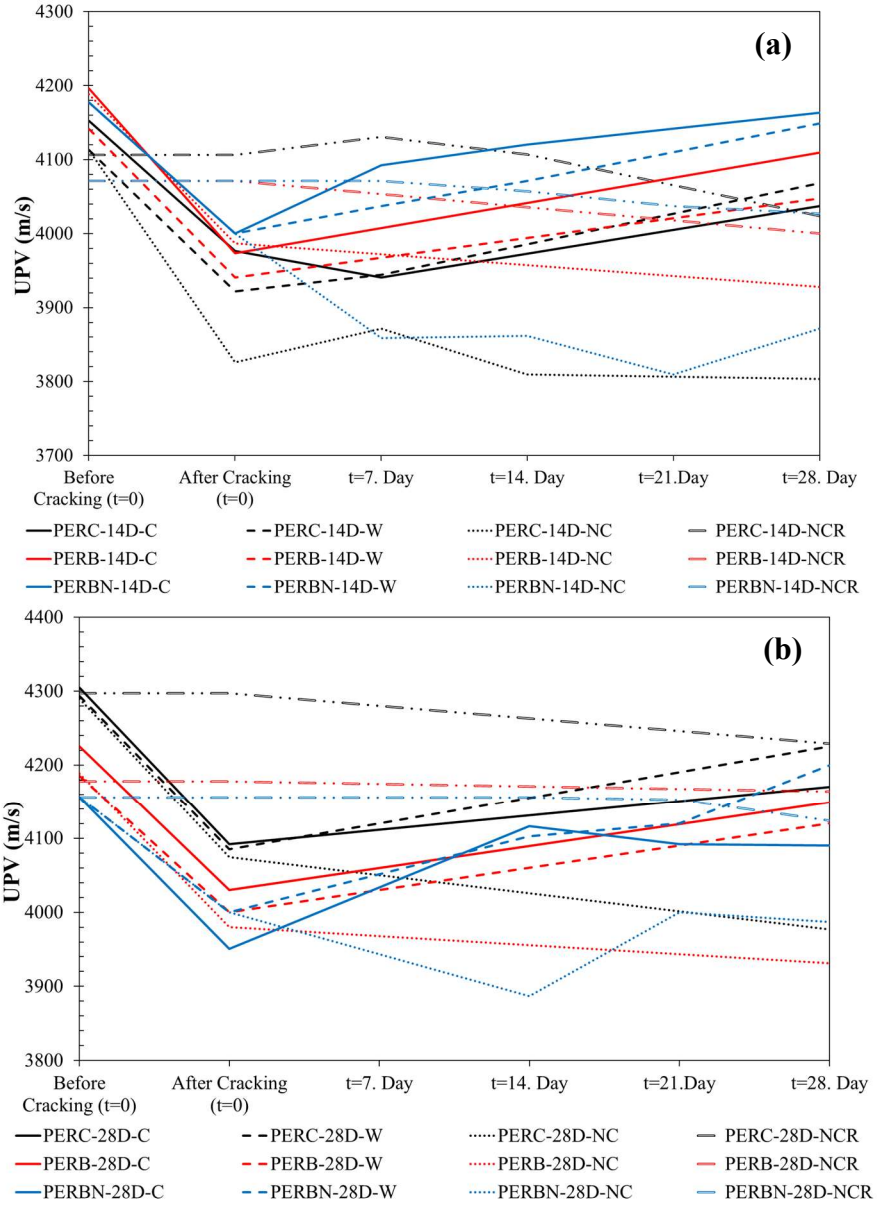

Figure 22: Ultrasonic pulse velocity changes of samples containing perlite, after 28 days curing. (a) cracked on day 14th (b) cracked on day 28th. PER: perlite, C: only includes minerals, B: mineral was saturated with bacterial cells and PBS, BN: half of mineral was saturated with bacterial cells and PBS and the other half of mineral was saturated with UCSL-CA, C: UCSL-CA nutrient medium curing, W: water curing, NC: at ambient conditions, NCR: no crack

Figure 23 summarizes the water absorption coefficient of perlite-based specimens. The application of water and nutrient curing decreased the water absorption capacity of specimens independent of bacteria content by 40% approximately. Similar to the stereomicroscopy and UPV evaluation, the reduction in water absorption capacity was more pronounced in 14-day old samples, particularly those cured in UCSL-CA medium.

Herein, we can conclude that even there was a limited amount of sealing occurred in these samples, it was able to plug the ingress of water. Based all these three evaluations for PER series showed that perlite is not a suitable bedding source for the bacterial cells to trigger self-healing.

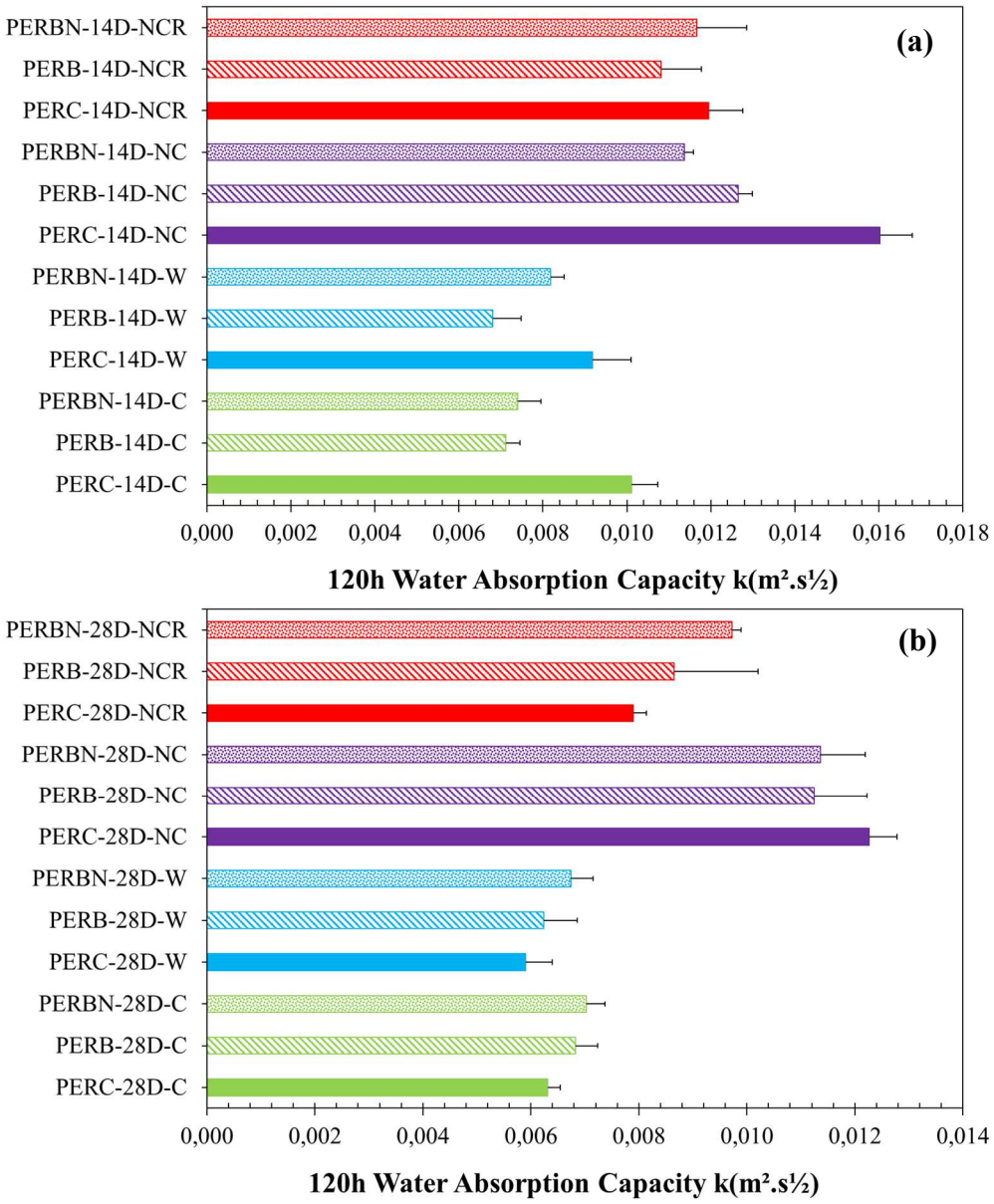

Figure 23: 120-hour water absorption capacities of samples containing perlite, after 28 days curing. (a) cracked on day 14th (b) cracked on day 28th. PER: perlite, C: only includes minerals, B: mineral was saturated with bacterial cells and PBS, BN: half of mineral was saturated with bacterial cells and PBS and the other half of mineral was saturated with UCSL-CA, C: UCSL-CA nutrient medium curing, W: water curing, NC: at ambient conditions, NCR: no crack.

4.1.4 Use of metakaolin as a protection barrier:

The stereoscopy images obtained from METC, METB and METBN series are shown in Figure 24, 25 and 26. The slight crack sealing was observed in METC samples. The crack sealing ratio in METC specimens was between the range of 20% to 15%. The sealing could be attributed to the pozzolanic reactivity of metakaolin which triggered to autogenous healing mechanism similar to ZEOC-200 specimens [64].

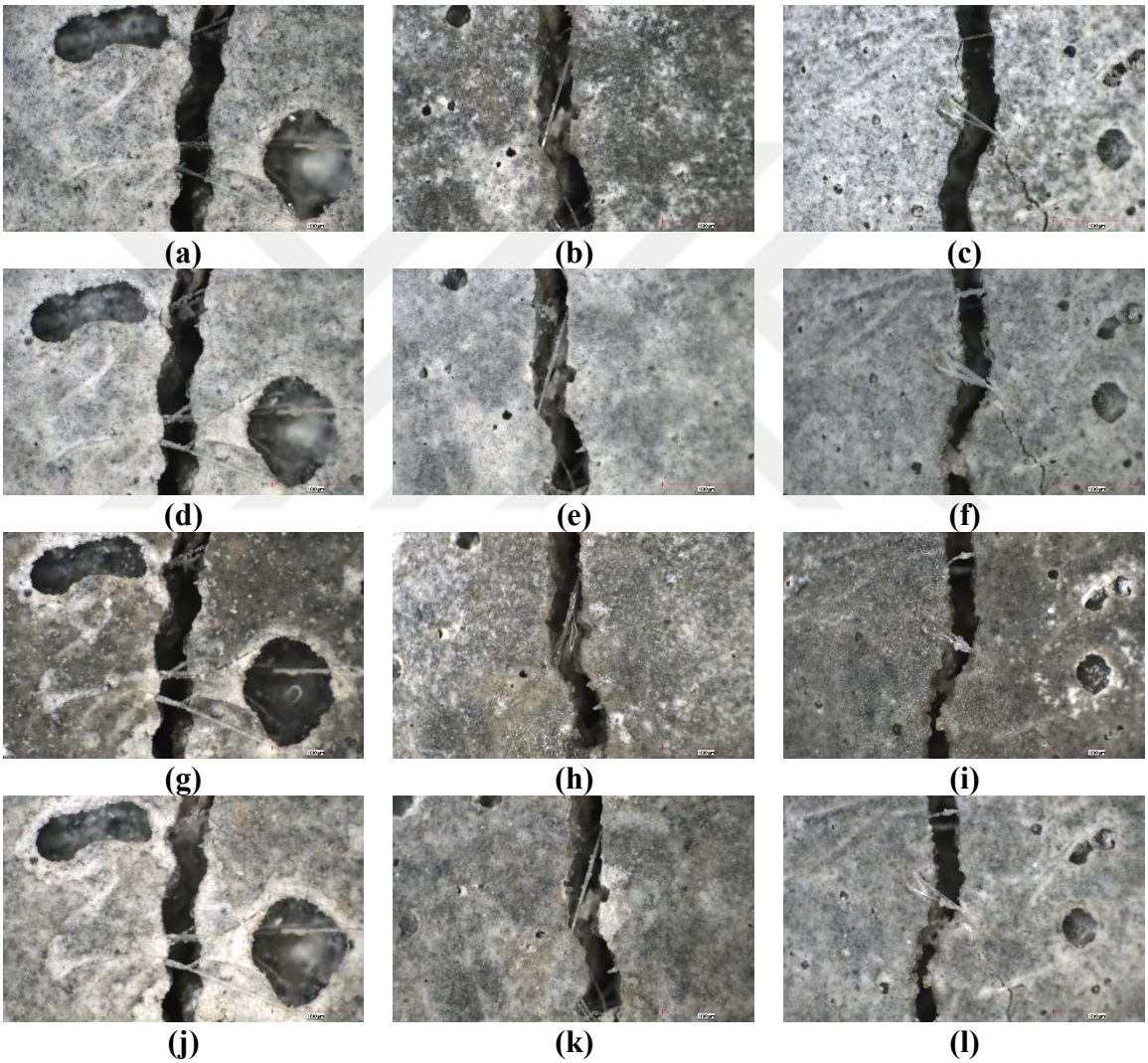

Figure 24: The crack images of 14-day old METC samples. (a, b, c) right after cracking, (d, e, f) after 7 days of water curing, (g, h, i) after 21 days of water curing, (j, k, l) after 28 days of water curing.

Inoculation of bacteria cells in metakaolin based samples was not effective to heal the cracks. However, when METC and METB samples were compared, slightly increased

in the crack closure was observed in METB samples. The crack closure rates of 14-day and 28-day old METB cured with UCSL-CA samples were 38% and 30%, respectively. Even it was insufficient to remediate the cracks in high ratio, the calcium carbonate was precipitated in small quantities by bacteria cells. The less efficient healing could be related to the pore size of metakaolin which might be not sufficient to absorb the bacteria cells. Since the bacteria cells were not immobilized on the protective barrier, they might be more incline to the high alkaline condition of the cement-matrix and consequently, the bacteria cells could not remain viable. This fact could also be seen by the comparison of METB samples cured with UCSL-CA and water separately.

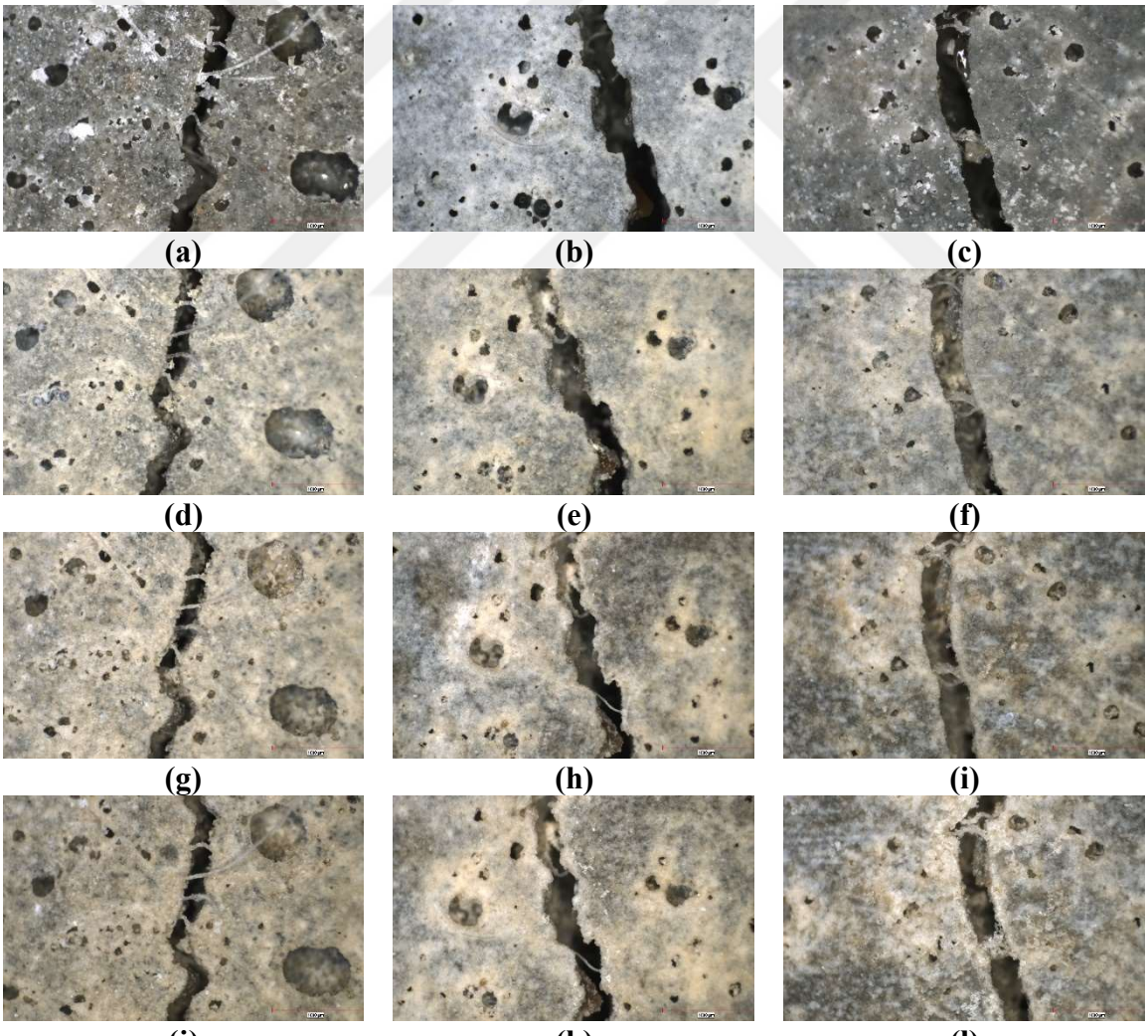

(m) (n) (o)

Figure 25: The crack images of 28-day old METB samples. (a, b, c) right after cracking, (d, e, f) after 7 days of UCSL-CA curing, (g, h, i) after 14 days of UCSL-CA curing, (j, k, l) after 21 days of UCSL-CA curing (m, n, o) after 28 days of UCSL-CA curing.

Lastly, METBN samples showed similar crack closure trend with METB samples. The crack closure rates of 14-day and 28-day old METBN cured with UCSL-CA samples were 25% and 33%, respectively. Therefore, the incorporation bacteria cells with their nutrients in METBN samples did not enhance the self-healing ability of biological additive. According to visual inspection, the maximum crack closure rate in MET samples was 38%. The crack closure rate results indicated that metakaolin based biological additive was not effective to heal the cracks.

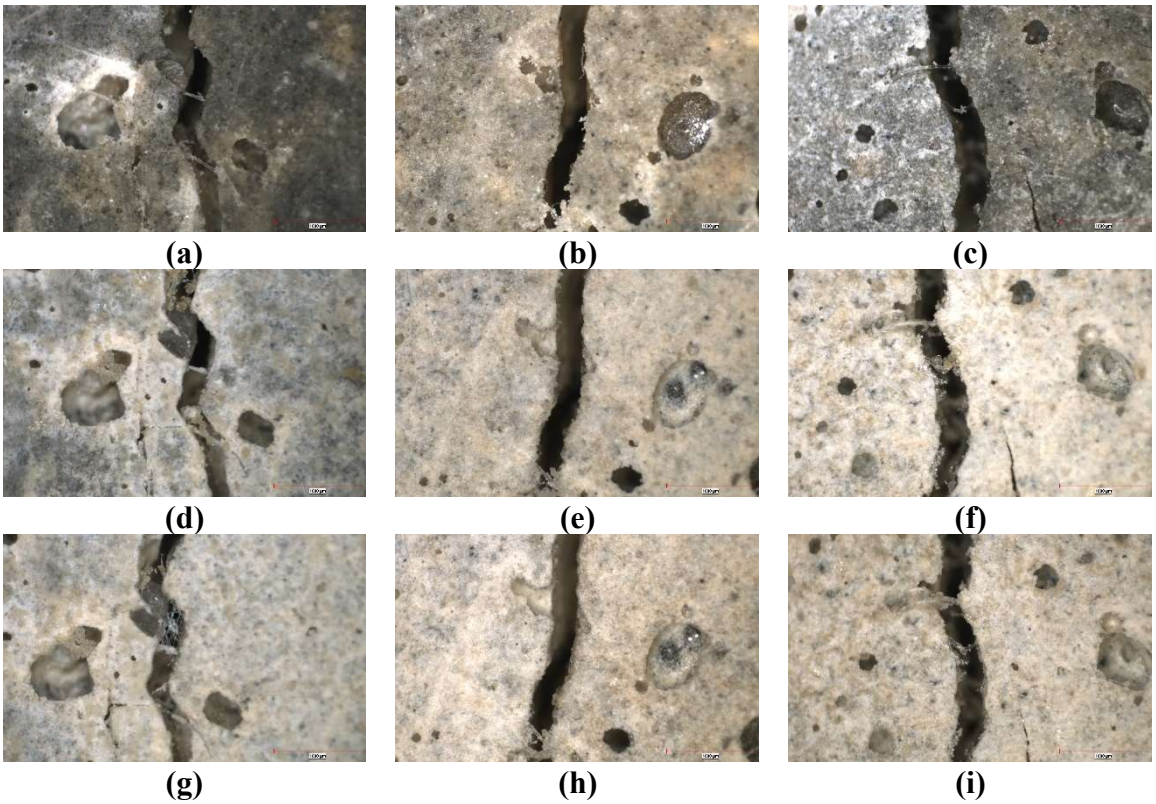

(a) (b) (c)

(d) (e) (f)

(g) (h) (i)

(j) **(k)** **(l)**

Figure 26: The crack images of 14-day old METBN samples. (a, b, c) right after cracking, (d, e, f) after 7 days of UCSL-CA curing, (g, h, i) after 14 days of UCSL-CA curing, (j, k, l) after 28 days of UCSL-CA curing.

Figure 27 shows the results of UPV measurements obtained from metakaolin based samples cracked after 14-day and 28-day. The higher UPV change was detected in 14-day old METC samples cured in nutrient medium and water. This again could be related to the pozzolanic reactivity of metakaolin. On the other hand, although the highest closure was measured in 14-day METB cured with UCSL-CA, no change in UPV of that sample was observed. Herein, it could be concluded that the amount of calcium carbonate precipitate was not enough to fill the cracks in samples including metakaolin.

Moreover, UPV changes of specimens cured with water or nutrient medium were almost same with specimens kept at ambient conditions. Hence, internal sealing observed in control specimens including zeolite and perlite especially cured with water, did not occur in specimens including metakaolin. This state could be attributed to the reduction effect of metakaolin on surface permeability of cement-based materials which prevents ingress of water and subsequently, the autogenous healing [65].

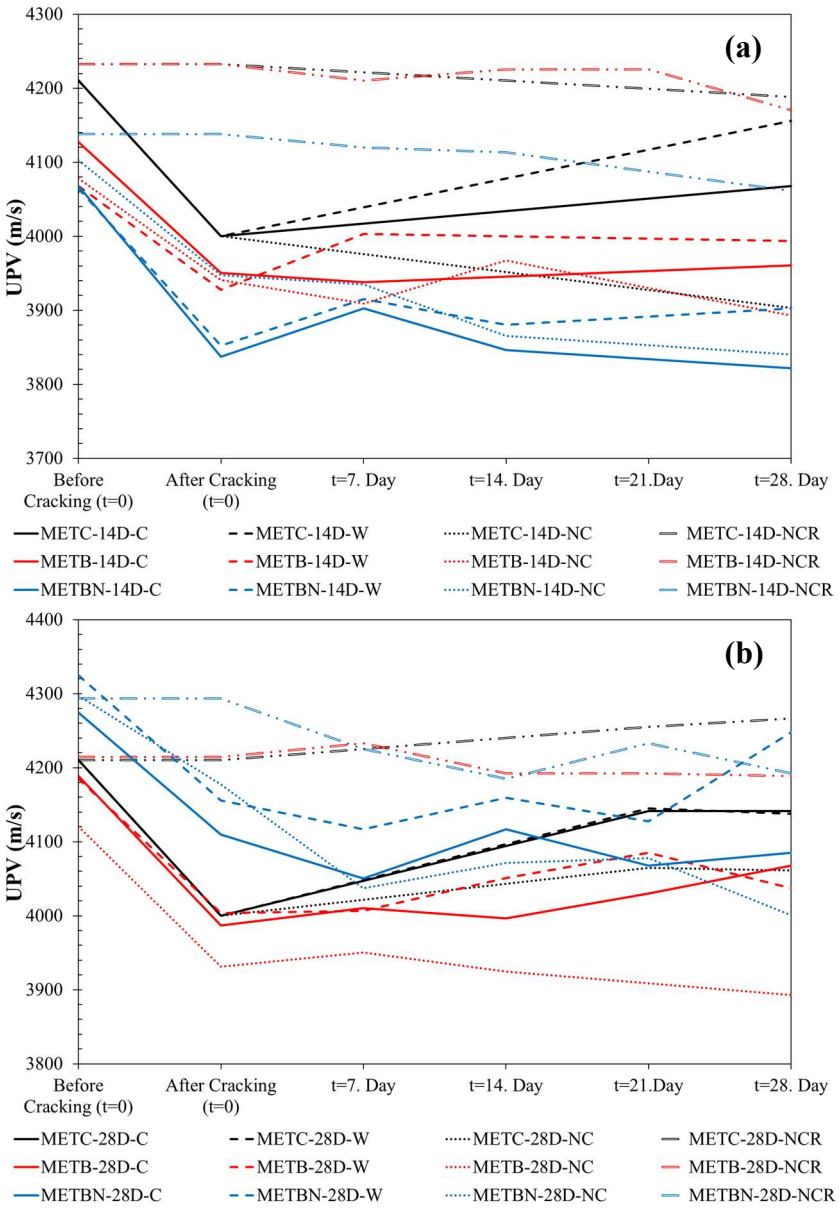

Figure 27: Ultrasonic pulse velocity changes of samples containing metakaolin, after 28 days curing. (a) cracked on day 14th (b) cracked on day 28th. MET: metakaolin, C: only includes minerals, B: mineral was saturated with bacterial cells and PBS, BN: half of mineral was saturated with bacterial cells and PBS and the other half of mineral was saturated with UCSL-CA, C: UCSL-CA nutrient medium curing, W: water curing, NC: at ambient conditions, NCR: no crack

The water absorption coefficients of metakaolin-based samples were presented in Figure 28. The distinct reduction in the water absorption was observed in METC samples. Especially, the water curing reduced the water absorption capacity of METC samples by approximately 40%. Again, this finding indicated the pozzolanic reactivity of metakaolin which triggered the autogenous healing in the cement mortar. In contrast with visual

inspection, the water absorption capacities of 14- day and 28-day old METB and METBN samples increased regard to corresponding samples kept at ambient conditions. Therefore, the results of the water absorption test indicates that the addition of metakaolin based biological additive has no sealing or healing impact on microcracks.

The findings of visual analysis, ultrasonic pulse velocity (UPV) test and the water absorption test shows that metakaolin is not a suitable bedding for bacteria cells. This result might be related to two different situations. Firstly, the metakaolin might not be a suitable protective barrier for bacteria cells regarding its pore structure. On the other hand, these inefficient crack sealing percentages might be due to limited curing time. Therefore, it is possible to acquire higher crack closures based on increase curing time.

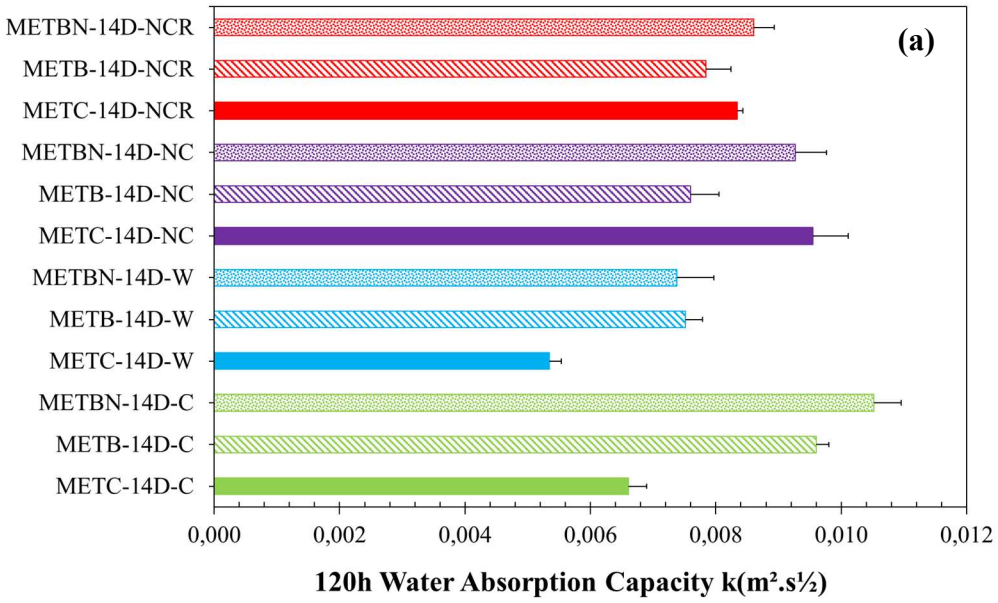

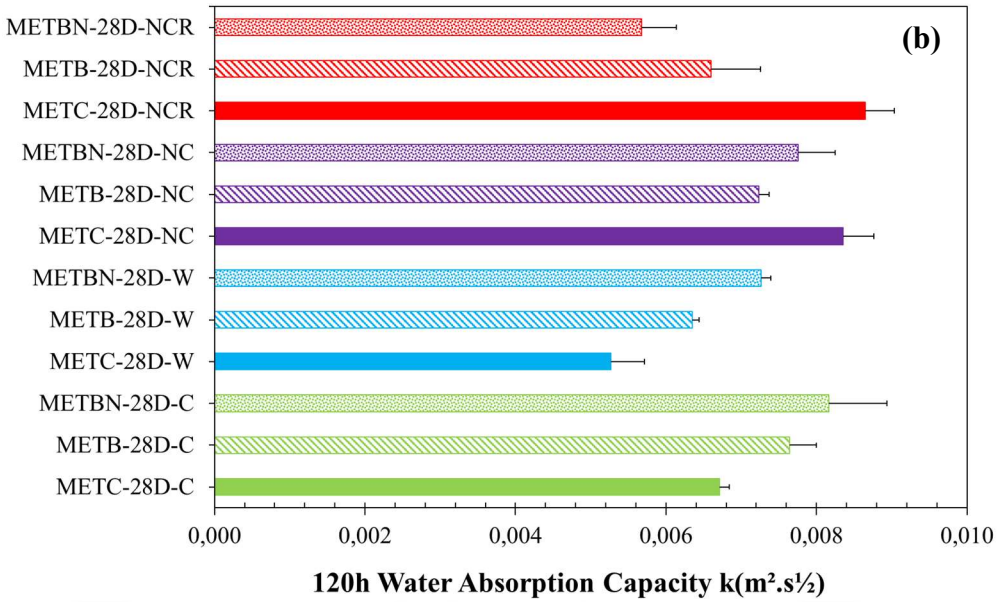

Figure 28: 120-hour water absorption capacities of samples containing metakaolin, after 28 days curing. (a) cracked on day 14th (b) cracked on day 28th. MET: metakaolin, C: only includes minerals, B: mineral was saturated with bacterial cells and PBS, BN: half of mineral was saturated with bacterial cells and PBS and the other half of mineral was saturated with UCSL-CA, C: UCSL-CA nutrient medium curing, W: water curing, NC: at ambient conditions, NCR: no crack

4.1.5 A comparative evaluation of mineral immobilization barriers:

While this study aims to use zeolite, metakaolin and perlite as protection barrier, a comparative evaluation was done for % crack healing for the previously used bentonite, sepiolite, diatomaceous earth, and pumice [42]. The % crack healing in each sample is summarized in Table 6.

Table 6: Crack closure rates %. BT: bentonite, DE: diatomaceous earth, SEP: sepiolite, ZEO: zeolite, PER: perlite, MET: metakaolin, PUM: pumice. C: only includes minerals, B: mineral was saturated with bacterial cells and PBS, BN: half of mineral was saturated with bacterial cells and PBS and the other half of mineral was saturated with UCSL-CA, UCSL-CA: nutrient medium curing, W: water curing, NC: at ambient conditions.

Crack Closure %						
Sample Name	**14. Day**			**28. Day**		
	UCSL-CA	**W**	**NC**	**UCSL-CA**	**W**	**NC**
BTC	25,08	0,74	-	34,92	1,86	-

DEC	6,06	6,52	-	2,78	0	-
SEPC	7,32	0,79	-	3,43	2,29	-
ZEOC-200	33,61	63,3	44,36	52,86	71,87	15,27
ZEOC-1.6	52,07	37,12	11,11	55,9	24,11	17,28
METC	20,05	12,91	10,35	15,83	9,57	16,81
PERC	42,39	17,73	3,2	32,6	8,69	4,73
PUMC	-	4,98	-	9,46	14,29	-
BTB	90,52	49,94	-	80,2	42,61	-
DEB	65,31	26,74	-	84,17	29,18	-
SEPB	92,81	25,79	-	68,06	53,3	-
ZEOB-200	84,19	23,6	15,05	69,55	61,48	13,77
ZEOB-1.6	37,1	30,43	2,27	34,55	23,3	12,64
METB	38,79	0,64	10,40	30,02	11,03	10,47
PERB	34,73	21,09	7,86	21,84	12,42	9,84
PUMB	81,38	22,1		84,4	17,25	-
BTBN	100	71,51	-	100	35,7	-
DEBN	100	68,69	-	96,8	45,98	-
SEPBN	94,54	48,58	-	100	17,08	-
ZEOBN-200	53,88	23,13	9,49	28,37	13,86	23,64
ZEOBN-1.6	40,16	43,02	29,14	29,65	24,65	23,19
METBN	25,7	8	15,11	33,42	17,03	8,36
PERBN	56,23	6,51	6,17	17,32	22,72	3,2
PUMBN	91,82	49,57	-	90,14	36,81	-

According to visual analysis, more than 80% crack sealing was observed in B and BN series (cured with UCSL-CA) samples including sepiolite, bentonite, diatomaceous earth, and pumice. In addition, the water absorption capacities of these samples were in the range of 0.002-0.003 equivalent to uncracked control samples [42]. Although, 84% crack closure was observed in 14-day old ZEOB-200 sample cured with UCSL-CA, this crack closure did not affect the water absorption capacity of sample. Herein, it was considered that the crack healing in ZEOB-200 sample was not based on bacteria, it was related to the reactivity of fine zeolite. On the other hand, the inefficient water absorption results of ZEOB-200 sample could be attributed to the precipitate triggered by zeolite was vaterite instead of stable calcite. Thus, shrinkage and corrosion tests were conducted with samples containing sepiolite, bentonite, diatomaceous earth, and pumice.

4.2 Performance evaluation of bio-based mortar samples

4.2.1 Evaluation of initial setting time

The impact of biological additive on the fresh state properties of mortar was examined in terms of initial setting time. Previous studies showed that addition of bacteria without any encapsulation increased the workability, at the same time increased the initial setting time significantly. This was attributed to the high sugar content in yeast extract used in the mixture [66]. Using CSL instead of yeast extract relatively reduced the negative impact on the initial setting time [23]. Within the scope of this study, the nutrient medium was only used in a very limited amount for BN series of samples. Figure 29 shows the initial setting times of 25 mixtures. Even though the cells and the nutrient medium were nor directly added to the mix water, they have a slight impact on the initial setting time if the immobilization barrier was not reactive such as zeolite-200 µm and metakaolin

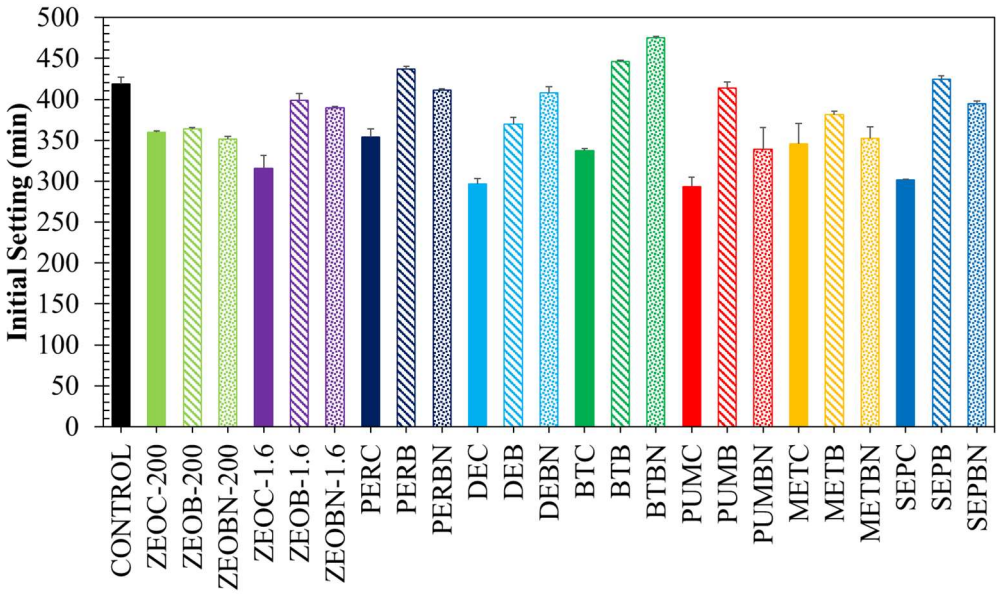

Figure 29: Vicat Needle test results. ZEO: zeolite, PER: perlite, DE: diatomaceous earth, BT: bentonite, PUM: pumice, MET: metakaolin, SEP: sepiolite, C: only includes minerals, B: mineral was saturated with bacterial cells and PBS, BN: half of mineral was saturated with bacterial cells and PBS and the other half of mineral was saturated with UCSL-CA.

Regardless of mineral type, the initial settings times of samples containing only mineral decreased by 20% compared to the control sample. It can be related to the reactivity of minerals which effects the reaction rate, like metakaolin and zeolite-200 μm and additionally the water holding properties of minerals retaining mix water, such as bentonite.

The influence of bacterial cells was more pronounced in samples containing non-reactive barriers. The initial setting time of B series samples for bentonite, sepiolite, pumice, perlite, zeolite-1.6 mm and diatomaceous earth showed a relatively longer setting times (a maximum of 35% increase) compared to their counterpart C series samples. For instance, the initial setting times of BTC and BTB samples were determined 337 and 446 min., respectively. Although, the addition of bacteria increased the initial setting time of sample including bentonite by 30%, the initial setting time of BTB sample increased by 7% compared to control sample. While the incorporation of cells increased the initial setting time, the use of nutrient medium in BN series samples did not yield a significant increase in setting compared to their counterpart B series samples. This indicates that the use of bacterial cells is the predominant parameter affecting the setting time rather than the use of nutrients. It should be noted that the influence of the nutrient medium was only seen when the bacterial cells were incorporated with their growth culture, so the nutrient medium was decomposed [66], [67]. Herein, the bacterial cells can carry ions from their growth culture (like sugars) and delay the initial set. The BN series of samples contains additional fresh nutrient and the bacterial cells collected from their growth culture. Therefore, the fresh nutrient medium did not impose an additional delay in the initial setting time.

4.2.2 Evaluation of compressive strength

The hardened performance of mortars containing biological additive were evaluated in terms of their compressive strength. Figure 30 summarizes the compressive strength of C, B and BN series specimens in reference to the negative control cement-based mortar without any mineral and bacteria. It should be noted that the results for sepiolite, diatomaceous earth, pumice and metakaolin were obtained from previous studies in our research group [68]. However, they are included in the analysis to establish an extended comparison among the protection barriers.

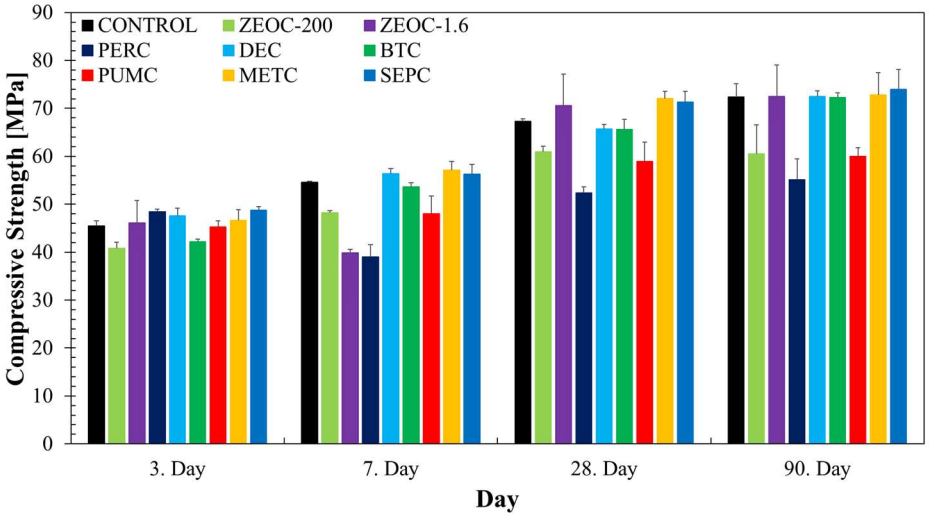

(a)

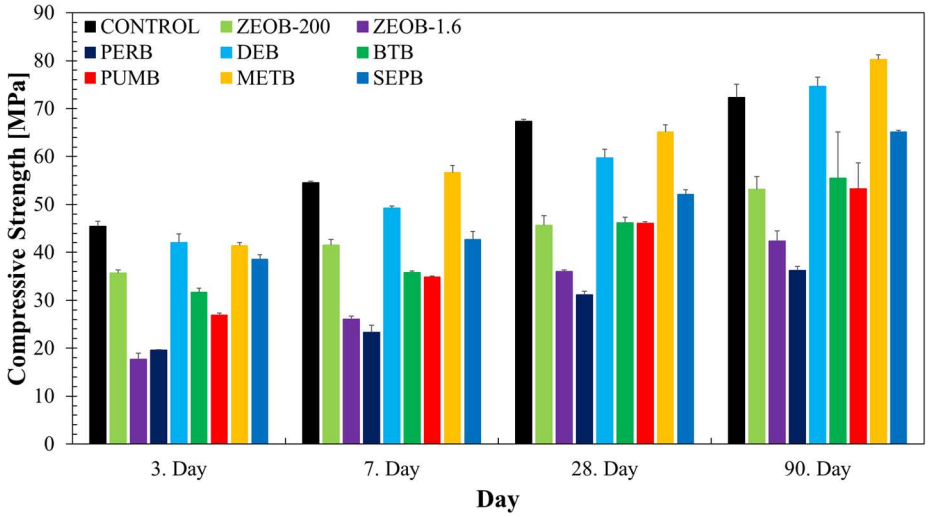

(b)

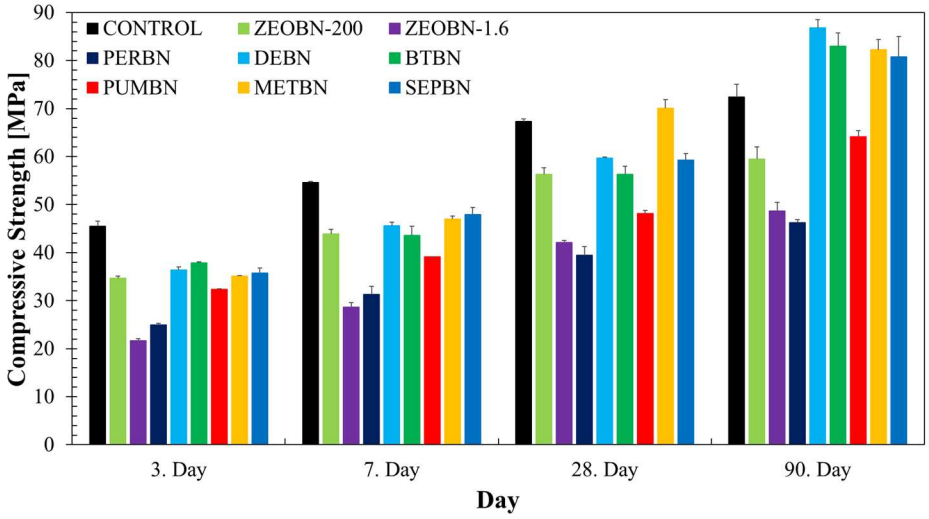

(c)

Figure 30: Compressive Strength test result. [68] (a) C series samples (b) B series samples (c) BN series samples. ZEO: zeolite, PER: perlite, DE: diatomaceous earth, BT: bentonite, PUM: pumice, MET: metakaolin, SEP: sepiolite, C: only includes minerals, B: mineral was saturated with bacterial cells and PBS, BN: half of mineral was saturated with bacterial cells and PBS and the other half of mineral was saturated with UCSL-CA.

While the mineral addition had no negative impact on the compressive strength, a decrease was observed in compressive strength of B and BN series specimens compared to their counterpart C series samples. The maximum decrease in compressive strength was observed in samples containing zeolite (1.6mm), pumice and perlite. The decrease in the compressive strength was attributed to the replacement of normal weight sand with saturated lightweight aggregate in the mix design. However, the addition of bacteria into the mixture also induced an additional a in the compressive strength at B series specimens, regardless of mineral type. This could again be related to presence of ions on the cells from the decomposed growth culture, decreasing the rate of hardening in the mortar samples.

Moreover, the decrease in compressive strength at BN series samples was slightly less pronounced than at B series samples except the samples containing diatomaceous earth and metakaolin. Table 7 summarizes the % change in compressive strength of each

sample compared to the negative control sample without any minerals and bacterial cells. For instance, while 30% decrease was observed in 3-day compressive strength of BTB sample, the reduction was determined by 17% in 3-day compressive strength of BTBN sample. Similarly, while 30% decrease was observed in 28-day compressive strength of BTB sample, the reduction was determined by 16% in 28-day compressive strength of BTBN sample. This difference could be explained by the precipitation of CaCO3 in consequence of the limited UCSL-CA nutrient medium [67].

For the C series specimens, although the addition of diatomaceous earth, metakaolin and sepiolite partially increased the compressive strength, adding bacteria and nutrient medium into the mixture decreased their impact and correspondingly decreased the compressive strength. However, while this impact was mostly observed in 3-day and 7-day compressive strengths, at rate of 10% increase in comparation to control sample was observed in the 28- day and following. Even, the increase was determined by 20% in the 90- day compressive strength of DEBN sample. Accordingly, the bacteria addition was only effective on early-stage compressive strength, and which was found to be less than 30%.

According to the compressive strength test results, the biological additive prepared with fine mineral has a lower impact on the compressive strength compared to that of what was observed in samples containing lightweight aggregate. Even though, the addition of bacteria into mixture affected the early-stage compressive strength negatively, this effect was reduced in time. When the 28-day compressive strength results were evaluated, BN series biological additive developed with fine mineral caused the reduction less than 20% in the compressive strength. Further, there was an increase in the 90-day compressive strength in comparison with control sample. Therefore, it was concluded that

the biological additive has no significant impact on the hardened performance in the long term.

Table 7: The variation at the compressive strength with respect to cement-based mortar without any mineral and bacteria. ZEO: zeolite, PER: perlite, DE: diatomaceous earth, BT: bentonite, PUM: pumice, MET: metakaolin, SEP: sepiolite, C: only includes minerals, B: mineral was saturated with bacterial cells and PBS, BN: half of mineral was saturated with bacterial cells and PBS and the other half of mineral was saturated with UCSL-CA.

Sample Name	3. Day	7. Day	28. Day	90. Day
Control	0%	0%	0%	0%
BTC	-7%	-2%	-3%	0%
DEC	5%	3%	-2%	0%
SEPC	7%	3%	6%	2%
ZEOC-200	-10%	-12%	-9%	-16%
ZEOC-1.6	1%	-27%	5%	0%
METC	2%	5%	7%	1%
PERC	7%	-29%	-22%	-24%
PUMC	0%	-12%	-12%	-17%
BTB	-30%	-34%	-31%	-23%
DEB	-7%	-10%	-11%	3%
SEPB	-15%	-22%	-23%	-10%
ZEOB-200	-22%	-24%	-32%	-27%
ZEOB-1.6	-61%	-52%	-47%	-41%
METB	-9%	4%	-3%	11%
PERB	-57%	-57%	-54%	-50%
PUMB	-41%	-36%	-32%	-26%
BTBN	-17%	-20%	-16%	15%
DEBN	-20%	-17%	-11%	20%
SEPBN	-22%	-12%	-12%	12%
ZEOBN-200	-24%	-20%	-16%	-18%
ZEOBN-1.6	-52%	-47%	-37%	-33%
METBN	-23%	-14%	4%	14%
PERBN	-45%	-43%	-41%	-36%
PUMBN	-29%	-28%	-29%	-11%

4.3 Influence of biological additive on free drying shrinkage

The influence of biological additive on free drying shrinkage was evaluated at a relative humidity of 50% and 23° C. In order to evaluate the impact of incorporating bacteria and mineral on the shrinkage of cement-based mortars separately, both C and BN series

specimens were casted. Herein, C and BN series specimens for biological additive containing diatomaceous earth, bentonite, sepiolite, and pumice were casted. These series were selected based on their relatively higher efficiency in visual crack healing as well as reducing the water absorption capacity (*see* Section 4.1.5).

Figure 31 and Figure 32 represent the drying % shrinkage in mortar samples. It was seen that the addition of minerals increased the % strain due to drying shrinkage compared to the control sample. The impact of mineral addition on the drying shrinkage can be due to the higher water absorption capacities of minerals which entraps the water content during mixing. Another possible explanation could be the pozzolanic reactivity of minerals [51]. Previous studies on evaluating the effects of clays on the performance of concrete showed that addition of montmorillonite by 4% of weight of cement showed a similar behavior and resulted with a higher increased drying shrinkage % [69]. The values obtained with montmorillonite was found to be very similar to bentonite used in this study. In fact, montmorillonite and bentonite are very similar, such that they have a high absorption capacity. Higher absorption rate of these clays can increase the drying shrinkage when they were used in cement-based systems. Throughout the literature, it was demonstrated that addition of 2% clay could increase the drying shrinkage due to the high-water adsorption of clays [70].

Other minerals used in this study, as diatomaceous earth, sepiolite, zeolite, and metakaolin could be classified as clays or clayey minerals. Therefore, they all have a tendency to interact with water [71]–[73]. The higher water absorption capacities of bentonite, diatomaceous earth, sepiolite, pumice, and zeolite used in this study were determined as 300%, 110%, 80%, 45% and 25% respectively [42]. According to water absorption capacities of natural minerals, it was expected that the higher shrinkage rate would occur in sample including bentonite and the lower shrinkage occurred in sample

containing zeolite. Except, zeolite this theory holds true (Figure 32). However, ZEOC sample exhibited almost the highest drying shrinkage % upon 112 days of observation. Moreover, while the shrinkage of samples including pumice and zeolite occurred in two weeks and then remained stable, significant increase in the shrinkage of samples containing bentonite and diatomaceous earth was observed approximately in the end of two months. Additional evaluation has to be done to further understand how the characteristics of minerals affect the water interaction and shrinkage of the material.

The impact of incorporating bacteria on shrinkage showed different results regarding mineral type. While adding bacteria increased shrinkage of samples including sepiolite and bentonite, shrinkage of sample including diatomaceous earth decreased. The decrease in shrinkage of DEBN sample could be explained by compressive strength results. The 20% increase in compressive strength in comparison to 90-day C series samples was observed in DEBN sample. Even similar trend in compressive strength was obtained in SEPBN and BTBN, such that the addition of bacteria cells increased shrinkage. Therefore, it was understood that the only factor affected shrinkage is not the compressive strength.

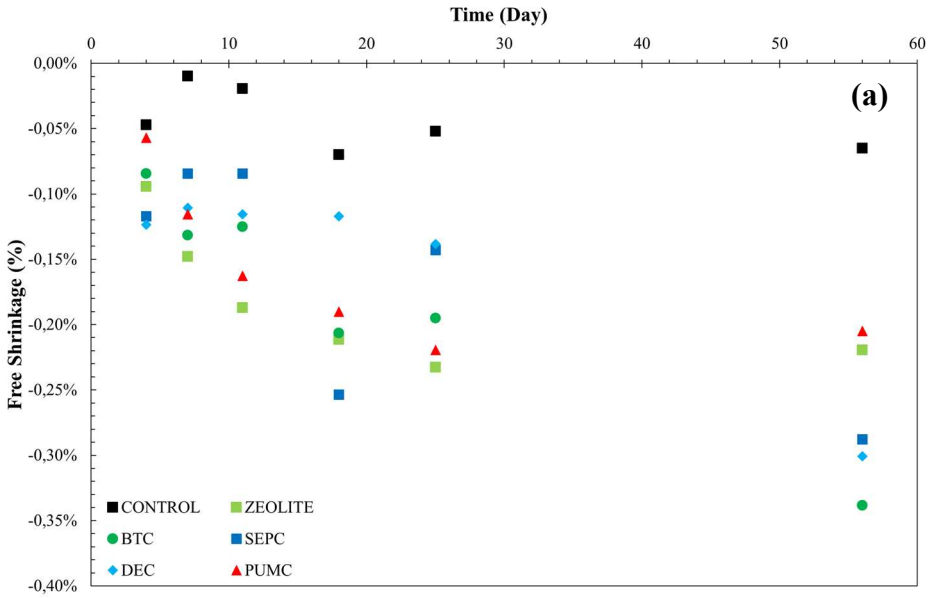

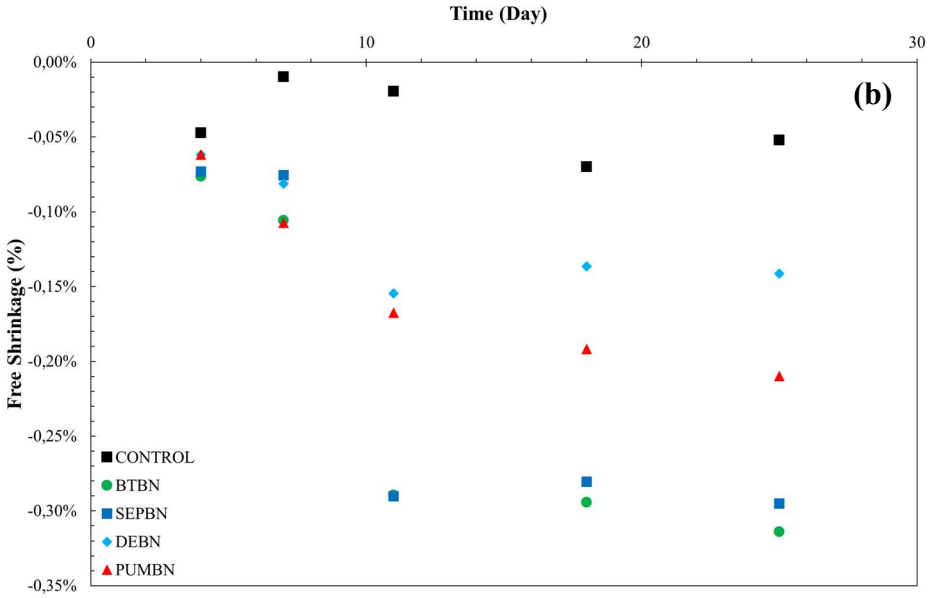

Figure 31: Free shrinkage by time. (a) C series (b) BN series. DE: diatomaceous earth, BT: bentonite, PUM: pumice, SEP: sepiolite, C: only includes minerals, BN: half of mineral was saturated with bacterial cells and PBS and the other half of mineral was saturated with UCSL-CA.

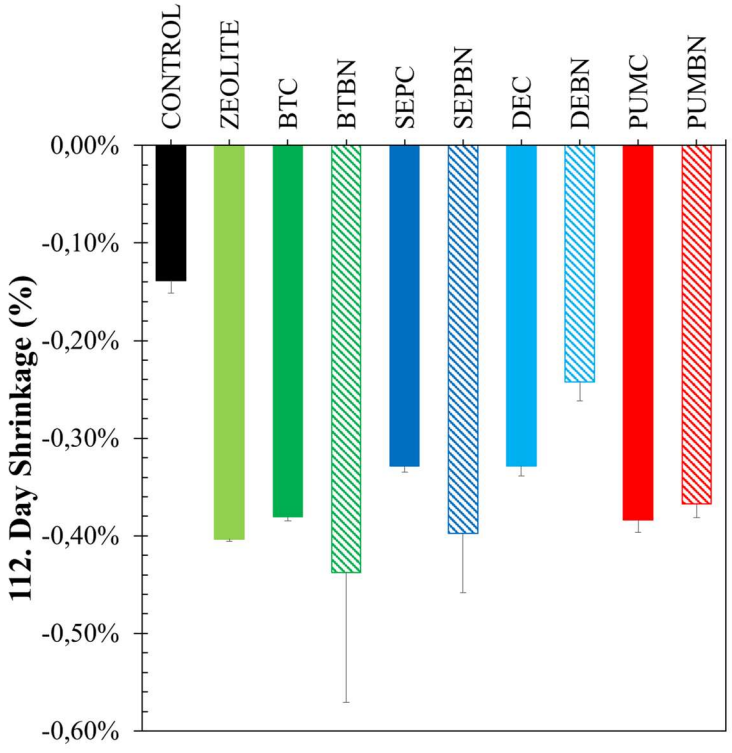

Figure 32: The change of length after 112 days. DE: diatomaceous earth, BT: bentonite, PUM: pumice, SEP: sepiolite, C: only includes minerals, BN: half of mineral was saturated with bacterial cells and PBS and the other half of mineral was saturated with UCSL-CA.

The weight loss of specimen means the water loss in cement-based mortars. According to Figure 33 and Figure 34, it was seen that the weight loss was not consistent with the results of length change. While control sample showed the lowest shrinkage in comparison with samples including mineral, it exhibited a higher weight loss than the samples including minerals. Hence, it could be said that the drying shrinkage is not due to the loss of water in the cement-based mortar. This finding was also reported by the prior study related to alkali-activated slag concrete and it was attributed the drying shrinkage to the pore size distribution and the qualification of the calcium silicate hydrate gel [74].

The addition of bacteria cells into the cementitious matrix increased the amount of weight loss in samples except sample containing pumice. It could be attributed to saturated minerals due to immobilization of bacteria cells and nutrient mediums. As abovementioned, further analysis has to be done to evaluate the pore size distribution, the chemistry and the pozzolanic reactivity of minerals affect shrinkage mechanism.

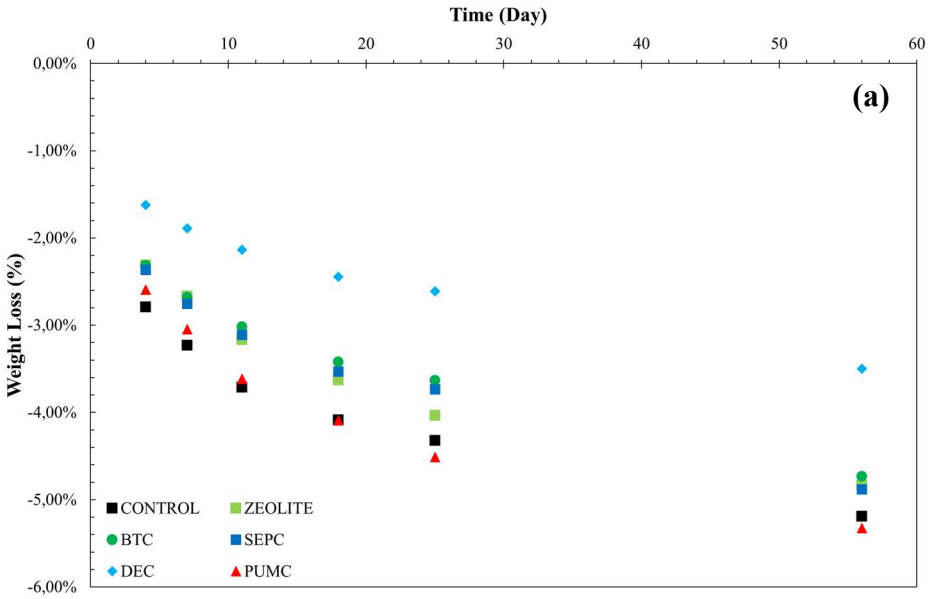

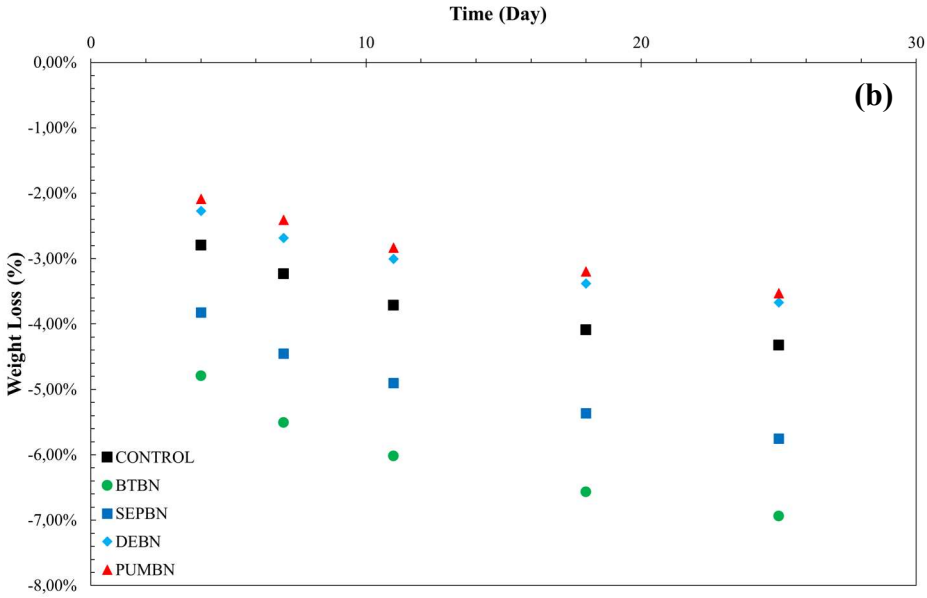

Figure 33: Weight loss by time. (a) C series (b) BN series. DE: diatomaceous earth, BT: bentonite, PUM: pumice, SEP: sepiolite, C: only includes minerals, BN: half of mineral was saturated with bacterial cells and PBS and the other half of mineral was saturated with UCSL-CA.

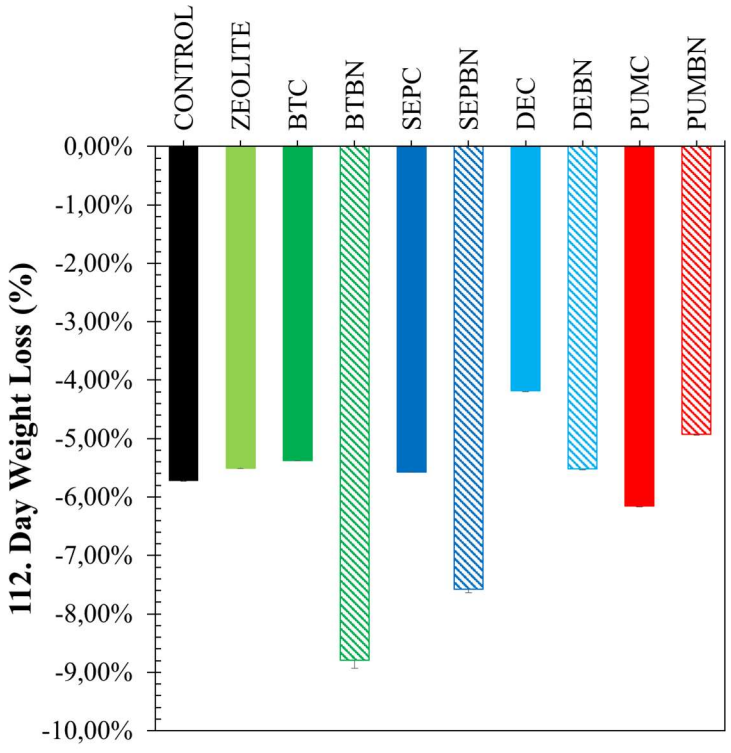

Figure 34: The change of weight after 112 days. DE: diatomaceous earth, BT: bentonite, PUM: pumice, SEP: sepiolite, C: only includes minerals, BN: half of mineral was saturated with bacterial cells and PBS and the other half of mineral was saturated with UCSL-CA.

4.4 Effects of crack sealing on corrosion resistance

At last, the influence of self-healing on corrosion resistance was evaluated. Similar to the drying shrinkage assessment, mortar samples were casted by using biological additive containing diatomaceous earth, sepiolite, bentonite, and pumice. Additionally, sample including zeolite without bacteria was also included in this analysis due its possible potential as an internal curing reservoir. Table 8 summarizes the electrical current measurements of the self-healed mortar samples after accelerated corrosion test.

Table 8: Assessment of corrosion by current measurement after crack healing. DE: diatomaceous earth, BT: bentonite, PUM: pumice, SEP: sepiolite, C: only includes minerals, BN: half of mineral was saturated with bacterial cells and PBS and the other half of mineral was saturated with UCSL-CA.

Sample Name	mV	Result
CONTROL	-605.23 ± 6.90	Corroded
SEPC	-518.10 ± 93.13	Corroded
SEPBN	-500.33 ± 150.80	Corroded
BTC	-590.20 ± 112.31	Corroded
BTBN	-634.53 ± 34.04	Corroded
DEC	-246.33 ± 22.84	Uncertain
DEBN	-632.47 ± 17.51	Corroded
PUMC	-272.13 ± 31.15	Uncertain
PUMBN	-623.00 ± 21.71	Corroded

Based on the results obtained from current measurements, it was determined that the rebars in the mortar samples were corroded in all samples regardless of the sample was healed or not, except those were in DEC and PUMC samples. The current measurements obtained from the DEC and PUMC did not provide clear information about the state of the rebar. The initial non-destructive measurements indicated that the crack healing by biomineralizations does not prevent corrosion. These findings contradict other studies in the literature [15], [54].

After the non-destructive evaluation of corrosion in the samples, a direct tensile strength test was applied to the rebars in the mortar samples. Figure 29 summarizes the tensile strength results obtained from the possibly corroded rebars. Herein, almost all the samples exhibited a relatively same tensile strength, except the negative control without any biological additive. The tensile strength of the rebars in the negative control samples (cracked but there was no self-healing) were 20% lower than the rest of the samples. On the other hand, these values were more than what was expected in a corroded rebar.

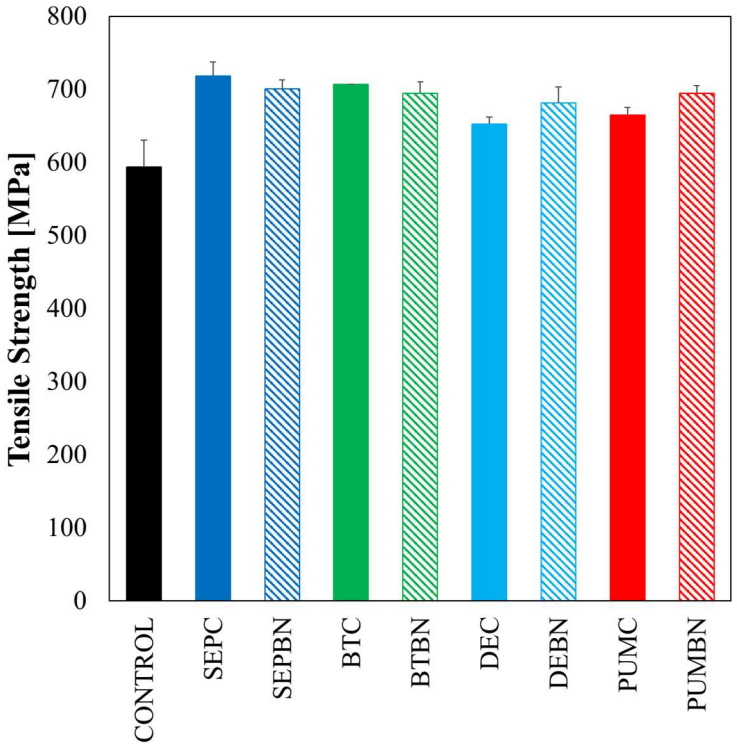

Figure 35: The tensile strength results after accelerated corrosion test**.** DE: diatomaceous earth, BT: bentonite, PUM: pumice, SEP: sepiolite, C: only includes minerals, BN: half of mineral was saturated with bacterial cells and PBS and the other half of mineral was saturated with UCSL-CA.

Upon tensile testing, the samples were broken into 2 pieces, and it was understood that the measurements in Table 8 were misleading. Herein, there was not any corrosion occurred in the rebars (Figure 42). This shows that the experimental process did not provide accurate results. It was understood that under these conditions, the samples should be subjected to wetting and drying cycles of NaCl solution for a longer time. At

this stage, it is necessary to develop a more reliable method to assess corrosion in these samples. Therefore, a new set series of mortars were casted and subjected to self-healing in our ongoing progress. However, the w/c ratio of these samples were kept at 0.6 to increase the permeability and decrease the quality of mortar to trigger corrosion. Upon self-healing, these samples will be subjected wetting and drying cycles of NaCl solution, and the solution will be refreshed in each cycle to increase the rate of Cl- ion penetration. The on-going works are presented in Appendix C.

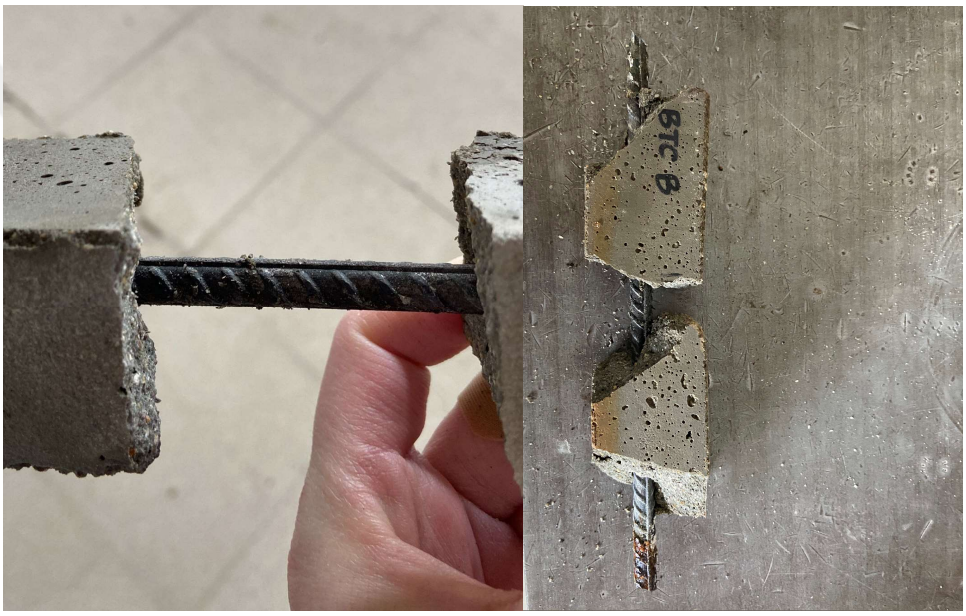

Figure 36: Conditions of rebars after the accelerated corrosion test

CHAPTER V

CONCLUSION AND FUTURE STUDIES

5.1 Key findings of the study

In this study, it was tried to develop a biological additive by immobilizing *sporosarcina pasteurii* vegetative cells on natural minerals to provide a self-healing mechanism in cement-based mortars. Zeolite, metakaolin and perlite were used to immobilize bacteria cells. The biological additive obtained by submerging minerals to bacteria cells and nutrient medium was added to cement-based mortar. After 14- and 28-days casting, 0.30-0.60 mm width cracks were formed, and subsequently crack healing was observed for 4 weeks. Samples were kept in three different conditions: UCSL-CA nutrient medium curing, water curing and ambient conditions. Crack remediation was monitored by stereomicroscope analysis and ultrasonic pulse velocity (UPV) test. After the completion of 4 weeks curing process, the water absorption capacities of specimens were measured and the characterization of precipitation in the crack zone was done. Finally, the impact of the biological additive on the drying shrinkage and the corrosion was tested.

The key findings of the study can be listed as follows:

- Zeolite-200 μm was found to be efficient in terms of sealing the cracks even without bacterial cells. The % crack healing was 70% ZEOC-200 samples cured with water. This was mainly attributed to the pozzolanic reactivity of fine zeolite particles.

- Incorporation of bacterial cells to this system (ZEOB-200) led to a higher degree of visual crack sealing which was attributed to additional biomineralization occurs along with the pozzolanic activity. Yet, incorporation of UCSL-CA medium in the mix (ZEOBN-200) or as curing solution decreased the efficiency of crack healing. This might be due to high pH and ionic concentration of UCSL-CA medium inhibits the cation exchange in zeolites and decrease its pozzolanic activity.

- Evaluations for ZEO-1.6 series showed that immobilization of bacterial cells on zeolite-1.6 mm is not an efficient source for self-healing mechanisms. Zeolite-200 μm is a more preferable protection barrier for the proposed biological additive. This could be explained by the different working mechanisms occur in these zeolites having 2 different sizes. While zeolite-200 μm reacts with water and induces a latent hydration, zeolite-1.6 mm can desorb a higher amount of absorbed water leading to a higher degree of internal curing but does not possess pozzolanic activity. Herein, we can conclude that pozzolanic activity becomes more predominant in healing process.

- Metakaolin and perlite were not found to be suitable bedding for the bacterial cells. It was considered that the pore structures and the water absorption capacities of these minerals were not sufficient to immobilize bacteria cells. In addition, the ion contents and the reactivities of these minerals can negatively impact the viability of bacteria cells.

- While the biological additive had not a significant impact on the initial setting time of cement-based mortar, in particular adding bacteria without nutrient medium into mixture caused decrease in the 3- and 7- days compressive strengths in comparison with control sample. Addition of bacteria cells with nutrient medium enhanced the

compressive strength of samples including fine powder mineral. On the other hand, the distinct reduction in the compressive strength of samples containing lightweight aggregate perlite and zeolite-1.6 mm.

- Drying shrinkage test was conducted to control and B series samples including sepiolite, diatomaceous earth, pumice, bentonite, and zeolite. Only mineral addition increased the free drying shrinkage 2.5 times compared to control sample.

- As a result of the accelerated corrosion test applied after crack healing observed in the samples including sepiolite, diatomaceous earth, pumice and bentonite, corrosion didn't occur in any of samples according to non-destructive corrosion measurement and tensile strength test. This result is likely to be related to the experimental protocol and the quality of samples regarding low w/c ratio.

5.2 Future works

This study has shown that metakaolin and perlite were not compatible to develop the biological additive. On the other hand, it was seen that only zeolite addition into mortar without any bacteria cells provided partially crack closure. Therefore, further works are required as follows:

- It was seen that zeolite addition triggered the autogenous healing of cement-based materials due to the pozzolanic reactivity and internal curing. Furter studies can be carried out to improve the autogenous self-healing cement-based mortar including zeolite.

- In order to understand the impact of natural minerals characteristic on biological self-healing, it is required to determine the pozzolanic reactivity and the chemical

component of minerals. Moreover, the pore size distribution of samples can be examined.

- The self-healing ability of developed biological additive should be evaluated with spray curing or air-curing which are more feasible in-situ.
- The findings of the drying shrinkage results suggested that high rate of cracks would occur in restrained slab. Therefore, mesoscale experiments should be carried out to detect the problems in practice.
- Lastly, to understand the efficiency of crack remediation obtained by biomineralization, chloride induced, and carbon induced corrosion test would be conducted to the cement-based mortars containing biological additive prepared with higher w/c ratio.

APPENDIX A – IMAGE ANAYLSES

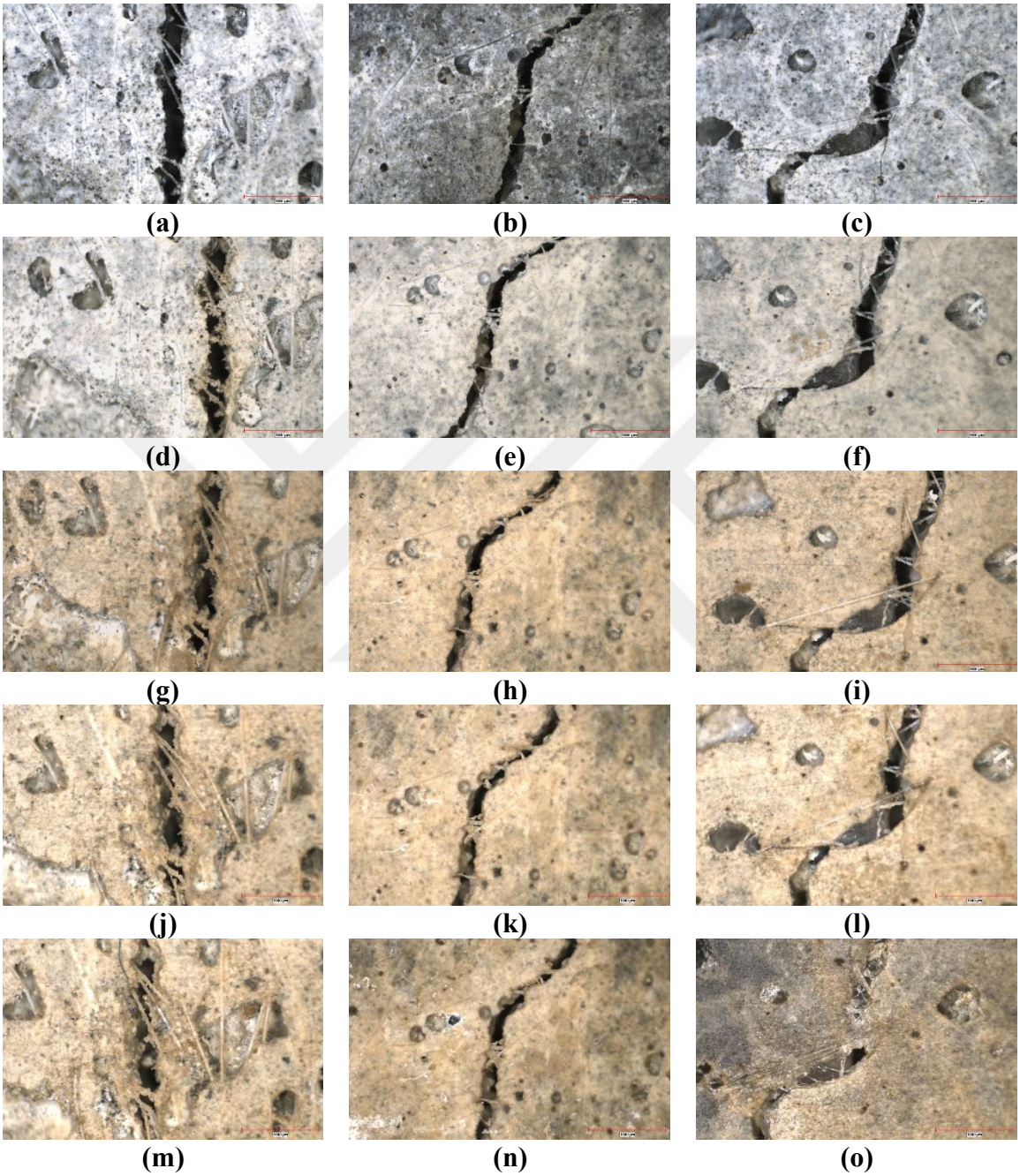

Figure A.1: The crack images of 14- day old ZEOC-200 samples. (a, b, c) right after cracking, (d, e, f) after 7 days of UCSL-CA curing, (g, h, i) after 14 days of UCSL-CA curing, (j, k, l) after 21 days of UCSL-CA curing, (m, n, o) after 28 days of UCSL-CA curing.

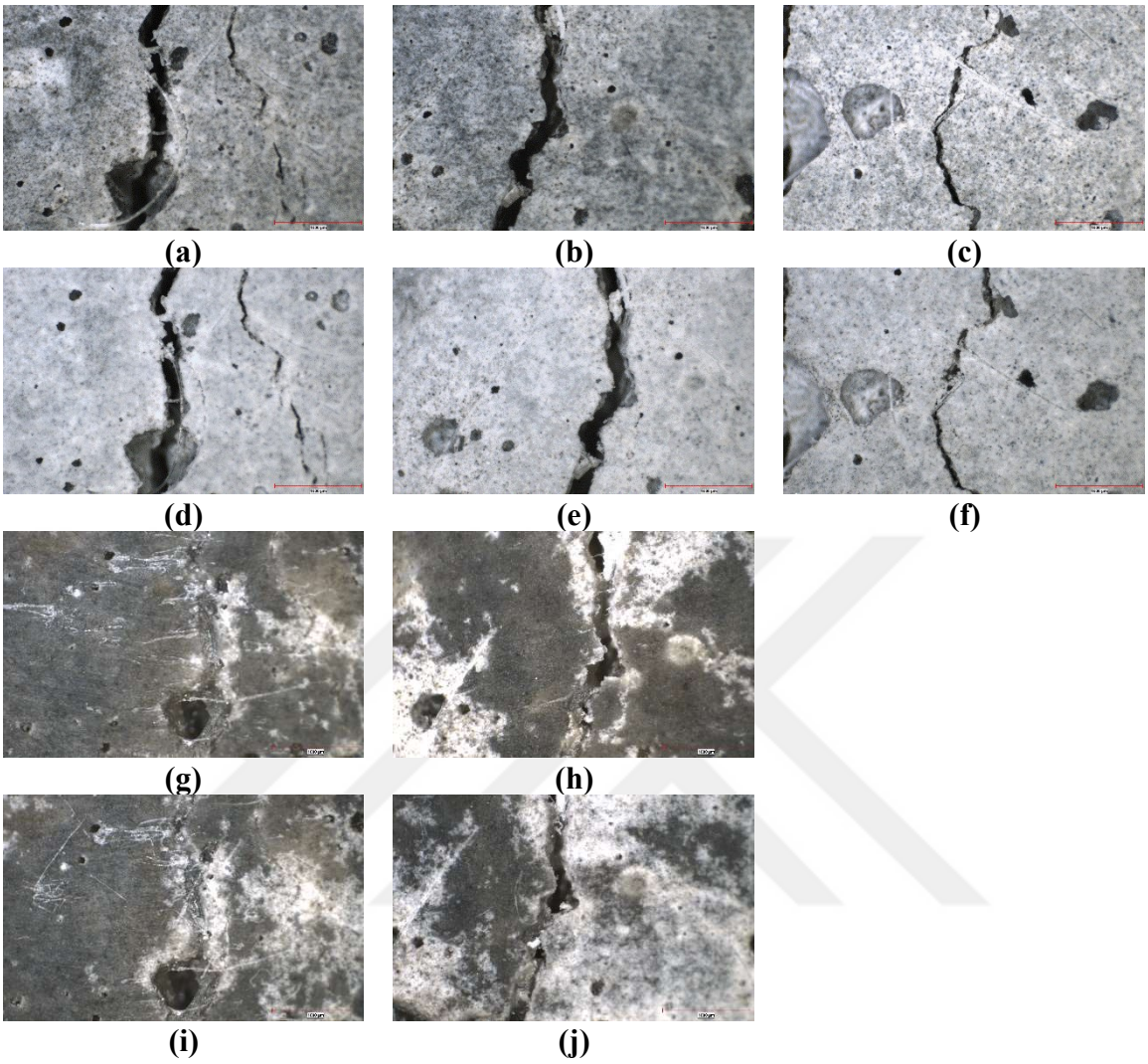

Figure A.2: The crack images of 14-day old ZEOC-200. (a, b, c) right after cracking, (d, e, f) after 7 days of water curing, (g, h) after 21 days of water curing, (i, j) after 28 days of water curing. (Due to crack sealing, the measurement point couldn't be found therefore some of images were missing.)

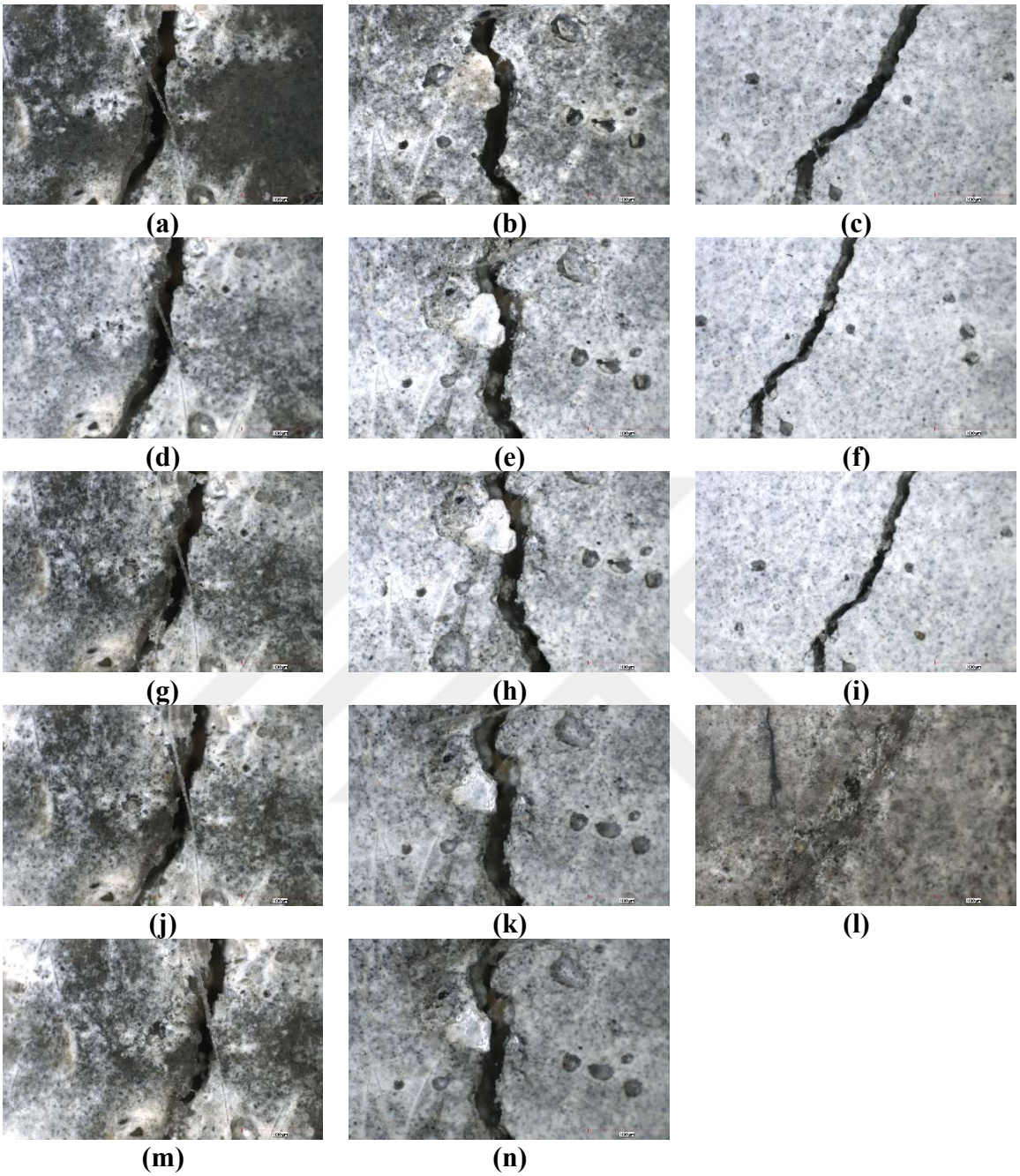

Figure A.3: The crack images of 14-day old ZEOC-200 samples. (a, b, c) right after cracking, (d, e, f) after 7 days, (g, h, i) after 14 days, (j, k, l) after 21 days, (m, n) after 28 days.

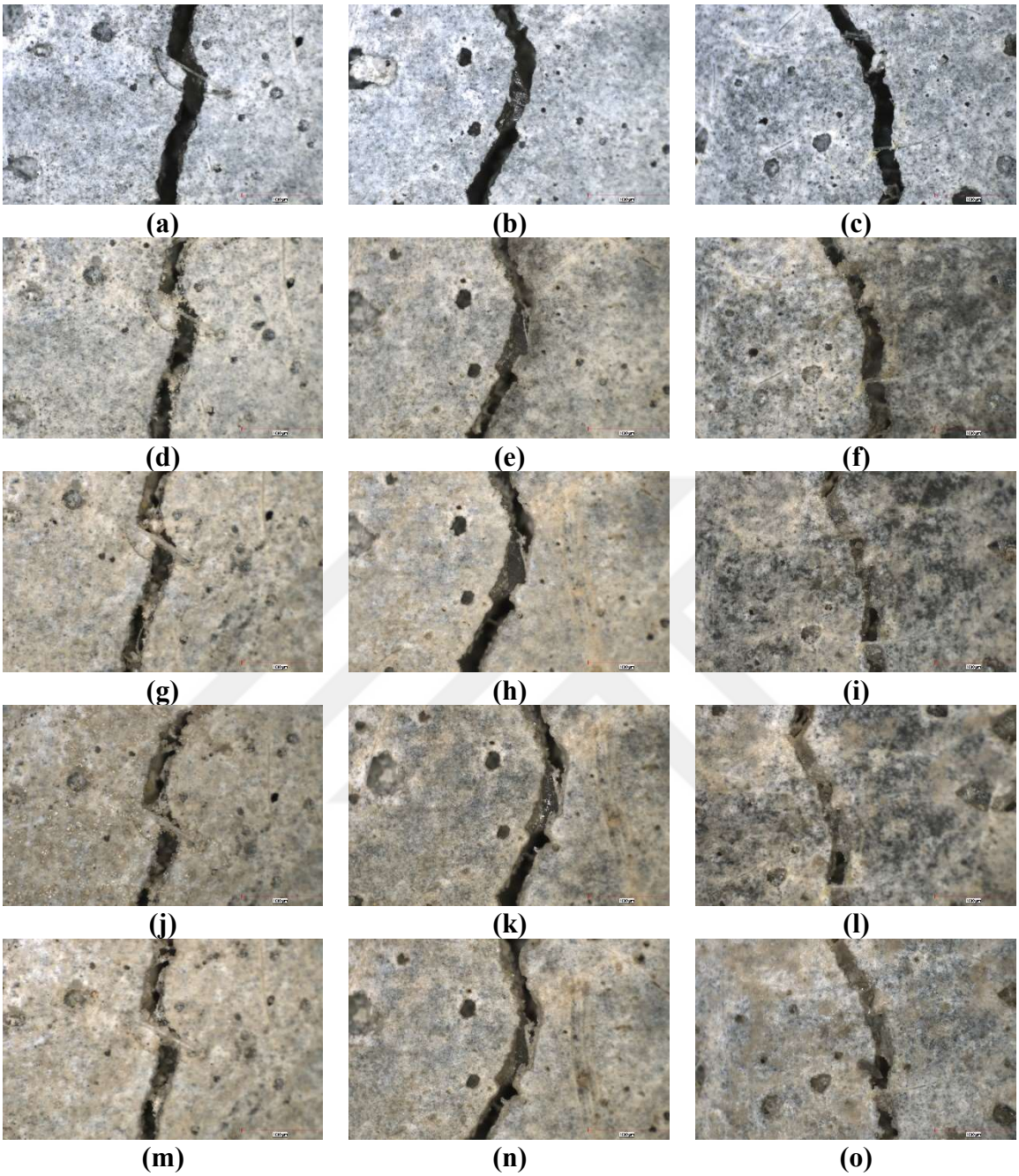

Figure A.4: The crack images of 28-day old ZEOC-200. (a, b, c) right after cracking, (d, e, f) after 7 days of UCSL-CA curing, (g, h, i) after 14 days of UCSL-CA curing, (j, k, l) after 21 days of UCSL-CA curing, (m, n, o) after 28 days of UCSL-CA curing.

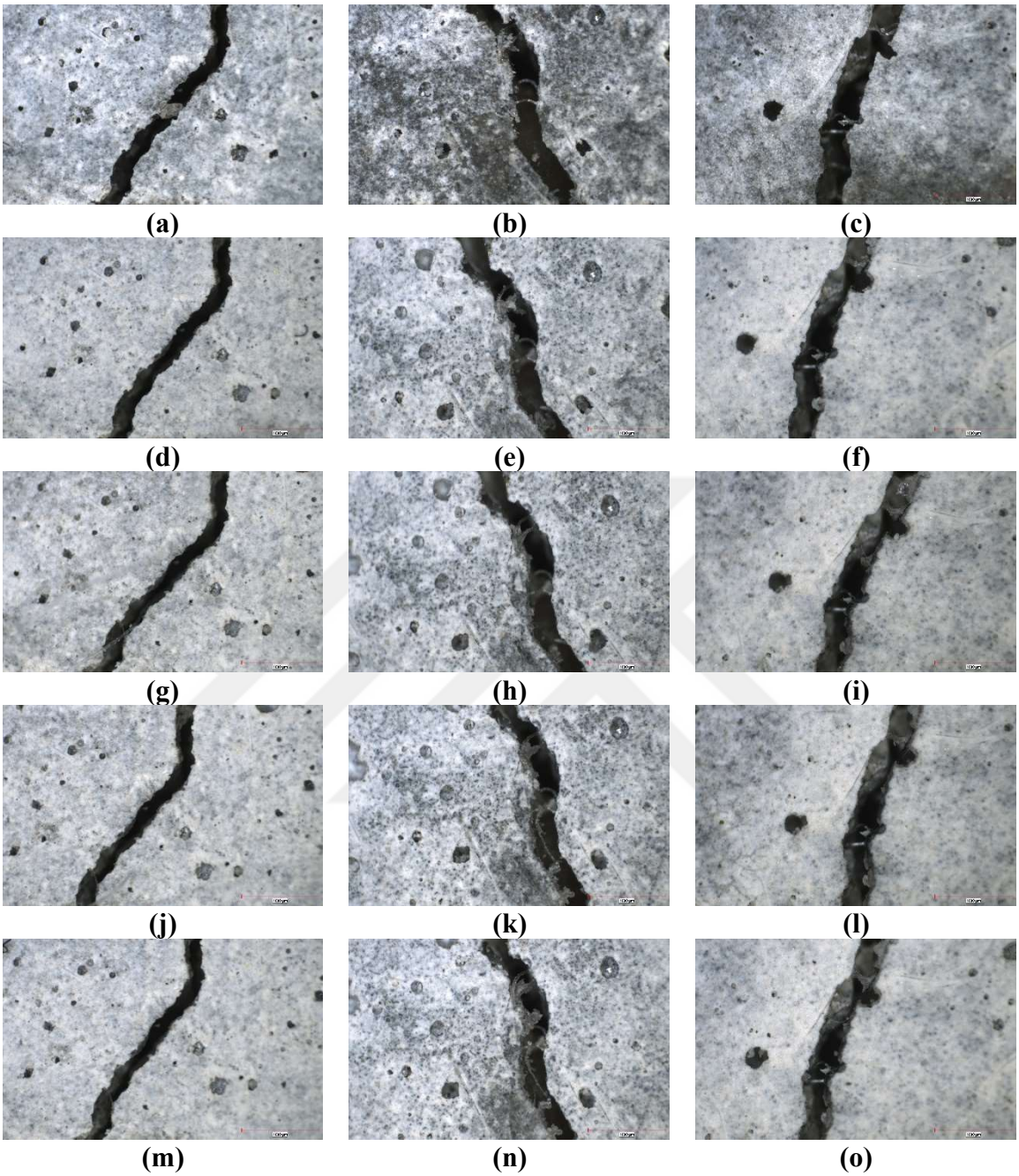

Figure A.5: The crack images of 28-day old ZEOC-200 samples kept at ambient conditions. (a, b, c) right after cracking, (d, e, f) after 7, (g, h, i) after 14 days, (j, k, l) after 21 days, (m, n, o) after 28 days.

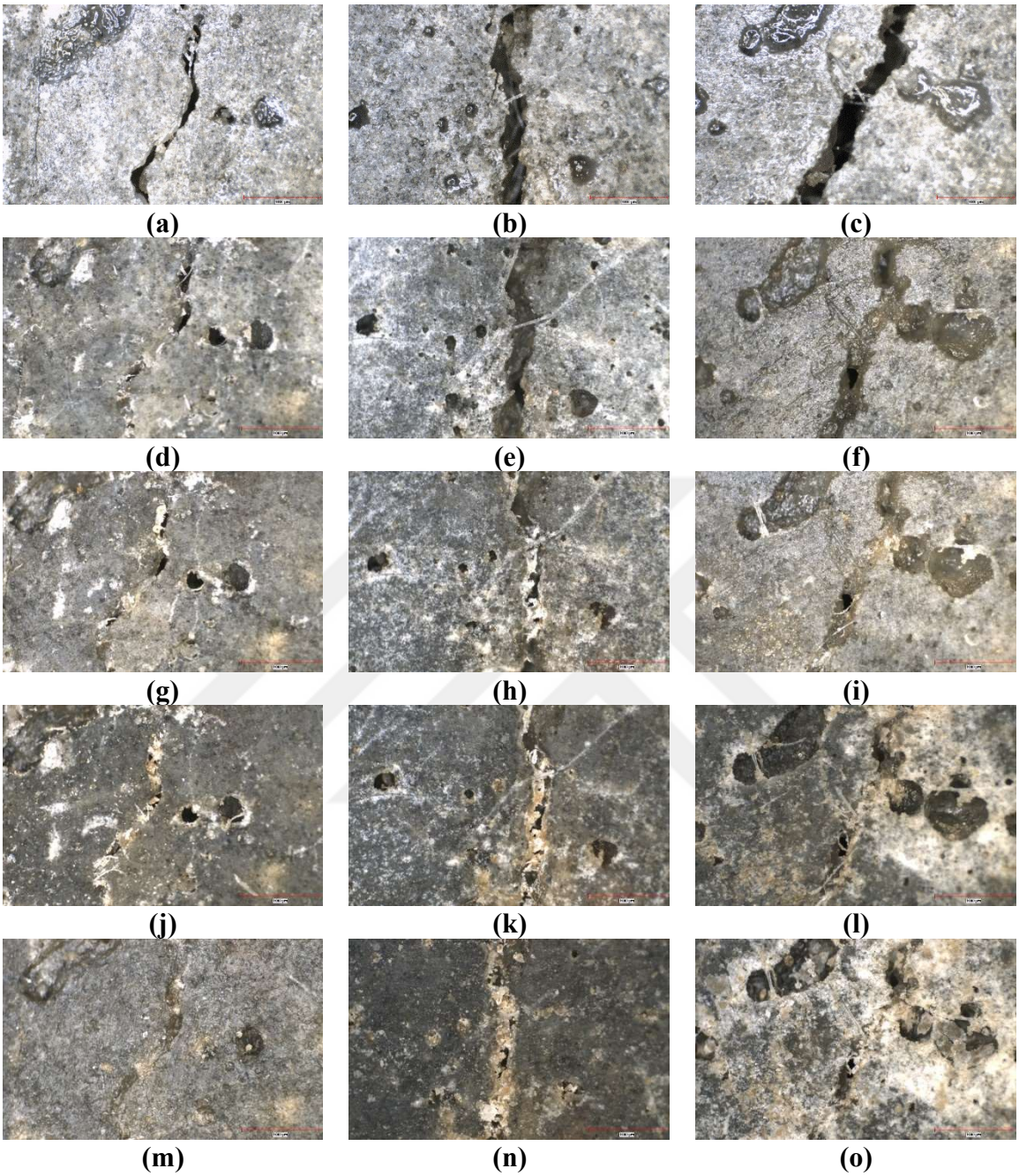

Figure A.6: The crack images of 14-day old ZEOB-200. (a, b, c) right after cracking, (d, e, f) after 7 days of UCSL-CA curing, (g, h, i) after 14 days of UCSL-CA curing, (j, k, l) after 21 days of UCSL-CA curing, (m, n, o) after 28 days of UCSL-CA curing.

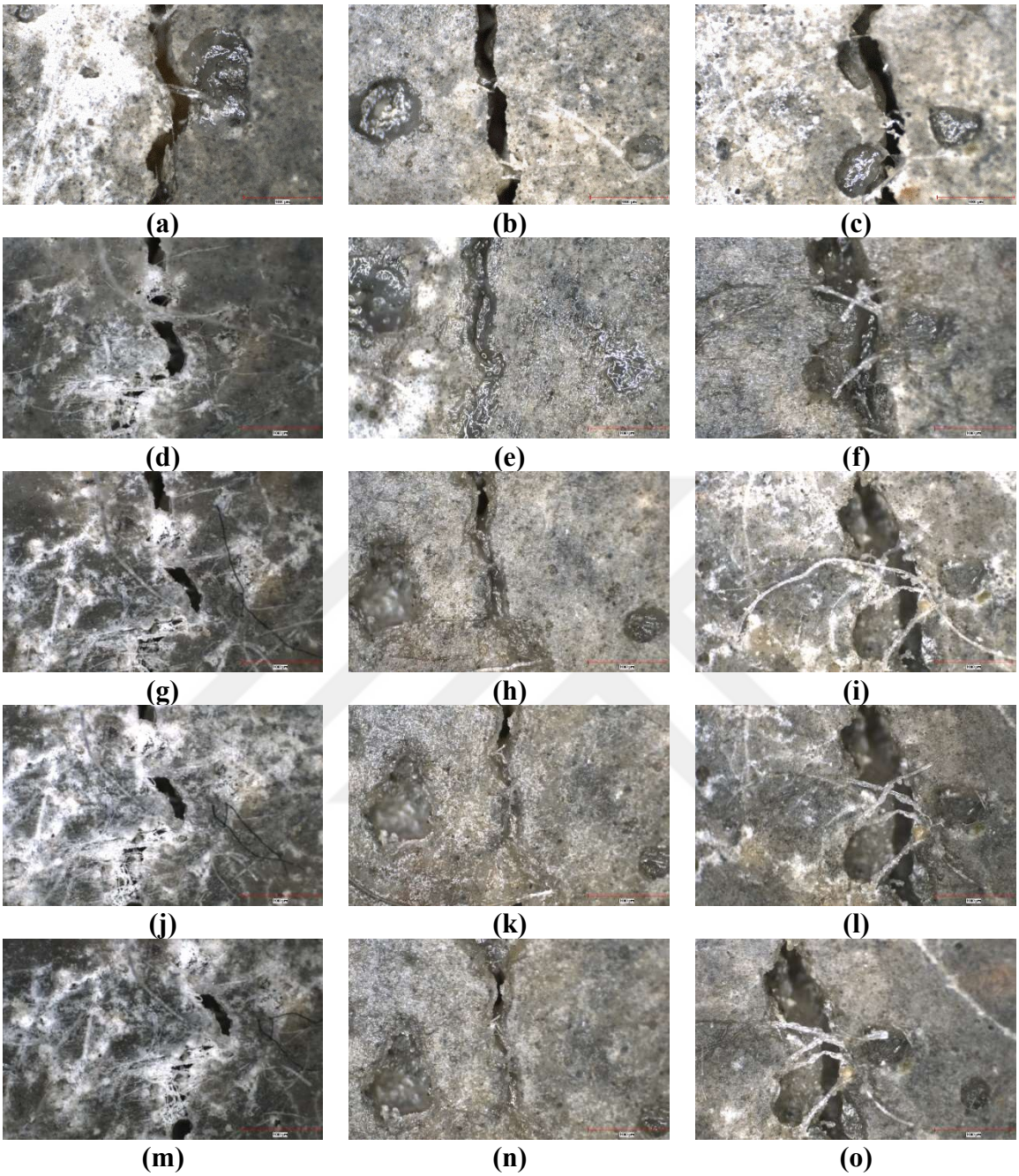

Figure A.7: The crack images of 14-day old ZEOB-200 samples. (a, b, c) right after cracking, (d, e, f) after 7 days of water curing, (g, h, i) after 14 days of water curing, (j, k, l) after 21 days of water curing, (m, n, o) after 28 days of water curing.

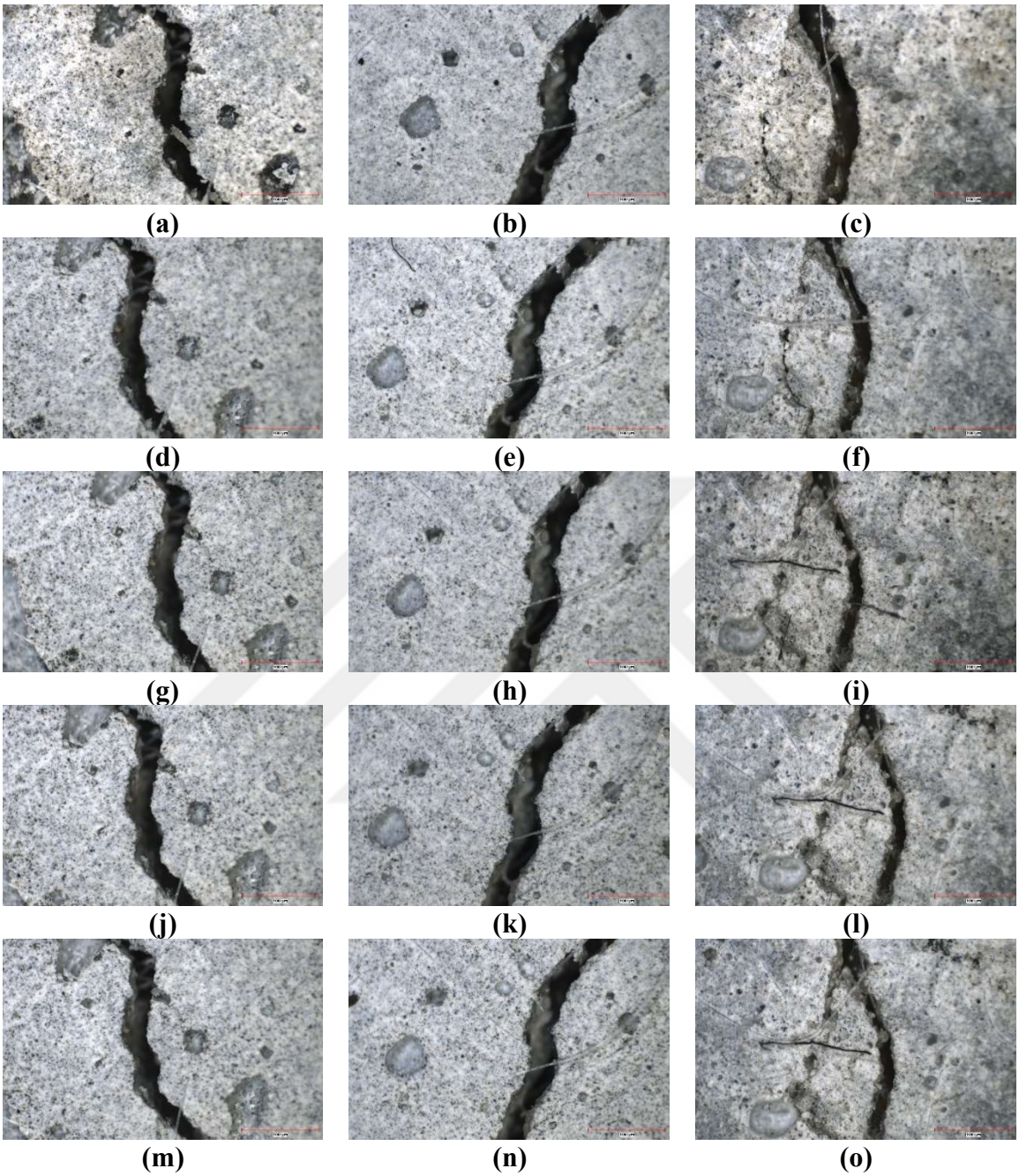

Figure A.8: The crack images of 14-day old ZEOB-200 samples kept at ambient conditions. (a, b, c) right after cracking, (d, e, f) after 7 days, (g, h, i) after 14 days, (j, k, l) after 21 days, (m, n, o) after 28 days.

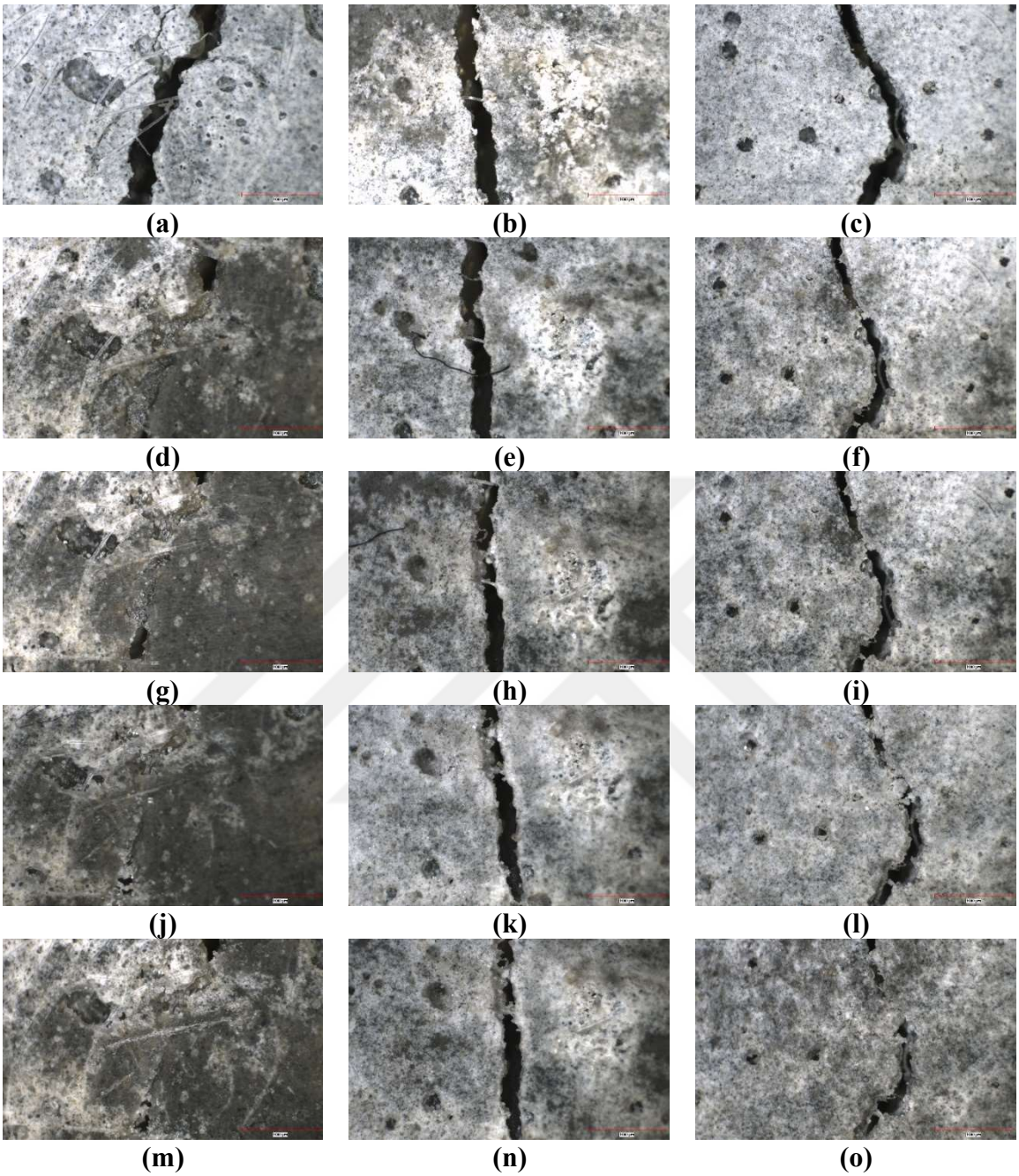

Figure A.9: The crack images of 28-day old ZEOB-200. (a, b, c) right after cracking, (d, e, f) after 7 days of water curing, (g, h, i) after 14 days of water curing, (j, k, l) after 21 days of water curing, (m, n, o) after 28 days of water curing.

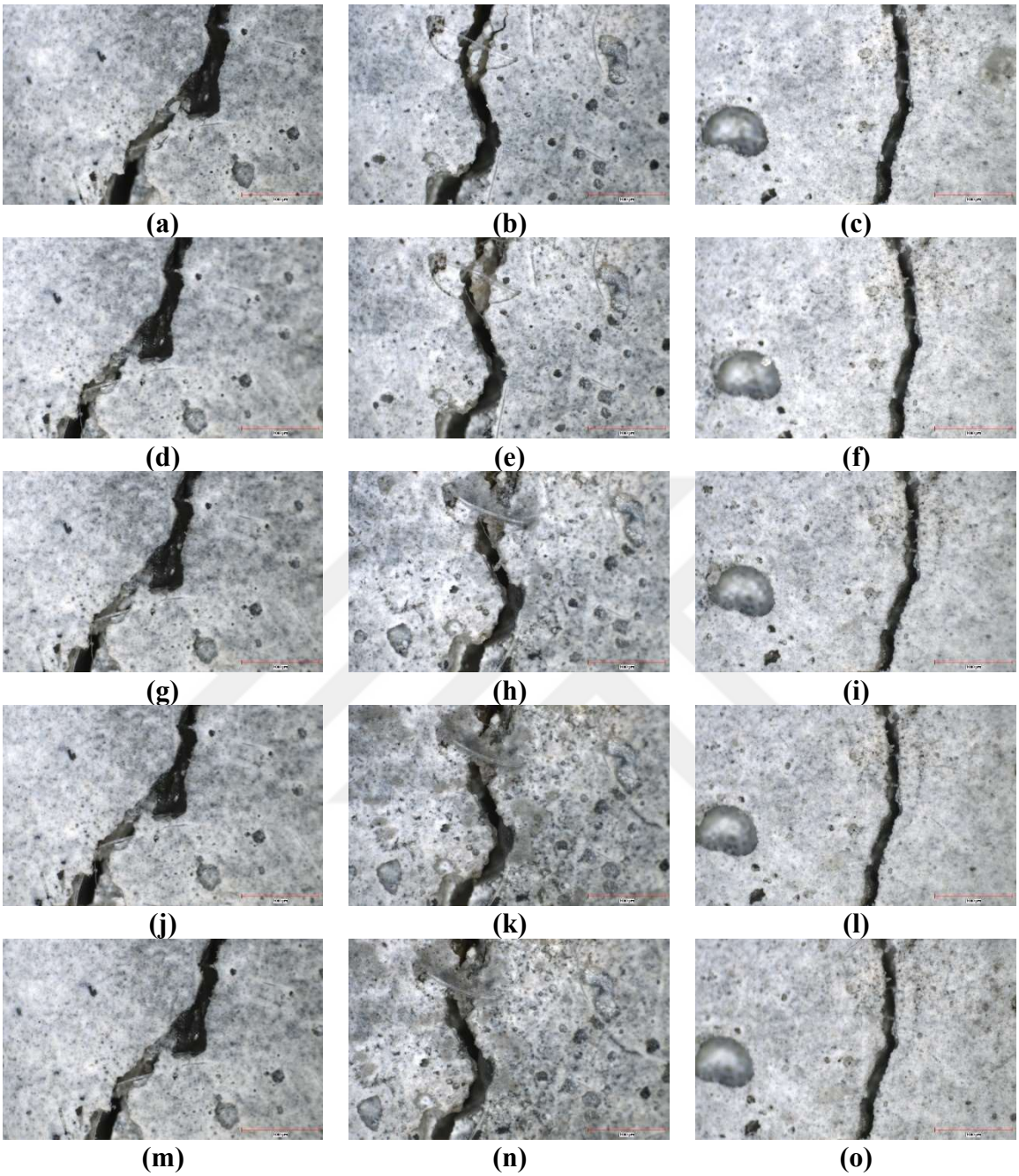

Figure A.10: The crack images of 28-day old ZEOB-200 samples kept at ambient conditions. (a, b, c) right after cracking, (d, e, f) after 7 days, (g, h, i) after 14 days, (j, k, l) after 21 days, (m, n, o) after 28 days.

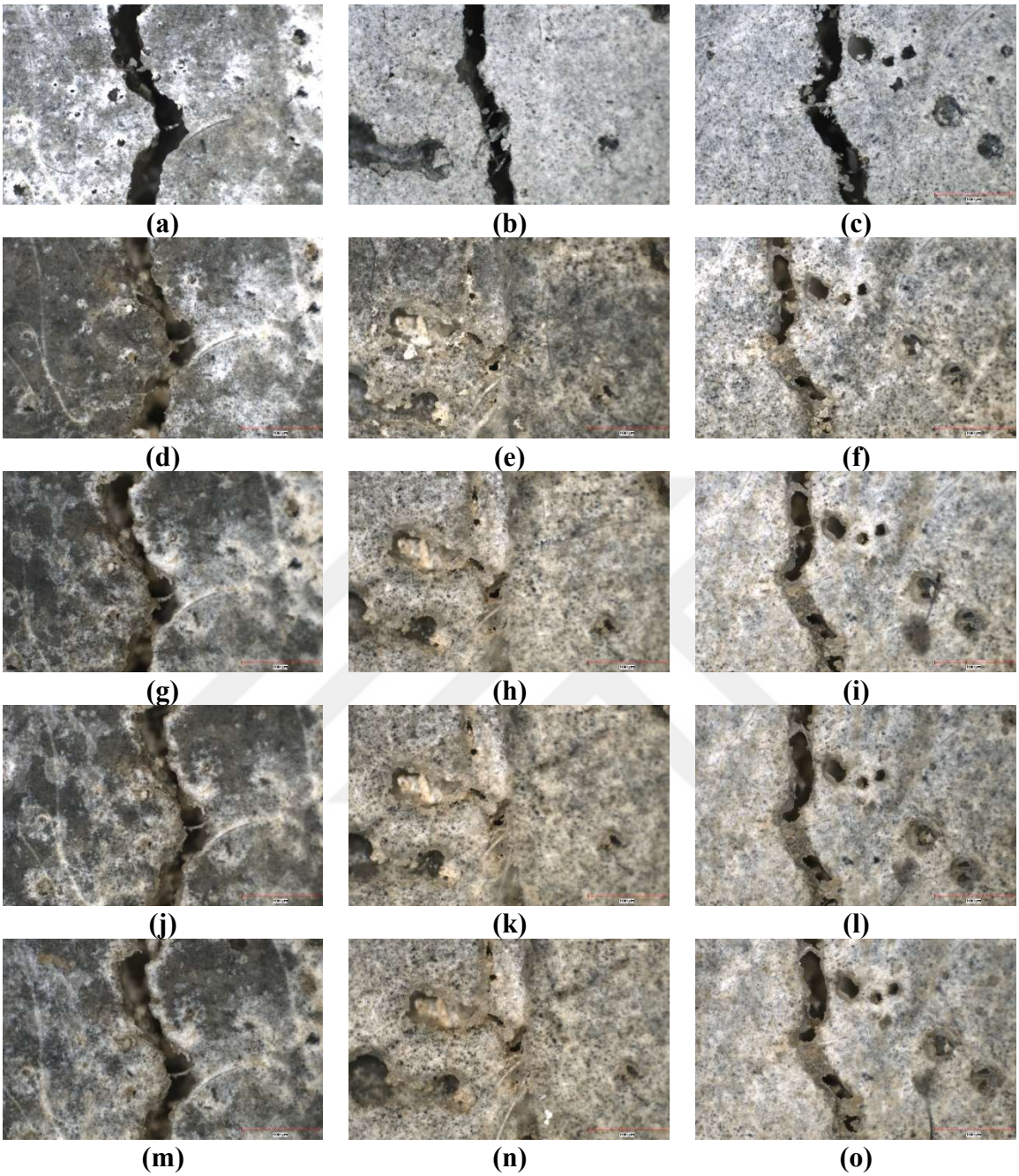

Figure A.11: The crack images of 14-day old ZEOBN-200 samples. (a, b, c) right after cracking, (d, e, f) after 7 days of UCSL-CA curing, (g, h, i) after 14 days of UCSL-CA curing, (j, k, l) after 21 days of UCSL-CA curing, (m, n, o) after 28 days of UCSL-CA curing.

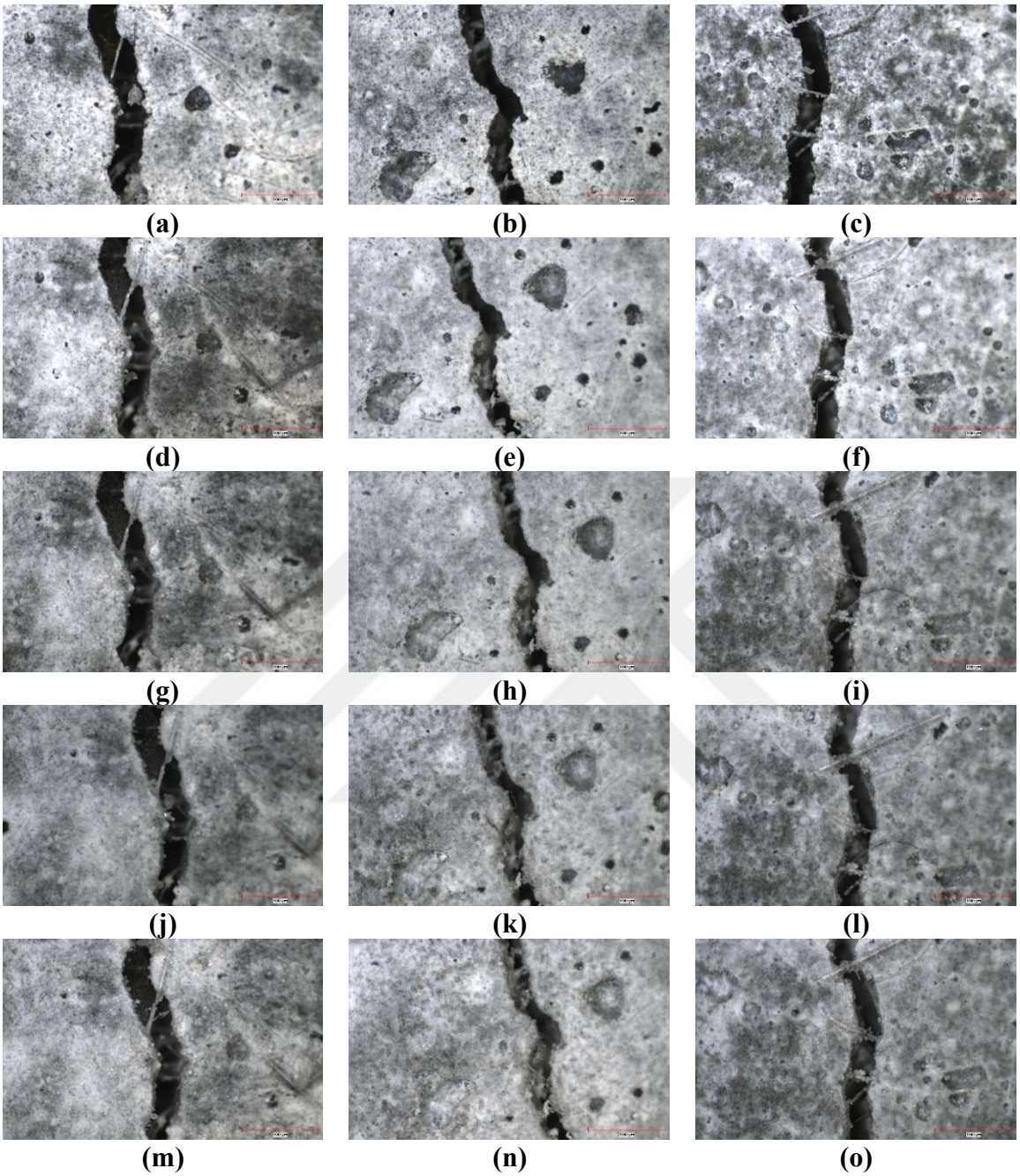

Figure A.12: The crack images of 14-day old ZEOBN-200. (a, b, c) right after cracking, (d, e, f) after 7 days of water curing, (g, h, i) after 14 days of water curing, (j, k, l) after 21 days of water curing, (m, n, o) after 28 days of water curing.

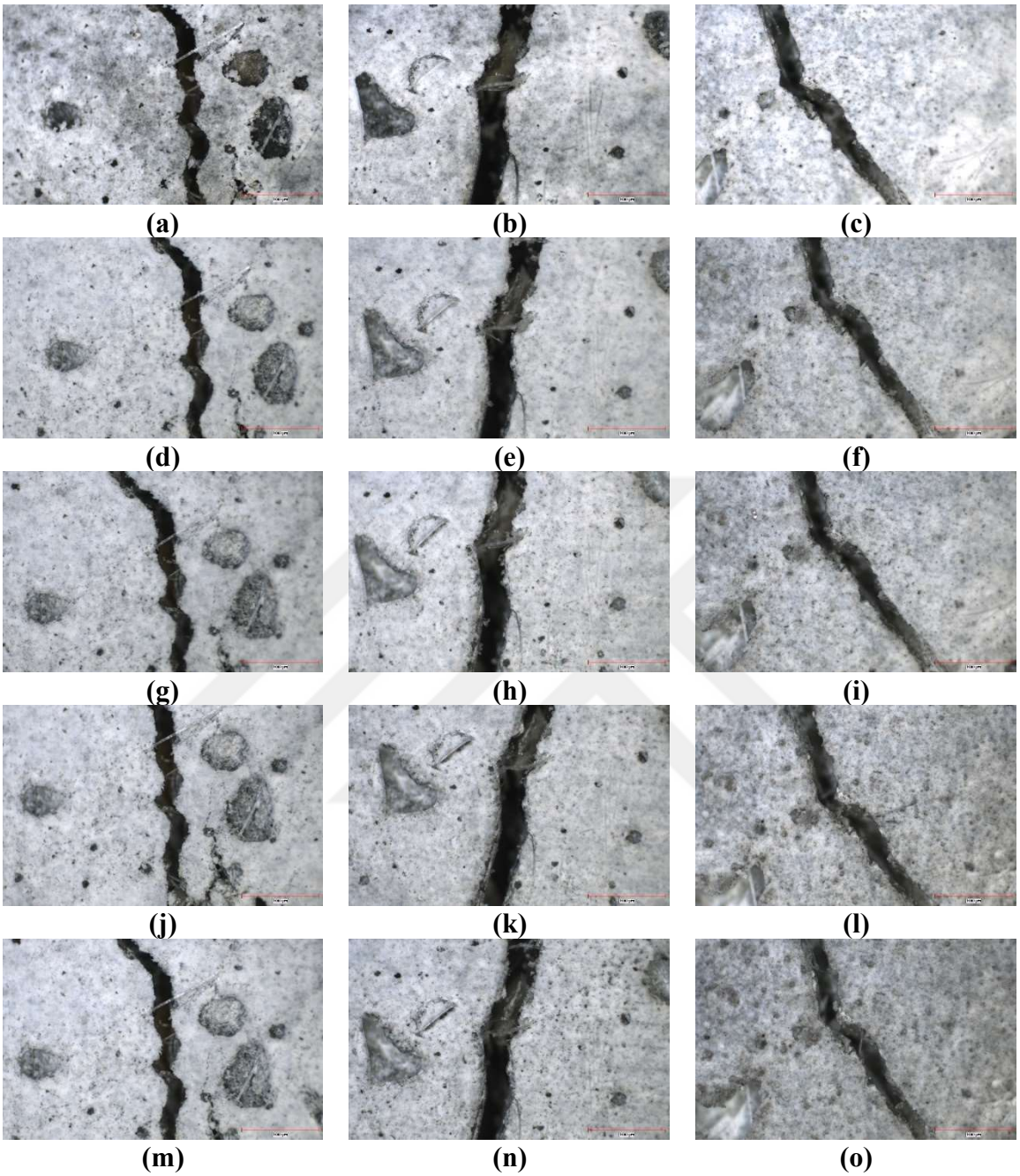

Figure A.13: The crack images of 14-day old ZEOBN-200 samples kept at ambient conditions. (a, b, c) right after cracking, (d, e, f) after 7 days, (g, h, i) after 14 days, (j, k, l) after 21 days, (m, n, o) after 28 days.

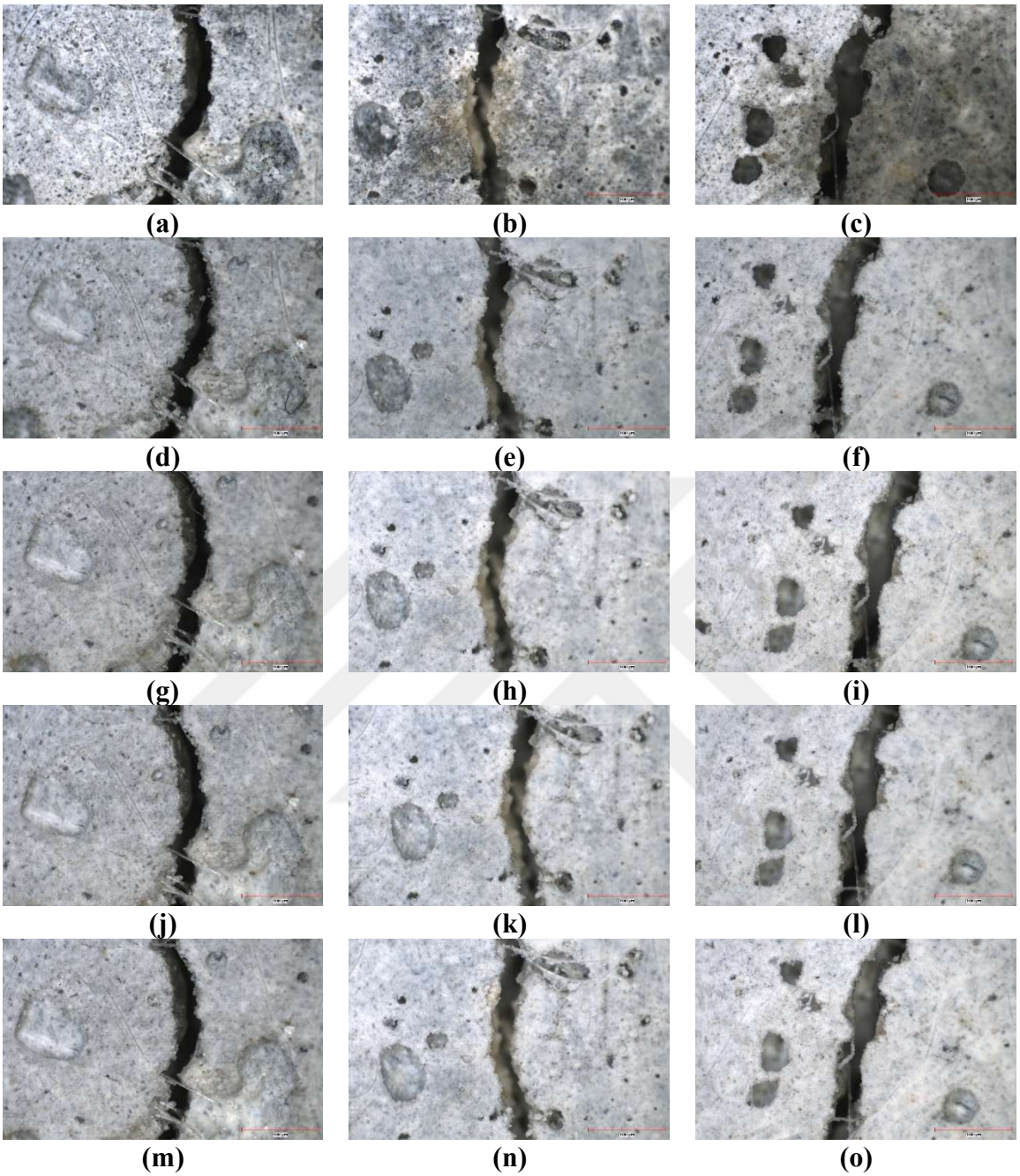

Figure A.14: The crack images of 28-day old ZEOBN-200 samples. (a, b, c) right after cracking, (d, e, f) after 7 days of water curing, (g, h, i) after 14 days of water curing, (j, k, l) after 21 days of water curing, (m, n, o) after 28 days of water curing.

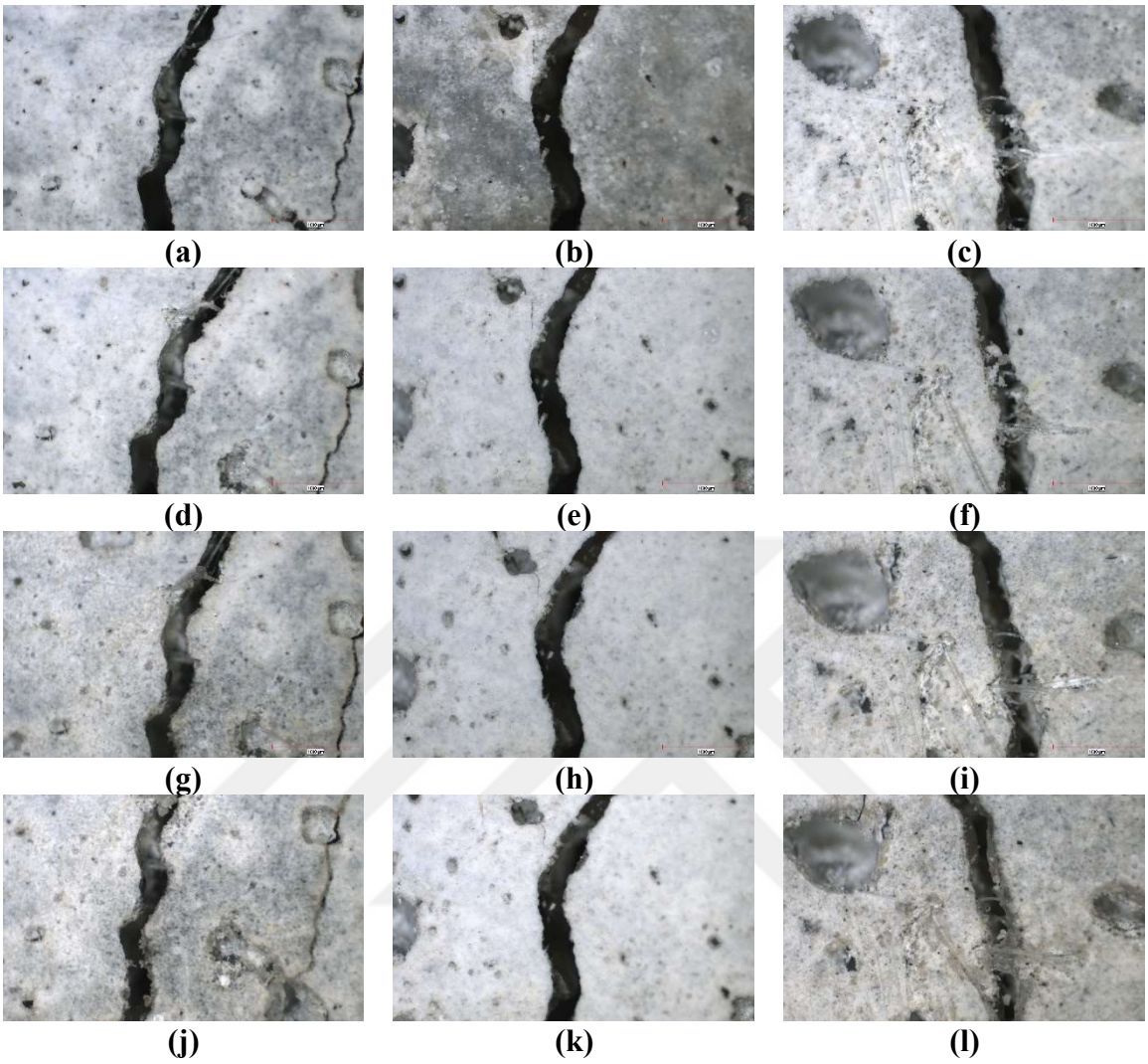

Figure A.15: The crack images of 28-day old ZEOBN-200 samples kept at ambient conditions. (a, b, c) right after cracking, (d, e, f) after 7 days, (g, h, i) after 14 days, (j, k, l) after 28 days.

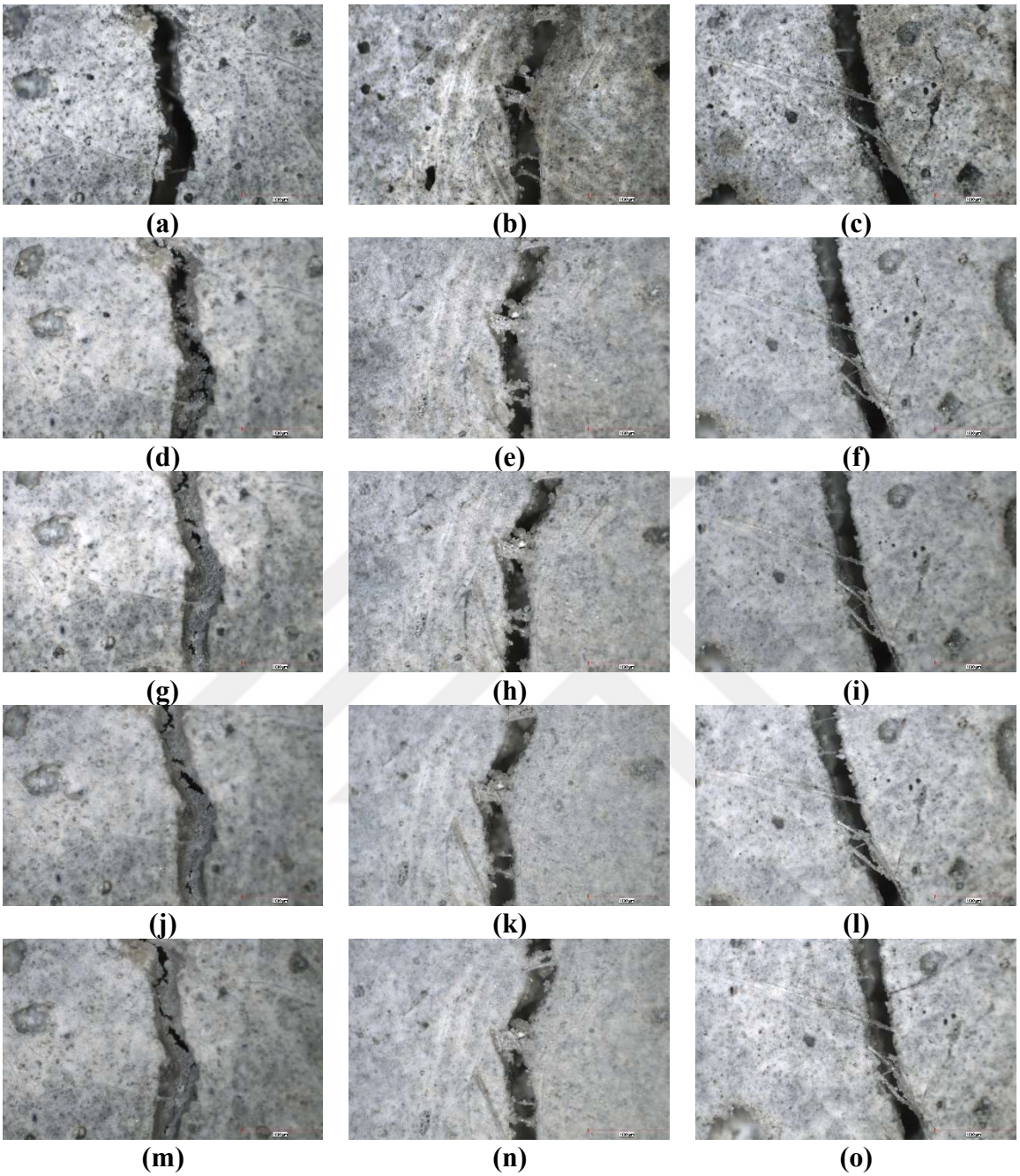

Figure A.16: The crack images of 14-day old ZEOC-1.6 samples. (a, b, c) right after cracking, (d, e, f) after 7 days of water curing, (g, h, i) after 14 days of water curing, (j, k, l) after 21 days of water curing, (m, n, o) after 28 days of water curing.

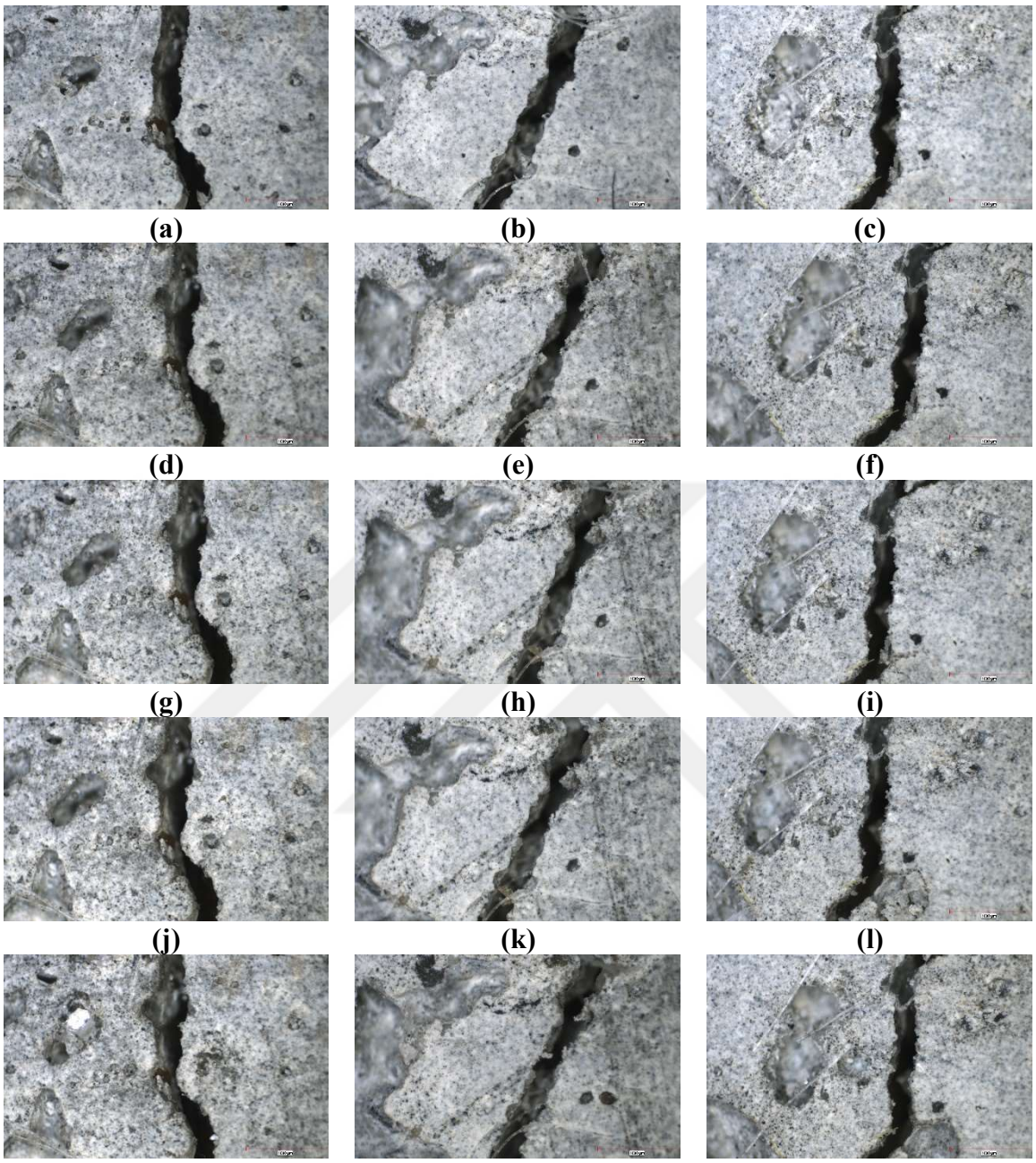

Figure A.17: The crack images of 14-day old ZEOC-1.6 samples kept at ambient conditions. (a, b, c) right after cracking, (d, e, f) after 7 days, (g, h, i) after 14 days, (j, k, l) after 21 days, (m, n, o) after 28 days.

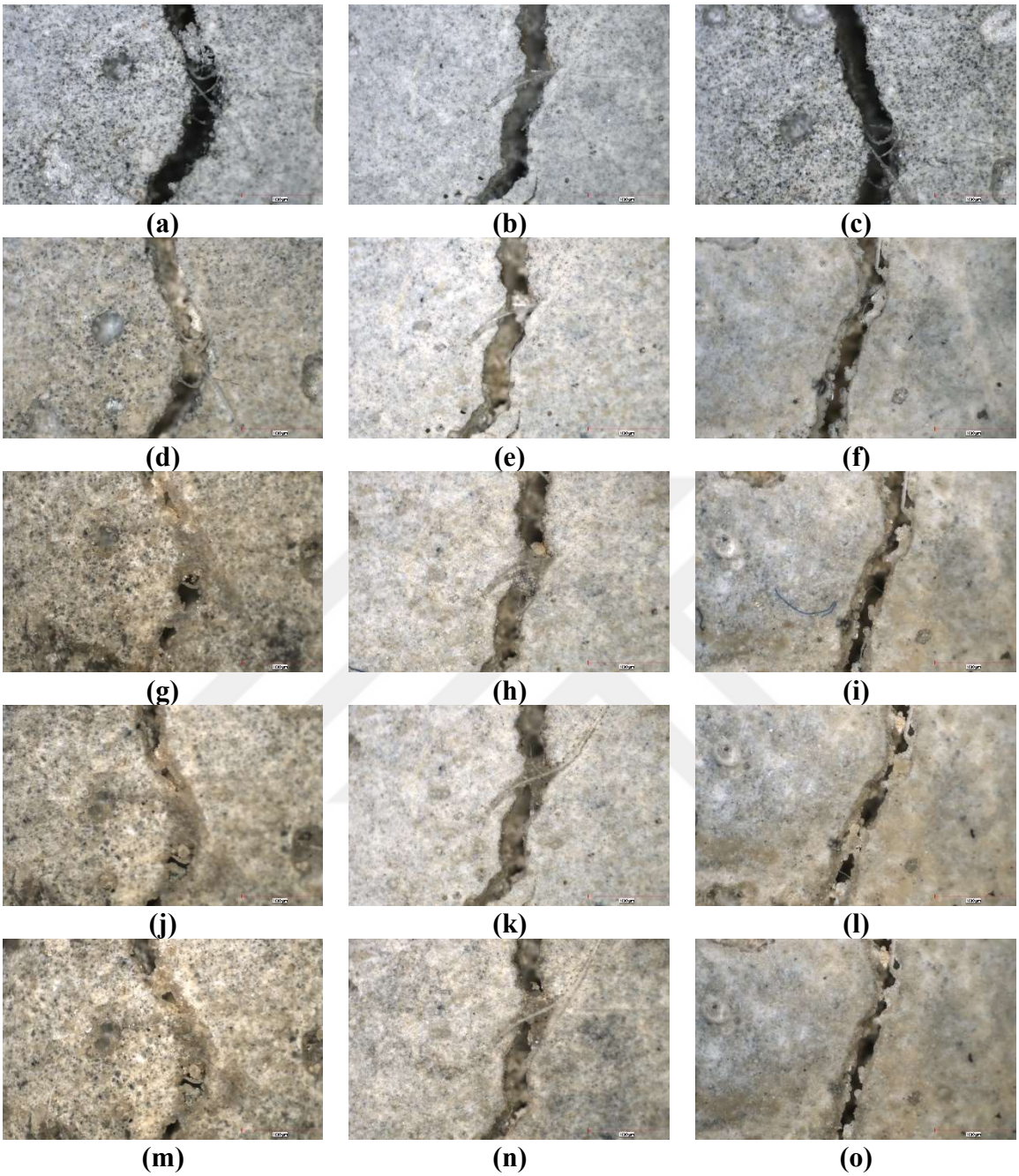

Figure A.18: The crack images of 28-day old ZEOC-1.6 samples. (a, b, c) right after cracking, (d, e, f) after 7 days of UCSL-CA curing, (g, h, i) after 14 days of UCSL-CA curing, (j, k, l) after 21 days of UCSL-CA curing, (m, n, o) after 28 days of UCSL-CA curing.

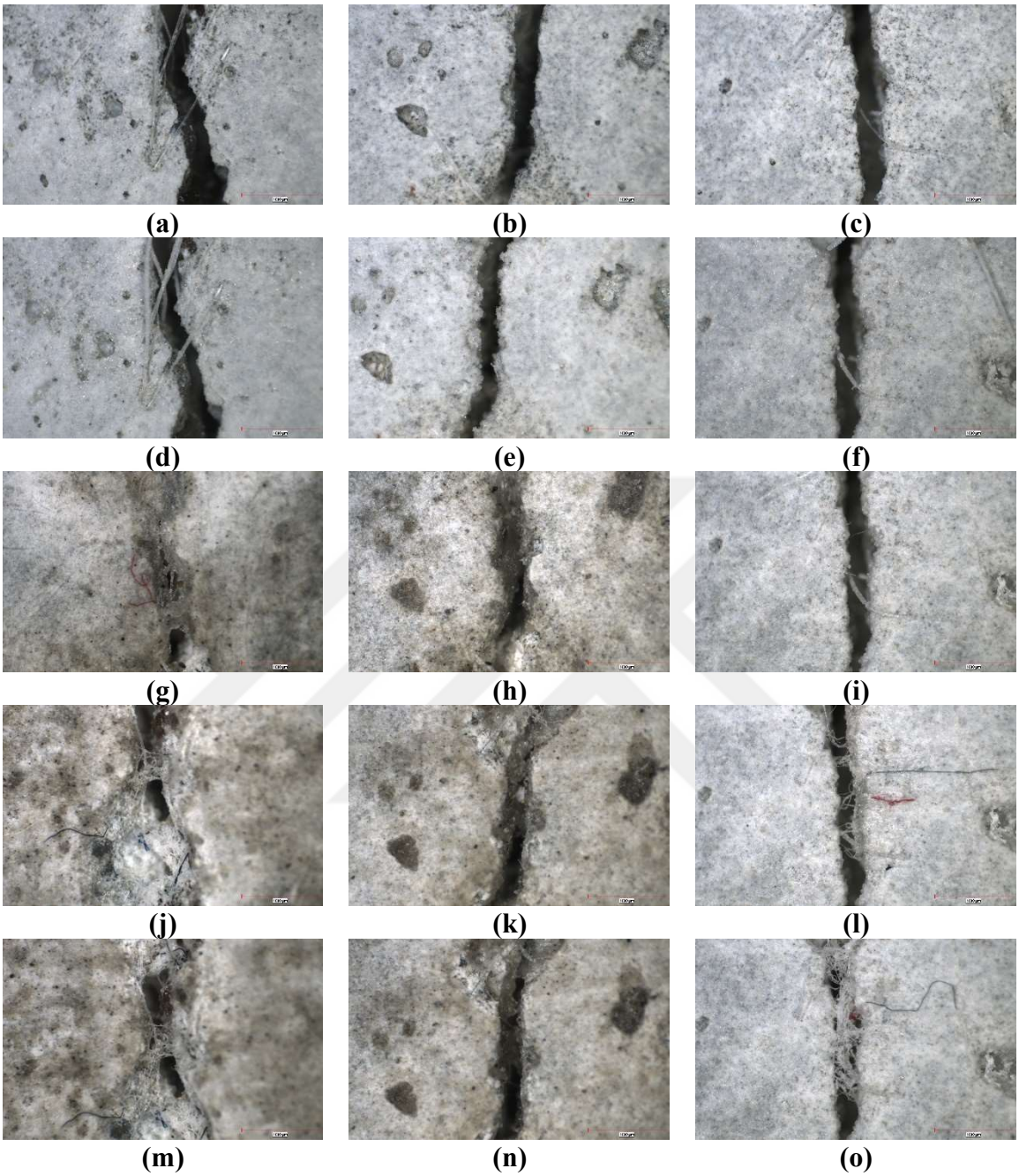

Figure A.19: The crack images of 28-day old ZEOC-1.6 samples. (a, b, c) right after cracking, (d, e, f) after 7 days of water curing, (g, h, i) after 14 days of water curing, (j, k, l) after 21 days of water curing, (m, n, o) after 28 days of water curing.

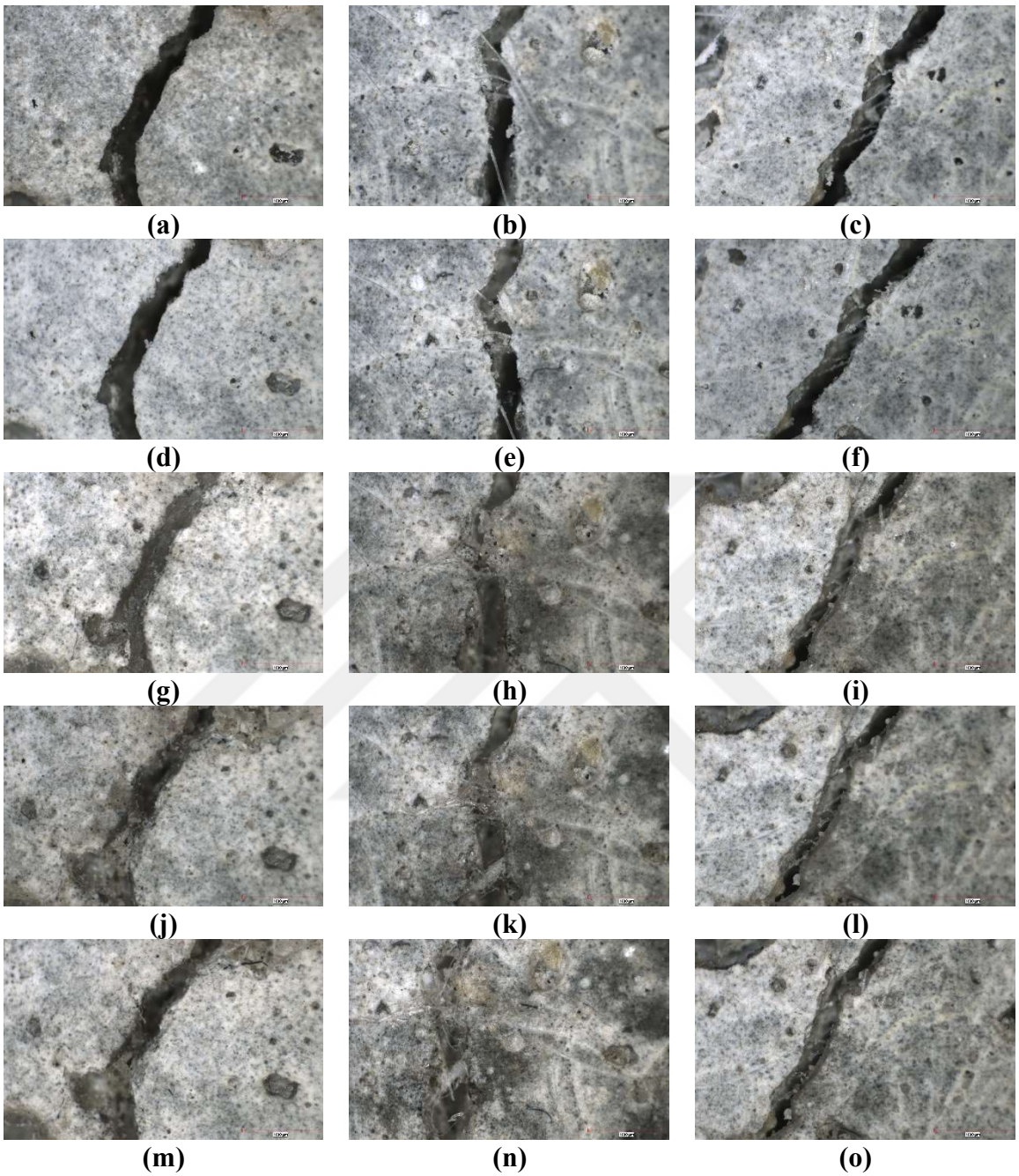

Figure A.20: The crack images of 28-day old ZEOC-1.6 samples kept at ambient conditions. (a, b, c) right after cracking, (d, e, f) after 7 days, (g, h, i) after 14 days, (j, k, l) after 21 days, (m, n, o) after 28 days.

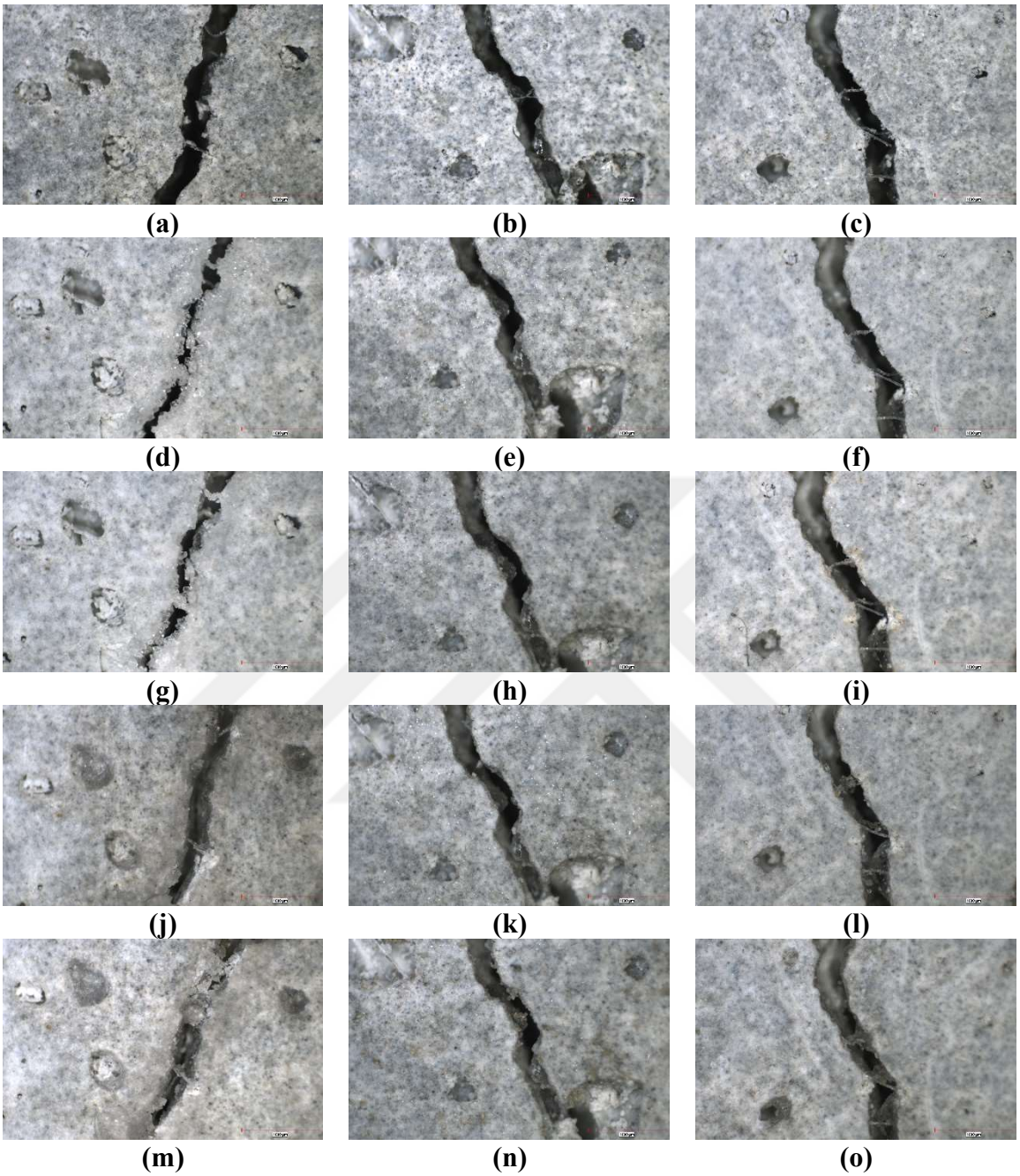

Figure A.21: The crack images of 14-day old ZEOB-1.6 samples. (a, b, c) right after cracking, (d, e, f) after 7 days of water curing, (g, h, i) after 14 days of water curing, (j, k, l) after 21 days of water curing, (m, n, o) after 28 days of water curing.

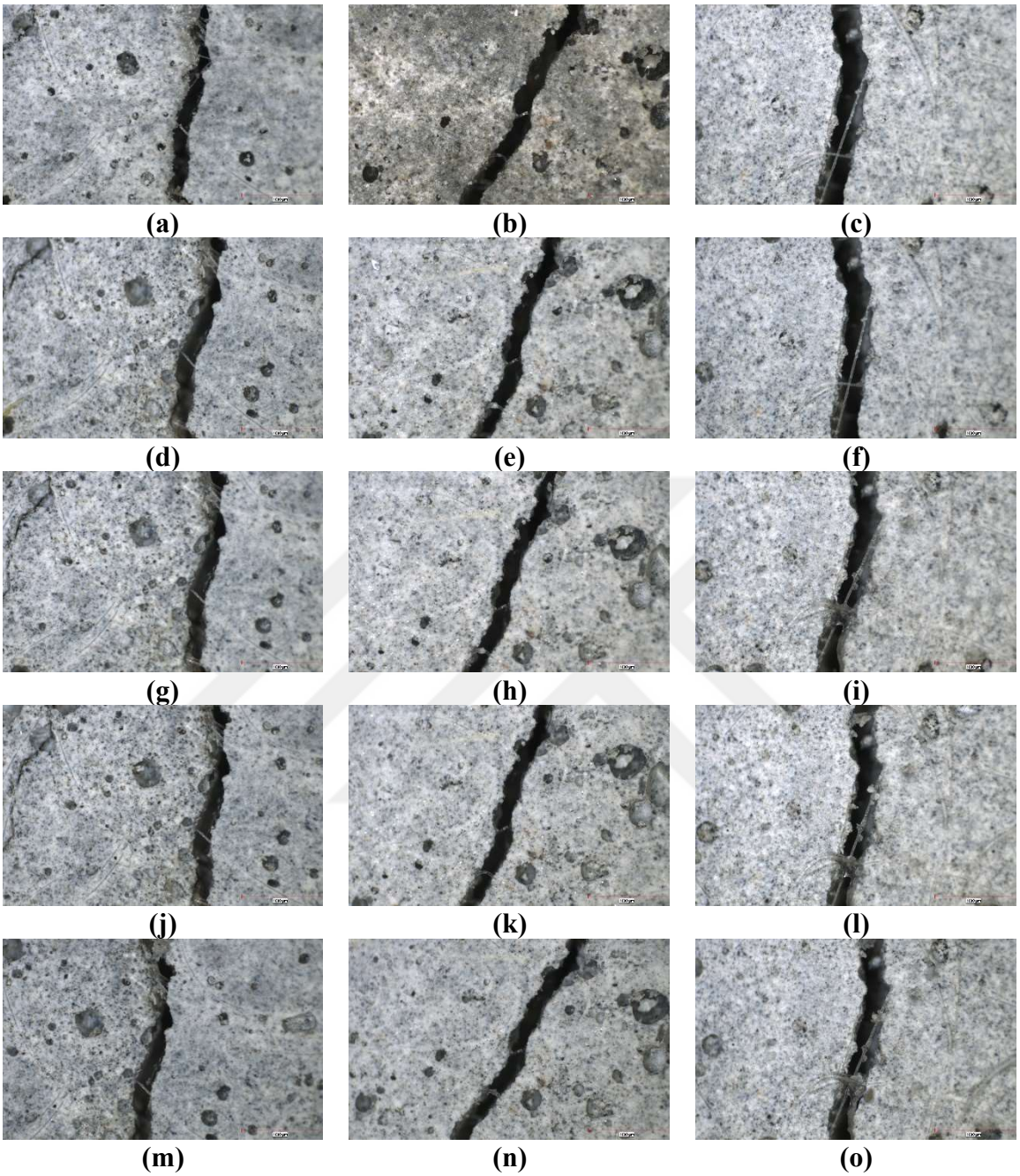

Figure A.22: The crack images of 14-day old ZEOB-1.6 kept at ambient conditions. (a, b, c) right after cracking, (d, e, f) after 7 days, (g, h, i) after 14 days, (j, k, l) after 21 days, (m, n, o) after 28 days.

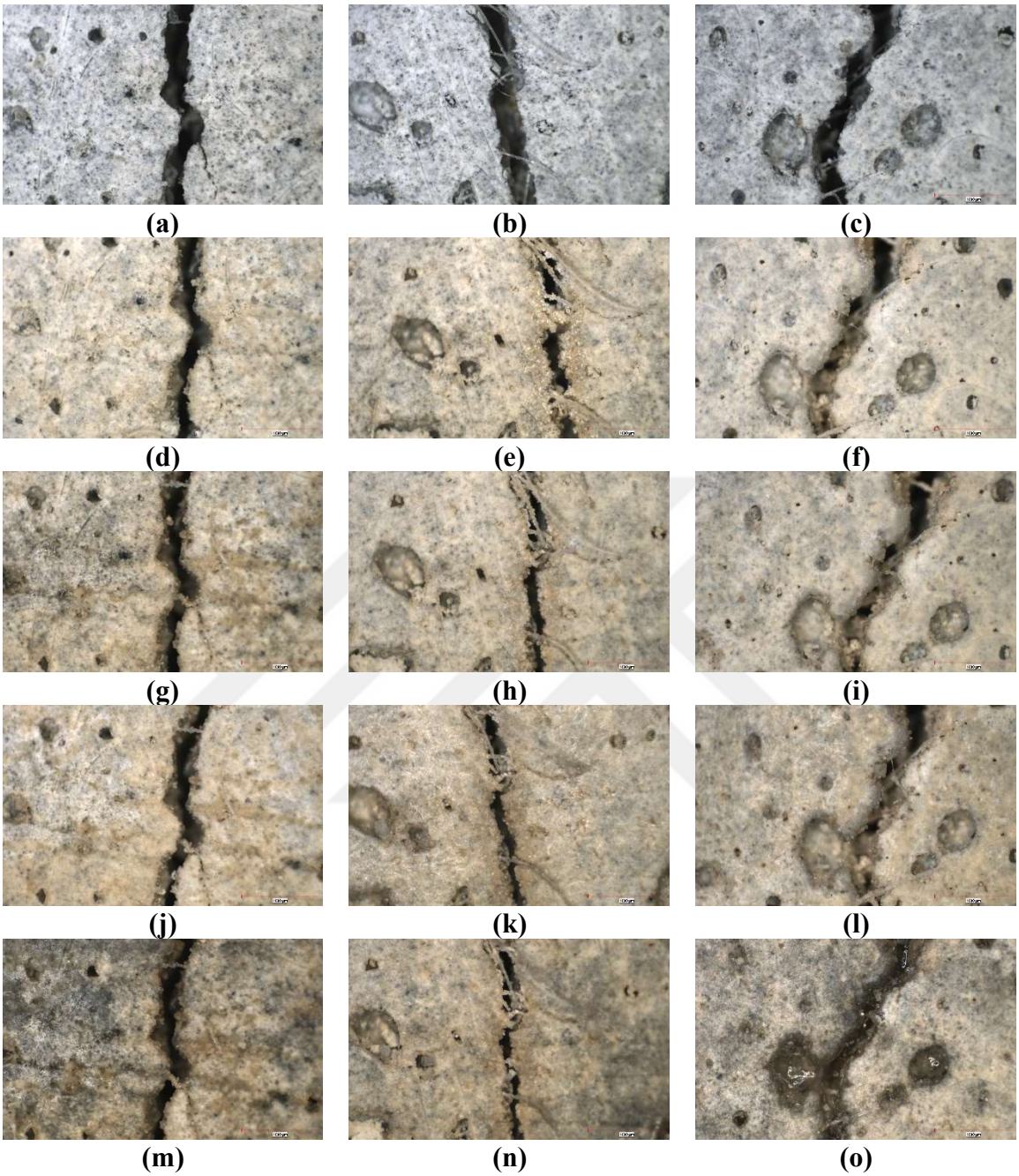

Figure A.23: The crack images of 28-day old ZEOB-1.6 samples. (a, b, c) right after cracking, (d, e, f) after 7 days of UCSL-CA curing, (g, h, i) after 14 days of UCSL-CA curing, (j, k, l) after 21 days of UCSL-CA curing, (m, n, o) after 28 days of UCSL-CA curing.

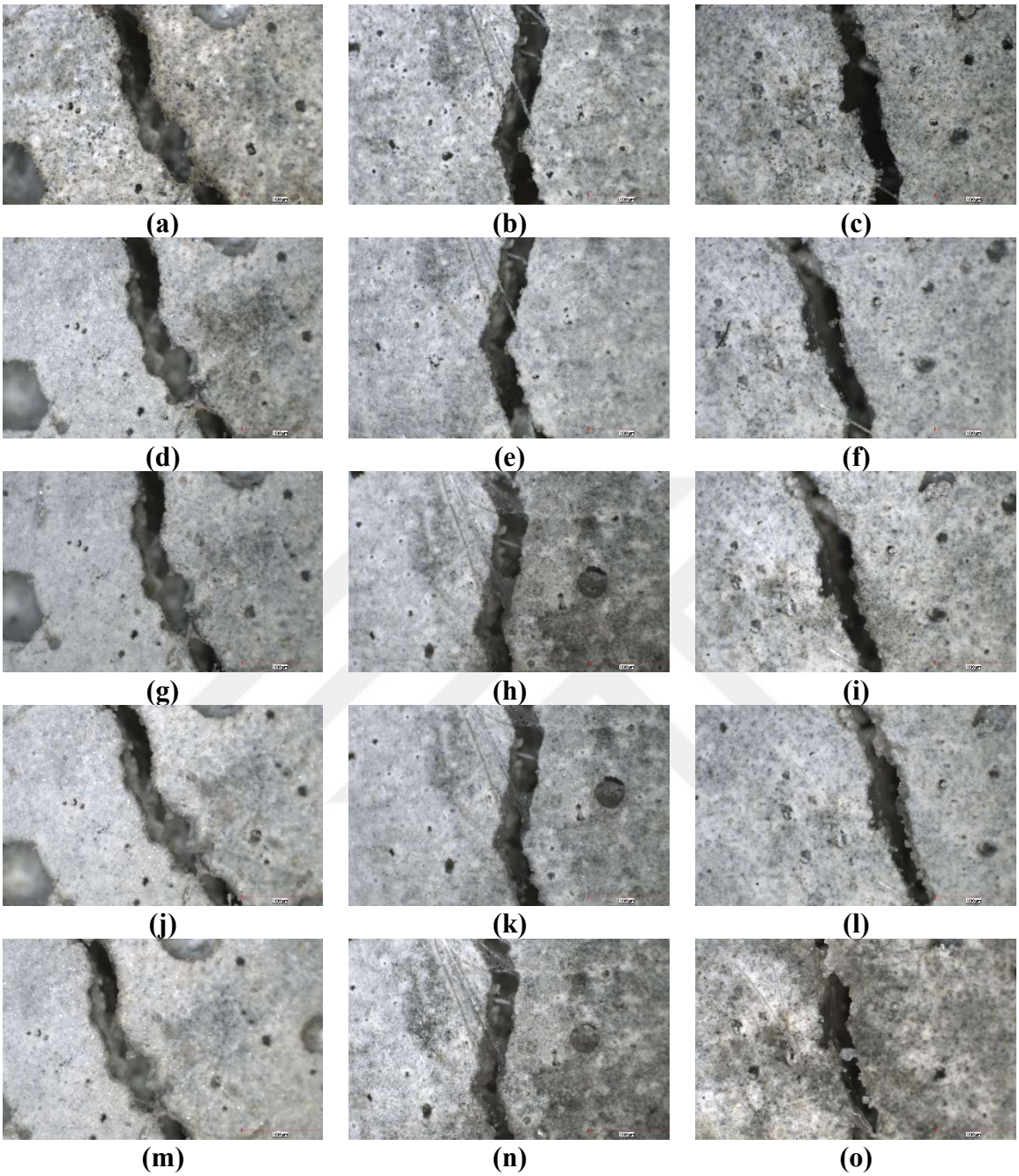

Figure A.24: The crack images of 28-day old ZEOB-1.6 samples. (a, b, c) right after cracking, (d, e, f) after 7 days of water curing, (g, h, i) after 14 days of water curing, (j, k, l) after 21 days of water curing, (m, n, o) after 28 days of water curing.

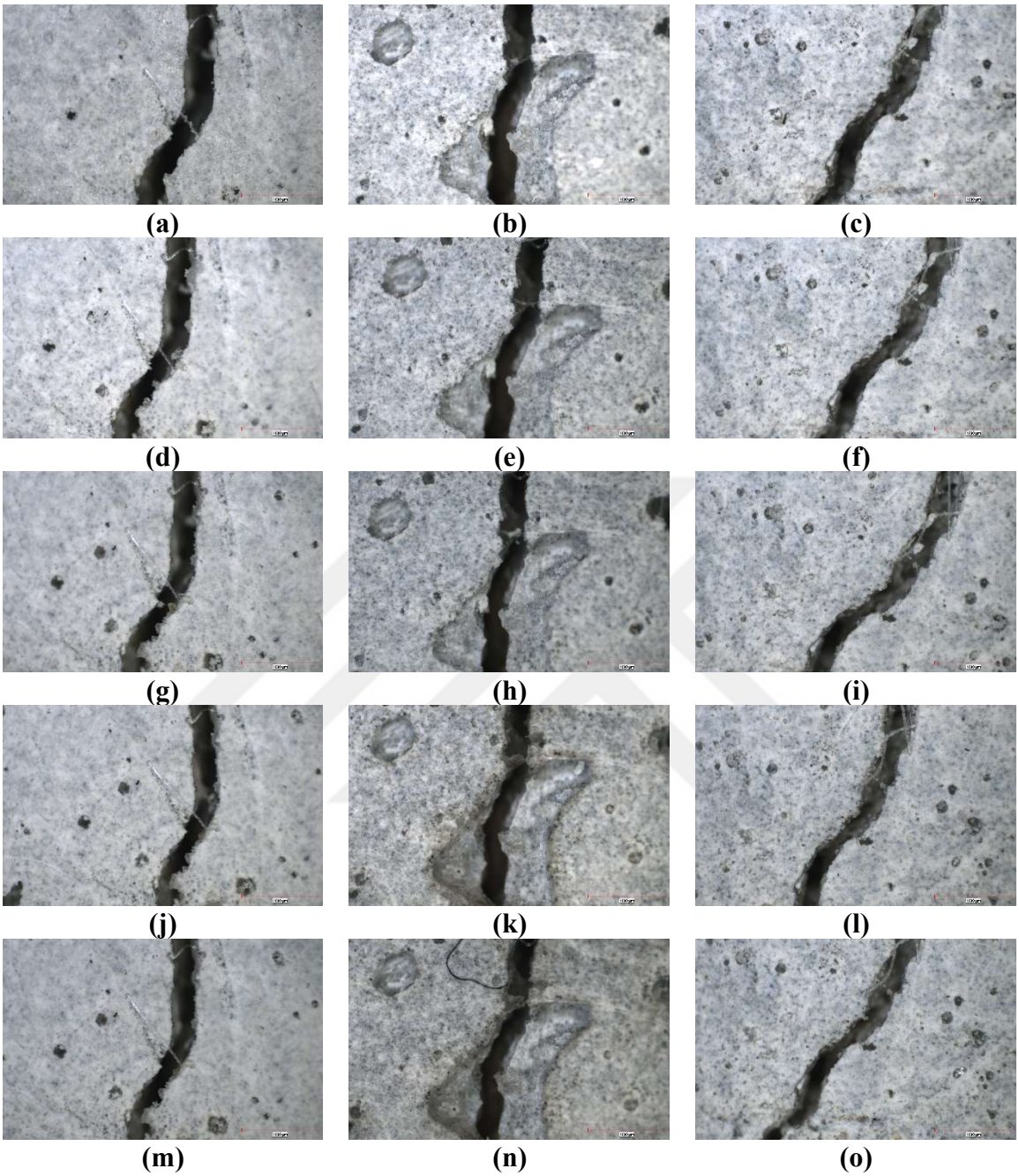

Figure A.25: The crack images of 28-day old ZEOB-1.6 samples kept at ambient conditions. (a, b, c) right after cracking, (d, e, f) after 7 days, (g, h, i) after 14 days, (j, k, l) after 21 days, (m, n, o) after 28 days.

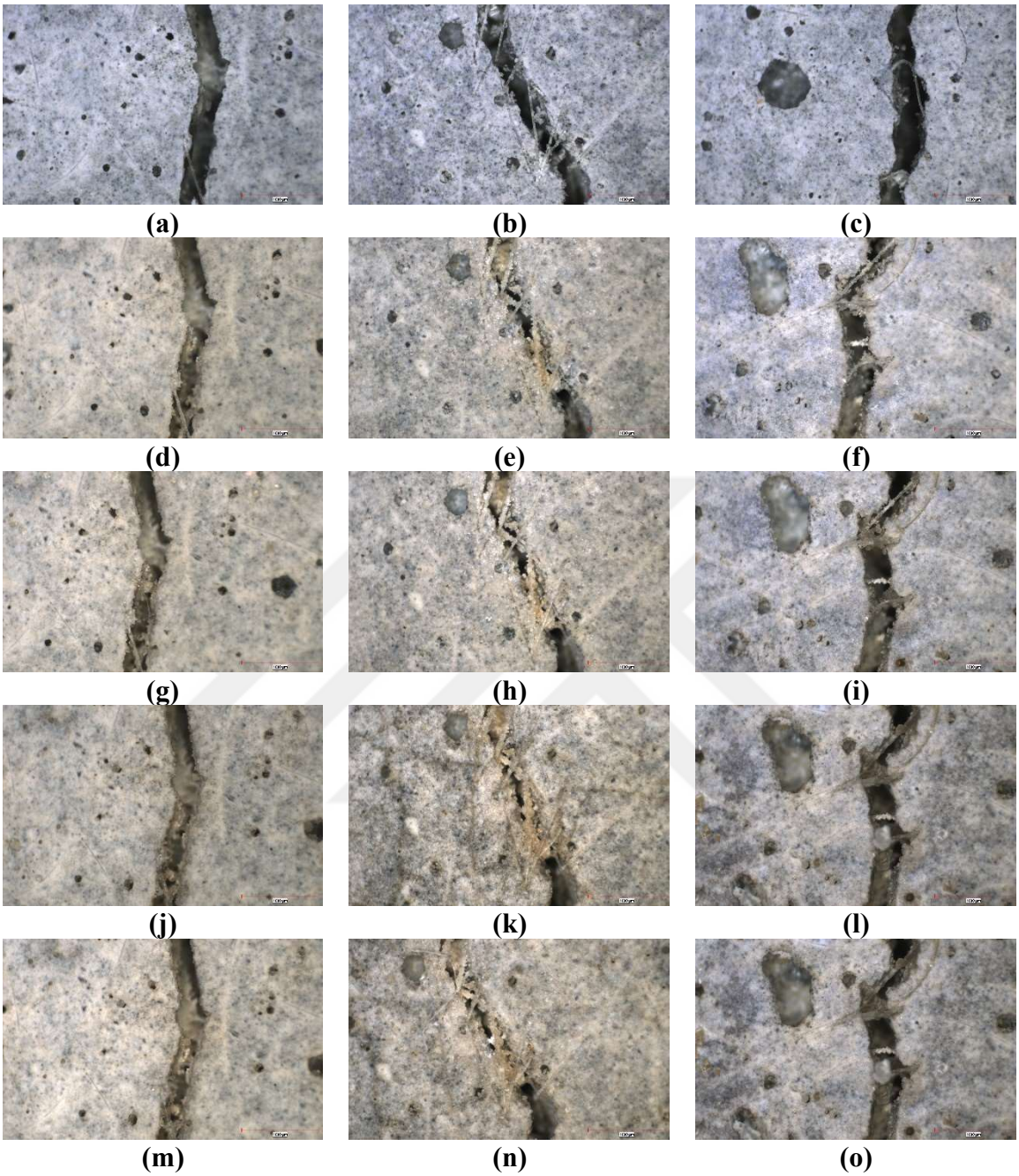

Figure A.26: The crack images of 14-day old ZEOBN-1.6 samples. (a, b, c) right after cracking, (d, e, f) after 7 days of UCSL-CA curing, (g, h, i) after 14 days of UCSL-CA curing, (j, k, l) after 21 days of UCSL-CA curing, (m, n, o) after 28 days of UCSL-CA curing.

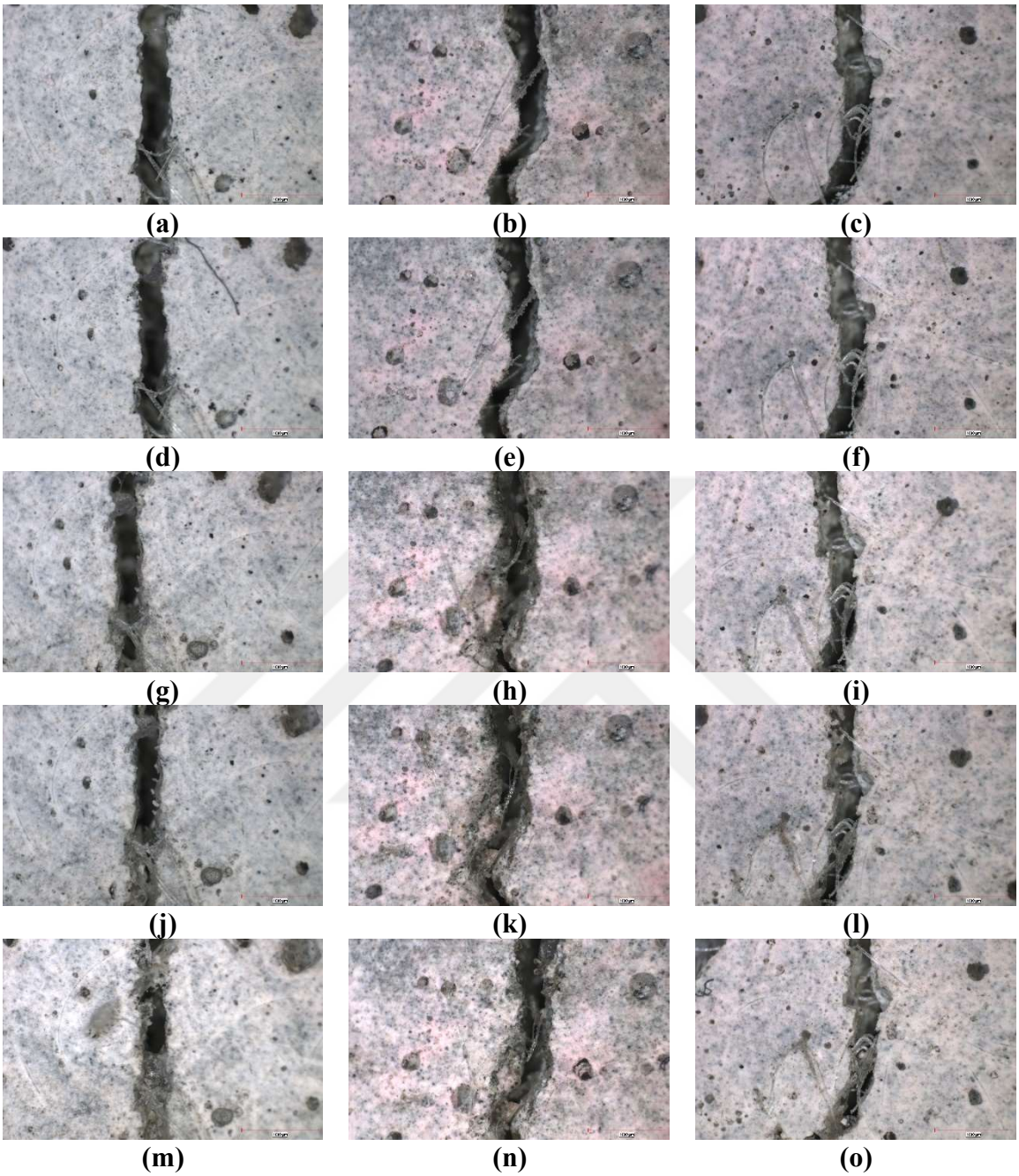

Figure A.27: The crack images of 14-day old ZEOBN-1.6 samples kept at ambient conditions. (a, b, c) right after cracking, (d, e, f) after 7 days, (g, h, i) after 14 days, (j, k, l) after 21 days, (m, n, o) after 28 days.

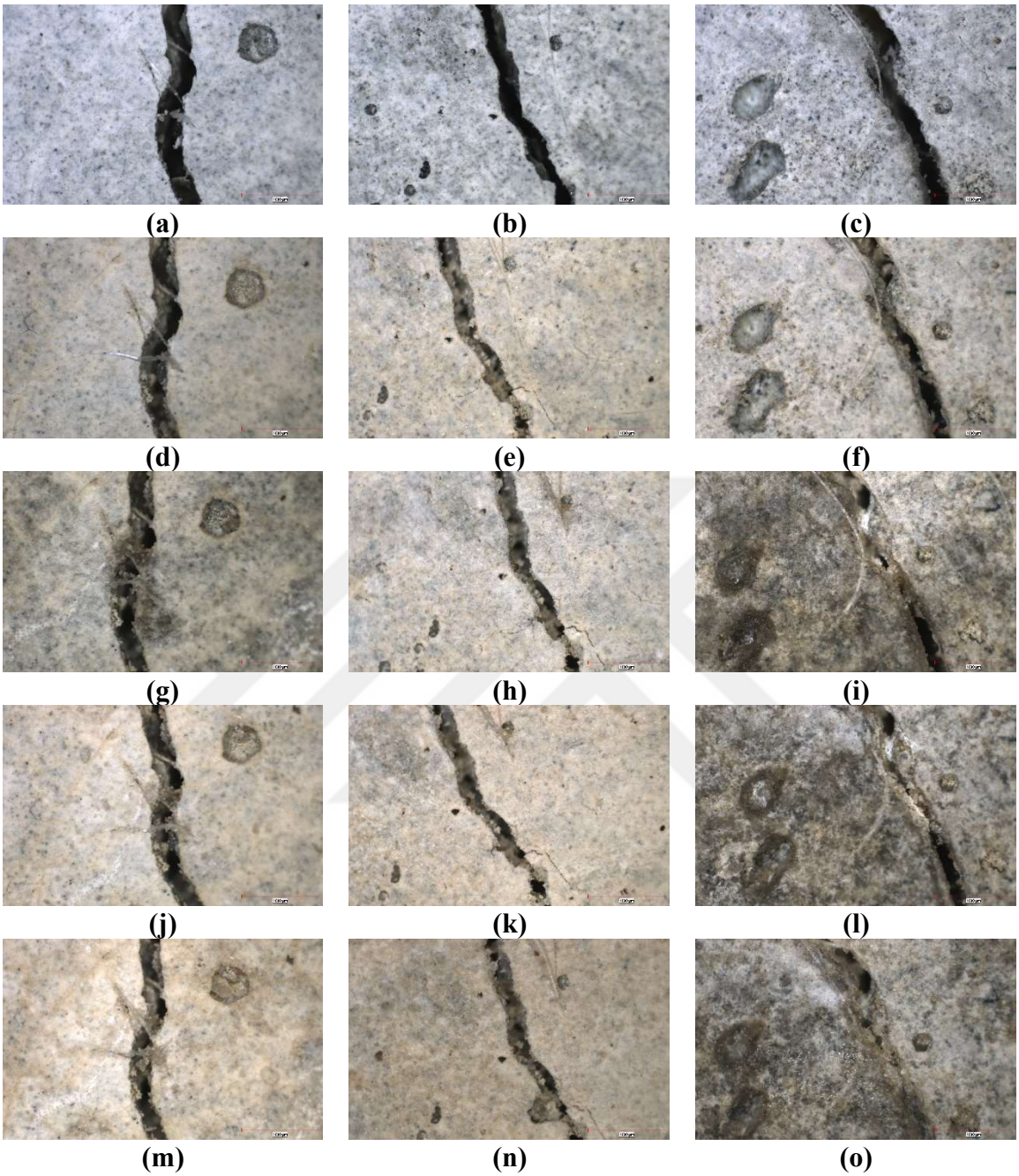

Figure A.28: The crack images of 28-day old ZEOBN-1.6 samples. (a, b, c) right after cracking, (d, e, f) after 7 days of UCSL-CA curing, (g, h, i) after 14 days of UCSL-CA curing, (j, k, l) after 21 days of UCSL-CA curing, (m, n, o) after 28 days of UCSL-CA curing.

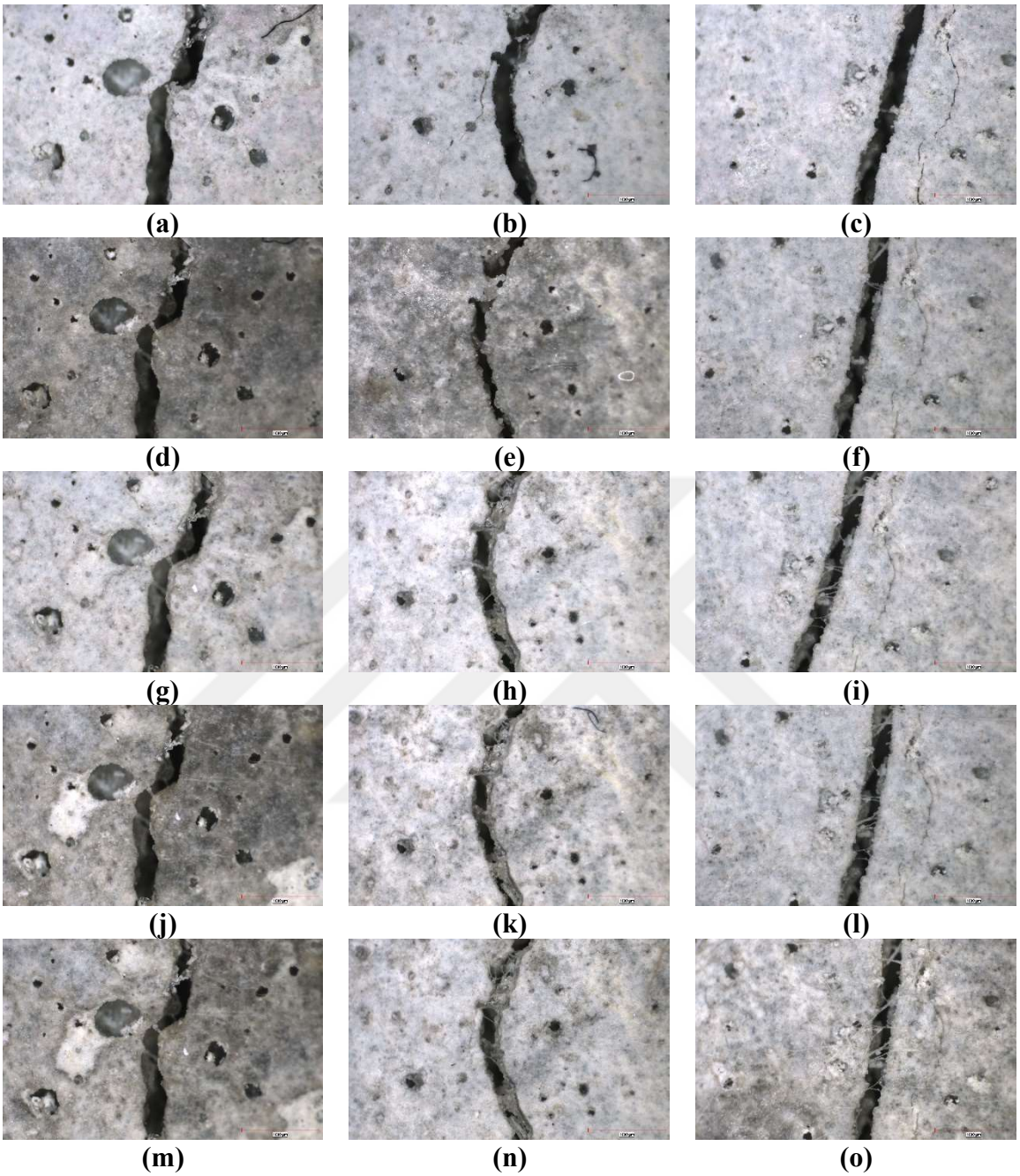

Figure A.29: The crack images of 28-day old ZEOBN-1.6 samples. (a, b, c) right after cracking, (d, e, f) after 7 days of water curing, (g, h, i) after 14 days of water curing, (j, k, l) after 21 days of water curing, (m, n, o) after 28 days of water curing.

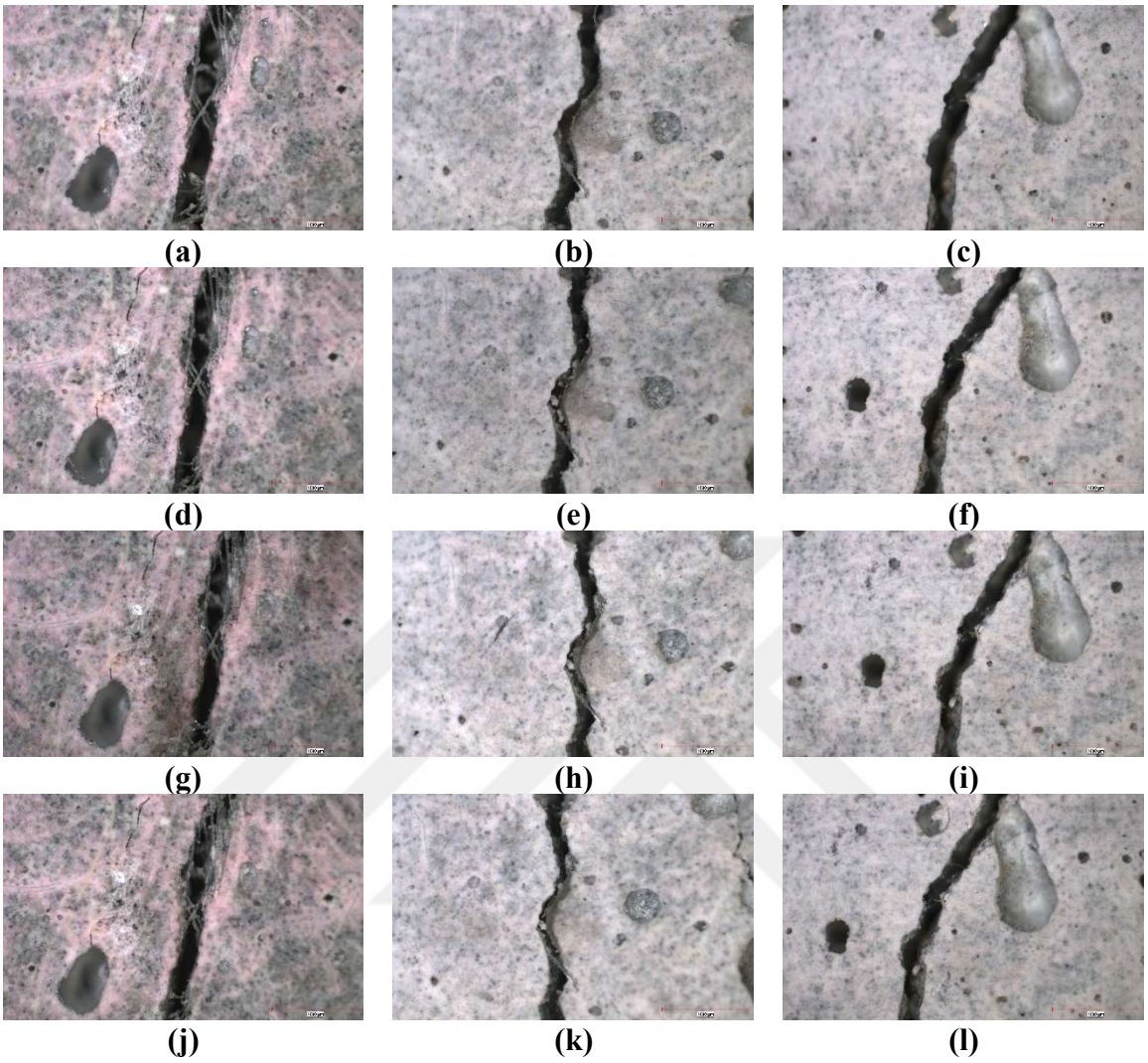

Figure A.30: The crack images of 28-day old ZEOBN-1.6 samples kept at ambient conditions. (a, b, c) right after cracking, (d, e, f) after 7 days, (g, h, i) after 14 days, (j, k, l) after 28 days

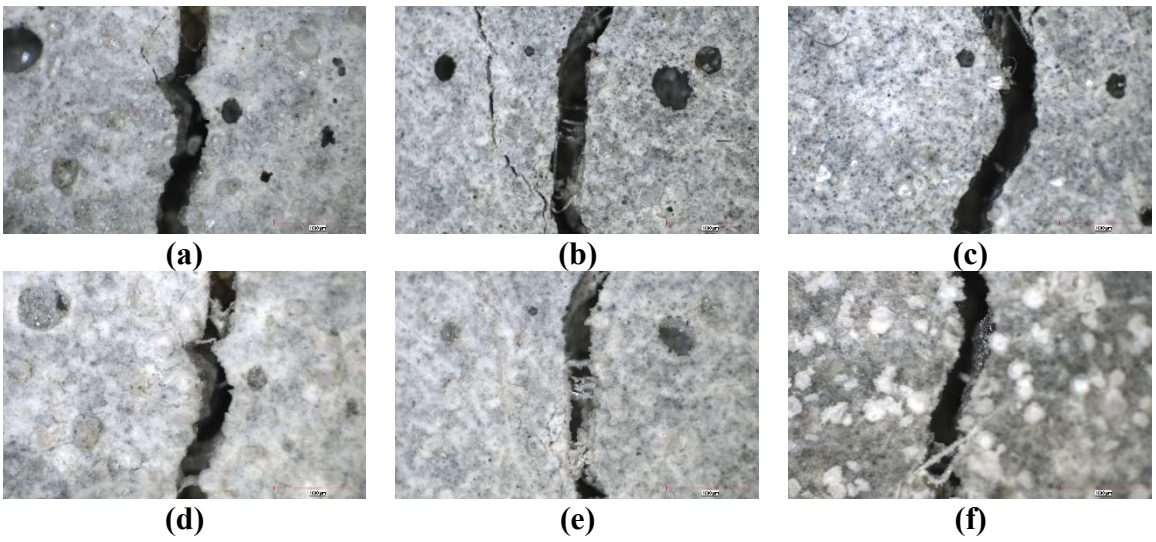

(g) (h) (i)

Figure A.31: The crack images of 14-day old PERC samples. (a, b, c) right after cracking, (d, e, f) after 7 days of water curing, (g, h, i) after 28 days of water curing.

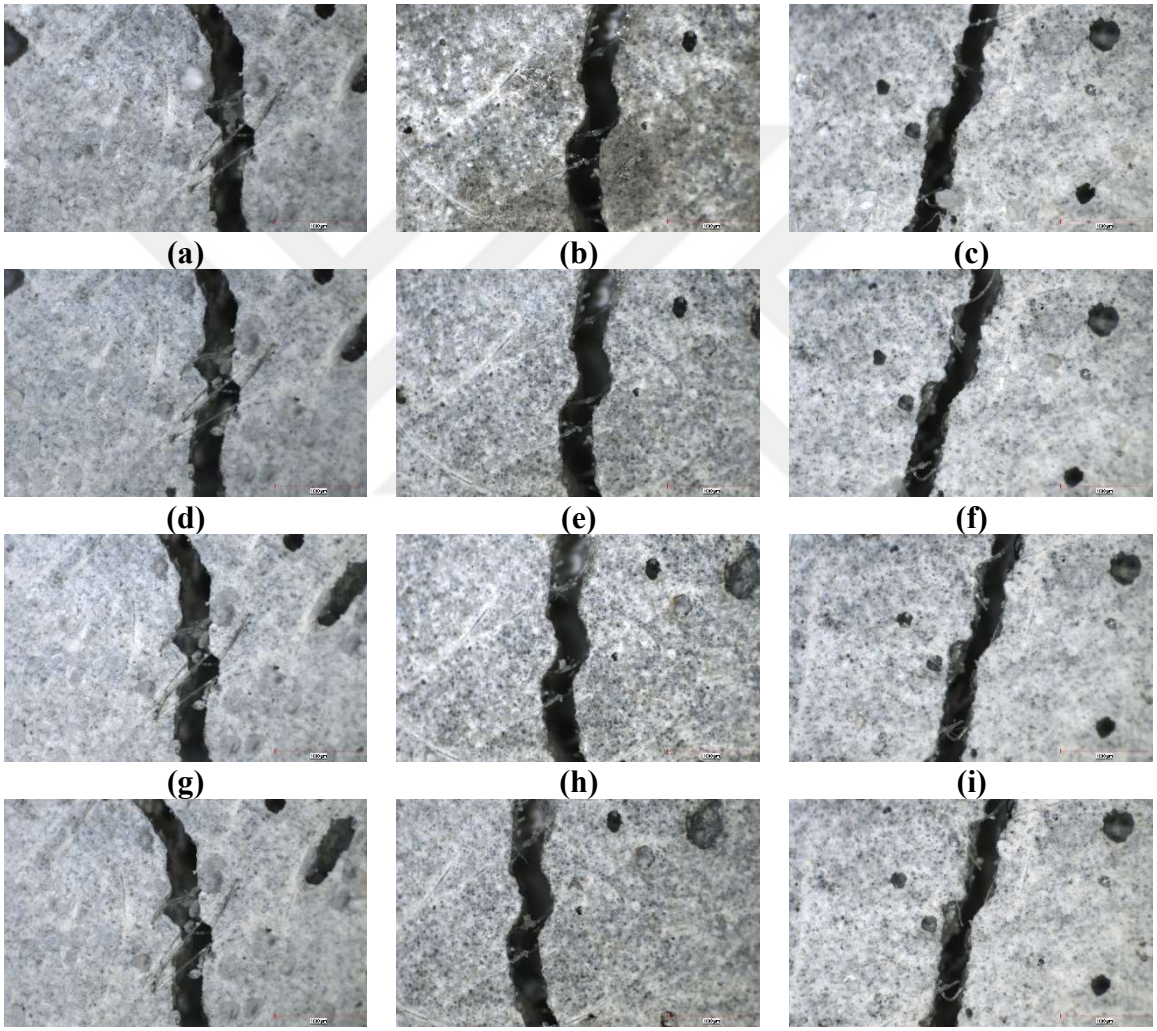

(a) (b) (c)

(d) (e) (f)

(g) (h) (i)

(j) (k) (l)

Figure A.32: The crack images of 14-day old PERC samples kept at ambient conditions. (a, b, c) right after cracking, (d, e, f) after 7 days, (g, h, i) after 14 days, (j, k, l) after 28 days.

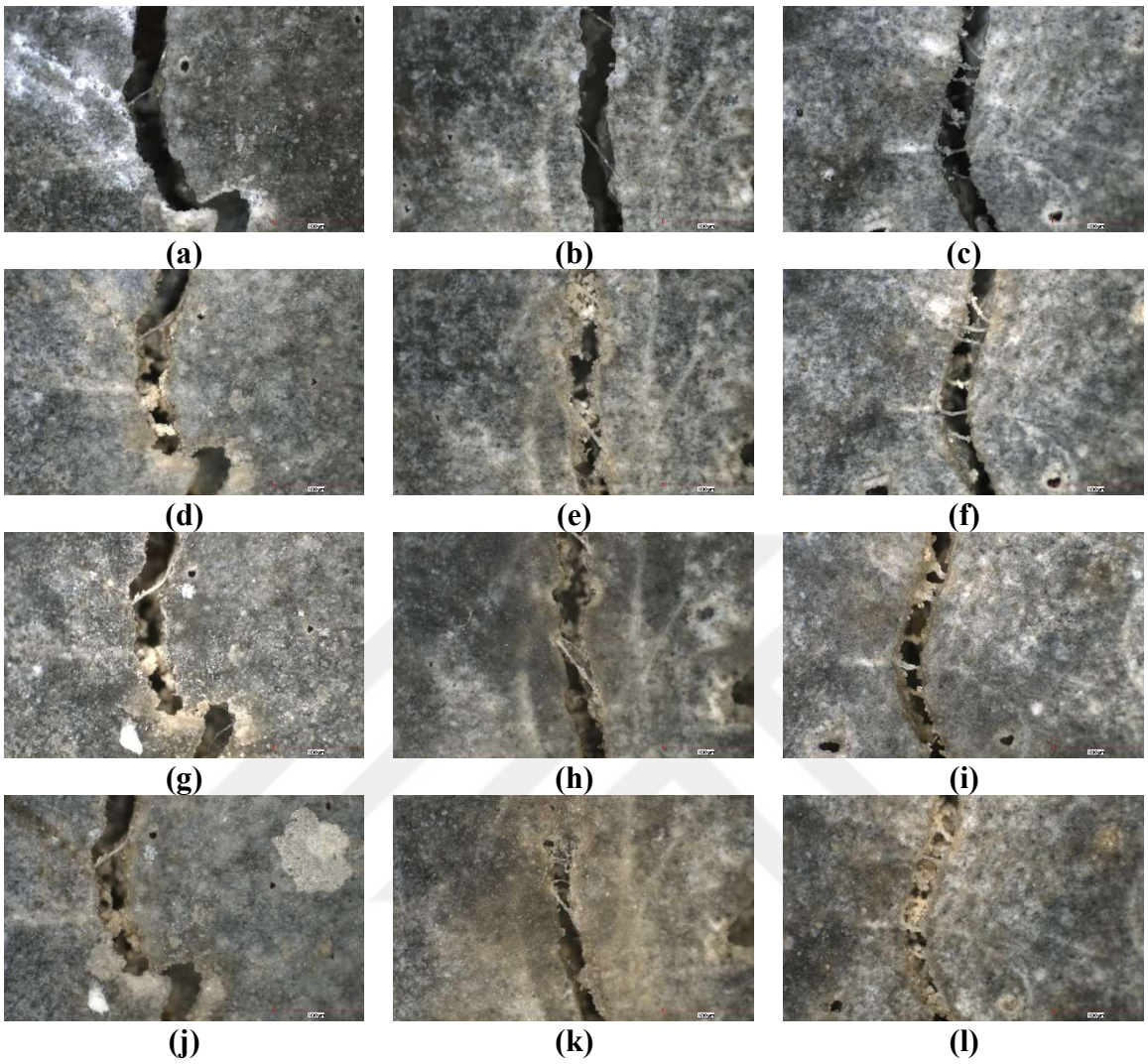

Figure A.33: The crack images of 28-day old PERC samples. (a, b, c) right after cracking, (d, e, f) after 7 days of UCSL-CA curing, (g, h, i) after 14 days of UCSL-CA curing. (j, k, l) after 28 days of UCSL-CA curing.

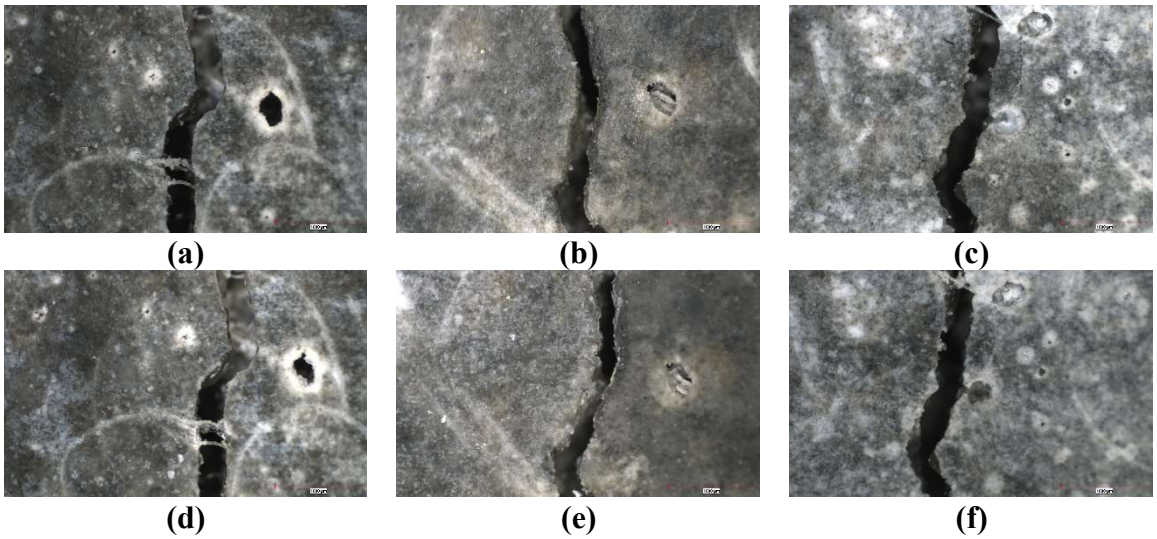

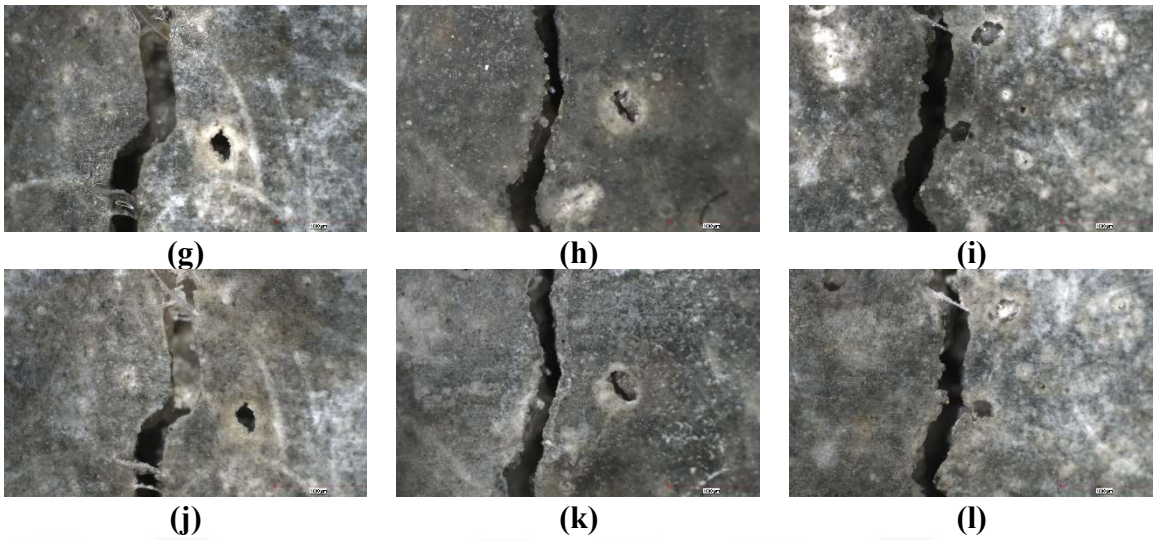

Figure A.34: The crack images of 28-day old PERC samples. (a, b, c) right after cracking, (d, e, f) after 7 days of water curing, (g, h, i) after 21 days of water curing. (j, k, l) after 28 days of water curing.

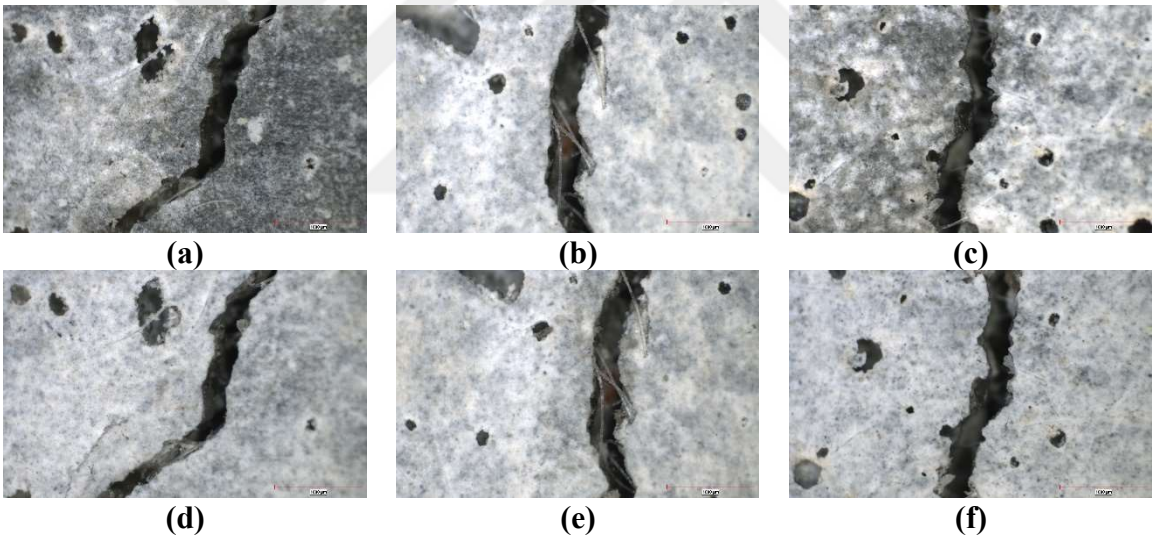

Figure A.35: The crack images of 28-day old PERC samples kept at ambient conditions. (a, b, c) right after cracking, (d, e, f) after 28 days.

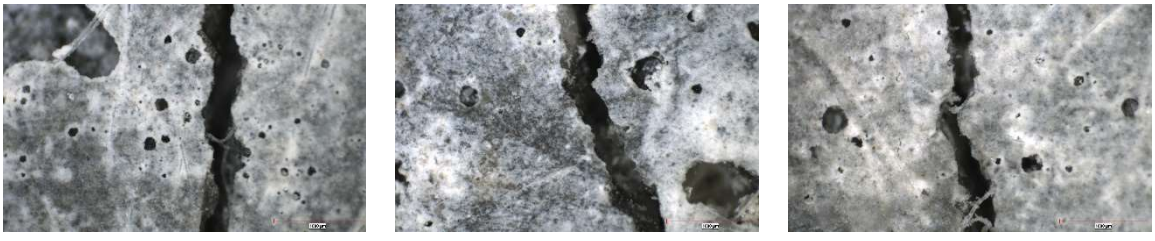

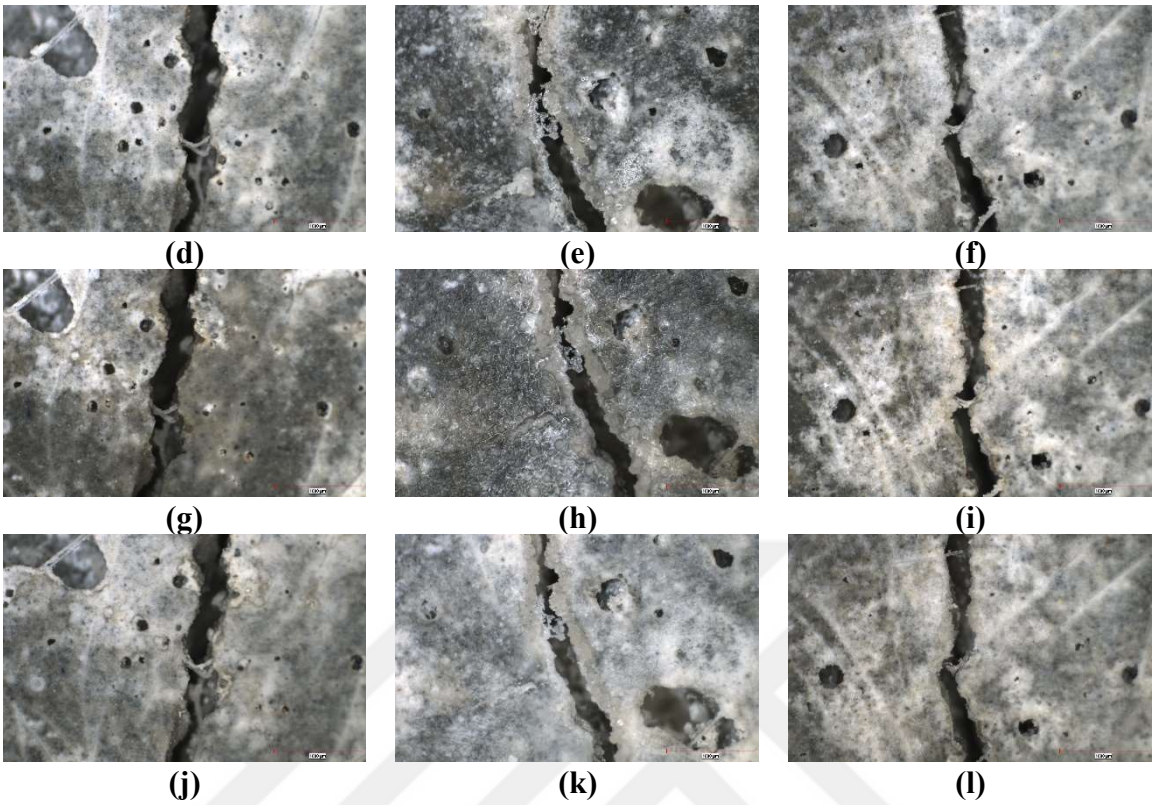

Figure A.36: The crack images of 14-day old PERB samples. (a, b, c) right after cracking, (d, e, f) after 7 days of water curing, (g, h, i) after 14 days of water curing. (j, k, l) after 28 days of water curing.

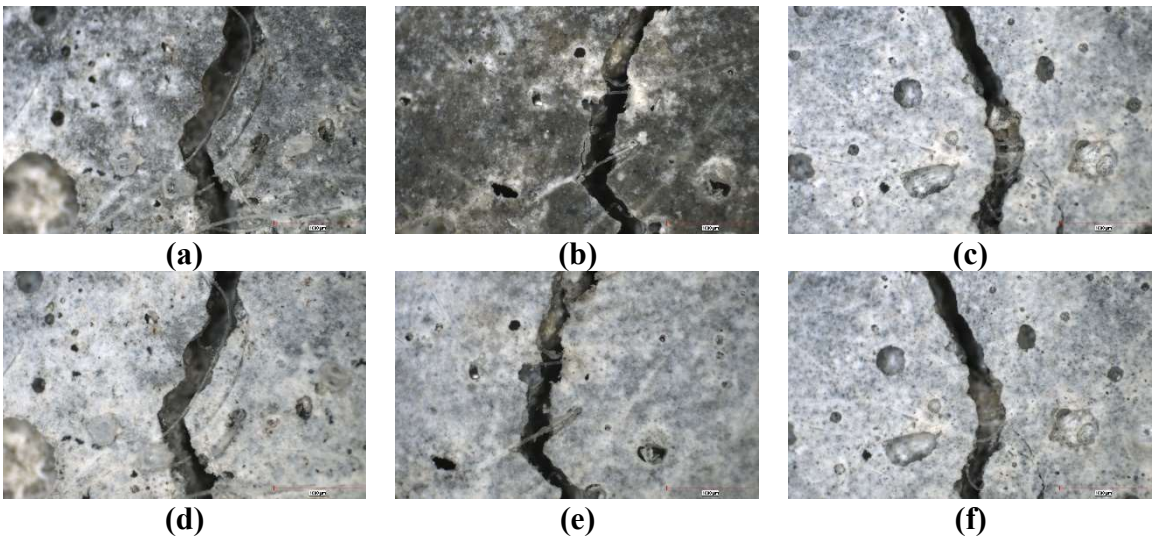

Figure A.37: The crack images of 14-day old PERB samples kept at ambient conditions. (a, b, c) right after cracking, (d, e, f) after 28 days.

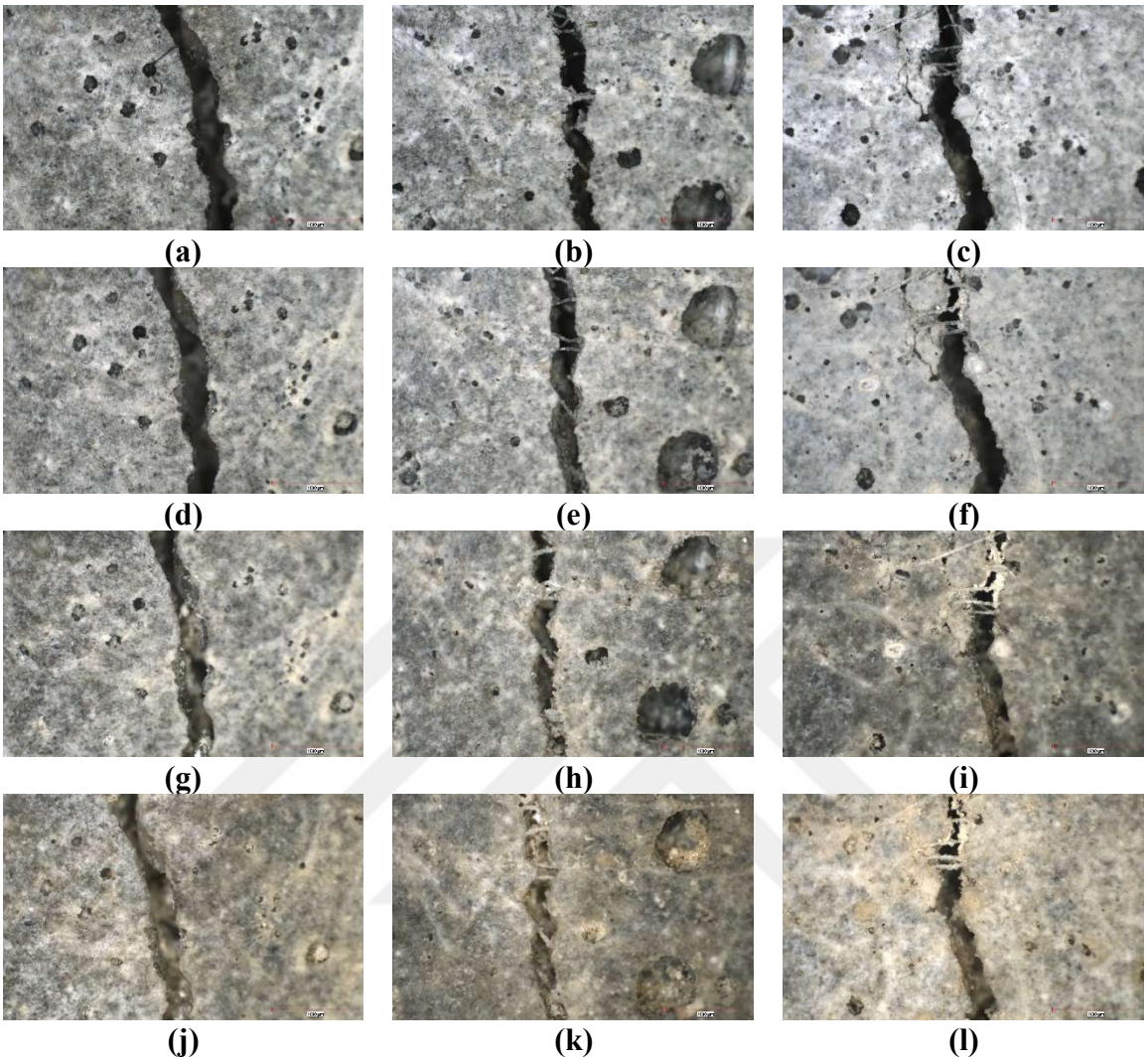

Figure A.38: The crack images of 28-day old PERB samples. (a, b, c) right after cracking, (d, e, f) after 7 days of UCSL-CA curing, (g, h, i) after 14 days of UCSL-CA curing. (j, k, l) after 28 days of UCSL-CA curing.

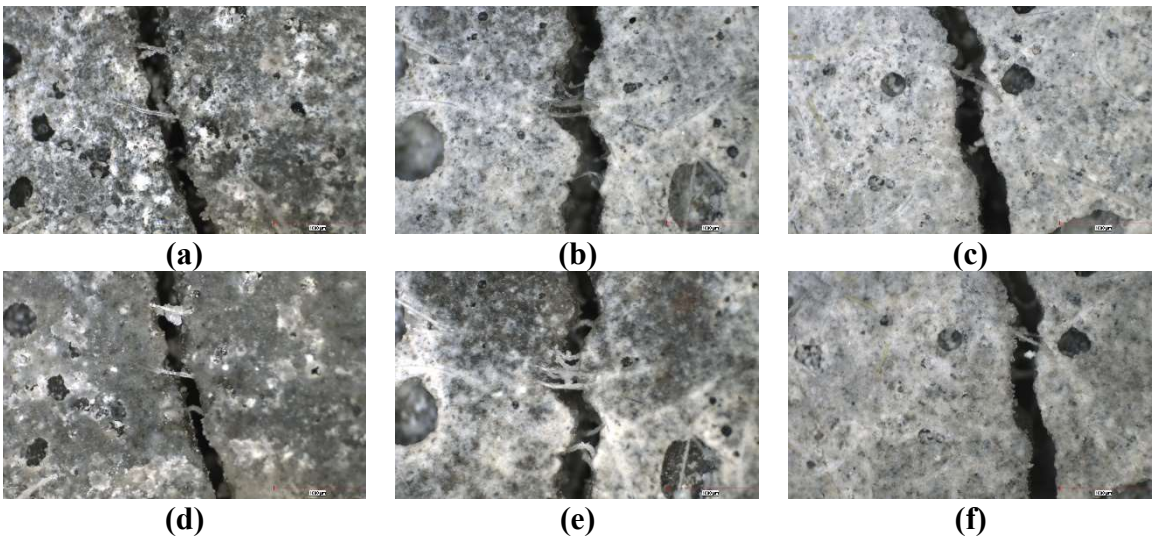

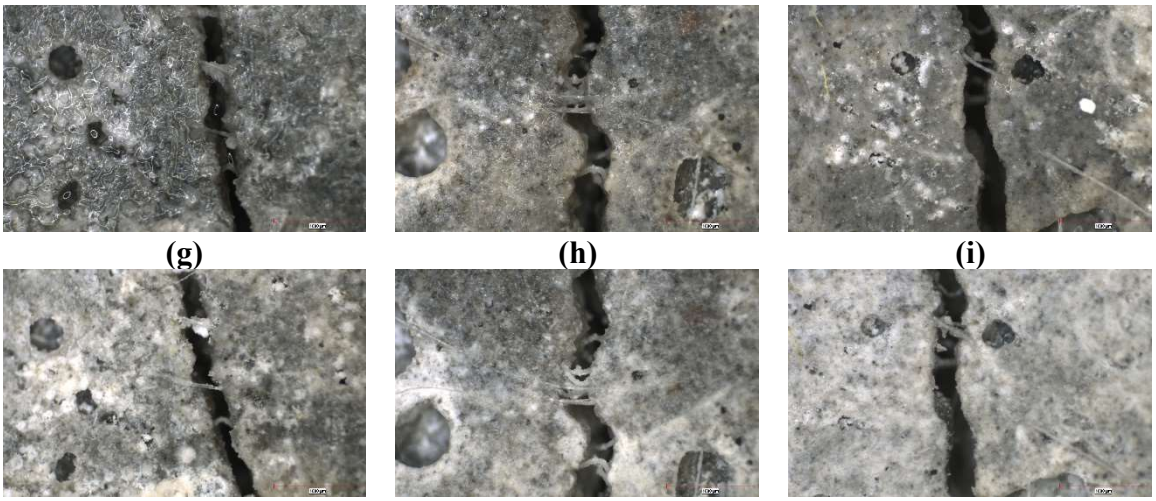

Figure A.39: The crack images of 28-day old PERB samples. (a, b, c) right after cracking, (d, e, f) after 7 days of water curing, (g, h, i) after 14 days of water curing. (j, k, l) after 28 days of water curing.

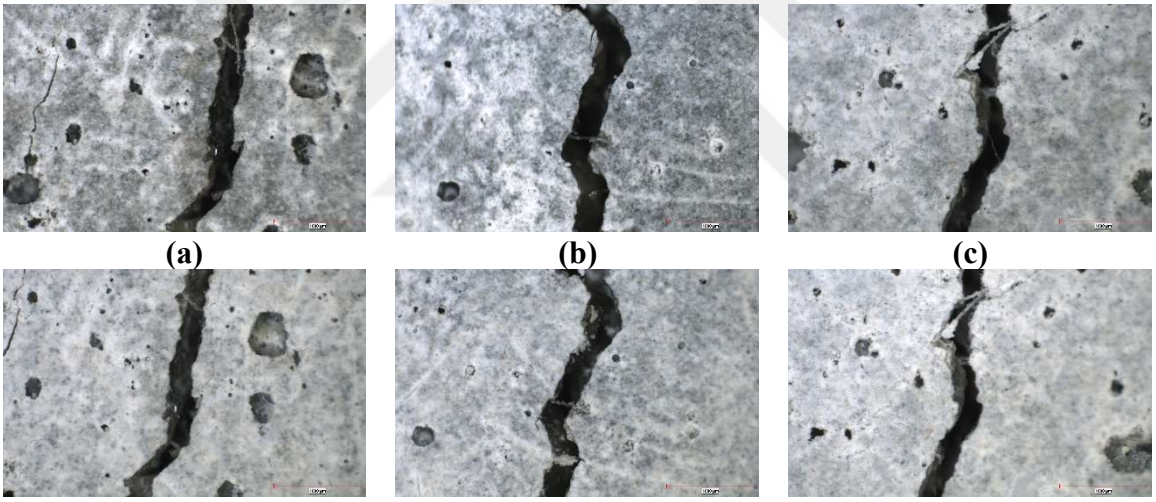

Figure A.40: The crack images of 28-day old PERB samples kept at ambient conditions. (a, b, c) right after cracking, (d, e, f) after 28 days.

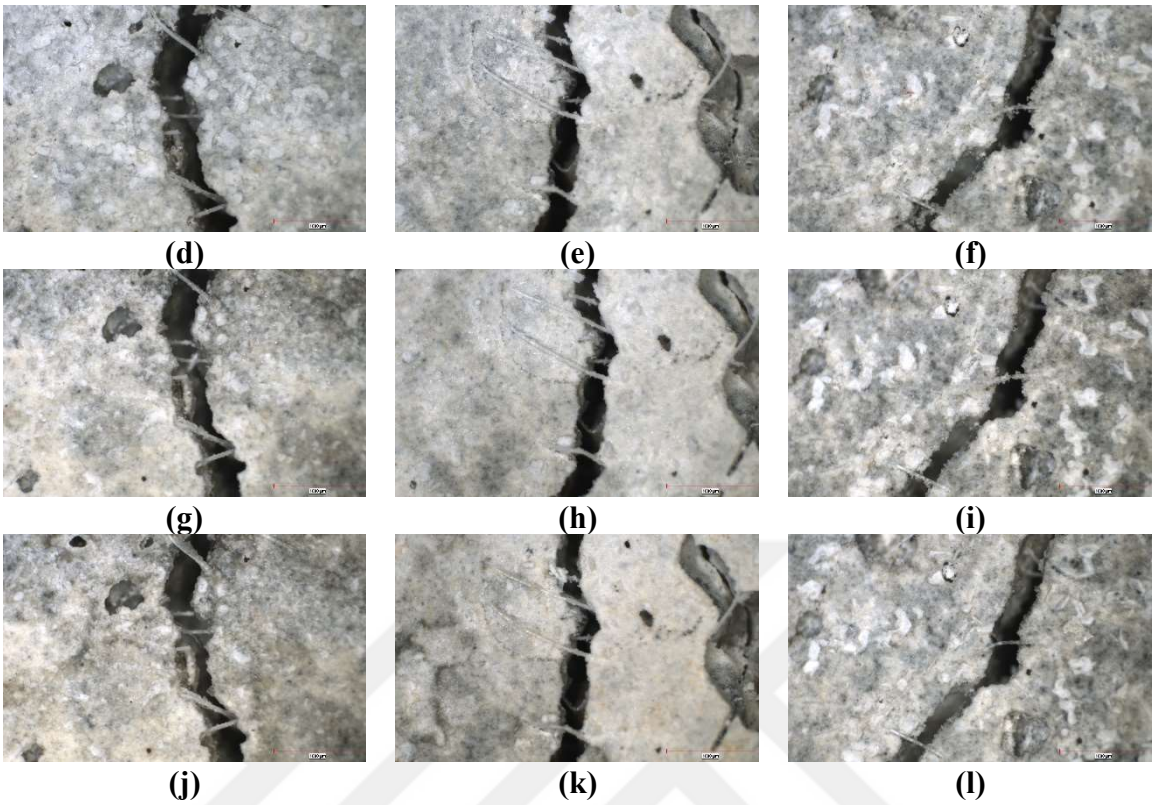

Figure A.41: The crack images of 14-day old PERBN samples. (a, b, c) right after cracking, (d, e, f) after 7 days of water curing, (g, h, i) after 21 days of water curing. (j, k, l) after 28 days of water curing.

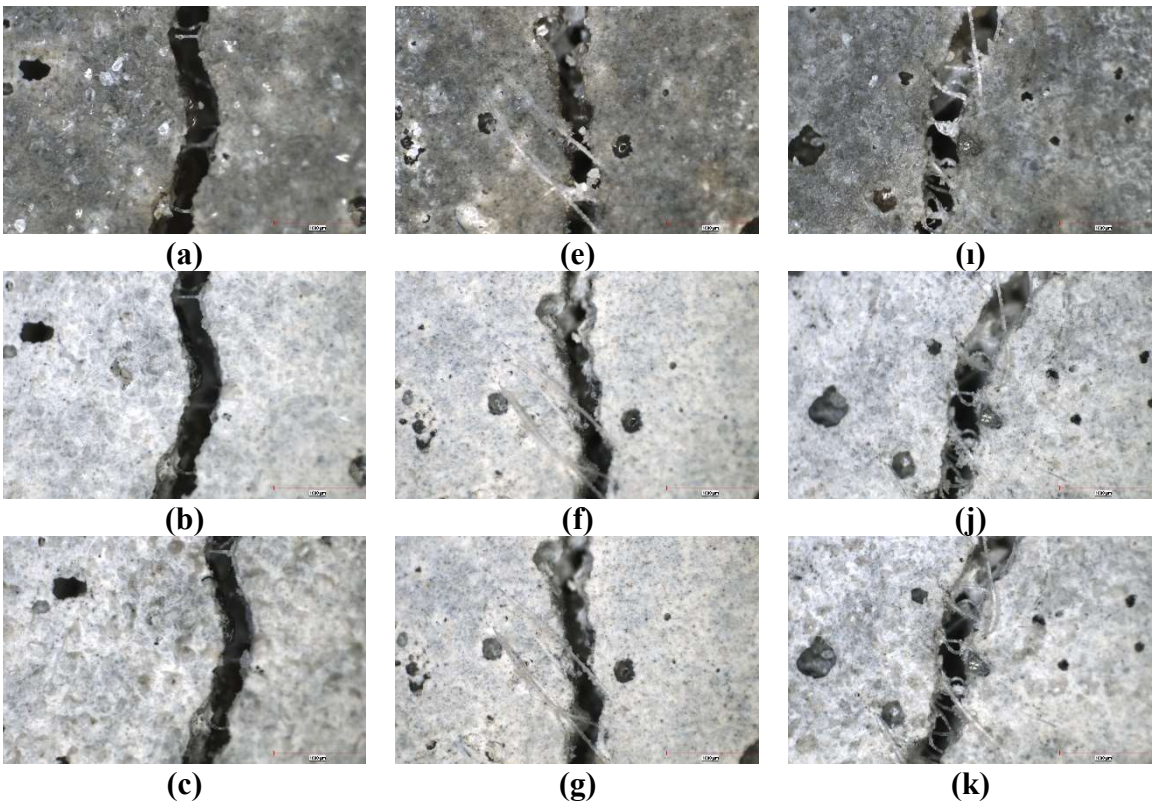

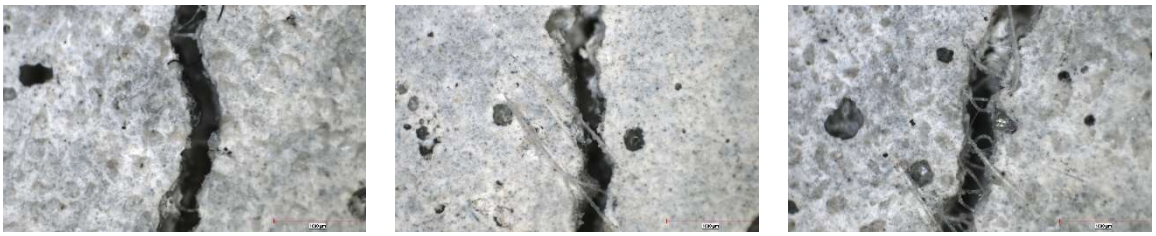

(d) (h) (l)

Figure A.42: The crack images of 14-day old PERBN samples kept at ambient conditions. (a, b, c) right after cracking, (d, e, f) after 7 days, (g, h, i) after 14 days, (j, k, l) after 28 days.

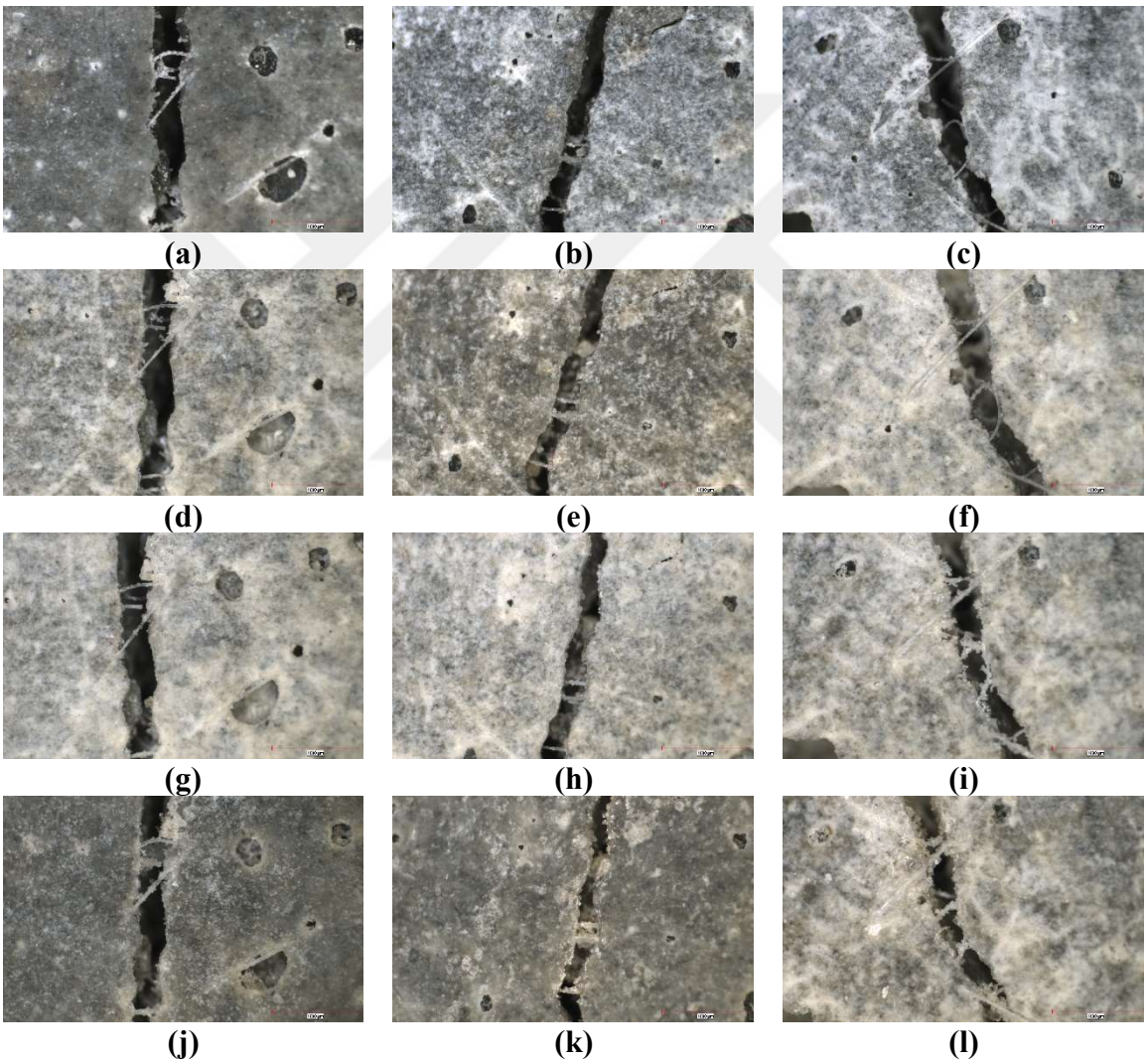

(a) (b) (c)

(d) (e) (f)

(g) (h) (i)

(j) (k) (l)

Figure A.43: The crack images of 28-day old PERBN samples. (a, b, c) right after cracking, (d, e, f) after 7 days of UCSL-CA curing, (g, h, i) after 21 days of UCSL-CA curing, (j, k, l) after 28 days of UCSL-CA curing.

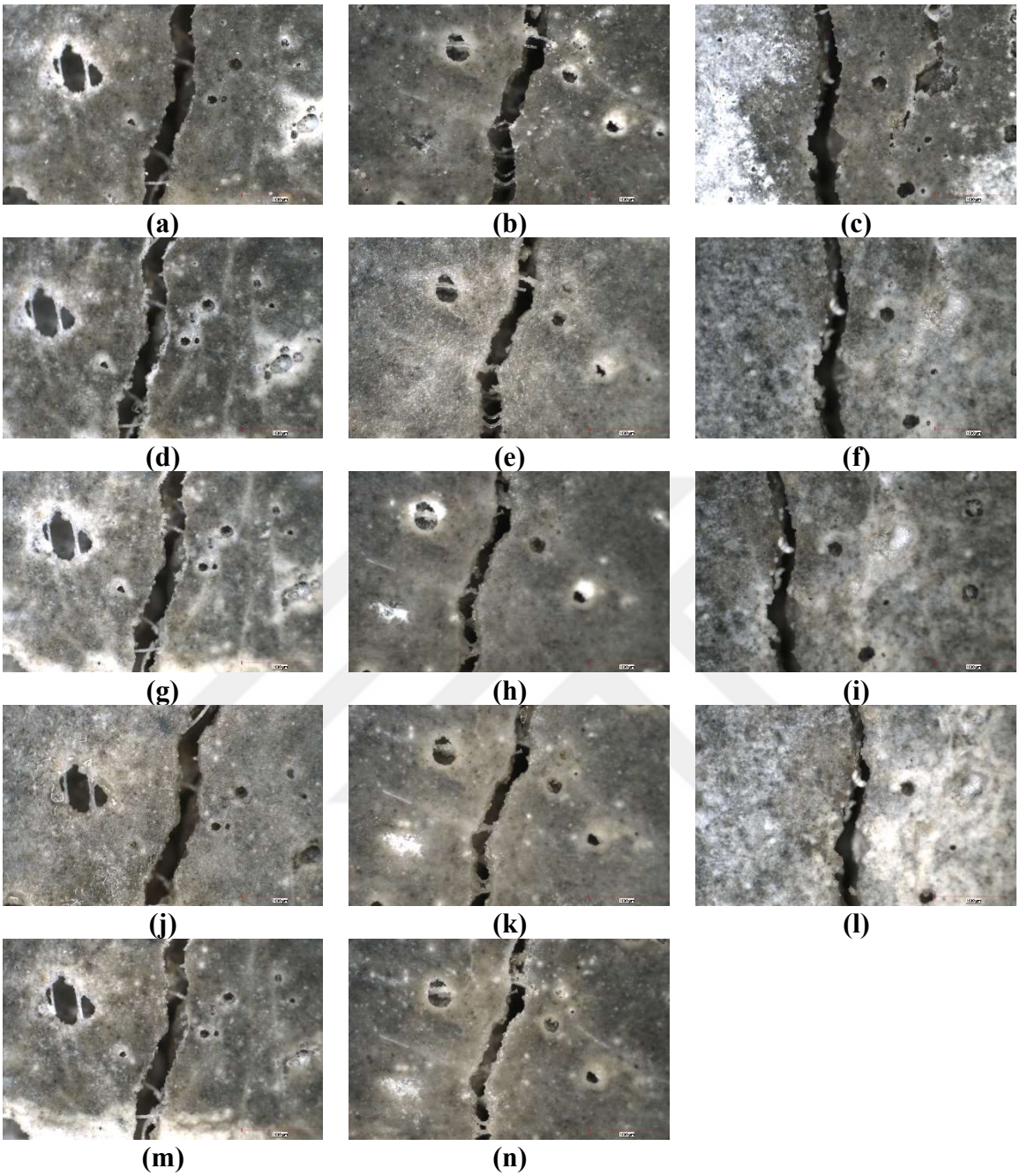

Figure A.44: The crack images of 28-day old PERBN samples. (a, b, c) right after cracking, (d, e, f) after 7 days of water curing, (g, h, i) after 14 days of water curing, (j, k, l) after 21 days of water curing, (m, n) after 28 days of water curing.

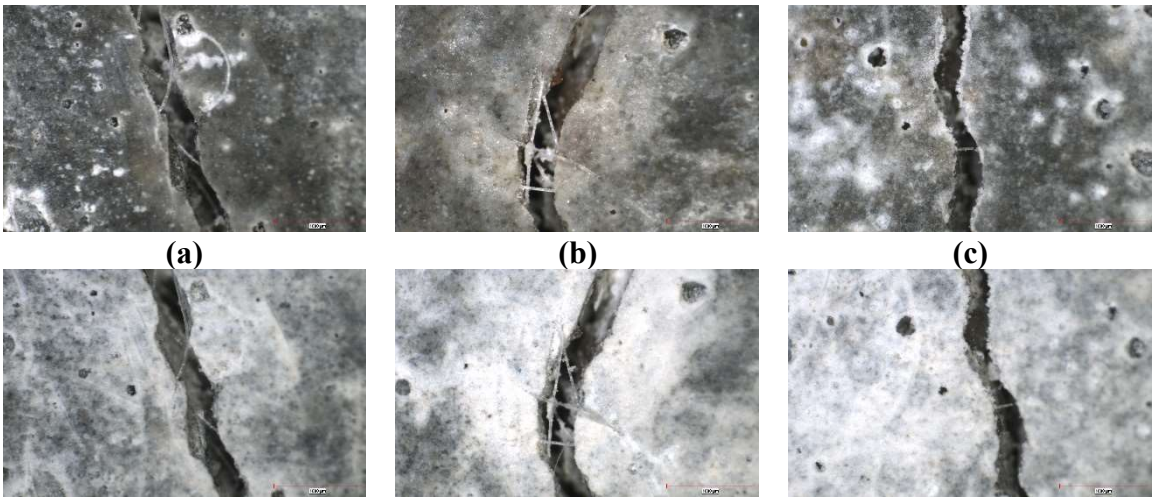

Figure A.45: The crack images of 28-day old PERBN samples kept at ambient conditions. (a, b, c) right after cracking, (d, e, f) after 28 days.

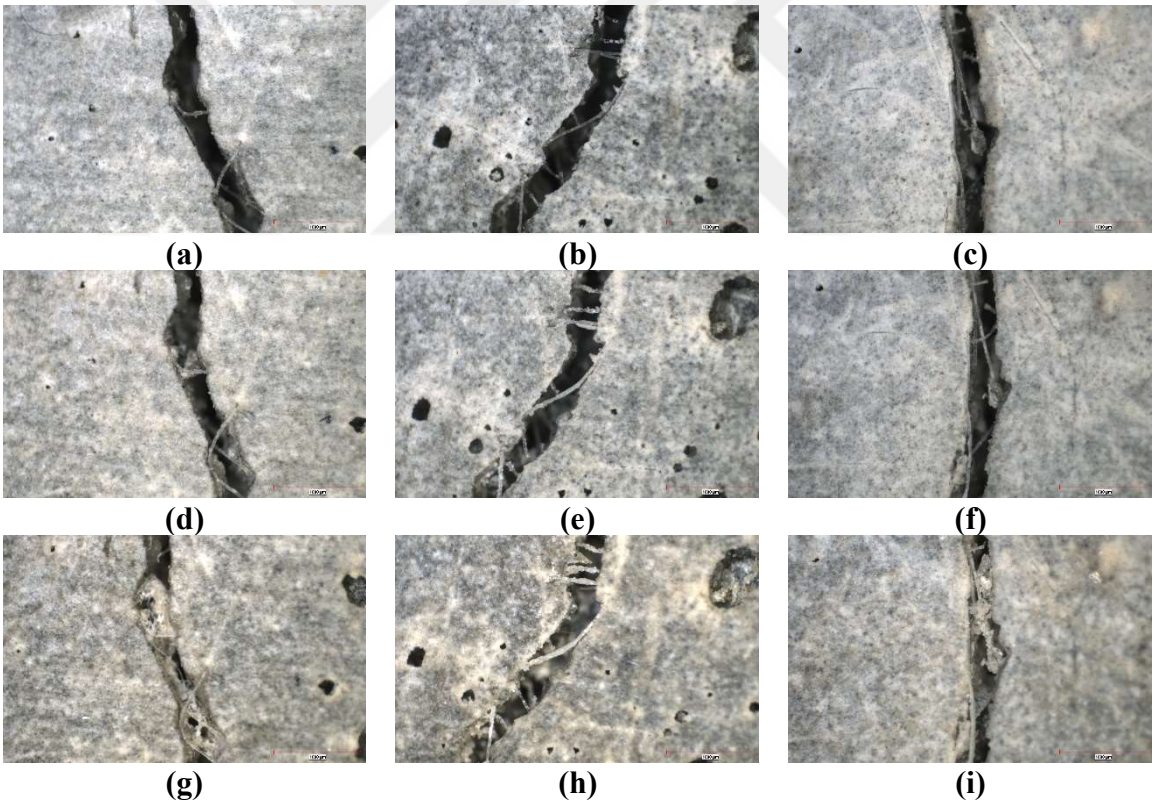

(j) (k) (l)

Figure A.46: The crack images of 14-day old METC samples. (a, b, c) right after cracking, (d, e, f) after 14 days of UCSL-CA curing, (g, h, i) after 21 days of UCSL-CA curing, (j, k, l) after 28 days of UCSL-CA curing.

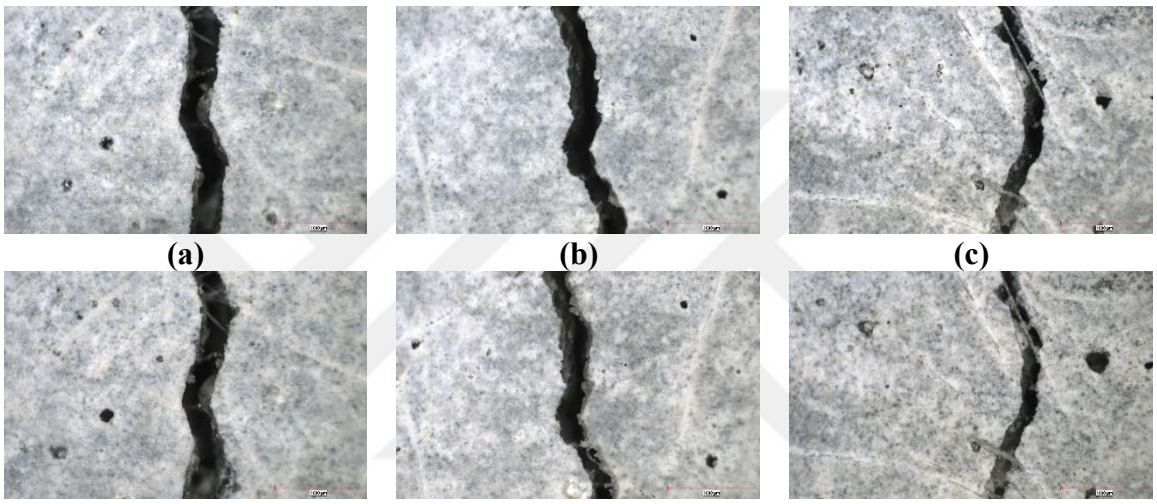

(a) (b) (c)

(d) (e) (f)

Figure A.47: The crack images of 14-day old METC samples kept at ambient conditions. (a, b, c) right after cracking, (d, e, f) after 28 days.

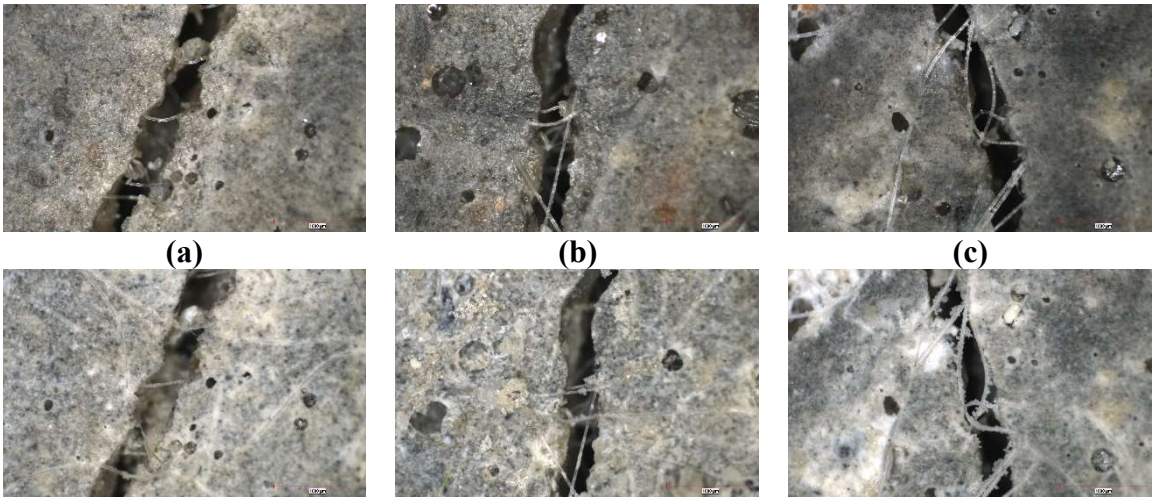

(a) (b) (c)

(d) (e) (f)

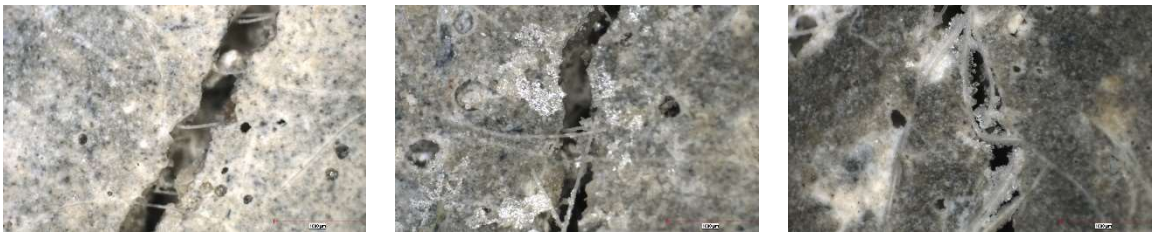

(g) (h) (i)

Figure A.48: The crack images of 28-day old METC samples. (a, b, c) right after cracking, (d, e, f) after 21 days of UCSL-CA curing, (g, h, i) after 28 days of UCSL-CA curing.

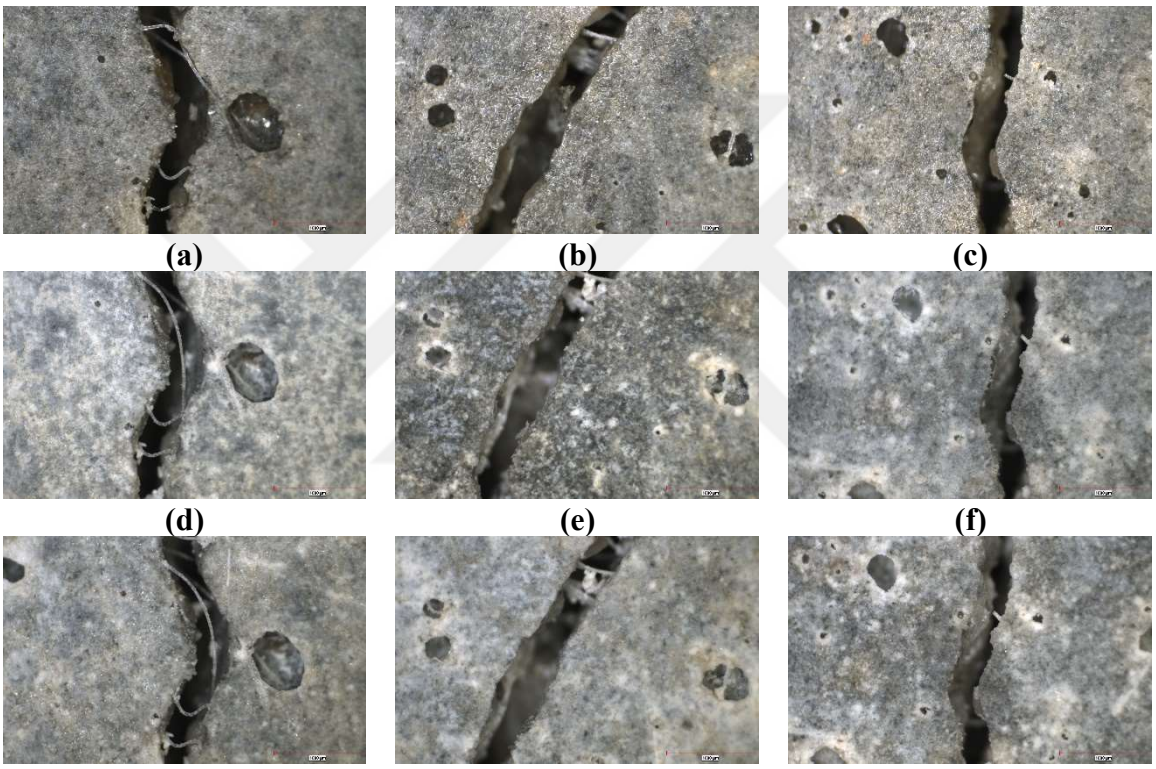

(a) (b) (c)

(d) (e) (f)

(g) (h) (i)

Figure A.49: The crack images of 28-day old METC samples. (a, b, c) right after cracking, (d, e, f) after 14 days of water curing, (g, h, i) after 28 days of water curing.

(a) (b) (c)

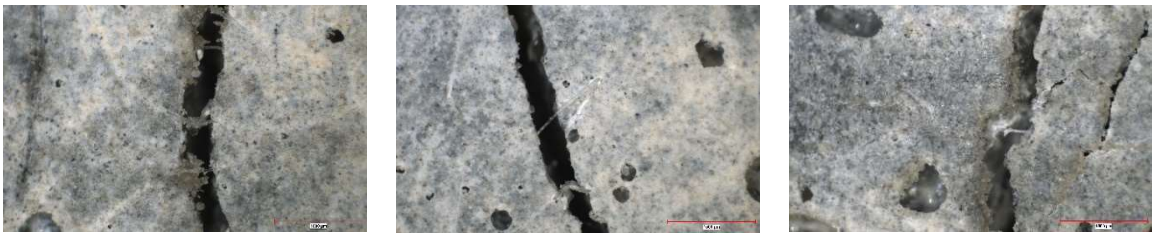

(d) (e) (f)

Figure A.50: The crack images of 28-day old METC samples kept at ambient conditions. (a, b, c) right after cracking, (d, e, f) after 28 days.

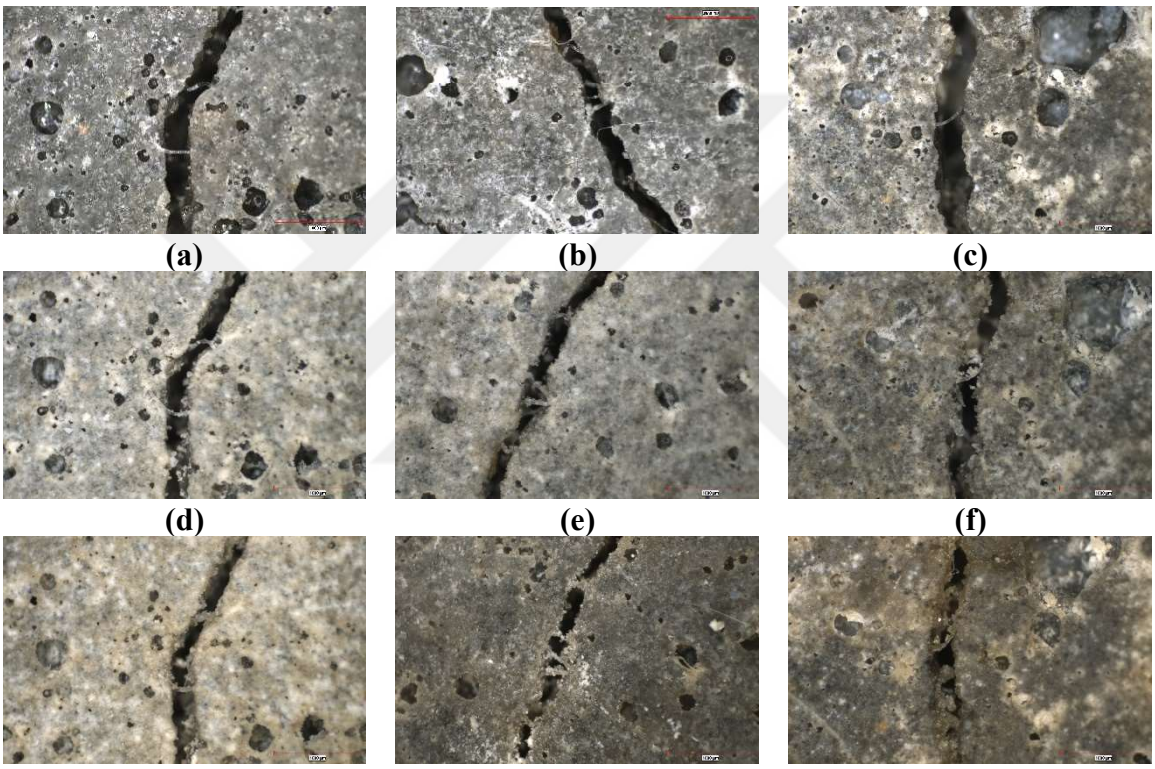

(a) (b) (c)

(d) (e) (f)

(g) (h) (i)

Figure A.51: The crack images of 14-day old METB samples. (a, b, c) right after cracking, (d, e, f) after 21 days of UCSL-CA curing, (g, h, i) after 28 days of UCSL-CA curing.

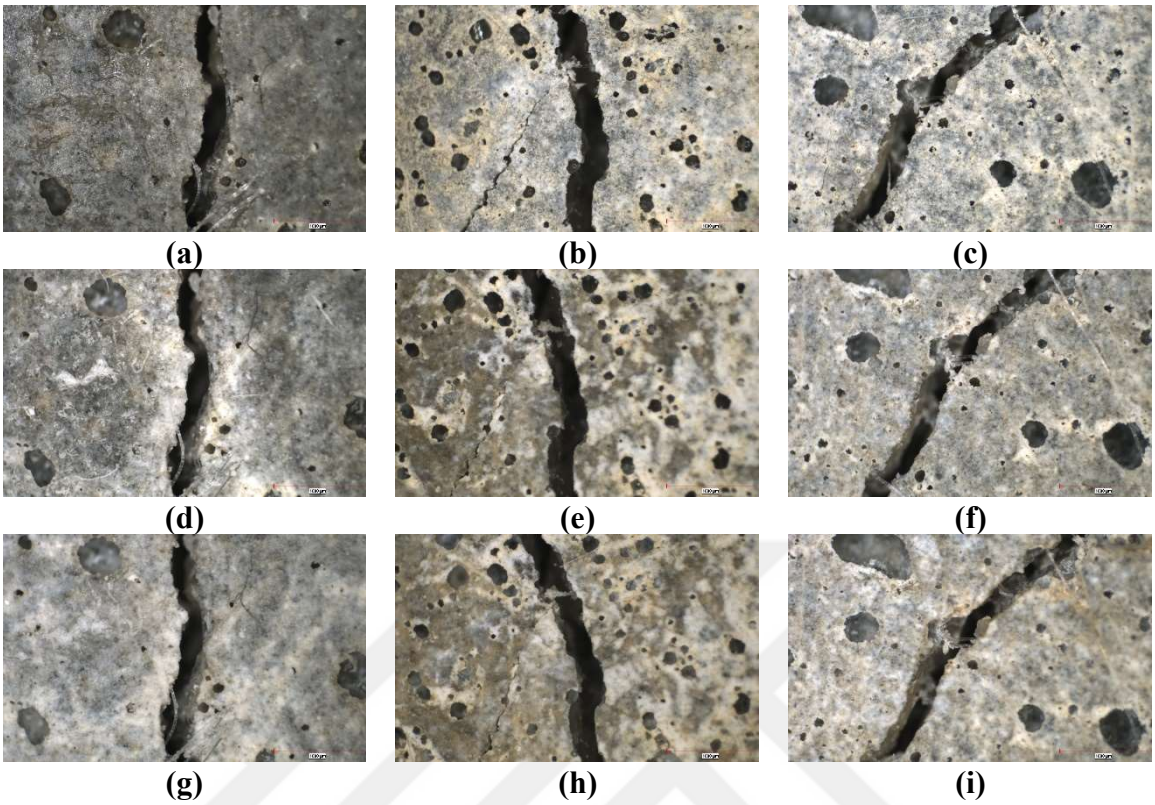

Figure A.52: The crack images of 14-day old METB samples. (a, b, c) right after cracking, (d, e, f) after 14 days of water curing, (g, h, i) after 28 days of water curing.

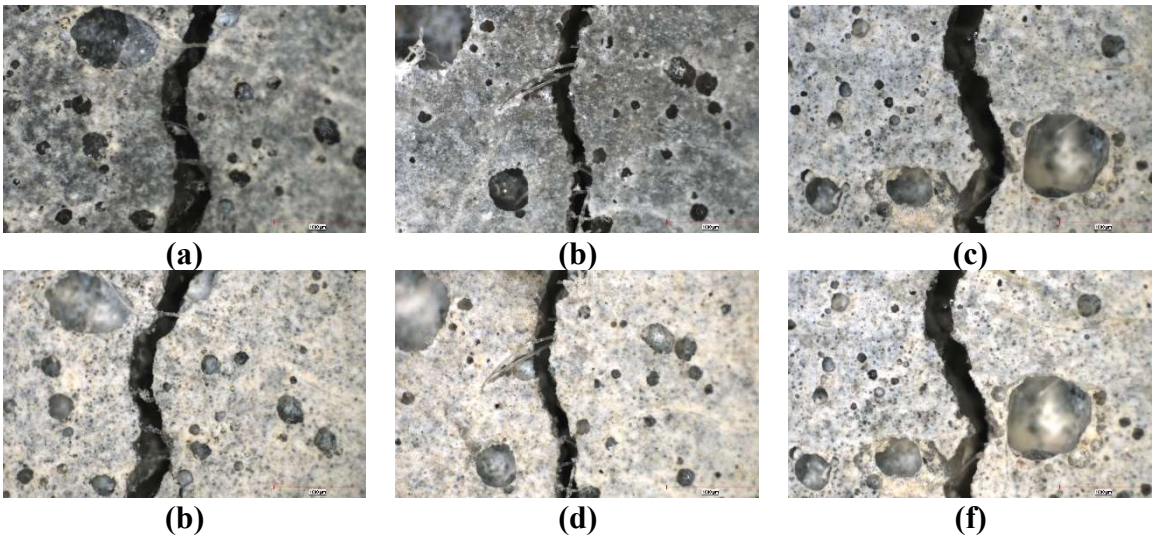

Figure A.53: The crack images of 14-day old METB samples kept at ambient conditions. (a, b, c) right after cracking, (d, e, f) after 28 days.

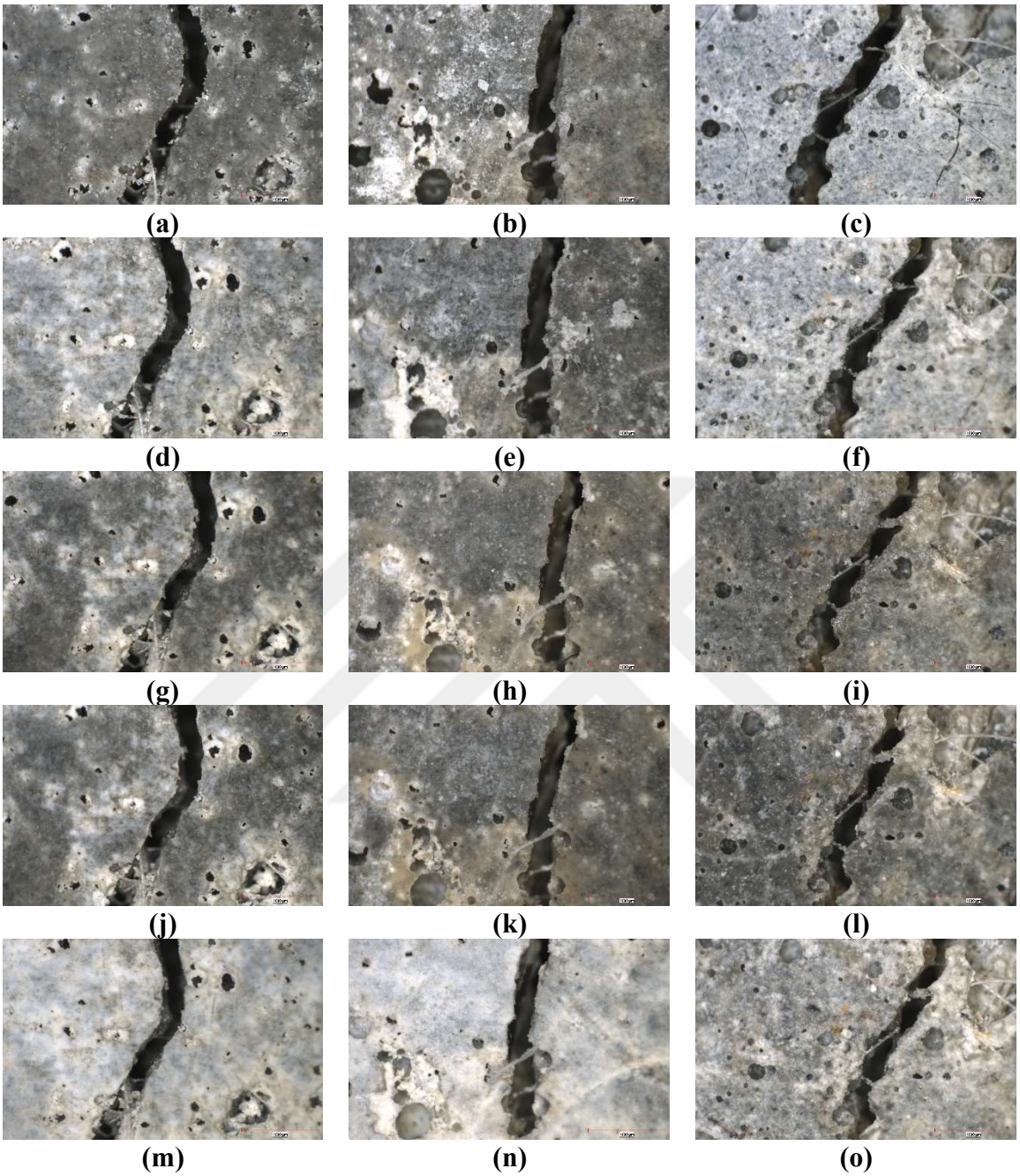

Figure A.54: The crack images of 28-day old METB samples. (a, b, c) right after cracking, (d, e, f) after 7 days of water curing, (g, h, i) after 14 days water curing, (j, k, l) after 21 days of water curing (m, n, o) after 28 days of water curing.

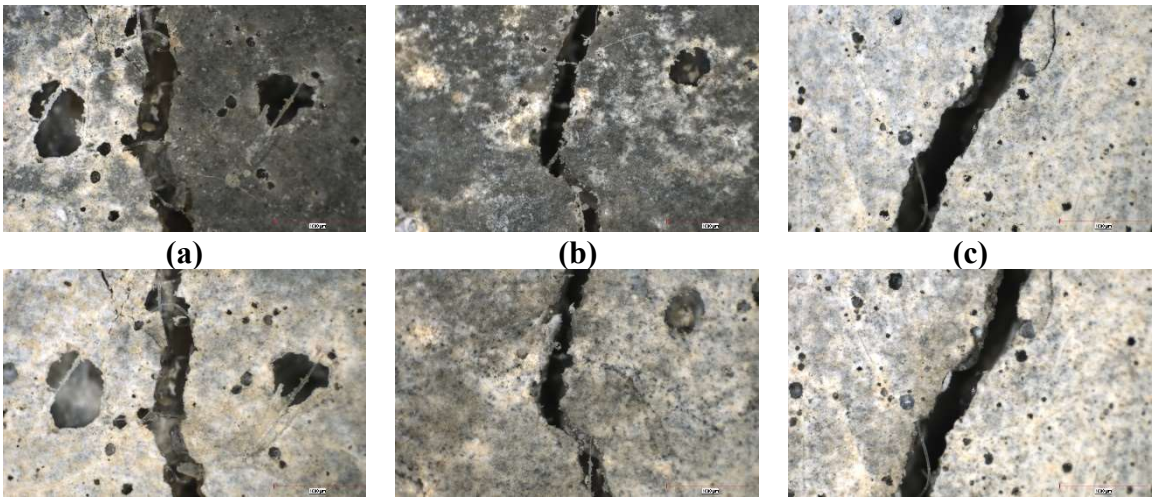

(a) (b) (c)

(d) (e) (f)

Figure A.55: The crack images of 28-day old METB samples kept at ambient conditions. (a, b, c) right after cracking, (d, e, f) after 28 days.

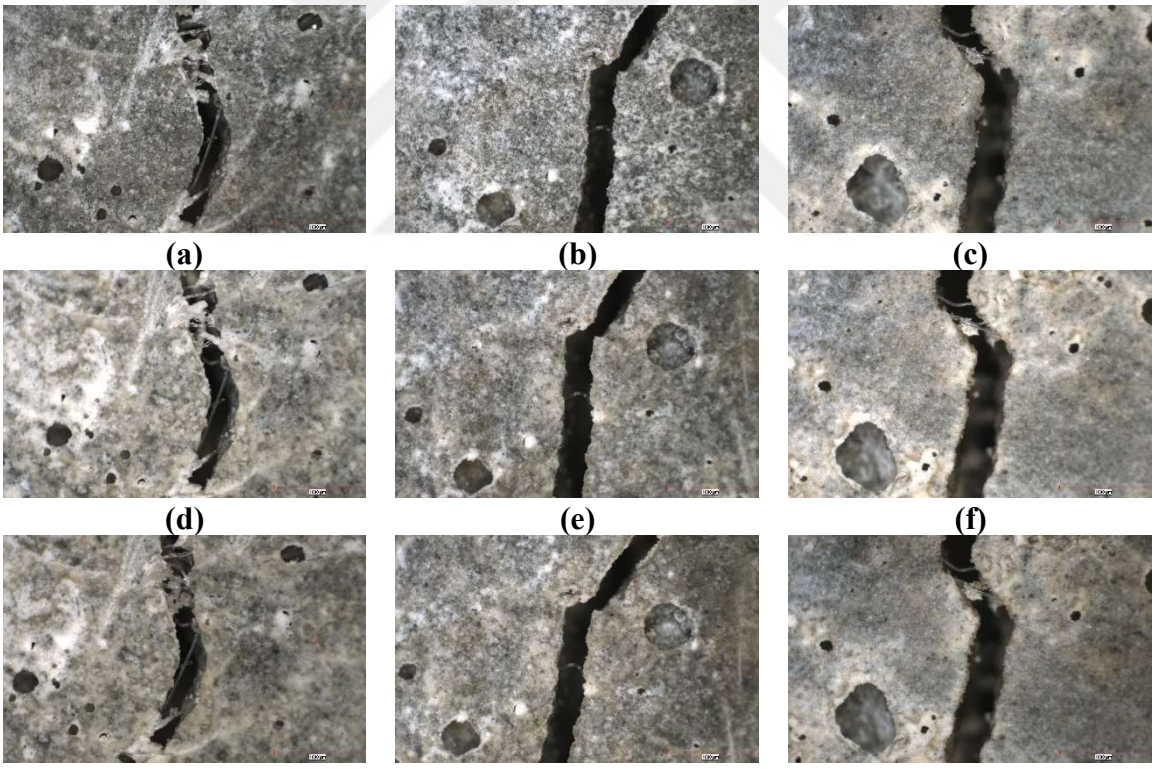

(a) (b) (c)

(d) (e) (f)

(g) (h) (i)

(j) (k) (l)

Figure A.56: The crack images of 14-day old METBN samples. (a, b, c) right after cracking, (d, e, f) after 7 days of water curing, (g, h, i) after 14 days of water curing, (j, k, l) 28 days of water curing.

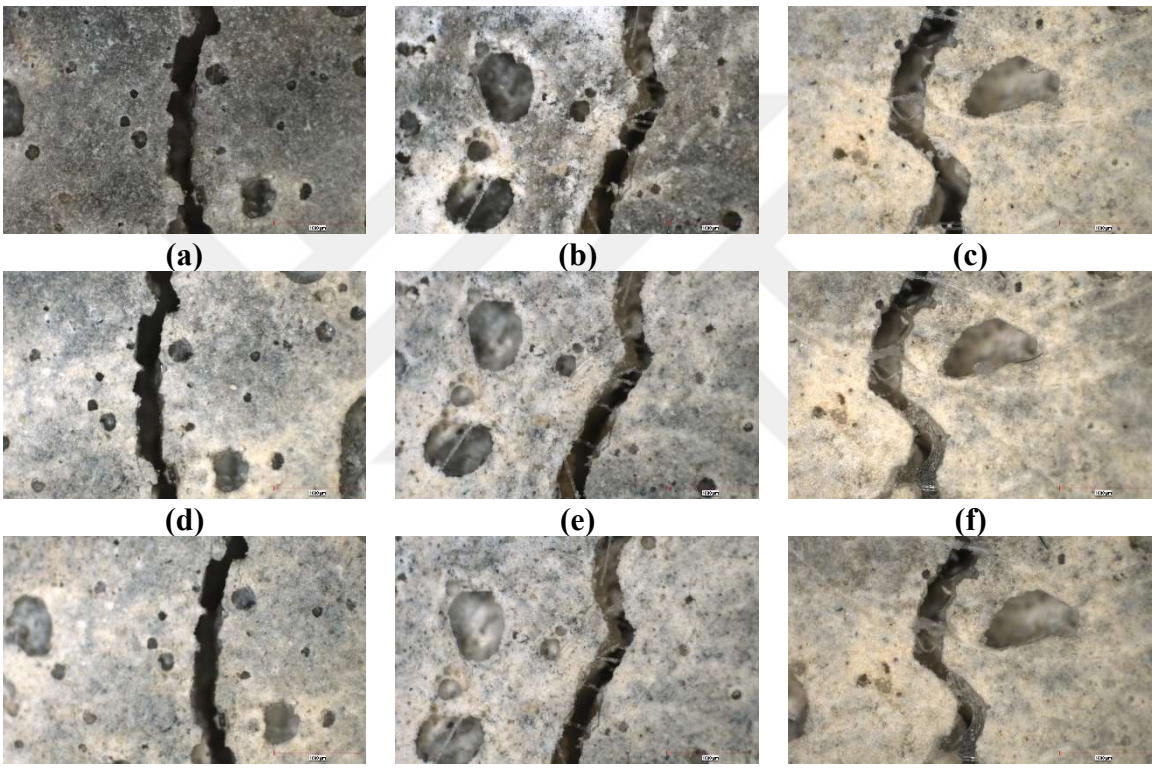

(a) (b) (c)

(d) (e) (f)

(g) (h) (i)

Figure A.57: The crack images of 14-day old METBN samples kept at ambient conditions. (a, b, c) right after cracking, (d, e, f) after 7 days, (g, h, i) after 28 days.

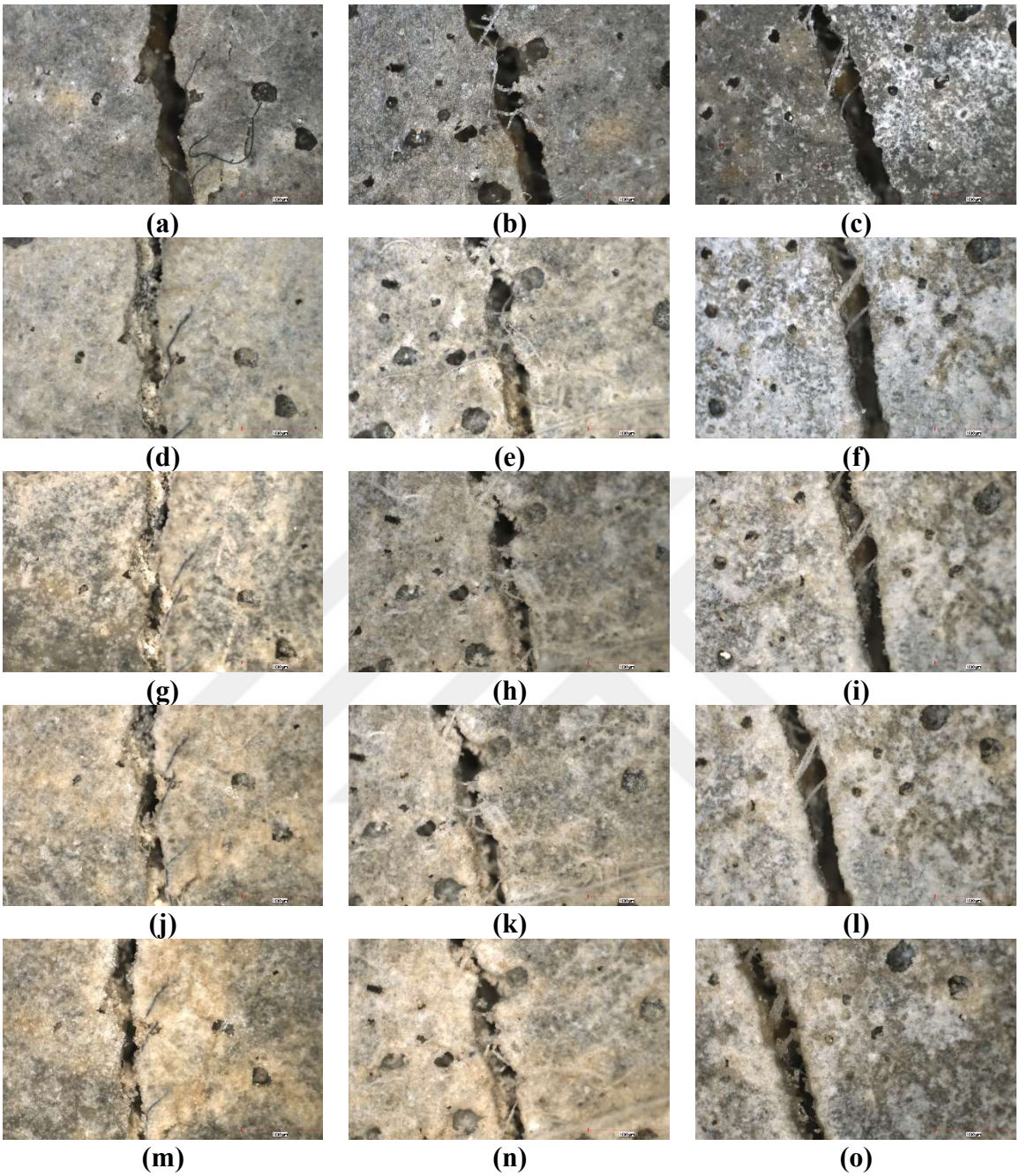

Figure A.58: The crack images of 28-day old METBN samples. (a, b, c) right after cracking, (d, e, f) after 7 days of UCSL-CA curing, (g, h, i) after 14 days of UCSL-CA curing, (j, k, l) after 21 days of UCSL-CA curing (m, n, o) after 28 days of UCSL-CA curing.

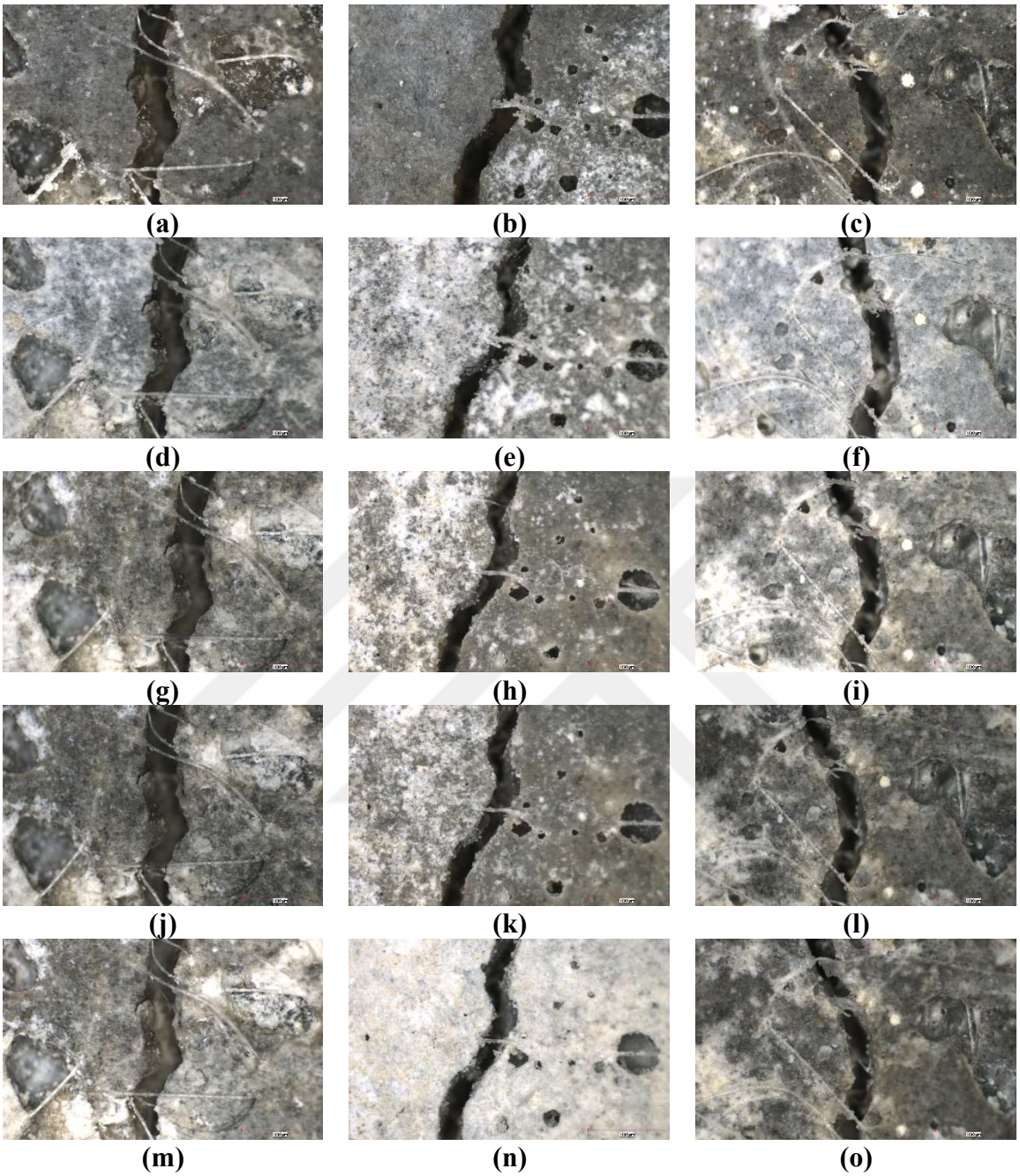

Figure A.59: The crack images of 28-day old METBN samples. (a, b, c) right after cracking, (d, e, f) after 7 days of water curing, (g, h, i) after 14 days of water curing, (j, k, l) after 21 days of water curing (m, n, o) after 28 days of water curing.

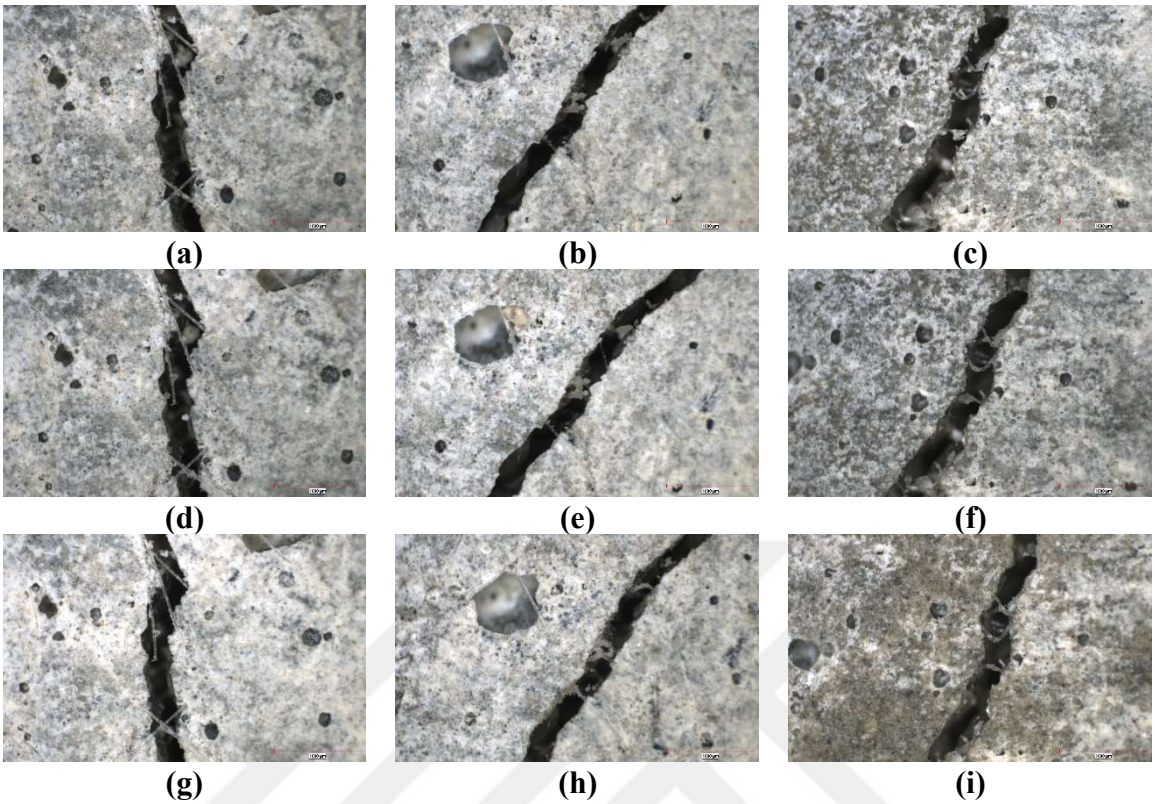

Figure A.60: The crack images of 28-day old METBN samples kept at ambient conditions. (a, b, c) right after cracking, (d, e, f) after 7 days, (g, h, i) after 28 days.

Table A.1: The crack width analysis of 14-day old samples cured with UCSL-CA nutrient medium. BT: bentonite, DE: diatomaceous earth, SEP: sepiolite, ZEO: zeolite, PER: perlite, MET: metakaolin, PUM: pumice. C: only includes minerals, B: mineral was saturated with bacterial cells and PBS, BN: half of mineral was saturated with bacterial cells and PBS and the other half of mineral was saturated with UCSL-CA.

14. DAY UCSL-CA NUTRIENT MEDIUM CURING					
Sample Name	**Crack Closure Rate (%)**	**Maximum Crack Width (µm)**	**Minimum Crack Width (µm)**	**Average Crack Width (µm)**	**Average Crack Width of Non Closure Part (µm)**
BTC	25,08	703,22	191,40	288,39	216,06
DEC	6,06	976,34	298,93	406,95	382,29
SEPC	7,32	1208,60	270,97	494,41	458,21
ZEOC-200	33,61	666,67	163,44	255,05	169,32
ZEOC-1.6	52,07	361,29	230,11	307,81	147,53
METC	20,05	533,33	279,57	369,03	295,05
PERC	42,39	473,12	266,67	331,47	190,97
PUMC	0,50	-	-	-	-
BTB	90,52	660,22	191,40	345,16	32,74
DEB	85,31	563,44	187,10	294,10	102,01
SEPB	92,81	812,90	279,57	393,69	28,30
ZEOB-200	84,19	546,24	96,77	321,86	50,90
ZEOB-1.6	37,10	610,75	227,96	377,77	237,63
METB	38,79	425,81	232,26	291,61	178,50
PERB	34,73	507,53	227,96	367,03	239,57
PUMB	81,38	617,20	189,25	332,98	61,98
BTBN	100	662,37	231,90	346,76	0
DEBN	100	412,90	215,05	303,08	0
SEPBN	94,54	606,45	296,77	365,43	20,61
ZEOBN-200	53,88	415,05	258,07	340,22	156,92
ZEOBN-1.6	40,16	468,82	283,87	340,93	204,01
METBN	25,70	430,11	172,04	316,85	235,41
PERBN	56,23	460,22	262,37	338,35	148,10
PUMBN	91,82	451,61	251,61	333,33	27,26

Table A.2: The crack width analysis of 28-day old samples cured with UCSL-CA nutrient medium. BT: bentonite, DE: diatomaceous earth, SEP: sepiolite, ZEO: zeolite, PER: perlite, MET: metakaolin, PUM: pumice. C: only includes minerals, B: mineral was saturated with bacterial cells and PBS, BN: half of mineral was saturated with bacterial cells and PBS and the other half of mineral was saturated with UCSL-CA.

28. DAY UCSL-CA NUTRIENT MEDIUM CURING					
Sample Name	**Crack Closure Rate (%)**	**Maximum Crack Width (µm)**	**Minimum Crack Width (µm)**	**Average Crack Width (µm)**	**Average Crack Width of Non Closure Part (µm)**
BTC	34,92	612,90	197,85	319,21	207,74
DEC	2,78	458,07	277,42	330,47	321,29
SEPC	3,43	756,99	154,84	331,97	320,57
ZEOC-200	52,86	369,89	236,56	275,84	130,04
ZEOC-1.6	55,90	466,67	311,83	397,42	175,27
METC	15,83	593,55	313,98	401,15	337,63
PERC	32,6	404,30	258,07	346,52	233,55
PUMC	9,46	690,32	234,41	373,69	320,29
BTB	80,20	408,60	165,59	270,90	50,43
DEB	84,17	430,11	167,74	272,19	43,08
SEPB	98,06	406,45	174,19	269,11	85,95
ZEOB-200	69,55	313,98	165,59	214,70	65,38
ZEOB-1.6	34,55	533,33	270,97	350,40	229,32
METB	30,02	468,82	215,06	335,77	234,98
PERB	21,84	503,23	219,36	303,23	236,99
PUMB	84,40	563,44	215,05	314,12	49,0
BTBN	100	765,59	169,89	313,08	0
DEBN	96,8	564,98	214,82	300,08	9,60
SEPBN	100	458,07	101,08	290,32	0
ZEOBN-200	28,37	533,33	210,75	359,28	257,35
ZEOBN-1.6	29,65	419,36	245,16	329,53	231,83
METBN	33,42	451,61	236,56	365,59	243,41
PERBN	17,32	421,51	193,55	298,78	247,03
PUMBN	90,14	490,32	270,10	359,14	227,00

Table A.3: The crack width analysis of 14-day old samples cured with water. BT: bentonite, DE: diatomaceous earth, SEP: sepiolite, ZEO: zeolite, PER: perlite, MET: metakaolin, PUM: pumice. C: only includes minerals, B: mineral was saturated with bacterial cells and PBS, BN: half of mineral was saturated with bacterial cells and PBS and the other half of mineral was saturated with UCSL-CA.

14. DAY WATER CURING					
Sample Name	**Crack Closure Rate (%)**	**Maximum Crack Width (µm)**	**Minimum Crack Width (µm)**	**Average Crack Width (µm)**	**Average Crack Width of Non Closure Part (µm)**
BTC	0,74	698,93	116,13	298,21	295,99
DEC	6,52	541,94	251,61	328,82	307,38
SEPC	0,79	886,02	227,96	397,28	394,12
ZEOC-200	63,30	769,89	120,43	270,11	99,14
ZEOC-1.6	37,12	494,62	251,61	346,52	217,88
METC	12,91	524,73	335,48	392,11	341,51
PERC	17,73	455,91	296,77	359,00	295,34
PUMC	4,98	473,12	167,74	279,07	265,16
BTB	49,94	658,07	156,99	293,54	146,93
DEB	26,74	522,58	245,16	324,59	237,78
SEPB	25,79	662,37	264,52	384,59	285,41
ZEOB-200	23,60	778,50	124,73	305,23	233,19
ZEOB-1.6	30,43	402,15	245,16	336,56	234,16
METB	0,64	477,42	245,16	325,95	323,87
PERB	21,09	524,73	206,45	329,03	259,64
PUMB	22,10	587,10	200,00	313,05	243,87
BTBN	71,51	453,76	180,65	285,34	81,29
DEBN	68,69	780,65	262,37	408,84	126,34
SEPBN	48,58	679,57	266,67	353,48	227,81
ZEOBN-200	23,13	509,68	260,22	347,67	267,24
ZEOBN-1.6	43,02	511,83	253,76	359,28	204,73
METBN	8,00	434,41	249,46	337,06	310,11
PERBN	6,51	529,03	215,05	326,17	304,95
PUMBN	49,57	380,65	208,60	286,38	144,41

Table A.4: The crack width analysis of 28-day old samples cured with water. BT: bentonite, DE: diatomaceous earth, SEP: sepiolite, ZEO: zeolite, PER: perlite, MET: metakaolin, PUM: pumice. C: only includes minerals, B: mineral was saturated with bacterial cells and PBS, BN: half of mineral was saturated with bacterial cells and PBS and the other half of mineral was saturated with UCSL-CA.

28. DAY WATER CURING					
Sample Name	**Crack Closure Rate (%)**	**Maximum Crack Width (µm)**	**Minimum Crack Width (µm)**	**Average Crack Width (µm)**	**Average Crack Width of Non Closure Part (µm)**
BTC	1,86	488,17	219,36	342,37	335,99
DEC	0	929,03	290,32	400,00	437,28
SEPC	2,29	612,90	161,29	278,85	272,47
ZEOC-200	71,87	754,84	103,23	285,45	80,27
ZEOC-1.6	24,11	636,56	275,27	359,14	272,55
METC	9,57	623,66	361,29	444,88	402,29
PERC	8,69	361,29	159,14	301,94	275,70
PUMC	14,29	490,32	193,55	304,34	275,56
BTB	42,61	361,29	187,10	239,82	137,63
DEB	29,18	348,39	210,75	278,42	197,17
SEPB	53,30	634,41	184,95	346,17	161,65
ZEOB-200	61,48	464,52	187,10	279,50	107,67
ZEOB-1.6	23,30	673,12	294,62	428,71	328,82
METB	11,03	602,15	275,27	361,43	321,58
PERB	12,42	486,02	219,36	329,03	288,17
PUMB	17,25	539,79	206,45	322,95	276,46
BTBN	35,70	447,31	210,75	289,43	186,09
DEBN	45,98	882,92	190,32	341,10	220,42
SEPBN	17,08	548,39	261,82	338,78	280,93
ZEOBN-200	13,86	526,88	249,46	333,69	287,45
ZEOBN-1.6	24,65	406,45	247,31	295,48	222,65
METBN	17,03	580,65	322,58	390,68	324,16
PERBN	22,72	503,23	223,66	284,88	220,14
PUMBN	36,81	490,32	270,97	359,14	226,97

APPENDIX B – FTIR ANALYSES

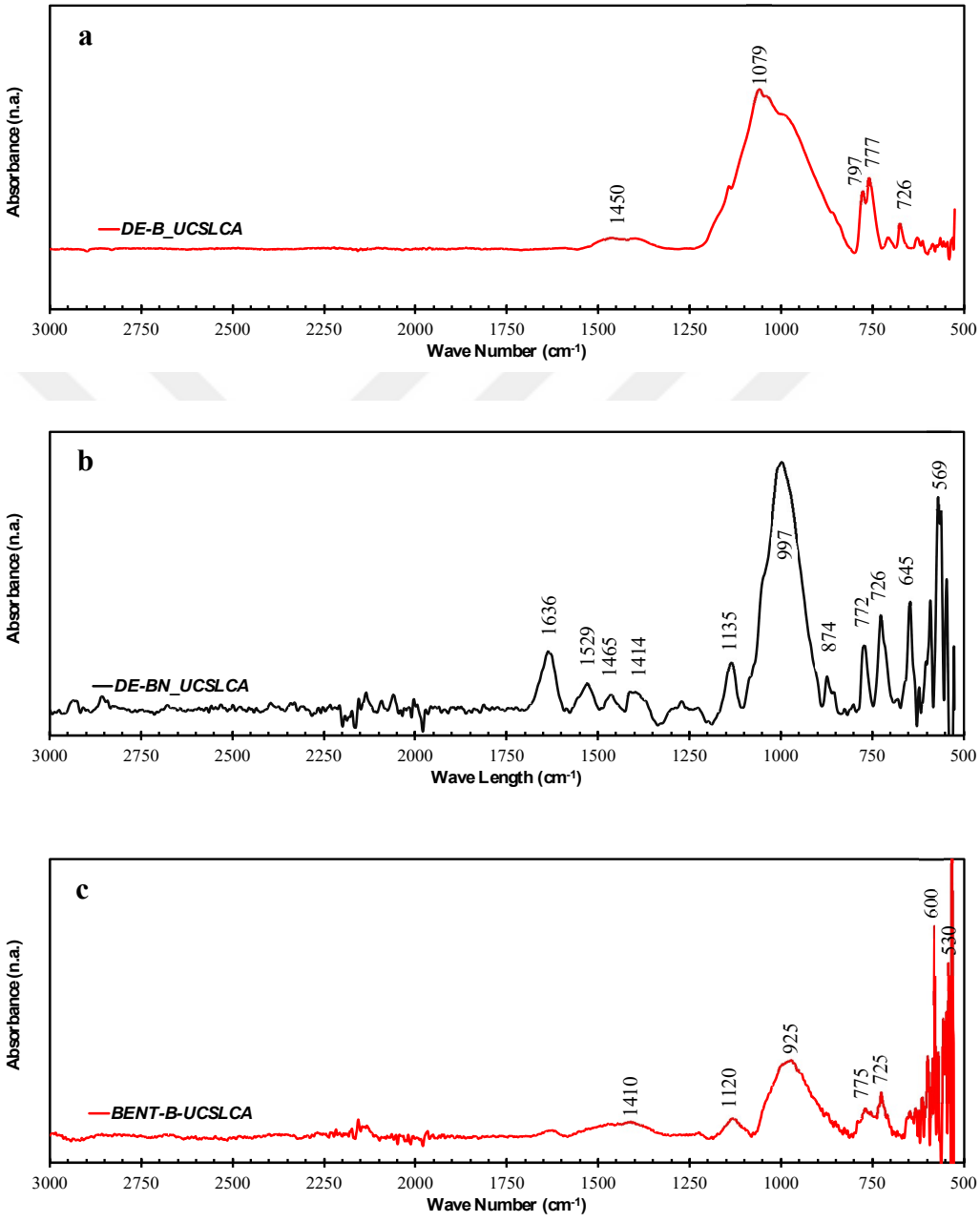

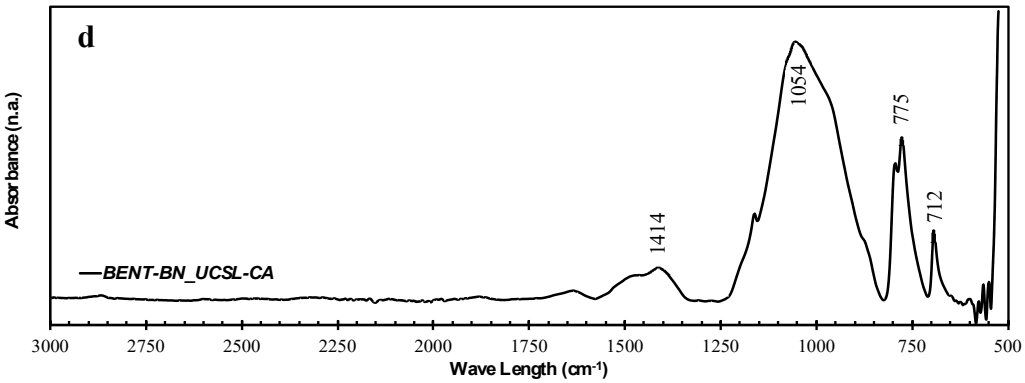
d
Absorbance (n.a.)
1414
1054
775
712
BENT-BN_UCSL-CA
3000 2750 2500 2250 2000 1750 1500 1250 1000 750 500
Wave Length (cm-1)

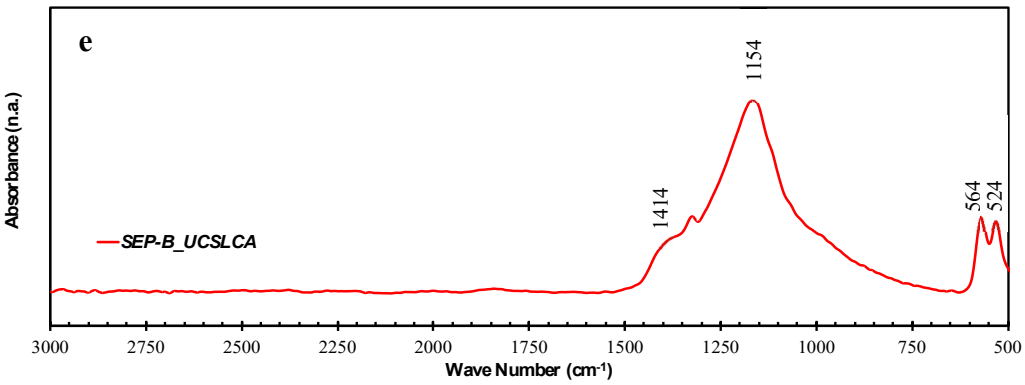
e
Absorbance (n.a.)
1414
1154
564
524
SEP-B_UCSLCA
3000 2750 2500 2250 2000 1750 1500 1250 1000 750 500
Wave Number (cm-1)

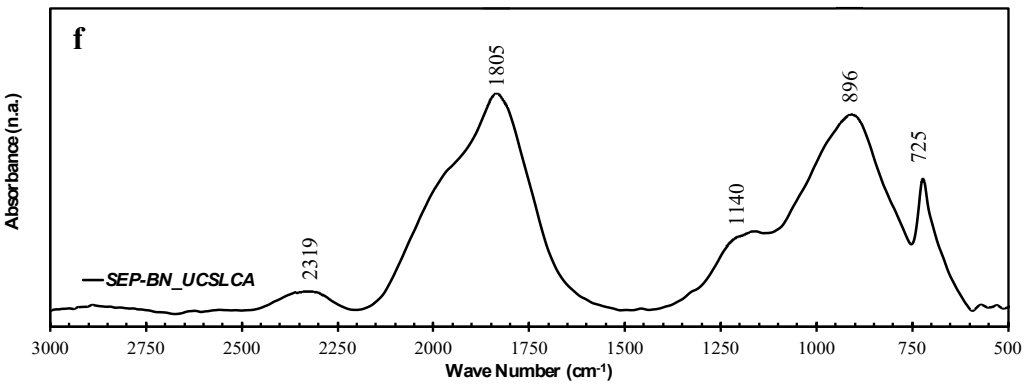
f
Absorbance (n.a.)
2319
1805
1140
896
725
SEP-BN_UCSLCA
3000 2750 2500 2250 2000 1750 1500 1250 1000 750 500
Wave Number (cm-1)

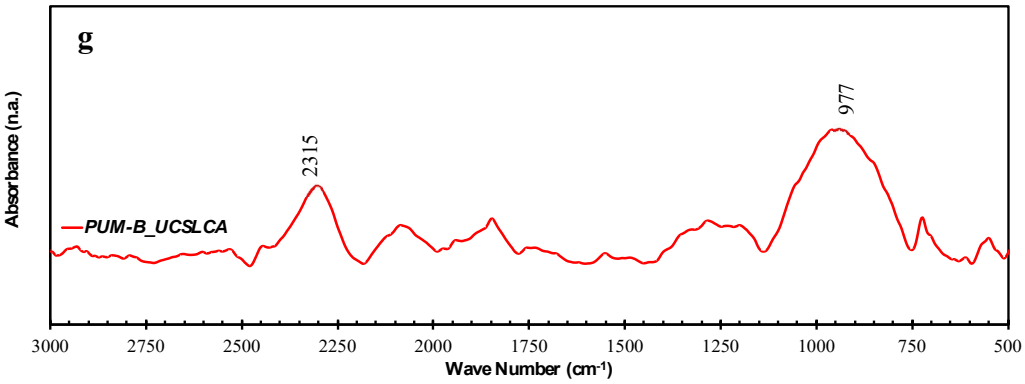
g
Absorbance (n.a.)
2315
977
PUM-B_UCSLCA
3000 2750 2500 2250 2000 1750 1500 1250 1000 750 500
Wave Number (cm-1)

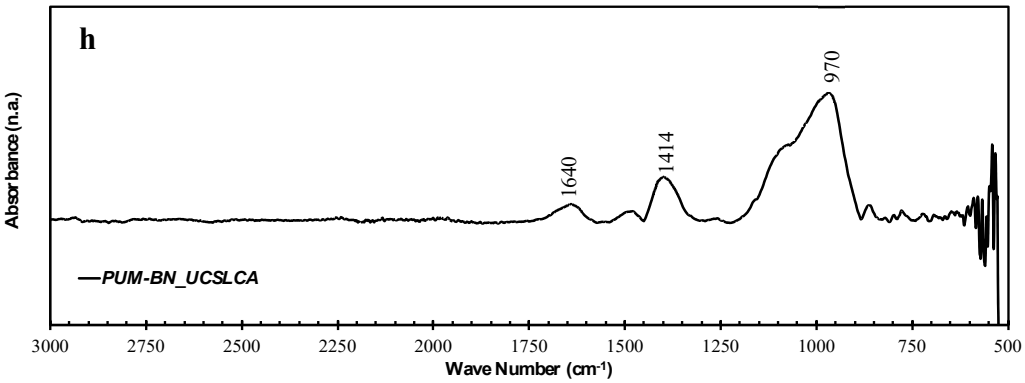

Figure B.1: FTIR spectra of 28-day old samples cured with UCSL-CA nutrient medium. (a) DEB (b) DEBN (c) BTB (d) BTBN (e) SEPB (f) SEPBN (g) PUMB (h) PUMBN

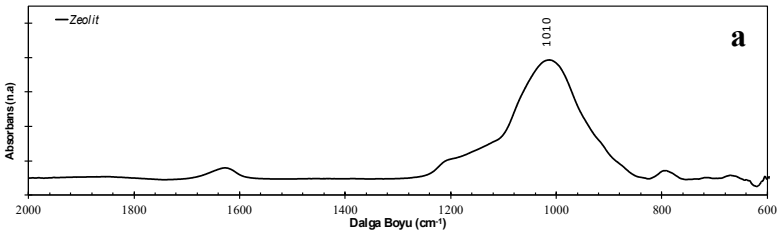
Zeolit
1010
a
Absorbans (n.a)
2000 1800 1600 1400 1200 1000 800 600
Dalga Boyu (cm-1)

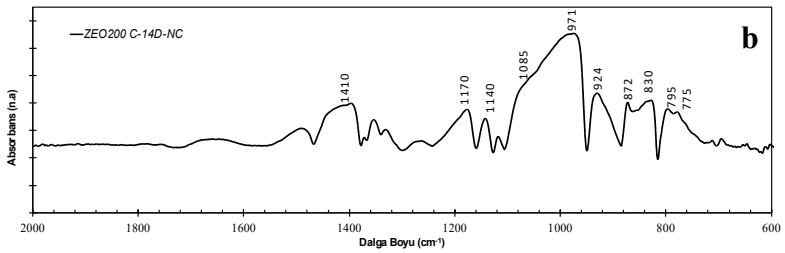
ZEO200 C-14D-NC
1410
1170
1140
1085
971
924
872
830
795
775
b
Absorbans (n.a)
2000 1800 1600 1400 1200 1000 800 600
Dalga Boyu (cm-1)

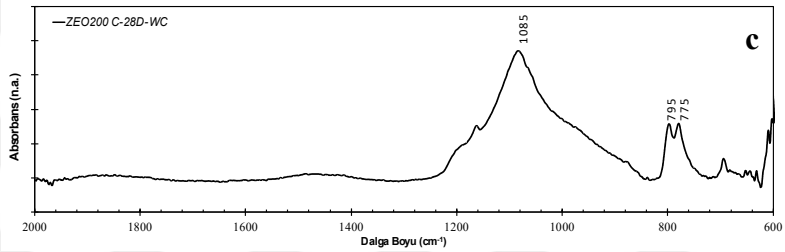
ZEO200 C-28D-WC
1085
795
775
c
Absorbans (n.a.)
2000 1800 1600 1400 1200 1000 800 600
Dalga Boyu (cm-1)

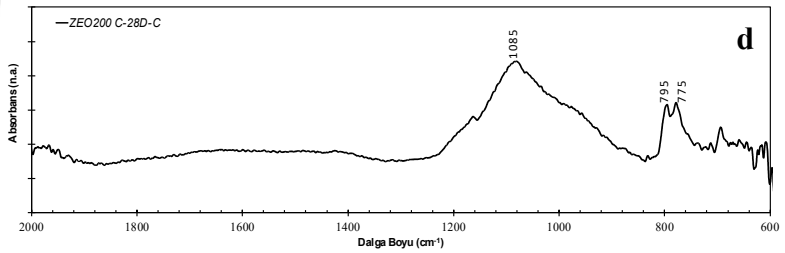
ZEO200 C-28D-C
1085
795
775
d
Absorbans (n.a.)
2000 1800 1600 1400 1200 1000 800 600
Dalga Boyu (cm-1)

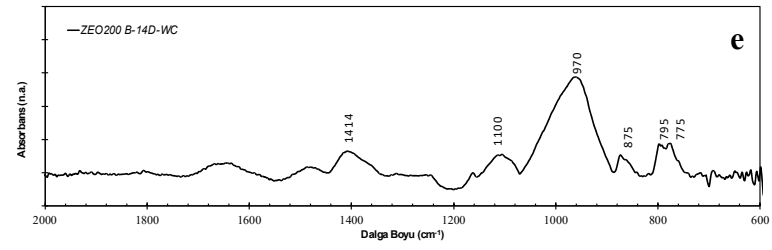
ZEO200 B-14D-WC
1414
1100
970
875
795
775
e
Absorbans (n.a.)
2000 1800 1600 1400 1200 1000 800 600
Dalga Boyu (cm-1)

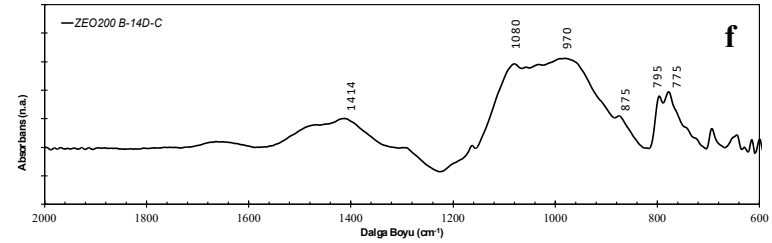
ZEO200 B-14D-C
1414
1080
970
875
795
775
f
Absorbans (n.a.)
2000 1800 1600 1400 1200 1000 800 600
Dalga Boyu (cm-1)

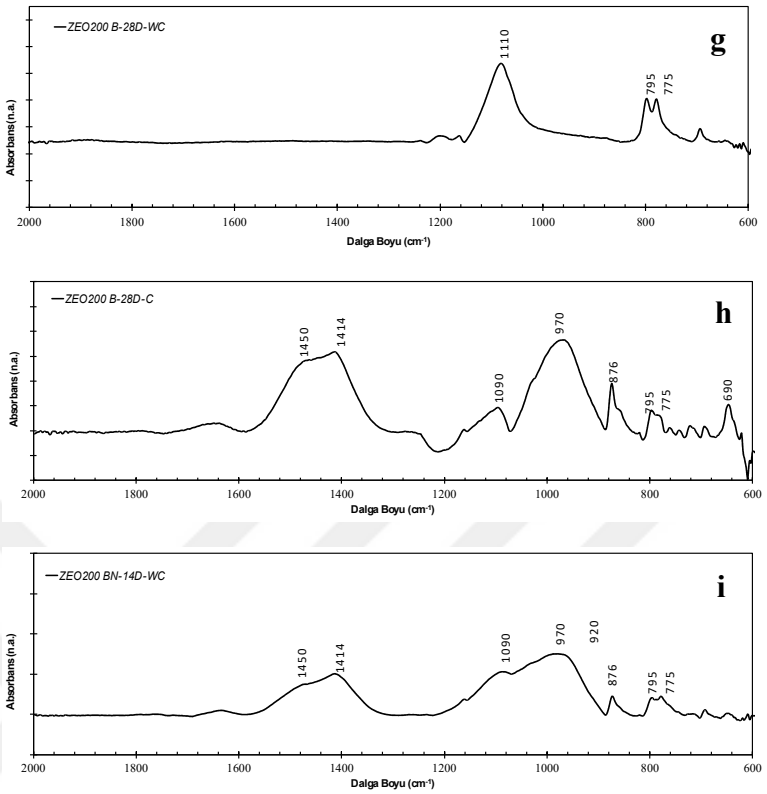

Figure B.2: FTIR spectra of ZEO-200 samples. (a) Zeolite-200µm (b) ZEOC-200-14D-NC (c) ZEOC-200-28D-W (d) ZEOC-200-28D-C (e) ZEB-200-14D-W (f) ZEOB-200-14D-C (g) ZEOB-200-28D-W (h) ZEOB-200-28D-C (i) ZEOBN-200-14D-W

APPENDIX C – ONGOING WORKS

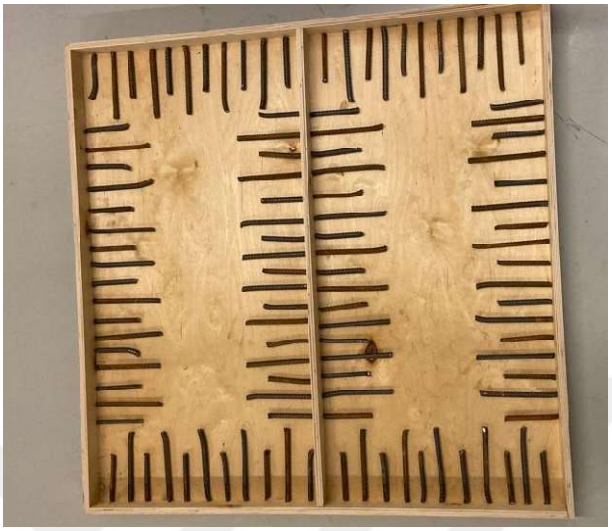

Figure C.1: The designed restrained shrinkage system to obtain micro cracks.

Figure C.2: First trial of restrained shrinkage (a) control sample (b) BTBN sample (c) the initial crack was observed in BTBN sample after 15 days without any curing.

Figure C. 3: The reinforced cement-based mortars for corrosion test.

BIBLIOGRAPHY

[1] K. L. Scrivener, V. M. John, and E. M. Gartner, "Eco-efficient cements: Potential economically viable solutions for a low-CO2 cement-based materials industry," *Cem Concr Res*, vol. 114, pp. 2–26, Dec. 2018, doi: 10.1016/J.CEMCONRES.2018.03.015.

[2] "Technology Roadmap: Low-Carbon Transition in the Cement Industry," *IEA, CSI & WBCSD*, 2018. https://www.wbcsd.org/Sector-Projects/Cement-Sustainability-Initiative/Resources/Technology-Roadmap-Low-Carbon-Transition-in-the-Cement-Industry (accessed Jul. 13, 2022).

[3] "The Paris Agreement | UNFCCC," *United Nations*, 2015.

[4] "The European Green Deal," *European Comission*, 2019.

[5] W. Zhang, Q. Zheng, A. Ashour, and B. Han, "Self-healing cement concrete composites for resilient infrastructures: A review," *Compos B Eng*, vol. 189, p. 107892, May 2020, doi: 10.1016/J.COMPOSITESB.2020.107892.

[6] H. Mihashi and T. Nishiwaki, "Development of engineered self-healing and self-repairing concrete-state-of-the-art report," *Journal of Advanced Concrete Technology*, vol. 10, no. 5, pp. 170–184, 2012, doi: 10.3151/JACT.10.170.

[7] N. de Belie *et al.*, "A Review of Self-Healing Concrete for Damage Management of Structures," *Adv Mater Interfaces*, vol. 5, no. 17, p. 1800074, Sep. 2018, doi: 10.1002/ADMI.201800074.

[8] D. Snoeck, K. van Tittelboom, S. Steuperaert, P. Dubruel, and N. de Belie, "Self-healing cementitious materials by the combination of microfibres and superabsorbent polymers," *J Intell Mater Syst Struct*, vol. 25, no. 1, pp. 13–24, Jan. 2014, doi: 10.1177/1045389X12438623.

[9] T. H. Ahn and T. Kishi, "Crack self-healing behavior of cementitious composites incorporating various mineral admixtures," *Journal of Advanced Concrete Technology*, vol. 8, no. 2, pp. 171–186, Jun. 2010, doi: 10.3151/JACT.8.171.

[10] R. Maddalena, H. Taha, and D. Gardner, "Self-healing potential of supplementary cementitious materials in cement mortars: sorptivity and pore structure," *Developments in the Built Environment*, vol. 6, p. 100044, Feb. 2021, doi: 10.1016/j.dibe.2021.100044.

[11] Z. Jiang, W. Li, and Z. Yuan, "Influence of mineral additives and environmental conditions on the self-healing capabilities of cementitious materials," *Cem Concr Compos*, vol. 57, pp. 116–127, Mar. 2015, doi: 10.1016/J.CEMCONCOMP.2014.11.014.

[12] B. Dong *et al.*, "Performance recovery concerning the permeability of concrete by means of a microcapsule based self-healing system," *Cem Concr Compos*, vol. 78, pp. 84–96, Apr. 2017, doi: 10.1016/j.cemconcomp.2016.12.005.

[13] R. Alghamri, A. Kanellopoulos, and A. Al-Tabbaa, “Impregnation and encapsulation of lightweight aggregates for self-healing concrete,” *Constr Build Mater*, vol. 124, pp. 910–921, Oct. 2016, doi: 10.1016/J.CONBUILDMAT.2016.07.143.

[14] J. Y. Wang, H. Soens, W. Verstraete, and N. de Belie, “Self-healing concrete by use of microencapsulated bacterial spores,” *Cem Concr Res*, vol. 56, pp. 139–152, Feb. 2014, doi: 10.1016/J.CEMCONRES.2013.11.009.

[15] Y. Ç. Erşan, H. Verbruggen, I. de Graeve, W. Verstraete, N. de Belie, and N. Boon, “Nitrate reducing CaCO3 precipitating bacteria survive in mortar and inhibit steel corrosion,” *Cem Concr Res*, vol. 83, pp. 19–30, May 2016, doi: 10.1016/J.CEMCONRES.2016.01.009.

[16] K. van Tittelboom, N. de Belie, D. van Loo, and P. Jacobs, “Self-healing efficiency of cementitious materials containing tubular capsules filled with healing agent,” *Cem Concr Compos*, vol. 33, no. 4, pp. 497–505, Apr. 2011, doi: 10.1016/J.CEMCONCOMP.2011.01.004.

[17] K. van Tittelboom, N. de Belie, W. de Muynck, and W. Verstraete, “Use of bacteria to repair cracks in concrete,” *Cem Concr Res*, vol. 40, no. 1, pp. 157–166, Jan. 2010, doi: 10.1016/J.CEMCONRES.2009.08.025.

[18] Y. Shields, N. de Belie, A. Jefferson, and K. van Tittelboom, “A review of vascular networks for self-healing applications,” *Smart Mater Struct*, vol. 30, no. 6, p. 063001, Apr. 2021, doi: 10.1088/1361-665X/ABF41D.

[19] P. Minnebo *et al.*, “A novel design of autonomously healed concrete: Towards a vascular healing network,” *Materials*, vol. 10, no. 1, 2017, doi: 10.3390/MA10010049.

[20] Y. Kuang and J. Ou, “Self-repairing performance of concrete beams strengthened using superelastic SMA wires in combination with adhesives released from hollow fibers,” *Smart Mater Struct*, vol. 17, no. 2, Apr. 2008, doi: 10.1088/0964-1726/17/2/025020.

[21] W. Tang, O. Kardani, and H. Cui, “Robust evaluation of self-healing efficiency in cementitious materials – A review,” *Constr Build Mater*, vol. 81, pp. 233–247, Apr. 2015, doi: 10.1016/J.CONBUILDMAT.2015.02.054.

[22] Z. Basaran, “Biomineralization in cement based materials: inoculation of vegetative cells,” 2013.

[23] A. Amiri, M. Azima, and Z. B. Bundur, “Crack remediation in mortar via biomineralization: Effects of chemical admixtures on biogenic calcium carbonate,” *Constr Build Mater*, vol. 190, pp. 317–325, Nov. 2018, doi: 10.1016/J.CONBUILDMAT.2018.09.083.

[24] “Sustainable Development Goals (SDGs),” *United Nations (UN)*. 2015.

[25] S. Mann, “Biomineralization: principles and concepts in bioinorganic materials chemistry,” 2001.

[26] S. Stocks-Fischer, J. K. Galinat, and S. S. Bang, “Microbiological precipitation of CaCO3,” *Soil Biol Biochem*, vol. 31, no. 11, pp. 1563–1571, Oct. 1999, doi: 10.1016/S0038-0717(99)00082-6.

[27] K. L. Bachmeier, A. E. Williams, J. R. Warmington, and S. S. Bang, “Urease activity in microbiologically-induced calcite precipitation,” *J Biotechnol*, vol. 93, no. 2, pp. 171–181, Feb. 2002, doi: 10.1016/S0168-1656(01)00393-5.

[28] W. de Muynck, K. Cox, N. de Belie, and W. Verstraete, “Bacterial carbonate precipitation as an alternative surface treatment for concrete,” *Constr Build Mater*, vol. 22, no. 5, pp. 875–885, May 2008, doi: 10.1016/J.CONBUILDMAT.2006.12.011.

[29] W. de Muynck, N. de Belie, and W. Verstraete, “Microbial carbonate precipitation in construction materials: A review,” *Ecol Eng*, vol. 36, no. 2, pp. 118–136, Feb. 2010, doi: 10.1016/J.ECOLENG.2009.02.006.

[30] Z. Başaran Bundur, S. Bae, M. J. Kirisits, and R. D. Ferron, “Biomineralization in Self-Healing Cement-Based Materials: Investigating the Temporal Evolution of Microbial Metabolic State and Material Porosity,” *Journal of Materials in Civil Engineering*, vol. 29, no. 8, p. 04017079, Aug. 2017, doi: 10.1061/(asce)mt.1943-5533.0001838.

[31] V. Wiktor and H. M. Jonkers, “Quantification of crack-healing in novel bacteria-based self-healing concrete,” *Cem Concr Compos*, vol. 33, no. 7, pp. 763–770, Aug. 2011, doi: 10.1016/j.cemconcomp.2011.03.012.

[32] H. M. Jonkers, A. Thijssen, G. Muyzer, O. Copuroglu, and E. Schlangen, “Application of bacteria as self-healing agent for the development of sustainable concrete,” *Ecol Eng*, vol. 36, no. 2, pp. 230–235, Feb. 2010, doi: 10.1016/j.ecoleng.2008.12.036.

[33] S. S. Bang, J. K. Galinat, and V. Ramakrishnan, “Calcite precipitation induced by polyurethane-immobilized Bacillus pasteurii,” *Enzyme Microb Technol*, vol. 28, no. 4–5, pp. 404–409, Mar. 2001, doi: 10.1016/S0141-0229(00)00348-3.

[34] E. Tziviloglou, V. Wiktor, H. M. Jonkers, and E. Schlangen, “Bacteria-based self-healing concrete to increase liquid tightness of cracks,” *Constr Build Mater*, vol. 122, pp. 118–125, Sep. 2016, doi: 10.1016/j.conbuildmat.2016.06.080.

[35] J. Wang, K. van Tittelboom, N. de Belie, and W. Verstraete, “Use of silica gel or polyurethane immobilized bacteria for self-healing concrete,” *Constr Build Mater*, vol. 26, no. 1, pp. 532–540, Jan. 2012, doi: 10.1016/J.CONBUILDMAT.2011.06.054.

[36] S. S. Bang, J. J. Lippert, U. Yerra, S. Mulukutla, and V. Ramakrishnan, “Microbial calcite, a bio-based smart nanomaterial in concrete remediation,” *http://dx.doi.org/10.1080/19475411003593451*, vol. 1, no. 1, pp. 28–39, 2010, doi: 10.1080/19475411003593451.

[37] J. Y. Wang, N. de Belie, and W. Verstraete, “Diatomaceous earth as a protective vehicle for bacteria applied for self-healing concrete,” *J Ind Microbiol Biotechnol*, vol. 39, no. 4, pp. 567–577, Apr. 2012, doi: 10.1007/S10295-011-1037-1.

[38] J. Zhang *et al.*, “Immobilizing bacteria in expanded perlite for the crack self-healing in concrete,” *Constr Build Mater*, vol. 148, pp. 610–617, Sep. 2017, doi: 10.1016/j.conbuildmat.2017.05.021.

[39] M. Alazhari, T. Sharma, A. Heath, R. Cooper, and K. Paine, “Application of expanded perlite encapsulated bacteria and growth media for self-healing concrete,” *Constr Build Mater*, vol. 160, pp. 610–619, Jan. 2018, doi: 10.1016/j.conbuildmat.2017.11.086.

[40] M. T. Mustafa and B. B. Zeynep, “Use of Natural Minerals to Immobilize Bacterial Cells for Remediating Cracks in Cement-Based Materials,” *Journal of Materials in Civil Engineering*, vol. 34, no. 3, p. 04021461, Mar. 2022, doi: 10.1061/(ASCE)MT.1943-5533.0004098.

[41] L. Jiang, G. Jia, C. Jiang, and Z. Li, “Sugar-coated expanded perlite as a bacterial carrier for crack-healing concrete applications,” *Constr Build Mater*, vol. 232, p. 117222, Jan. 2020, doi: 10.1016/j.conbuildmat.2019.117222.

[42] M. M. Tezer, “Development of two-phase biological self-healing agents for cement-based mortar,” 2020.

[43] “ASTM C136/C136M-19, Standard Test Method for Sieve Analysis of Fine and Coarse Aggregates,” *ASTM International*. 2019.

[44] “ASTM C305-14, Standard Practice for Mechanical Mixing of Hydraulic Cement Pastes and Mortars of Plastic Consistency,” *ASTM International*. 2014.

[45] “ASTM C230/C230M-21, Standard Specification for Flow Table for Use in Tests of Hydraulic Cement,” *ASTM International*. 2021.

[46] “ASTM C597-16, Standard Test Method for Pulse Velocity Through Concrete,” *ASTM International*. 2016.

[47] J. Xu and W. Yao, “Multiscale mechanical quantification of self-healing concrete incorporating non-ureolytic bacteria-based healing agent,” *Cem Concr Res*, vol. 64, pp. 1–10, Oct. 2014, doi: 10.1016/J.CEMCONRES.2014.06.003.

[48] Commission 25-PEM Protection et Érosion Des Monuments, “Essais Recommandés Pour Mesurer l’altération Des Pierres et Évaluer l’efficacité Des Méthodes de Traitement/Recommended Tests to Measure the Deterioration of Stone and to Assess the Effectiveness Of,” *Matériaux et constructions. Paris: International Union of Laboratories and Experts in Construction Materials, Systems and Structures*. 1980.

[49] “ASTM C191-19, Standard Test Methods for Time of Setting of Hydraulic Cement by Vicat Needle,” *ASTM International*. 2019.

[50] “ASTM C109/C109M-21, Standard Test Method for Compressive Strength of Hydraulic Cement Mortars (Using 2-in. or [50 mm] Cube Specimens),” *ASTM International*. 2021.

[51] C. Wu and S. Kou, “Effects of high-calcium sepiolite on the rheological behaviour and mechanical strength of cement pastes and mortars,” *Constr Build Mater*, vol. 196, pp. 105–114, Jan. 2019, doi: 10.1016/J.CONBUILDMAT.2018.11.130.

[52] “ASTM C596-18, Standard Test Method for Drying Shrinkage of Mortar Containing Hydraulic Cement,” *ASTM International*. 2018.

[53] “ASTM C157/C157M-17, Standard Test Method for Length Change of Hardened Hydraulic-Cement Mortar and Concrete,” *ASTM International*. 2017.

[54] A. M. Varenyam Achal Shweta Goyal and M. Sudhakara Reddy, “Corrosion Prevention of Reinforced Concrete with Microbial Calcite Precipitation,” *ACI Mater J*, vol. 109, no. 2, doi: 10.14359/51683702.

[55] S. Seraj, R. D. Ferron, and M. C. G. Juenger, “Calcining natural zeolites to improve their effect on cementitious mixture workability,” *Cem Concr Res*, vol. 85, pp. 102–110, Jul. 2016, doi: 10.1016/J.CEMCONRES.2016.04.002.

[56] G. Mertens, R. Snellings, K. van Balen, B. Bicer-Simsir, P. Verlooy, and J. Elsen, “Pozzolanic reactions of common natural zeolites with lime and parameters affecting their reactivity,” *Cem Concr Res*, vol. 39, no. 3, pp. 233–240, Mar. 2009, doi: 10.1016/J.CEMCONRES.2008.11.008.

[57] Y. Lv, G. Ye, and G. de Schutter, “Investigation on the potential utilization of zeolite as an internal curing agent for autogenous shrinkage mitigation and the effect of modification,” *Constr Build Mater*, vol. 198, pp. 669–676, Feb. 2019, doi: 10.1016/j.conbuildmat.2018.12.001.

[58] Y. F. Su *et al.*, “Autogenous healing performance of internal curing agent-based self-healing cementitious composite,” *Cem Concr Compos*, vol. 114, p. 103825, Nov. 2020, doi: 10.1016/J.CEMCONCOMP.2020.103825.

[59] Z. B. Bundur, A. Amiri, Y. C. Ersan, N. Boon, and N. de Belie, “Impact of air entraining admixtures on biogenic calcium carbonate precipitation and bacterial viability,” *Cem Concr Res*, vol. 98, pp. 44–49, Aug. 2017, doi: 10.1016/J.CEMCONRES.2017.04.005.

[60] V. S. Ramachandran and J. J. Beaudoin, *Handbook of analytical techniques in concrete science and technology: principles, techniques and applications*. Elsevier, 2000.

[61] Z. B. Bundur, A. Amiri, Y. C. Ersan, N. Boon, and N. de Belie, “Impact of air entraining admixtures on biogenic calcium carbonate precipitation and bacterial viability,” *Cem Concr Res*, vol. 98, pp. 44–49, Aug. 2017, doi: 10.1016/j.cemconres.2017.04.005.

[62] S. Bhaskar, K. M. Anwar Hossain, M. Lachemi, G. Wolfaardt, and M. Otini Kroukamp, “Effect of self-healing on strength and durability of zeolite-immobilized bacterial cementitious mortar composites,” *Cem Concr Compos*, vol. 82, pp. 23–33, Sep. 2017, doi: 10.1016/J.CEMCONCOMP.2017.05.013.

[63] H. Yuan *et al.*, "Application of zeolite as a bacterial carrier in the self-healing of cement mortar cracks," *Constr Build Mater*, vol. 331, p. 127324, May 2022, doi: 10.1016/J.CONBUILDMAT.2022.127324.

[64] A. R. Suleiman, A. J. Nelson, and M. L. Nehdi, "Visualization and quantification of crack self-healing in cement-based materials incorporating different minerals," *Cem Concr Compos*, vol. 103, pp. 49–58, Oct. 2019, doi: 10.1016/J.CEMCONCOMP.2019.04.026.

[65] R. Siddique and E. H. Kadri, "Effect of metakaolin and foundry sand on the near surface characteristics of concrete," *Constr Build Mater*, vol. 25, no. 8, pp. 3257–3266, Aug. 2011, doi: 10.1016/J.CONBUILDMAT.2011.03.012.

[66] A. Amiri and Z. B. Bundur, "Use of corn-steep liquor as an alternative carbon source for biomineralization in cement-based materials and its impact on performance," *Constr Build Mater*, vol. 165, pp. 655–662, Mar. 2018, doi: 10.1016/j.conbuildmat.2018.01.070.

[67] Z. Basaran Bundur, M. J. Kirisits, and R. D. Ferron, "Biomineralized cement-based materials: Impact of inoculating vegetative bacterial cells on hydration and strength," *Cem Concr Res*, vol. 67, pp. 237–245, 2015, doi: 10.1016/j.cemconres.2014.10.002.

[68] A. G. Güldoğan, "Bio-based rheology modifying agents for cement-based materials," Özyeğin University, İstanbul, 2020.

[69] J. K. Norvell, J. G. Stewart, M. C. Juenger, and D. W. Fowler, "Influence of Clays and Clay-Sized Particles on Concrete Performance," *Journal of Materials in Civil Engineering*, vol. 19, no. 12, pp. 1053–1059, Dec. 2007, doi: 10.1061/(ASCE)0899-1561(2007)19:12(1053).

[70] X. Gao, S. Kawashima, X. Liu, and S. P. Shah, "Influence of clays on the shrinkage and cracking tendency of SCC," *Cem Concr Compos*, vol. 34, no. 4, pp. 478–485, Apr. 2012, doi: 10.1016/J.CEMCONCOMP.2012.01.002.

[71] J. A. Carmona, P. Ramírez, L. A. Trujillo-Cayado, A. Caro, and J. Muñoz, "Rheological and microstructural properties of sepiolite gels. Influence of the addition of ionic surfactants," *Journal of Industrial and Engineering Chemistry*, vol. 59, pp. 1–7, Mar. 2018, doi: 10.1016/J.JIEC.2017.09.030.

[72] J. Pinilla Melo, A. Sepulcre Aguilar, and F. Hernández Olivares, "Rheological properties of aerated cement pastes with fly ash, metakaolin and sepiolite additions," *Constr Build Mater*, vol. 65, pp. 566–573, Aug. 2014, doi: 10.1016/J.CONBUILDMAT.2014.05.034.

[73] H. Yang *et al.*, "Effects of bentonite on pore structure and permeability of cement mortar," *Constr Build Mater*, vol. 224, pp. 276–283, Nov. 2019, doi: 10.1016/J.CONBUILDMAT.2019.07.073.

[74] F. Collins and J. G. Sanjayan, "Effect of pore size distribution on drying shrinkage of alkali-activated slag concrete," *Cem Concr Res*, vol. 30, no. 9, pp. 1401–1406, 2000, doi: 10.1016/S0008-8846(00)00327-6.

VITA

Ilgın Sandalcı is a research assistant in OZU SAM (Sustainable and Adaptive Materials) research group. She received her B.Sc. from Civil Engineering Department at Yıldız Technical University in 2017. She had worked as a quality control and quality assurance engineer for 1.5 years in-situ. She started her M.Sc. at Özyeğin University under the supervision of Assoc. Prof. Dr. Zeynep Başaran Bundur in 2019. She has been working on the development of bacteria-natural mineral system for self-healing cement-based mortars and its impact on shrinkage and corrosion. She had worked as a visitor scholar on the analysis of mitigating concrete cracks with bacteria at the Ohio State University. She will continue her Ph.d studies in Özyeğin University.